UNIVERSITY OF CALIFORNIA,

IRVINE

Early Life Unpredictability Alters Circuits Involved with Emotional and Cognitive Outcomes

DISSERTATION

Submitted in partial satisfaction of the requirements

for the degree of

DOCTOR OF PHILOSPHY

in Biological Sciences

by

Steven Jay Granger

Dissertation Committee:

Professor Michael A. Yassa, Chair

Professor Tallie Z. Baram

Assistant Professor Stephen V. Mahler

Professor Georg F. Striedter

2022

DEDICATION

To

Gale A. “Morrie” Granger

for inspiring a life in science and discovery

TABLE OF CONTENTS

Page

LIST OF FIGURES

LIST OF TABLES

Page

ACKNOWLEDGEMENTS

I would like to thank my advisor, Michael Yassa for his outstanding mentorship, friendship, guidance, and creating an environment that allowed for my creativity and thirst for discovery to flourish. I would like to thank Liv McMillan for her role as Chief of Operations, assistance with all the data collection, and for her constant support. I would like to thank Luis-Colon Perez for his mentorship and his work on the high-resolution diffusion imaging projects. I would like to thank Tallie Z. Baram for her continued support and expertise throughout my time in collaboration with the Conte Center at UC Irvine and beyond. I would like to thank Georg Striedter for his encouragement and belief in my ability as a neuroscientist. I would like to thank Steve Mahler for his role as a committee member and advice on my research projects. I would like to thank David Keator for his advice, mentorship, and collaboration on many projects within and outside of UC Irvine. I would like to thank Julian Thayer for his role as a co-sponsor and advisor. I would like to thank my colleagues from various Centers across campus including the many faculty of the Conte Center at UC Irvine and the faculty involved in BEACoN. I would like to thank John Janecek for programming assistance. I thank the many members of the Yassa Lab for their encouragement and contributions to this research over the years. I would like to thank my undergraduate mentor Dr. Heather Bimonte-Nelson for providing an exceptional early training environment. I would like to thank my wife, Lexie Granger, for being my biggest supporter. I would like to thank my family for their constant support and for listening to my experience through the highs and lows. I can't thank all of you enough. This work was supported by P50 MH096889 (PI: Baram), R01AG053555 (PI: Yassa) and R01MH102392 (PI: Yassa). My graduate training was supported by T32MH119049 (PIs: Yassa, McNaughton).

VITA

Steven J. Granger

Graduate Student Researcher
Neurobiology and Behavior, University of California Irvine

Education

University of California, Irvine 2016-2022
GPA: 3.93
Graduate Student (Neurobiology and Behavior)

Barrett The Honors College at Arizona State University 2013-2016
GPA: 3.88
Psychology B. S.

The Pennsylvania State University 2012-2013
GPA: 3.91
Psychology B. S.

State College Area High School 2008-2012
GPA: 3.88

Publications

Published Manuscripts

Granger, S. J., Colon-Perez, L., Larson, M. S., Phelan, M., Keator, D. B., Janecek, J. T., Sathishkumar, M. T., Smith, A. P., McMillan, L., Greenia, D., Corrada, M. M., Kawas, C. H., & Yassa, M. A. (2022). Hippocampal dentate gyrus integrity revealed with ultrahigh resolution diffusion imaging predicts memory performance in older adults. Hippocampus, 10.1002/hipo.23456. Advance online publication.

Granger, S. J., Adams, J. G., Kark, S. M., Sathishkumar, M. T., Chen, I. Y., Benca, R. M., McMillan, L., Janecek, J. T., & Yassa, M. A. (2022). Latent anxiety in clinical depression is associated with worse recognition of emotional stimuli. *Journal of affective disorders,* 301, 368–377.

Granger, S. J., Glynn, L. M., Sandman, C. A., Small, S. L., Obenaus, A., Keator, D. B., Baram, T. Z., Stern, H., Yassa, M. A., & Davis, E. P. (2021). Aberrant Maturation of the Uncinate Fasciculus Follows Exposure to Unpredictable Patterns of Maternal Signals. *Journal of Neuroscience*, 41(6), 1242–1250.

Granger, S. J., Leal, S. L., Larson, M. S., Janecek, J. T., McMillan, L., Stern, H., & Yassa, M. A. (2021). Integrity of the uncinate fasciculus is associated with emotional pattern separation-related fMRI signals in the hippocampal dentate and CA3. *Neurobiology of Learning and Memory*, 177, 107359.

Matin, M. J., Li, D., Peterson, J., Taylor, M. K., Laurent, H. K., Lucas, T., **Granger, S. J.**, Granger, D. A., and Granger, S. W. (2015). Measuring Nerve Growth Factor in

Saliva by Immunoassay: A Cautionary Note. *Psychoneuroendocrinology,* 63: 235-237.

In Revision

Granger, S. J., Colon-Perez, L., Larson, M. S., Bennet, L. J., Phelan, M., Keator, D. B., Janecek, J. T., Sathishkumar, M. T., Smith, A. P., McMillan, L., Greenia, D., Corrada, M. M., Kawas, C. H., Yassa, M. A. Reduced structural connectivity of the medial temporal lobe including perforant path-related connectivity is associated with aging and memory impairment. *In review at Neurobiology of Aging.*

Kark, S., Adams, J., Sathishkumar, M., McMillan, L., **Granger, S. J.**, Baram, T. Z., Yassa, M. A. Why Do Mothers Never Stop Grieving for Their Deceased Children? Enduring Alterations of Brain Connectivity and Function. *In review at Frontiers in Human Neuroscience.*

Rizvi, B., Sathishmukar, M., Marquez, F., **Granger, S. J.,** McMillan, L., Brickman, A. M., Tustison, N. J., Yassa, M. A. Associations between regional white matter hyperintensities, medial temporal lobe subregional volumes, and memory in older adults. *In review at Alzheimer's and Dementia: Diagnosis, Assessment and Disease Monitoring.*

In Preparation

Granger, S. J., Harhen, N., Bornstein, A. M., Yassa, M. A., A simplified neuro-computational framework for the influence of early life unpredictability on hedonic processing. *In preparation.*

Poster Abstracts

Hiroi, R., Lavery, C.N., **Granger, S.J**., Quihuis, A.M., Weyrich, G., Bimonte-Nelson, H.A. (2014). Sex differences, spatial cognition, and antidepressant treatment: Chronic citalopram administration in middle-aged rats improves memory retention in a sex-dependent manner, and impairs working memory in both sexes. Presented at Society for Neuroscience (2014)

Palmer, J.M., Hiroi, R., **Granger, S.J**., Poisson, M., Berns-Leone, C., Kirby, D., Patel, S., Hadder, B., Ciaramitaro, V., Bimonte-Nelson, H. (2016). 17-β estradiol versus conjugated equine estrogens: Differential interaction of androstenedione with two commonly used hormone therapy estrogens for spatial memory in mice. Presented at Society for Neuroscience (2016)

Granger, S. J., Montchal, M. E. Haddad, E., Obenaus, A., Keator, D., Solodkin, A., Small, S. L., Stern, H. S., Sandman, C. A., Davis, E. P., Glynn, L., Baram, T. Z.,

Yassa, M.A. (2017) Emotional and pleasure circuit alterations associated with fragmented and unpredictable early-life sensory signals. Presented at Society for Neuroscience (2017)

Granger, S.J., Leal, S. L., Murray, E. A. Yassa, M. A. (2018) Structural Integrity Deficits of Uncinate Fasciculus Predict Medial Temporal Lobe Subfield Activity During an Emotional Pattern Separation Task. Presented at Cognitive Neuroscience Society (2018)

Granger, S.J., Leal, S. L., Murray, E. A. Yassa, M. A. (2018) Structural Integrity Deficits of Uncinate Fasciculus Predict Medial Temporal Lobe Subfield Activity During an Emotional Pattern Separation Task. Presented at Conte Center at UC Irvine Annual Symposium (2018)

Granger, S.J., Leal, S. L., Murray, E. A. Yassa, M. A. (2018) Structural Integrity Deficits of Uncinate Fasciculus Predict Medial Temporal Lobe Subfield Activity During an Emotional Pattern Separation Task. Presented at the Annual Conference of the National Institute of Physiological Sciences (NIPS), Okazaki, Japan (2018)

Granger, S. J. M.S. Larson, M.T. Sathishkumar, R.J. Jirsaraie, A.P. Smith, L. Mcmillan, D. Greenia, M.M. Corrada, C.H. Kawas, M.A. Yassa. (2019) Ultrahigh Resolution Diffusion Imaging Reveals Abnormal Medial Temporal Lobe Integrity and Predicts Poor Performance on RAVLT Delayed Recall in the Oldest Old. Presented at Society for Neuroscience (2019)

Granger, S. J., Glynn, L. M., Sandman, C. A., Small, S. L., Obenaus, A., Keator, D. B. Baram, T. Z., Stern, H., Yassa, M. A., Davis, E. P. (2019) Accelerated Maturation of the Uncinate Fasciculus After Early-Life Unpredictable Patterns of Maternal Signals. Presented at Conte Center Annual Symposium (2019)

Granger, S. J., Adams, J. G., Kark, S. M., Sathishkumar, M. T., Chen, I. Y., Benca, R., McMillan, L., Janecek, J. T., Yassa, M. A. (2021). Latent anxiety in clinical depression is associated with worse recognition of emotional stimuli. Presenting at Society for Neuroscience (2021)

Adams, J. G., Kark, S., Sathishkumar, M., McMillan, L., **Granger, S. J.**, Baram, T. Z., Yassa, M. A. (2021) Enduring maternal grief impacts cognitive functioning and alters related resting-state functional connectivity. Cognitive Neuroscience Society (2021)

Kark, S., Adams, J., Sathishkumar, M., McMillan, L., **Granger, S. J.**, Baram, T. Z., Yassa, M. A. (2021) Enduring maternal grief following adult child loss alters resting connectivity of the paraventricular thalamic nucleus. Cognitive Neuroscience Society (2021)

Rizvi, B., Sathishmukar, M., Marquez, F., **Granger, S. J**., McMillan, L., Brickman, A. M., Tustison, N. J., Yassa, M. A. (2021) Regional white matter hyperintensities are associated with reduced medial temporal lobe regional volumes in older adults. Society for Neuroscience (2021)

Kark, S. M., **Granger, S. J.,** Adams, J. G., McMillan, L., Chen, I., Benca, R. M., Yassa, M. A. (2021) Sex-specific effects of paraventricular thalamic nucleus functional connectivity on depressed and anxiety symptoms in humans. Society for Neuroscience (2021)

Oral Presentations

- "17- beta-estradiol versus conjugated equine estrogens: Differential interaction of androstenedione with two commonly used hormone therapy estrogens for spatial memory in mice"
    - Honors Thesis Colloquium, Barrett the Honors College at Arizona State University 2016
- **"**Diffusion Weighted Imaging: A Comprehensive Guide"
    - Presented at Program in Exercise Biochemistry, University of Tsukuba, 2018
- "Guided Activity: What is the most connected Brain Region?"
    - Guest lecture Advanced Neurobiology N115, 2019 (Professor: Georg Striedter)
- "Uncinate Fasciculus structural and functional integrity predicts dentate gyrus activity during discrimination of similar emotional scenes"
    - Park City Winter Conference 2018
- "In-vivo microdissection of MTL subfields using ultrahigh-resolution diffusion imaging in the oldest old"
    - 2019 Center for the Neurobiology of Learning and Memory Conference
- "Emotional and Pleasure circuit alterations associated with early life fragmentation and unpredictability of environmental signals"
    - Neurobiology and Behavior Data Blitz, 2017
- "Associations between white matter integrity and fragmentation of prenatal maternal mood in female children."
    - Neurobiology and Behavior Data Blitz, 2018
- "Ultrahigh Resolution Diffusion Imaging Reveals Abnormal Medial Temporal Lobe Integrity and Predicts Poor Performance on RAVLT Delayed Recall in the Oldest Old"
    - Neurobiology and Behavior Data Blitz, 2019
- "Latent anxiety in clinical depression is associated with worse recognition of emotional stimuli"
    - Neurobiology and Behavior Data Blitz, 2020

Research Experience/Employment

Research Assistant to John Peterson, PhD, Salimetrics, LLC, Carlsbad, CA

- 06/2011-09/2011, 06/2012-09/2012

My work here challenged a widely held understanding and established that the off-purpose use of an assay for Neuronal Growth Factor (NGF) might have significant cross-reactivity when attempting to measure from saliva. My work resulted in a publication.

Undergraduate Researcher with Janae Neiderhiser, PhD, Pennsylvania State University

- 02/2013-05/2013

Worked predominantly in administration contacting high schools to participate in a state-wide twin study for gene x environment research.

Undergraduate Researcher with Heather Bimonte-Nelson, PhD, Arizona State University

- 10/2013-06/2016

Conducted research on memory function among women undergoing menopause and contributed to a study that showed significantly different responses based on sex. In this lab I completed my Honors Thesis via the Honors Thesis Seminar Series and Fellowship. My responsibilities included conducting various animal behavioral paradigms related to memory functioning and depressive-like behavior, animal ovariectomy surgery preparation and recovery, drug preparation and administration, and immunohistochemistry preparation (cryostat). My work in the lab resulted in two posters as well as the completion of my honors thesis.

Research Assistant to Michael Yassa, PhD, University of California, Irvine

- 06/2014-08/2014, 06/2015-08/2015

Worked as an undergraduate research assistant where my primary responsibilities were data entry as well as working on the implementation of a skin conductance device for research purposes. I also was involved in participant recruitment, consenting, and running preliminary behavioral experiments.

Graduate Student Researcher with Michael Yassa, PhD, University of California, Irvine

- 08/2016-Present

As a graduate student researcher my interest primarily lies in emotional memory systems. I work collaboratively across several large research institutes at UC Irvine including the Conte Center at UC Irvine, UCI MIND, and the Center for the Neurobiology of Learning and Memory. I implement analysis techniques including graph theoretical analysis using Diffusion weighted imaging (DSI Studio/FSL), task-based fMRI (high resolution; AFNI), and assay memory performance using a variety of mnemonic discrimination tasks. My work in the lab thus far has resulted in two published first-author research articles involving the structural integrity of the uncinate fasciculus. Two first-author research articles are in review. Two additional first-author publications will be submitted in the coming months.

Consultant: Hoag Hospital

- July 2021- January 2022

Worked with Dr. David Keator at UC Irvine (Operations Director of the UCI Neuroscience Imaging Center) to design a fully automated Diffusion Weighted Imaging processing software for clinical usage. The software creates an html report for each patient of quality metrics, connectometry analyses, and graph theoretical measures derived from multimodal MRI data

Honors/Awards

Paterno Fellows Program, Pennsylvania State University (2012)

- Honors program that requires advanced undergraduate coursework

Dean's List, Pennsylvania State University (2012-2013)
- Maintained a 3.5 GPA or higher

Dean's List, Barrett Honors College at Arizona State (2013-2016)
- Maintained a GPA of 3.5 or higher

Honors Thesis Sequence Fellowship/Series, Barrett Honors College at Arizona State (2016)
- Accepted to an Honor Thesis Fellowship Program that supplied financial aid, required advanced statistical coursework, undergraduate student research, and the completion of an approved Honors Thesis topic

RenéeHarwick Advanced Graduate Student Award (2021)
- Award is given to a graduate student of a Fellow of the Center for the Neurobiology of Learning and Memory who shows outstanding scientific promise as evidence by research accomplishments as well as the quality of his/her advancement document

James L. McGaugh Award for Excellence in Graduate Research (2021)
- Award is given to a graduate student of a Fellow of the Center for the Neurobiology of Learning and Memory based on the quality of in-press or published research

Extracurricular/Volunteer/Mentoring Experience

CNLM Brain Awareness Day/Week (currently)
- Educate and organize activities for Elementary school students to learn about the brain

CNLM Ambassador Program
- Co-chair of Communications Committee (2019-present)

Conte Center Jr Researchers Meeting
- Organizer/Co-organizer 2019-present

ASU Brain Fair for Children (2013-present)
- Educate Elementary school students about neuroanatomy

Brain Awareness (2013-present)
- Educate Elementary school students about college and the brain

ASU Night of the Open Door
- Educate local community about science and the brain (2014, 2015)

Hebb Club
- Center for the Neurobiology of Learning and Memory (2016-present)

REU Student Research Experiences for Undergraduates
- Co-mentor (lead mentor Dr. Luis Colon-Perez)

Relevant Training/Courses

Teacher Assistantship in Neurobiology (N113L)
- Independent instruction and grading of an introductory neuroscience laboratory course consisting of approx. 30 undergraduate students

HPC's Computing Facility Training Course
- An introduction to working with the High Performance Computing Cluster at UCI, taught by Dr. Harry Mangalam.

Analysis of Functional Neuroimages (AFNI) Bootcamp

- Full week instruction at NIH with Dr. Bob Cox and Colleagues

MRI Operator Certification (UC Irvine)
- Obtained at the Neuroscience Imaging Center at UC Irvine

UC Irvine Data Science Initiative Python Training Course
- Introductory courses in coding in python

Programming for Neuroscience Research
- Python course taught by Dr. Craig Stark for the analysis of rodent behavioral data

Activate to Captivate
- 8-week communication certificate program taught by Bri McWorter of Graduate Division at UCI

Noteworthy Neuroimaging and Analytical Skills

FSL (https://fsl.fmrib.ox.ac.uk/fsl/fslwiki/FSL)
DSI-Studio (http://dsi-studio.labsolver.org)
DIPY (https://dipy.org)
Advanced Normalization Tools (http://stnava.github.io/ANTs/)
Analysis of Functional Neuroimaging (AFNI) experience (https://afni.nimh.nih.gov)
ASHS: Automated Segmentation of Hippocampal Subfields (https://www.nitrc.org/projects/ashs)
R programming (https://www.r-project.org)
Python (https://www.python.org)
Shell scripting

ABSTRACT OF THE DISSERTATION

Early Life Unpredictability Alters Circuits Involved with Emotional and Cognitive Outcomes

By

Steven Jay Granger

Doctor of Philosophy in Biological Sciences

University of California, Irvine, 2022

Professor Michael A. Yassa, Chair

Decades of research have investigated the impact of the quantity and quality of maternal care on the development of healthy cognitive and emotional function in both human and rodent offspring. Emerging from this literature is the notion that the (un)predictability of maternal signals in early infancy is an important factor influencing the development of these systems. In animal models, exposure to unpredictable patterns of maternal behavior alters brain circuit maturation and cognitive and emotional outcomes, including impaired memory performance and anhedonia (the loss of pleasure or lack of reactivity to pleasurable stimuli). However, whether exposure to such signals in humans alters the development of brain pathways is unknown. In Chapter 2 of this Dissertation, in mother–child dyads, we tested the hypothesis that exposure to unpredictable maternal signals in infancy is associated with aberrant maturation of corticolimbic pathways. We focused on the uncinate fasciculus, the primary fiber bundle connecting the amygdala to the orbitofrontal cortex and a key component of the medial temporal lobe–prefrontal cortex circuit. Using high angular resolution diffusion imaging,

we discovered that higher maternal unpredictability during infancy was associated with greater uncinate fasciculus generalized fractional anisotropy (a correlate of fractional anisotropy with distinct advantages). In a separate experiment, Chapter 3 of this Dissertation tested the hypothesized role of the uncinate fasciculus in adjudicating between competing memory representations at retrieval. Using multimodal imaging, we discovered that greater uncinate fasciculus integrity is associated with reduced hippocampal dentate and CA3 activity during correct discrimination of similar emotional stimuli. Together, this work yields novel insight into neurobiological mechanisms of vulnerability to cognitive deficits and advances our knowledge of the function of medial prefrontal white matter connectivity with the temporal lobe.

Chapter 1: Background and Significance

Origins of Research on the Impact of Early Life Environment on Emotional and Cognitive Outcomes

In 2020, there was an estimated 52.9 million adults over 18 years old (roughly 21%) in the United States with some form of mental illness (National Survey on Drug Use and Health, 2020). The lifetime prevalence of any mental health disorder among U.S. adolescents aged 13-18 was estimated to be 49.5% (National Survey on Drug Use and Health, 2020; Merikangas, 2010). Major Depressive Disorder (MDD) is one of the most prominent of all mental health disorders with an estimated 21 million adults in the U.S. having at least one major depressive episode in 2020 (National Survey on Drug Use and Health, 2020). While MDD is one of the most prominent mental health disorders, it is also highly comorbid with anxiety disorders (Mineka et al., 1998) with the prevalence of comorbidity with MDD as high as 60% of cases (Kaufman & Charney, 2000). Although reported in 2018, the most updated economic burden of Major Depression is approximately $326.2 billion, a figure which is likely rising with the addition of the COVID-19 pandemic and inflation (Greenberg et al., 2021). Due to the human and economic costs of mental health burden, it is imperative to understand the etiology and pathophysiology of cognitive and emotional deficits associated with mental illness.

Major Depressive Disorder is accompanied by various pathological mood states including (a) altered incentive and reward processing, evidenced by amotivation, apathy, and anhedonia; (b) impaired modulation of anxiety and worry, accompanied by oversensitivity to negative feedback; (c) inflexibility of thought and behavior in

association with changing reinforcement contingencies; (d) altered integration of sensory and social information, as evidence by mood-congruent processing biases; (e) impaired attention and memory; and (f) visceral or somatic disturbances including altered weight, appetite, sleep, and endocrine and autonomic function (Rolls, 2016; Drevets, 2007; Gotlib & Hammen, 2009).

Interactions between environmental and genetic factors influence the development of neurological changes that result in adolescent psychopathology (McEwen et al., 2015, Jaworska-Andryszewska & Rybakowski, 2019; Heim et al., 2012, Bale et al., 2010, Anderson et al., 2008). Of particular interest is the contribution of environmental signals during sensitive and critical periods of development that contribute to the neurobiological and behavioral characteristics observed in various mental illnesses including depression (Hasler et al., 2004; Andersen et al., 2008). While contemplated for generations prior, the first empirical evidence for the notion that early life environment may influence the development of cognitive and emotional function came from the pioneering work of John Bowlby. This work focused on the specific role of the caregiver as a necessary component to develop healthy cognitive and emotional function (Bowlby, 1952).

Patricia M. Crittenden writes in her *Test of Time* review entitled, *Gifts from Mary Ainsworth and John Bowlby,* that Bowlby's work planted three crucial stakes in the ground to make way for the study and development of attachment theory (the theory that healthy cognitive and emotional development is dependent on healthy interaction between infants and their primary caregivers; Crittenden, 2017). First, in 1944, Bowlby's investigation of the lives of juvenile thieves led to the idea that extended separation from

their mothers might have been one common factor in criminal behavior (Bowlby, 1944). In 1949, Bowlby proposed the idea that family processes were perhaps a mediating factor between extended separation and impaired emotional and cognitive function by observing that children brought to guidance clinics signaled problems with their families and the need for reconciliation with the family (Bowlby, 1949). Finally, in 1951, Bowlby suggested that exposure to the bombing in WWII England was less dangerous to the child's psychological wellbeing than separation from their parents with the care of a stranger (Bowlby, 1951; Crittenden, 2017). In 1968, Bowlby published his formal theory of attachment in a work entitled *Attachment and Loss. Volume I: Attachment* where he described attachment as 'a lasting psychological connectedness between human beings' of which was evolutionarily conserved to promote survival in early life (Bowlby, 1969; Bowlby, 1983).

It wasn't until the contributions from Mary Ainsworth that different patterns of attachment were empirically investigated and described. In 1978, the results from the "Strange Situation" experiment were detailed (Ainsworth et al., 1978). The "Strange Situation" experiment consisted of close observation of a mother-infant dyad in a laboratory setting and was designed to assess the quality of the child's attachment to the caregiver. More specifically, the experiment consists of multiple rounds of brief maternal separation followed by the presence of a stranger who attempts to console the infant while the mother is away. The infant's behavior is systematically observed while separated from the mother and left alone briefly, separated from the mother and cared for by the stranger, and while reunited with the mother (Ainsworth & Bell, 1970). As a result of this work, three predominant attachment styles were observed: secure (child

uses the mother as a secure base, is exploratory and happy), insecure-avoidant (the child is not very explorative and is emotionally distant), insecure-ambivalent (the child is anxious, insecure, and angry) (Ainsworth & Bell, 1970; Ainsworth et al., 1978). A fourth attachment style was provided later by Main & Solomon known as insecure-disorganized (the child is depressed, angry, completely passive, and non-responsive; Main & Solomon, 1986). Of importance, it was proposed by Ainsworth, that different attachment styles (or patterns of attachment) were mirrored by specific maternal care qualities. This notion deemed “the caregiver sensitivity hypothesis”, suggested that secure attachment styles were encouraged by mothers who are sensitive to their needs, insecure-avoidant attachment styles were encouraged by mothers who were distant or disengaged, and insecure-ambivalent attachment styles were encouraged by mothers who were inconsistent, sometimes sensitive and sometimes neglectful (Ainsworth et al., 1974).

The combined work by Bowlby and Ainsworth (as well as others) inspired a vast amount of research on attachment theory and the impact of the quantity and quality of maternal care on infant mental health outcomes. A recent meta-analysis captures the breadth of research linking insecure attachment styles to impaired cognitive and emotional outcomes later in life. This analysis, which was conducted across 643 effect sizes and 123 independent samples, revealed a significant overall effect size ($r = 0.31$) showing that insecure attachment to primary caregivers is associated with depression-like phenotypes later in life (Spruit et al., 2020) adding to the existing literature that robustly ties insecure attachment styles to internalizing and externalizing symptoms (Colonnesi et al. 2011; Groh et al. 2017; Hoeve et al. 2012; Madigan et al. 2016; Lee &

Hankin, 2009).

The impact of absence of maternal care via maternal separation (Rutter, 1979; Gunnar, 2010; Nelson et al., 2007) and lack of sensitive maternal care via exposure to maternal depression and anxiety (Goodman, 2007; Murray et al., 2011; Dawson et al., 2003; Feldman et al., 2009; Halligan et al., 2004; Beck, 1998; Verbeek et al., 2021) has also been extensively studied. One of the most salient examples regarding the lack of quality maternal care in humans comes from the study of Romanian orphans and the research conducted by the Bucharest Early Intervention Project (Zeanah et al., 2003). In 1966, under the dictatorial rule of Nicolae Ceausescu, both abortion and contraception were banned in Romania under the assumption that population growth would enhance economic growth. In response to drastic increase in birth rates, many children were abandoned to be raised in overcrowded and impoverished orphanages and institutions. Investigation into children exposed to this environment showed institutionalized children exhibited impaired responses to emotional stimuli assessed with electroencephalogram recording (Parker et al., 2005), widespread disturbances in attachment (Zeanah et al., 2005), impaired memory and cognitive/executive function (Bos et al., 2009), impaired language development (Windsor et al., 2007), and displayed a variety of psychiatric symptoms (Ellis et al., 2004; Bos et al., 2012). These effects mirrored the larger literature that children raised in institutions are subject to greater risk for developmental delays and mental health disorders including depression (MacLean, 2003). Attempts to reverse these negative impacts were then causally investigated by randomized controlled trials where institutionalized children were either assigned to continued institutionalized care or foster care, the latter of which was shown to improve psychiatric

and developmental outcomes in previously institutionalized children (Vanderwert et al., 2016; Nelson et al., 2007; Humphreys et al., 2015).

As a part of this literature, it was suggested that “for normal development to occur, mammalian brains require an optimal level of environmental input, a so-called ‘*expectable’* environment. Examples of an expectable environment might include exposure to patterned light information, normal language exposure, and access to responsive caregivers” (Nelson et al., 2007; Curtis & Nelson, 2003; Bruer & Greenough, 2001). This hypothesis originated from the observation that “children reared in impoverished institutions are subjected to unfavorable caregiver-to-child ratios, highly regimented routines, impoverished sensory, cognitive, and linguistic stimulation, and unresponsive caregiving practices” (Nelson et al., 2007). Together, research from the Bucharest Early Intervention project helped to identify the notion that in addition to impoverished conditions, abuse, and neglect, whether or not maternal care was expectable (predictable) or not (unexpected/unpredictable) may be important to developing infant emotional and cognitive circuits.

Other work suggested that the relationship between Ainsworth’s sensitivity hypothesis and insecure attachment styles is partially dependent on the perception of maternal predictability (Ross & Hill, 2002; Hill et al., 1997). To assess early environmental unpredictability, Ross and Hill (2000) developed *The Family Unpredictability Scale* to retrospectively measure lack of consistency in family behaviors and regulatory systems in childhood and suggest that environmental unpredictability results in unpredictability schemas or the pervasive belief that people are undependable and the world is chaotic. Ross and Hill suggested that seven interrelated schemas are

generated by an unpredictable childhood environment including (1) lack of self-efficacy (the belief that there will not be predictable outcomes due to their own behavior), (2) external locus of control (unpredictable forces outside of one's actions determine one's destiny), (3) helplessness (result of chronic external locus of control; others who may be unpredictable must be relied on for desired outcomes), (4) causal uncertainty (one's beliefs about whether or not good and bad events that happen to oneself and others are due to certain, predictable reasons), (5) interpersonal trust (unpredictable environments result in a lack of interpersonal trust), (6) sense of coherence (the extent to which one has a pervasive enduring feeling of confidence that one's internal and external environments are predictable and that there is a high probability that things will work out as expected), and (7) future orientation (those who experience unpredictability will be less future oriented; Ross & Hill, 2002). It is critical to note in this work that the difference between maternal sensitivity, maternal consistency, and environmental predictability is not well operationalized and while the authors suggest predictability lends itself to different styles of attachment, it does not strongly establish a link between environmental unpredictability and mental health outcomes but rather focuses on establishing a link between environmental unpredictability and risk-taking behaviors. In addition, it is unclear how or which kinds of unpredictability at certain developmental windows may impact or aid the development of these schemas.

Of interest, the concept that specific types of maternal sensory signals may contribute to the development of cognitive and emotional systems was not altogether new at this time. In 1994, Myron Hoffer's work highlighted the importance of patterning and intensity of maternal stimulation in young rats as a result of experimental work

directed at early behavioral systems on which attachment is grounded (Hofer, 1994; Walker et al., 2017). This theory, which birthed the concept of “hidden regulators” states that the foundations of psychological attachment in early infancy are laid down through a web of sensory and behavioral interactions that characterize the parent-infant relationship and by the early emotion and physiological states that are induced by these events (Hofer, 1994). Evidence for this idea came from Hofer (1973) showing that rats separated from their mothers for 24 hours had reduced heart rates, slow movements, and reduced body temperatures. However, exchanging maternal body heat with thermoregulated heat through the cage floor resulted in hyperactive movements but no change in heart rate. Hofer noticed that different aspects of a mother’s care appeared to have relatively specific effects on the separated pups. In a series of experiments, he showed that the reduced cardiac rate could be rescued by supplying milk during the separation period, but milk did not change hyperactivity. Behavioral hyperactivity on the part of the infant could however be rescued with the presence of a non-lactating foster mother while not impacting infant heart rate (Hofer, 1973). Additional examples that different stimuli and their patterns impact specific biological systems are briefly outlined by Walker et al., (2017) which highlights evidence showing the role of maternal tactile stimulation of pups in maintaining high levels of pups’ growth hormone and neural proteins, maternal odor keeping stress hormones low, and warmth controlling behavioral motor activity levels (Chatterjee et al., 2007; Eghbal-Ahmadi et al., 1999; Hofer, 1973, 1984; Hostinar, et al., 2014). Together, this literature has been used as an early basis for the idea that patterns of parental behavior, in addition to the “caregiver sensitivity hypothesis” from Ainsworth and maternal deprivation originating from

Bowlby's work, are key to maintaining homeostatic balance in specific systems (Walker et al., 2017).

Another overlapping, non-mutually exclusive, and widely accepted theory focuses on the notion that exposure to an abnormal early life environment induces chronic stress. Increased adrenocortical hormone secretion, including cortisol, as a mechanism for the link between abnormal early life environment and Major Depression is one of the most consistent findings in neuropsychiatry (Juruena, 2014; McEwen, 2007; McEwen, 2008; Smith & Pollack, 2020; Koss & Gunnar, 2018). Early life stress can come in many forms but can be defined as an emotional experience in response to a stressor and can manifest itself by biochemical, physiological, cognitive, and behavioral changes (Juruena, 2014). A stressor, as Juruena (2014) writes, is a physical or imagined stimulus that disturbs or threatens to disturb homeostasis and can come in many forms. Chen & Baram (2016) describe stress as a signal indicating a potential or perceived threat (Calabrese et al, 2007; Joëls & Baram, 2009; Ulrich-Lai & Herman, 2009; McEwen & Gianaros, 2011).

It is important to note here, that the terminology 'early life adversity' has also been used to describe the impact of abnormal early life environment and is often used interchangeably with early life stress (Koss & Gunnar, 2018; Purewal et al., 2018; Van Tieghem & Tottenham, 2018). Nelson & Gabard-Durnam (2020) attempt to adjudicate between these two overlapping constructs by suggesting that adversity is best considered through the lens of violations in the expectable environment (i.e. experiences that are atypical such as patterned light diffused through a cataract) or entirely absent (such as congenital deafness). In this fashion, not all forms of adversity

are interpreted and/or encoded as stressful. Nelson & Gabard provide examples including a scenario where a child may experience preparation for an exam as stressful, but this would not be considered a form of adversity or perhaps in the instance of an impoverished language environment where a child is exposed to fewer words and less complex language may be a form of adversity, but it is in itself not stressful and does not activate the stress response system. This is not to say that aberrant maternal care does one or the other, rather, Nelson & Gabard suggest that aberrant maternal care may act as both an adverse early life experience which can produce a stress response albeit dependent on brain maturity and developmental history.

As briefly mentioned previously, aberrant early life experience that produces a biological stress response can come in many forms. Studies have shown that lifetime history of maternal depression and anxiety has been associated with increased baseline infant cortisol levels which can be partially attenuated with prenatal maternal psychotropic medication (Brennan et al., 2008). Maternal depression is well known to induce a wide variety of impaired cognitive and emotional function (Ahun et al., 2020; Cummings & Davies, 1994; Cicchetti et al., 1998). Insecurely attached infants show larger increases in cortisol levels from the Strange Situation Procedure, an effect which was augmented if the mothers had depressive symptoms (Luijk et al., 2010). Early life maltreatment, abuse, and neglect are known to produce similar deviations in the biological stress response involving hypothalamic-pituitary-adrenal (HPA) axis disruption and is known to result in adolescent cognitive and emotional deficits (Gonzalez, 2013; Cicchetti & Rogosch, 2001). Children raised in poverty are also highly vulnerable to develop impaired cognitive and emotional function later in life, a

relationship thought to be mediated by aberrant stress responses (Yoshikawa et al., 2012; Blair & Raver, 2016).

Due to the various ways in which early life stress may be induced, some researchers in the field have sought to determine how specific forms of childhood adversity map onto specific symptom profiles underlying impaired cognitive and emotional function in mental illness; *The Specificity Approach* (Lumley & Harkness, 2007; Myman et al., 2003; Lui & Fisher, 2022). Lumley and Harkness (2007) provide evidence that individuals who perceived their childhood adversity (whether it be emotional maltreatment, physical abuse, or sexual abuse) as preferentially dangerous presented with more anxious symptoms in adolescence. Individuals who perceived their childhood adversity with themes of loss or worthlessness presented with more anhedonic symptoms in adolescence (Lumley & Harkness, 2007). Data from the Netherlands Study of Depression and Anxiety has shown that emotional neglect seems to be differentially related to depression, dysthymia, and social phobia (Spinhoven et al., 2010) furthering the idea that specific types of adverse experiences impact particular developmental outcomes through distinguishable pathways (Lui & Fisher, 2022; Wyman et al. 2003).

Early life adversity has also been assessed through the cumulative risk model which approaches early life adversity as a composite of multiple risk factors (Evans & Whipple, 2013). The Adverse Childhood Experiences (ACEs) questionnaire is a widely used tool to measure the amount of cumulative early life adverse factors that predispose impaired cognitive and emotional function later in life (Lanier et al., 2018; Anda et al., 1999; Anda et al., 2006; Felitti et at., 1998; Hughes et al., 2017).

HPA-axis dysfunction, as a result of early life adversity, has been extensively studied (van Bodegom et al., 2017; McEwen et al., 2007). Briefly, it is thought that upon exposure to a stressor, corticotrophin releasing hormone (CRH), also known as corticotropin releasing factor or CRF, is secreted by the paraventricular nucleus of the hypothalamus (as well as the hippocampus and central nucleus of the amygdala), the hypothalamus in-turn releases adrenocorticotropic hormone (ACTH) which stimulates the adrenals to release cortisol in humans and corticosterone in rodents (Stratakis & Chrousos, 1995; van Bodegom et al., 2017). These corticosteroids are thought to bind to glucocorticoid receptors (GR) in the hypothalamus and pituitary in a negative feedback loop (de Kloet et al., 1993; Herman & Cullinan, 1997). CRH is thought to bind to several G-protein coupled receptors in the cell membrane including CRHR1 (expressed in the prefrontal cortex, hippocampus, paraventricular nucleus of the hypothalamus, and basolateral amygdala) and CRHR2 (expressed in the hypothalamus, dorsal raphe nucleus, and medial nucleus of the amygdala; van Bodegom et al., 2017). Corticosteroids readily cross the blood brain barrier having been released from the adrenal cortex and bind to GR (canonically located in the hypothalamus and pituitary) or mineralocorticoid receptors (MR; canonically located in the limbic system including hippocampus) in the intracellular membrane to regulate gene transcription (van Bodegom et al., 2017). Decades of research have sought to understand the impact of CRH and corticosteroids as a mediating influence between chronic stress in early life and its impact on hippocampal (Bale, 2011; Bagot et al., 2014), amygdala (Lupien et al., 2016; Bohacek & Mansuy, 2016), and prefrontal cortex function and structure (Lupien et al., 2016; McGowan et al., 2009; Liu et al., 1997; Bolton et al., 2018). These

mechanisms include altered neurotransmitter exposure, gene transcription, or neuronal differentiation within the key nodes of the stress circuitry (van Bodegom et al., 2017; Chen & Baram, 2016). It is also worth mentioning that the biological stress response involves more than the above-mentioned players and includes monoamines such as serotonin, noradrenaline, and dopamine which work in concert with the neuropeptides and steroids mentioned above (for review see Joëls & Baram, 2009).

Importantly, the effects of early life adversity on impaired emotional and cognitive outcomes later in life are influenced by the age at which the adversity was experienced. Bowlby was among the first to recognize this concept by providing evidence that the period from 6 months to 3 years seemed to be critical for the formation of attachment between mother-infant dyads finding that infants separated from their mothers past the age of 3 did not recover as well (Michel & Tyler, 2005; Bowlby, 1969). Findings from the Bucharest Early Intervention Project provided evidence that infants moved from institutionalized care to foster care earlier (before the age of 2) resulted in improved outcomes (Vanderwert et al., 2016; Nelson et al., 2007; Humphreys et al., 2015).

Broadly, it is generally thought that exposure to chronic early life stress (via aberrant maternal care) during critical periods of development contribute to disruption in brain development by several overlapping mechanisms including altered neurotransmitter exposure, gene transcription, or neuronal differentiation within key nodes of the stress circuitry (van Bodegom et al., 2017; Chen & Baram, 2016). However, the outcomes of exposure to early life stress are critically dependent on several aspects including the timing, quality, severity, and duration (Chen & Baram, 2016). To conclude, the quantity and quality of maternal care on cognitive and

emotional outcomes has been extensively studied, however, relatively less research has focused on the specific role of patterns of maternal care.

Maternal Sensory Unpredictability as a Novel Antecedents of Impaired Cognitive and Emotional Function

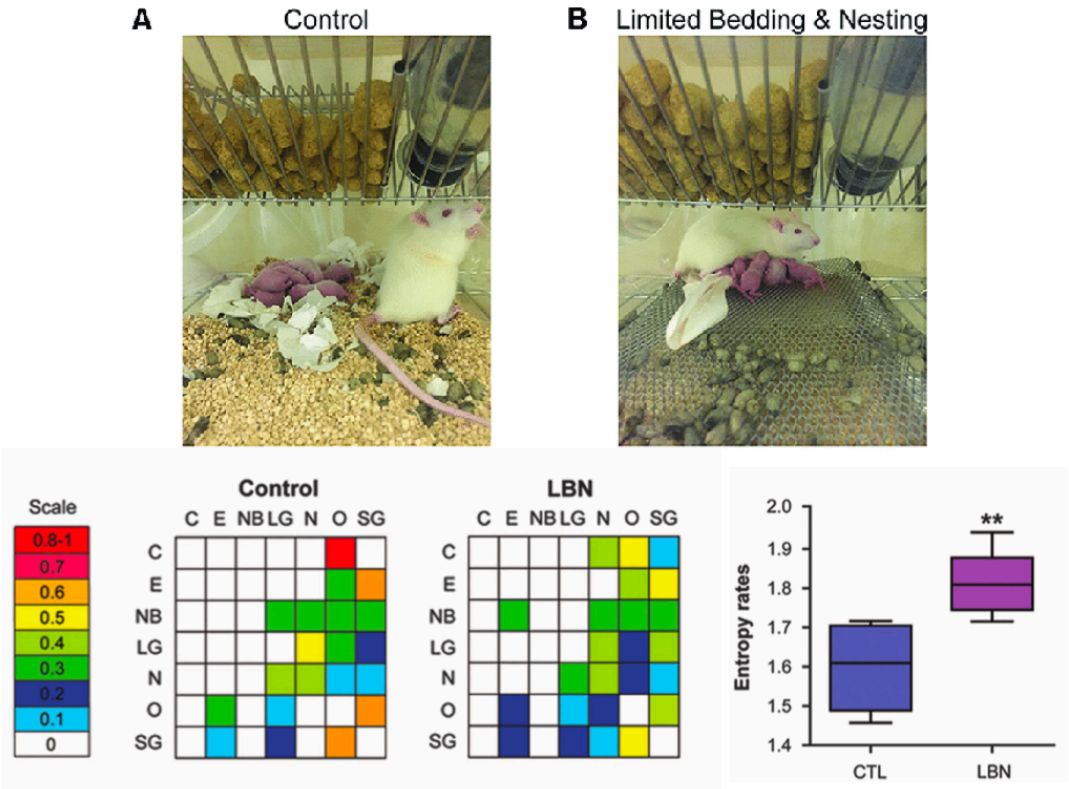

Figure 1: Top row of figures show Control (CLT) and LBN model. The LBN model consists of limiting the nesting and bedding material available to the dam typically during postnatal day 2-9. The effect of limited nesting material induces changes in maternal behavior currently captured as an entropy rate: the measure of the degree to which a future behavior can be predicted from the current behavior. The middle row shows the differences in the time-homogenous transition matrix to and from the following behaviors: licking/grooming (LG), carrying pups (C), eating (E), nursing (N), nest building (NB), no activity (O), or self-grooming (SG). In the control dam, in the most extreme case, there is a high probability from transitioning to one behavior given another. In the dam exposed to LBN, in the extreme case, there is a very low probability from transitioning to one behavior given another. The dam in this case has a dispersed range of next possible behaviors following a given behavior. The bottom right plot shows increase in entropy rate in LBN exposed animals compared to CLT animals. (Figure adapted from Molet et al., 2016a and Bolton et al., 2019)

More recently, research has focused directly on the influence of experiencing predictable or unpredictable maternal sensory signals on cognitive and emotional outcomes. Neurobiological and behavioral evidence for the developmental scenario in which early life maternal unpredictability predisposes emotional vulnerability have been primarily described in the rodent model of limited bedding and nesting (LBN; Gilles et al., 1996). The LBN model is an experimental manipulation of simulated poverty in which the amount of bedding material available to the dam is restricted during the offspring's early postnatal life (although variable, often occurring during postnatal day 2 to 9). The LBN model has been shown to produce fragmented behavior in dams including an increase in the average number of epochs spent away from the pups and decreases in average duration of licking and grooming bouts (Molet et al., 2016a). In addition, the LBN model is also known to result in an increase in the unpredictability of maternal transitions from behavior to behavior in interaction with their pups (Molet et al., 2016a, Ivy et al., 2008). Importantly, while the LBN-model induces unpredictability of maternal sensory signals, LBN leaves other qualities of maternal care such as the total duration of nursing, the total duration of licking and grooming, and total duration of dam-pup interaction undisturbed (Molet et al., 2016a; Arp, et al., 2016; Walker et al., 2017).

Maternal unpredictability induced via exposure to the LBN paradigm is captured as an entropy rate: a scaler value describing the likelihood of transitioning from one behavior given another. Figure 1 demonstrates the LBN model and resulting differences in entropy values observed across groups. Here, separate matrices are shown for both the Control and LBN-exposed animals that describe the differences in the time-

homogenous transitional probability matrix to and from the following behaviors: licking/grooming (LG), carrying pups (C), eating (E), nursing (N), nest building (NB), no activity (O), or self-grooming (SG). These matrices are first composed of the raw counts to and from the behaviors mentioned here and then converted to transition probabilities within each cell. In the Control dam, one can observe that there is a high probability of transitioning to one behavior given another. In the LBN-exposed dam, there is a low probability of transitioning from one behavior to another. In other words, the LBN-exposed dam displays a dispersed range of next possible behaviors following a given behavior. These transitional probability matrices can be captured by a single value, an entropy rate, using a Markov chain model described in Vegetabile et al. (2019). Larger entropy values reflect greater unpredictability of transitions from one type of behavior to another (Molet et al., 2016a).

In humans, a similar measure known as maternal sensory unpredictability has been quantified to reflect the entropy rate in animals exposed to LBN. This measure quantifies the unpredictability of tactile, auditory, and visual stimulus experienced by children in early postnatal life based on one to two 10-minute naturalistic observation periods occurring between 6 and 12-months post-partum. Similar to the LBN model, the number of transitions to and from a given behavior is summarized in a time-homogenous probability matrix. The degree of unpredictability of auditory, visual, and tactile stimuli between mother-infant dyads is quantified using the same Markov chain models as animals exposed to LBN and is described in Vegetabile et al. (2019). Similar to the entropy rates quantified in animals, larger values indicate greater maternal sensory unpredictability experienced by the infant within observation periods.

Research in both humans and rodents has shown that exposure to greater unpredictable sensory signals during infancy is associated with memory deficits later in life (Ivy et al., 2008, 2010; Molet et al., 2016b; Bath et al., 2017; Davis et al., 2017). In rodents, pup exposure to unpredictable maternal behavior leads to abnormal maturation of brain circuits involved with memory (Brunson, 2005; Ivy et al., 2010; Guadagno et al., 2016; Molet et al., 2016b; Walker et al., 2017). More specifically, rat pups exposed to the LBN paradigm from post-natal day 2-9, showed augmented CRH expression in the hippocampus assessed in middle age and impaired performance on the Morris water maze. Impaired memory performance as a result of exposure to LBN was rescued by peripheral administration of a CRF_1 blocker which also prevented dendritic atrophy and prevented reduced long-term-potentiation in the CA1 (Ivy et al., 2010). In a separate study, rat pups exposed to the LBN paradigm showed impaired object recognition at 12 months of age and impaired spatial memory performance assessed via a discrimination index that compares time spent exploring the novel vs. familiar locations. These behavioral deficits of pups exposed to LBN were accompanied by reduced dorsal hippocampal volumes assessed through structural MRI and increased fractional anisotropy of the CA1 assessed through ultra-high resolution diffusion MRI. Interestingly, increased fractional anisotropy of the CA1 was histologically validated in this investigation by providing evidence that animals exposed to LBN as a chronic early life stressor had reduced dendritic arborization of the CA1 (Molet et al., 2016b). As an aside, this work among others, served as an impetus for the utilization of high-resolution diffusion imaging directed at the medial temporal lobe in Appendices B-C of this Dissertation.

As a result of these impoverished conditions and changes in maternal behavior, pups exposed to this early life environment have also been shown to exhibit symptoms of anhedonia which include decreased sucrose preference and social play (Molet et al., 2016a, Bolton et al., 2018a). One such study implemented the LBN paradigm from post-natal day 8 to 12 and measured c-fos expression in the nucleus accumbens after a social behavior test. As a response of early life exposure to LBN, rats displayed social avoidance behavior measured as less time spent in a “social chamber” and decreased c-fos expression in the nucleus accumbens shell and core at postnatal day 20-22 and postnatal day 42-48 (Rincòn- Cortés & Sullivan, 2016). Another study implemented LBN from post-natal day 2-9 and investigated differences in pleasure-reward seeking. It was found that rats exposed to LBN exhibited reduced voluntary chocolate intake as well as administered lower doses of cocaine under lower reinforcement schedules. Further, rats exposed to LBN in this study exhibited increased c-fos expression in the nucleus accumbens core after cocaine administration. In this case, the authors attributed an increased c-fos expression in the accumbens core to maintaining similar cocaine demand elasticity to that of control animals (Bolton et al., 2018b). Additionally, animals exposed to LBN showed impairment on a probabilistic reward learning task which mirrored findings observed in human clinical populations (Kangas et al., 2022).

In addition, the LBN and analogous Scarcity model (a less severe impoverished environment occurring usually from postnatal day 8-12) have been shown to produce a wide variety of neurobiological changes including increased expression of c-fos, an activity-dependent immediate-early gene and increased spine density in the amygdala (Gaudagno et al., 2018, Guadagno et al., 2016, Raineki et al., 2012, Walker et al.,

2017). Within the LBN model, abnormalities of the prefrontal cortex have also been reported. Specifically, functional connectivity differences between the prefrontal cortex and amygdala across adolescence and adulthood have been found as an outcome of LBN occurring during postnatal day 8-12 (Yan et al., 2017). Additionally, it has been reported that rats exposed to LBN during postnatal day 8-12 showed decreased c-fos activity across the prefrontal cortex (including infralimbic) after a social behavior testing paradigm (Rincón-Cortés & Sullivan, 2016). Histological evidence from this model has indicated that there are layer specific dendritic reductions in the prefrontal cortex, a relationship which is thought to be mediated by CRF-1 (Yang et al., 2015).

Pups exposed to unpredictable maternal care through the LBN paradigm show increased plasma corticosterone levels (Rice et al., 2008). Importantly, exposure to augmented maternal care (which relies on the brief separation of dam and pup) is able to promote the overall time spent with rat pups, reverse exaggerated CRH expression in the hypothalamus (Korosi et al., 2010), and reduce basal CRH expression (Plotsky & Meaney, 1993; Plotsky et al., 2005; van Bodegom et al., 2017).

Although the amygdala, hippocampus, and several prefrontal cortical regions have been implicated in studies of LBN, it is less clear as to how connections between these regions might impact behavioral outcomes associated with impaired cognitive and emotional function. One investigation from the LBN paradigm using ex-vivo high-resolution diffusion imaging suggests that the amygdala-prefrontal cortex circuits become hyperconnected as a result of early life maternal unpredictability and perhaps also with more variability in the reconstructed white-matter connecting these two regions (Bolton et al., 2018a). Thus, it is possible that differences in the top-down inhibitory

control of the prefrontal cortex over limbic structures during synaptic pruning in childhood leads to aberrant cognitive and emotional processes later in life (Anderson et al., 2008). Whether the same corticolimbic circuits are impacted by unpredictable maternal sensory signals in humans remains unknown.

Medial Temporal Lobe and Prefrontal White Matter: Association with Early Life Adversity and Psychopathology

Figure 2: Partial dissections of the human brain showing large white matter association tracts that are most intricately linked with the development and presence of depressive symptoms. (a) Adapted from Bubb et al., 2018. Shows a mid-sagittal cut of the human brain with the anterior portion of the corpus callosum removed. In a, the cingulum bundle is depicted which consists of two portions: the superior component (depicted as '*a*') as well as the hippocampal cingulum (parahippocampal radiation; depicted as '*j*'). It is important to note here, the cingulum is a large tract innervating multiple components of cortex some of which are situated more medial to this cut, however, fiber projections toward posterior parietal (retrosplenial) cortex are visible in this view. Other white matter association tracts of interest are visible which include the body and column of the fornix ('*c*'). (b) Adapted from Leng et al., 2016. Shows the uncinate fasciculus bundle in reference to the inferior longitudinal fasciculus (IFOF). It is clear that the uncinate fasciculus and IFOF share overlapping prefrontal areas which make the dissociation of the respective uncinate fasciculus and IFOF components difficult when it comes to tractography. Further, tractography of the uncinate fasciculus often contains "falsely-continuing" streamlines posteriorly and backwards along the IFOF axis. (c) Depicts the general morphology of the uncinate fasciculus. Here it is important to note the tightly packed portion of the uncinate fasciculus known as the uncus (packed/bending portion) as well as the branching of the uncinate in the orbitofrontal cortex into a (dorso-) lateral and fronto-polar (more ventral) component.

Decades of research have been dedicated to understanding the neurobiological sequalae resultant from exposure to early life adversity. Although the amygdala, hippocampus, and several prefrontal cortical regions have been implicated in studies of early life adversity, it is less clear as to how connections between these regions might be impacted. In rodents, amygdala-prefrontal connections are relatively slow to develop and continue into adolescence with very rapid growth during the first 10 postnatal days of life followed by synaptic pruning in adolescence (Cunningham et al., 2002; Johnson et al., 2016). Interestingly, the development of glucocorticoid expression in the prefrontal cortex follows a similar pattern (Andersen et al., 2008; Perlman et al., 2007).

The use of diffusion weighted imaging methods in humans has yielded many insights into the development of white matter across the lifespan as well as provided unique insights into the circuit mechanisms of early life stress and depressive symptoms. Studies of white matter in early infancy have shown that white matter in general is developing at high rates with increasing fractional anisotropy (FA; representing the strength of diffusion) in many bundles continuing to develop into 30 years of age (Hermoye et al., 2006). Interestingly, specific white matter tracts connecting the medial temporal lobe and the prefrontal cortex are among the latest to develop (Asato et al., 2010; Olson et al., 2015). However, evidence points to very rapid limbic white matter change in the first 2 years of life, possibly indicating a period of sensitivity in which environmental stimuli could more drastically affect the development of limbic white matter (Yu et al., 2020). One such white matter tract known as the uncinate fasciculus is known to exhibit peak FA measures around the age of 35 whilst also rapidly developing in the first years of life (Olson et al., 2015, Von der Heide et al.,

2013; Simmonds et al., 2014; Yu et al., 2020).

The uncinate fasciculus is a largely understudied white matter pathway that generally connects the orbitofrontal cortex (OFC) with the anterior medial temporal lobe (Figure 2bc). It is a U-shaped fanning white matter bundle that is composed of three components: the temporal, the insular, and the frontal segments (Ebeling & von Cramon, 1992). Within the frontal segment, the uncinate fasciculus fans into three dominant branches extending toward the lateral OFC, fronto-polar cortex, as well as medially beneath the ventral striatum (Bhatia et al., 2012, 2017, 2018; Riva-Posse et al., 2014; Vergani et al., 2016). Within the temporal component, the uncinate is known to terminate in a variety of regions including the entorhinal/perirhinal cortices and the basolateral amygdala (Ebeling & Von Cramon, 1992; Von Der Heide et al., 2013; Thiebaut et al., 2012).

Although its function is poorly understood, some have suggested that the role of the uncinate fasciculus is situated between episodic memory processes, language, and socioemotional processing (Von Der Heide et al., 2013). While the functional significance of the uncinate fasciculus is still in question, it clearly undergoes major changes during development that are associated with psychiatric conditions and outcomes including depression, anxiety, exposure to early life stress and maltreatment. Children placed in Romanian orphanages who were exposed to severe socioeconomic deprivation early in life were shown to have decreased FA of the uncinate fasciculus at the age of 10 (Eluvathingal et al., 2006). In a similar study of socially deprived European orphans, decreased uncinate fasciculus FA was associated with greater duration spent in the orphanage (Govindan et al., 2010). In a large self-report study, decreases in

uncinate integrity were associated with greater scores on the Childhood Trauma Questionnaire (Hanson et al., 2015). Some studies have even shown that higher sensitivity to early life stress (regardless of the amount of stress) predicted reduced fractional anisotropy in the right uncinate fasciculus (Ho et al., 2017) and the amount of parental depressive symptoms also resulted in increased mean diffusivity of the uncinate fasciculus (Marroun et al., 2018). In general, these results suggest that early life stressful events result in abnormalities in fractional anisotropy of the uncinate fasciculus and poorer psychiatric outcome.

In studies of depression, the uncinate fasciculus appears to follow a very similar pattern. Studies generally find that decreases in uncinate fasciculus FA are prominent in those exhibiting depressive symptoms (Zhang et al., 2012; Vilgis et al., 2017; Carballedo et al., 2012; Yang et al., 2017; Bhatia et al., 2018). One study found that increases in FA were associated with better response to antidepressant treatment, a relationship which was moderated by genetic factors implicated in depression (Tatham et al., 2017). In contrast to these studies which suggest that decreased FA may be a consequence of early life stress and may be associated with depressive symptoms, other studies have reported opposing results. In one such study it was shown that uncinate fasciculus FA was increased in a sample of individuals with treatment resistant depression compared to healthy controls (Young et al., 2016). Additionally, it was found that high depression severity predicted increased FA of the uncinate fasciculus, a relationship which was moderated by both physical and emotional neglect (Tatham et al., 2016). Similar findings have reported that specific facets of the diffusion signal, primarily radial diffusivity (representing the diffusion perpendicular to the main axis of a

tensor – typically thought to associated with degree of myelination), are in fact increased in those exhibiting anticipatory anhedonia as well as depressive symptoms (Yang et al., 2017; Zhang et al., 2012). While it is unclear whether the dysmaturation of the uncinate fasciculus is the result of early life adversity, and whether it has a directional influence on psychiatric outcomes remains unclear, evidence for abnormalities in this specific pathway associated with both conditions is particularly salient in the literature.

In addition to the uncinate fasciculus, there are several other pathways that are also implicated in depression and aberrant early life experience. For instance, the genu of the corpus callosum (Lu et al., 2013; Wise et al., 2016) and the cingulum bundle (Figure 2a; Keedwell et al., 2012; Marroun et al., 2017; Henderson et al., 2013) have been implicated in several studies of depression and early life stress. Of importance, it was even found that reduced fractional anisotropy in the cingulum of adult females was related to familial history of depression as well as low hedonic capacity (Keedwell et al., 2012). While the genu (anterior segment) of the corpus callosum contains large prefrontal cortex projections across hemispheres, the cingulum has more complex connectivity. Like the uncinate fasciculus, it is a large white matter association tract aggregating axons from several different projection areas (for review see Bubb et al., 2018). From axon tracing studies, we know that the cingulum more specifically connects the posterior MTL to several cortical regions including the prefrontal, orbitofrontal, anterior cingulate, and retrosplenial cortex. Within the MTL, the cingulum in known to originate from cell bodies in the perirhinal cortex as well as the subiculum (Wouterlood et al., 1990; Van Groen et al., 1990; Shibata, 1993a; Shibata, 1993b.).

It is important to note that all of the aforementioned studies of white matter in humans do not dissociate between different portions of the white matter tracts of interest based on the location of their cell bodies. Rather, methods of white matter tractography as well as regions-of-interest based analysis lack the image resolution to properly dissociate individual connections that make up a white matter bundle (i.e. amygdala to the prefrontal cortex connection is found within a larger bundle containing axons from different projections sites). The majority of white matter studies thus often only refer to the white matter bundle as a whole without acknowledging their nuanced connections. Although it is methodologically challenging to dissociate portions of white matter bundles, it is possible that certain segments of the uncinate and cingulum play a more prominent role in the etiology of anhedonia and depression. One study has attempted to make such dissociations within the context of depression finding that reductions in FA were found in the body, subgenual stem (extending toward ventral striatum), and polar stem of the uncinate in depressed patients (Bhatia et al., 2018). Although in this case, the uncinate was modeled using diffusion-tensor informed tractography, new efforts are being made to more accurately delineate the uncinate's morphology using diffusion spectrum imaging (Leng et al., 2016).

Diffusion Weighted Imaging as a Method of Accessing Neuronal Structure on the Macro and Microstructural Scale

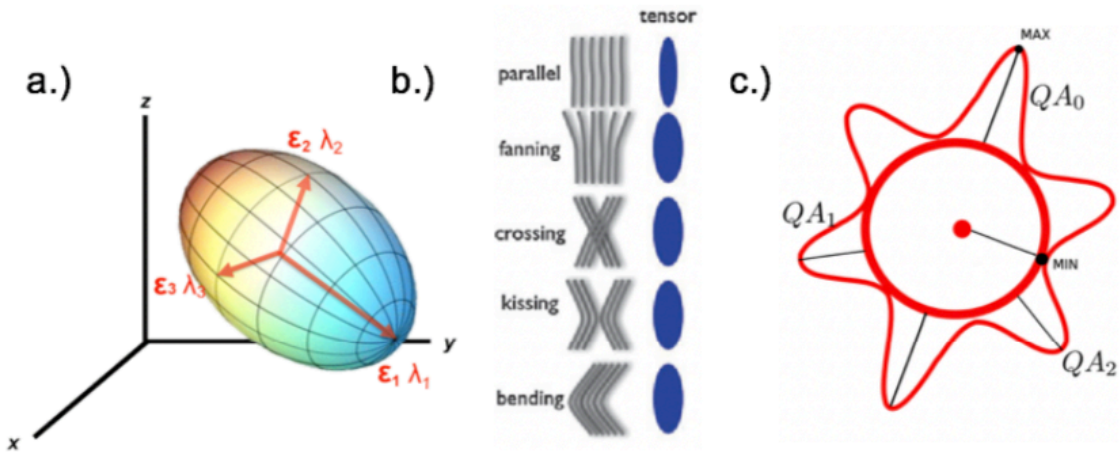

Figure 3: (a) The Tensor Model. Shows the primary eigenvector (e) and eigenvalue (Λ) components of a 3-dimensional tensor ellipsoid. Of note, the measure of fractional anisotropy is a summary measure of anisotropy ("diffusibility") among all three primary orientations of the tensor model. Other tensor-based measures include axial diffusivity which is composed of the primary eigenvalue/eigenvector (Λ_1). Radial diffusivity is the averaged second and third components of the tensor ((Λ_1+Λ_2)/2). Finally, mean diffusivity represents the average of all three eigenvalues ((Λ_1+Λ_2+Λ_3)/3) and is thought to relate to cellular density. (b) Shows one of the major limitations of the tensor model depicting 4 different intravoxel patterns (non-parallel fibers) that result in the same tensor model. The assumption of the tensor model is one primary direction of fibers when in fact we know biological tissue is more complicated than this. Further, the tensor model doesn't account for free water diffusion or isotropic diffusion compartments within a voxel. The use of other measures in areas of heterogeneous tissue structure (i.e. bending intravoxel patterns such as the uncus of the uncinate fasciculus) is clearly needed. (c) Shows one proposed solution, namely, the quantitative anisotropy model that accounts for the isotropic (free isotropic component: min) as well as multiple fiber orientations within the same voxel (i.e. QA_1, QA_2). Measures of generalized fractional anisotropy can be calculated from this model and reconstruction techniques work for many different types of sampling schemes. (Adapted from Jbabdi & Johansen-Berg, 2011 & Yeh et al., 2013).

Non-invasive neuroimaging is widely used as a tool to address questions in translational neurobiology. In particular, diffusion-weighted imaging allows us to assess differences in tissue microstructure, with the most popular method involving the use of diffusion tensor imaging (DTI) to study white matter in the brain. All diffusion-weighted imaging methods are based on the principle of Brownian motion, capturing the diffusion

of water within compartments along specific orientations (Jones, 2008; Figure 3). We can use DWI-based signals to construct models within voxels designed to represent the constrained or unconstrained diffusion of water in different brain compartments. Diffusion tensor imaging is one of the simplest models of this process where a 3-dimensional tensor ellipsoid is used to represent the underlying diffusion properties, allowing inferences about the underlying tissue properties (Feldman et al., 2014). DTI uses metrics based on the diffusion tensor. As mentioned previously, fractional anisotropy (FA) is a summary scalar measure based on three primary diffusion directions (eigenvectors/eigenvalues) to capture the overall degree of anisotropy or strength of diffusion across the entire voxel. The tensor's individual components are also used, namely axial and radial diffusivity, which represent diffusion along the primary and averaged secondary and tertiary components, respectively (Figure 3a). Although popular, DTI has several pitfalls including an inability to model crossing or multiple fibers within voxels and it suffers from partial volume effects due to resolution limitations (Alexander et al., 2007, Alexander et al., 2011; Jdabdi & Johansen-Berg, 2011). As demonstrated by Figure 3b, it is clear that multiple types of intra-voxel structural patterns might produce the same tensor-based reconstruction.

The use and interpretability of DTI is still largely a developing field. With a wide variety of data acquisition, processing, and reconstruction methods, there is very little consensus in the use and application of the technology and a number of common pitfalls (Jones & Cercignani, 2010) that make its use less than ideal for examining complex white matter architecture. New methods based on diffusion weighted imaging attempt to solve the shortcomings of the tensor-model by the use of "model-free"

methods designed to capture multiple fiber orientations by creating reconstructions based on each of the diffusion sampling directions. Examples of these methods include diffusion spectrum imaging (DSI) and high angular resolution diffusion imaging (HARDI) which calculate the orientational distribution of diffusing spins to model multiple fibers within each voxel. This results in much more anatomically plausible tractography (Tuch et al., 2002; Wedeen et al., 2005). More recently, the use of multiple b-value (multi-shell) high angular protocols (based on work by the Human Connectome Project) has provided significant advances. Implementation of opposite phase encoding to correct for magnetization-induced susceptibility distortions has also enhanced the quality of acquired images (Andersson et al., 2003). These distortions are particularly relevant in the prefrontal and medial temporal lobe cortices among protocols with a single-phase encoding direction.

While modeling the diffusion signal at the single voxel level is an interesting computational challenge, modeling the interpolation of the diffusion signal across voxels, a technique known as diffusion tractography, is even more complex. Tractography relies on the interpolation of diffusion signals from voxel-to-voxel which ultimately results in 3-dimensional models of short- and long-range projection fibers. When using tensor- derived measures to guide tractography algorithms there is a clear oversimplification of biological tissue indicating only one predominant fiber orientation per voxel. Modeling across voxels is thus likely to result in false-positive tracts that may not be representative of the underlying white matter. New methods in deterministic tractography refer to the use of quantitative anisotropy, which represents the strength of diffusion among many primary fiber orientations accounting for the isotropic free-water

component.

Several investigations have shown in phantom objects (microtubule objects of known structure) that the accuracy of deterministic tractography aided by the use of quantitative anisotropy resulted in more accurate modeling compared to FA aided tractography (Yeh et al., 2013). Further, efforts are being made in the field to compare across tractography methods to find the most accurate tractography algorithms to delineate human white matter bundles. In one such study, the use of quantitative anisotropy was found to produce fewer false-positive streamlines than over 96 different methods released by more than 20 other research groups around the world (Maier-Hein, 2017). Although the use of quantitative-anisotropy-informed-tractography has shown promise in properly delineating some of the largest white matter bundles in the brain, these techniques are still shown to produce false-fibers even within major white matter tracts (Maier-Hein, 2017). Validation with known anatomy is always an important step in these measurements.

Using quantitative anisotropy methods, one is also able to quantify the voxel-wise degree of anisotropy among many diffusion directions using a measure known as generalized fractional anisotropy (GFA; Tuch, 2004; Tuch et al., 2002). This measure is known to correlate well with fractional anisotropy of the tensor model but has the advantage of being able to model complex neural architecture (Glenn et al., 2015). In other words, GFA represents the degree of preferential directional diffusion mobility, with the benefit of being able to accommodate more complex diffusion profiles (Glenn et al., 2015). Figure 4 shows the differences and advantages of GFA compared to FA. As the fiber bundle orientation (top row) gets more complex, FA values (shown in blue) are reduced toward an anisotropy value of zero. GFA on the other hand is able to properly model fiber bundles of greater complexity. It should be noted however that there is variation in the accuracy to which GFA measures the degree of anisotropy across the type of tissue being evaluated as well as the b-value at which the raw data are collected (Fritzche et al., 2010; Gorczewski et al., 2008). Regardless of these issues, GFA is still used to assess structural integrity of complex tissues in a clinical setting particularly when there are heterogeneous fiber tissues (Koh et al., 2018; Yamada et al., 2018).

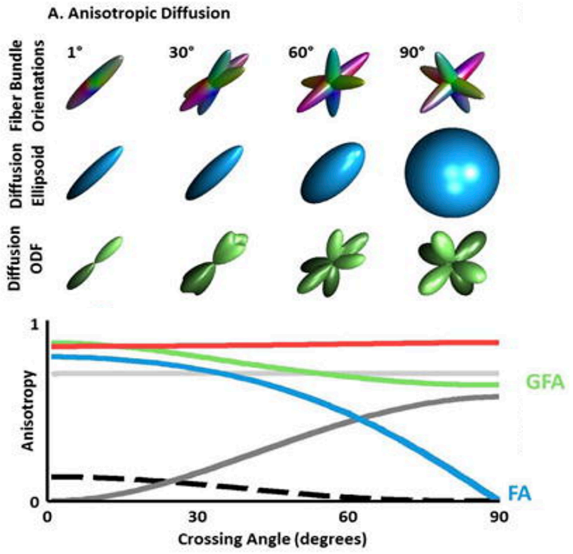

Figure 4. Adapted from Glenn et al., 2015 showing the advantage of modeling and detecting anisotropy within tissue using GFA.

Overall, while the technique is still in its development stages, DWI is able to

model white matter structure reasonably well and there is a general movement to move toward the use of high-angular, multi-shell data acquisition as well as implement more sophisticated “model-free” reconstruction techniques to model multiple fiber orientations within single voxels. While methods such as electrophysiology and resting state functional MRI can link regions together across time and even during task, they alone cannot determine the actual pathway signals must traverse in order to reach their destinations. Thus, the use of DWI as a complementary method has clear advantages, although the interpretation of the diffusion signal and the inference to cellular microstructure must be made with caution. Using variations of diffusion weighted imaging it is possible to shed light on aberrant neural circuitry associated with a wide variety of neurodegenerative and psychiatric diseases. Despite methodological limitations, this Dissertation aims to use the best available processing techniques to assess white matter connecting the medial temporal lobe and prefrontal cortex to address the hypotheses in question.

Approaches to Assess Memory and Interference Resolution

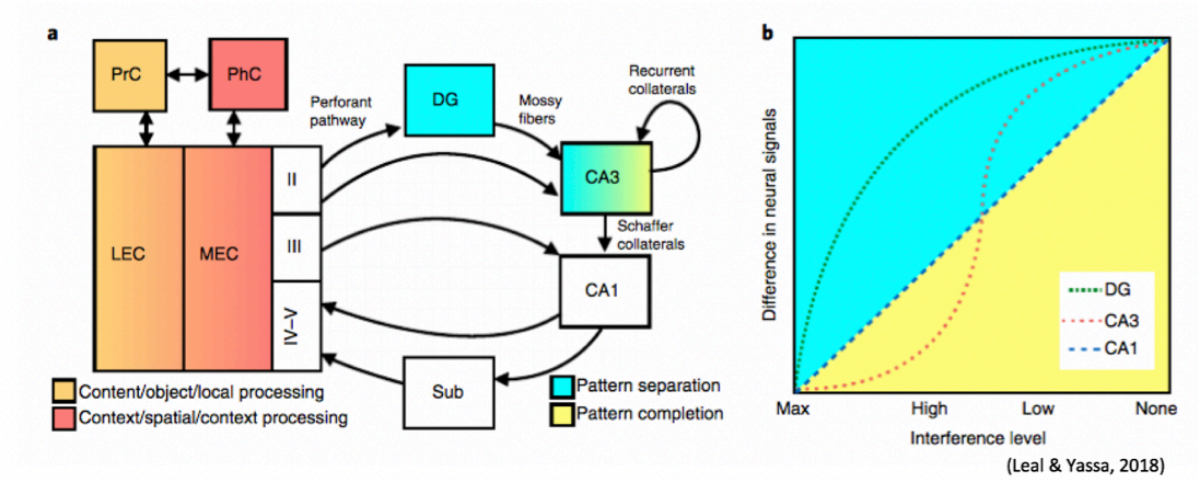

Figure 5: (a) Depicts a simplified version of known medial temporal lobe circuitry involved in episodic memory function. The lateral and medial entorhinal cortex are thought to be important for object and spatial processing, respectively. The entorhinal cortex communicates with the DG subfield of the hippocampus via the perforant pathway. Mossy fibers extent from the DG toward the CA3 region of the hippocampus which contains an autoassociative recurrent collateral network. (b) Of particular interest, the DG is thought to be critical for the neural computation of pattern separation while the CA3 is thought to contribute to both pattern separation as well as pattern completion (Leal & Yassa, 2018).

While the structural connections between the PFC and MTL are implicated in studies of early life stress and depression, the functional role of structural connectivity between these regions in episodic memory processes is still under investigation. Episodic memory is often defined as records of unique experiences and events that guide adaptive behavior; a feature of the brain that is thought to be reliant on the hippocampus (Milner et al., 1998; Squire et al., 2004). A key feature of episodic memory is the ability to discriminate among highly similar experiences thus creating dissociable experiences from one day to the next. Computational models suggest that the brain uses a neural computation known as pattern separation to distinguish among highly similar items during memory performance (Marr, 1971; O'Reilly & Norman, 2002). This computation is thought to be heavily reliant on the dentate gyrus (DG) and CA3 of the

hippocampus and serves to create orthogonalized representations from similar inputs (Yassa & Stark, 2011). More specifically, the DG is thought to be capable of pattern separation while the CA3 region acts in an autoassociative network capable of both pattern separation as well as pattern completion via its recurrent collateral network (see Figure 5 for review). Pattern completion in this sense, refers to the process by which incomplete representations are “filled in” based on previously stored information (Yassa & Stark, 2011).

Animal and human studies have begun to examine the influence of cortical areas in the pattern separation and completion process. Specifically, the entorhinal cortex (EC) has shown prominent influence in the pattern separation process as an integrating node that mediates the communication between the hippocampus and the rest of the neocortex (Reagh et al., 2018). Further, specific regions of the entorhinal cortex are known to have dissociable functions. Namely, the lateral EC (or the “content” pathway) comprises information associated with object processing while the medial EC (“context” pathway) comprises information associated with spatial/contextual processing (Eichenbaum et al., 2012; Knierim & Neuneubel, 2016; Reagh et al., 2018; Knierim et al., 2013). In addition, we know that the lateral and medial entorhinal cortex are innervated by different cortical inputs. Specifically, evidence from rodents indicates that the lateral entorhinal cortex is associated with cortical inputs including the orbitofrontal cortex and the amygdala while the medial entorhinal cortex is associated with cortical inputs such as the retrospenial cortex and postrhinal cortex, among others (Witter et al., 2017). It is thought that the functions of each of these regions are, in part, due to their connections with these cortical inputs. However, how these regions and their

computations are altered as a result of early life stress and the white matter pathways that may regulate them are still poorly understood.

Episodic memory disruption is a well-known outcome of the experience of chronic stress and is associated with poorer mental health outcomes including depression and anxiety among other disorders (Dillon & Pizzagalli, 2018; Pittenger, 2013; Leal & Yassa, 2018; Dalgeish et al., 2007; Williams et al., 2007). In a work entitled, *Mechanisms of Memory Disruption in Depression*, Dillon & Pizzagalli (2018) outline the impact of experiencing chronic stress on memory highlighting an overarching theory which suggests stress suppresses hippocampal neurogenesis, inhibits dopamine neurons, whilst sensitizing the amygdala. Dillon & Pizzagalli suggest that these phenomenon impair pattern separation processes, disrupt the encoding of positive experiences, and bias retrieval toward negative events.

Many labs have begun to investigate the pattern separation process in clinical applications such as depression, anxiety, schizophrenia, mild cognitive impairment and Alzheimer's Disease (reviewed in Leal & Yassa 2018). Leal et al., (2014ab) made significant contributions in understanding the link between pattern separation and mental health outcomes providing evidence that those exhibiting depressive symptoms presented enhanced discrimination of negative stimuli while also showing impaired target recognition for neutral items (Leal et al., 2014a). These findings were neurobiologically validated with evidence showing those with greater depressive symptoms had reduced DG/CA3 and increased amygdala activity during discrimination of negative items (Leal et al., 2014b). Other studies have demonstrated that those with greater symptoms of anxiety exhibit impaired memory of negative stimuli (Tofalini et al.,

2015; Inaba & Ohira, 2009) suggesting a cognitive affective bias that leads to overgeneralization of negative emotional memories (Leal & Yassa, 2018; Kheirbek et al., 2012; Balderston et al., 2017). Our recent work attempted to adjudicate between seemingly opposing impacts of anxiety and depressive symptoms in a clinical population (Granger et al., 2022; Appendix A).

In summary, episodic memory involves contributions from the medial temporal lobe (MTL), prefrontal cortex (PFC), and their interactions (Eichenbaum, 2017; Preston & Eichenbaum, 2013). Although contributions have been made to episodic memory dysfunction in various psychopathologies, less it known how different types of adversity experienced in early life may result in impaired mnemonic discrimination and what MTL-PFC pathways may be involved.

Unanswered Questions Related to Circuits Involved with Emotional and Cognitive Outcomes

A large literature has focused on the role of maternal care in shaping emotional and cognitive outcomes, however, relatively less research has focused exclusively on the role of patterns of maternal care. Chapter 2 of this Dissertation focuses on the role of unpredictable patterns of maternal sensory signals as a novel type of adversity that might predispose circuit dysfunction in MTL-PFC white matter. To determine the behavioral relevance of changes in MTL-PFC white matter, we utilize a mnemonic similarity task to probe episodic memory performance. Chapter 3 of this Dissertation is directed at understanding the function of the uncinate fasciculus using an emotional pattern separation paradigm. Each of the following Chapters attempts to address these using state-of-the-art measures to assess white matter.

Chapter 2: Impact of Early Life Maternal Sensory Unpredictability on White Matter Associated with Episodic Memory Performance and Neuropsychiatric Symptoms

All findings of this study have been published in Granger et al., (2021a)

Introduction

Experiences occurring during sensitive periods in early life are powerful factors influencing brain development and cognition (Hasler et al., 2004; Andersen & Teicher, 2008; Short & Baram, 2019). Although it is clear that the quality of maternal care affects the risk for offspring psychological disorders and neurobiological changes later in life (Bowlby, 1950; Lebel et al., 2016; Glynn & Baram, 2019), relatively less is known about how patterns of maternal behavior impact human development (Baram et al., 2012; Davis et al., 2017).

Patterns such as unpredictability of maternal sensory signals during early development are emerging as novel contributors to psychiatric illness later in life with unique neurobiological signatures (Chen & Baram, 2016, Walker et al., 2017, Glynn & Baram, 2019). It is possible that exposure to unpredictable maternal behavior results in aberrant synaptic pruning that leads to compromised structural integrity of neural circuitry vital to healthy cognitive and emotional processing (Glynn & Baram, 2019).

As mentioned in Chapter 1 of this Dissertation, across species, aberrant maturation of amygdala–prefrontal circuits is well recognized as a key outcome of exposure to stress (Burghy et al., 2012; Gee et al., 2013; Chen & Baram, 2016; Tottenham & Galván, 2016; Burgos-Robles et al., 2017). In rodents, amygdala-prefrontal connections are relatively slow to develop and continue into adolescence with

very rapid growth during the first 10 postnatal days of life followed by synaptic pruning in adolescence (Cunningham et al., 2002; Johnson et al., 2016). Interestingly, the development of glucocorticoid expression in the prefrontal cortex follows a similar pattern (Andersen at al., 2008; Perlman et al., 2007). Others have shown that accelerated maturation of amygdala–prefrontal cortex functional connectivity may be an adaptive response to early life adversity, which reprioritizes developmental goals to match the demands of adverse early life environments (Gee et al., 2013). In humans, the predominant anatomic connection between these two regions is the uncinate fasciculus (Ebeling & Von Cramon, 1992). The uncinate is thought to be important for episodic memory and has recently been hypothesized to play an important role in adjudicating among competing memory representations during retrieval (Von der Heide et al., 2013; Alm et al., 2016). Abnormal development of the uncinate could lead to impairments in cognitive and emotional functions (Carballedo et al., 2012; Zhang et al., 2012; Vilgis et al., 2017; Yang et al., 2017; Bhatia et al., 2018). Abnormal development of the uncinate has been associated with early life adversity including a history of institutionalization during childhood and paternal depressive symptoms (Eluvathingal et al., 2006; Govindan et al., 2010; Hanson et al., 2015; Ho et al., 2017; Marroun et al., 2018).

In this Chapter, we evaluate whether exposure to unpredictable maternal signals in infancy is associated with uncinate integrity, measured between the ages of 9 and 11 years. To determine whether the observed effects were specific to the uncinate or are general features of corticolimbic white matter, we conducted similar analyses in the hippocampal cingulum, which shares the fronto-temporal connectivity of the uncinate

but is spatially distinct (Bubb et al., 2018). As the functional output of brain circuits is a combinatorial sum of the activity of each of their components (Redish & Gordon, 2017), we also conducted analyses using the ratio of uncinate to hippocampal cingulum connectivity as a measure of imbalance across these two pathways.

To determine the behavioral relevance of changes in white matter connectivity associated with unpredictable maternal sensory signals, we focused on episodic memory function, which we assessed by using the mnemonic similarity task (MST), a well validated task (Stark et al., 2019) that is sensitive to the ability of the hippocampus to discriminate among highly similar experiences (i.e., pattern separation), which is thought to be a core facet of episodic memory (Marr, 1971; Yassa & Stark, 2011; Leal & Yassa, 2018; Leutgeb et al., 2007). This task was chosen as we have previously shown across species that greater unpredictability of maternal sensory signals in infancy is associated with differences in memory function (Davis et al., 2017). Further, MST performance is dependent on successful adjudication among competing memory representations during retrieval, which is thought to be a core function of the uncinate fasciculus (Von Der Heide et al., 2013; Alm et al., 2016).

Materials and Methods

Table 1. Sample characteristics for mother/infant dyads (N = 73)

Characteristics	Values
Maternal characteristics	
Cohabitation status (% married or cohabitating)	84.9
Education, years (SE)	16 (0.4)
Education (%)	
High school or less	11.1
Some college, associate degree, or vocational degree	28.7
4 year college degree	28.8
Graduate degree	23.3
Maternal race/ethnicity (%)	
White/European/North African/Middle Eastern	49.3
Asian	12.3
Hispanic white	30.1
Multiethnic/other	8.2
Maternal depression/anxiety (mean 6 SE)	
STAI	17.2222 ± 0.641
EPDS	4.95 ± 0.612
Maternal sensitivity (mean 6 SE)	9.85 ± 0.12
Income to needs ratio (mean 6 SE)	509.36 ± 59.5
Maternal unpredictable sensory signals (mean 6 SE)	0.81 ± 0.018
Age at MRI scan (mean 6 SE)	9.92 ± 0.078
Sex	43 males, 30 females
Days between scan and MST completion	99 ± 12.14

Participants A sample of 73 mother–offspring dyads (n = 30 females) from a prospective, longitudinal, prenatal cohort participated. Initial maternal recruitment criteria included the following: English-speaking, 18years old, nonsmokers, no evidence of drug/alcohol use, and singleton pregnancy. Unpredictable maternal sensory signals were assessed when the infants were 6 and 12 months of age, and the children

participated in a single MRI scan between 9 and 11 years of age. Demographic information for the full sample of participants is summarized in Table 1.

Measurement of unpredictability of maternal sensory signals:

Coding maternal sensory signals. Unpredictable maternal sensory signals were coded from a free play dyadic interaction between a mother and her child, as described in the study by Davis et al. (2019). Briefly, mothers were video recorded interacting with their child in a semi-structured 10 min play episode at 6 and 12 months of age. Mothers were given a standard set of age-appropriate toys and instructed to interact with their infants naturally as if they were at home. Behaviors from the mother that provided auditory, visual, or tactile sensory signals to the child were coded on a moment-to-moment basis from the video recordings using The Observer XT 11 (Noldus). Auditory signals included all maternal vocalizations, visual signals included maternal manipulation of toy or object while the infant was visually attending, and tactile signals involved all instances of physical contact (holding/touching) initiated by the mother. Coders were blind to all other information on study participants. Interrater reliability was calculated based on 20% of videos and averaged 89% (Davis et al., 2017).

Quantifying unpredictability of maternal sensory signals:

Unpredictability of maternal sensory signals were quantified by calculating the entropy rate of the sequences of visual, tactile, and auditory maternal signals assessed during the two 10 min naturalistic observation periods described above. The entropy rate is determined as follows. We first identify all transitions among visual, tactile, and

auditory maternal signals, accounting for all possible combinations of the different types of sensory signals. As an example, if a mother was speaking (auditory) to her child and then shows her a toy (visual) while labeling it (auditory), this would be classified as a transition from auditory only to auditory and visual. The resulting transitions are then modeled as changes in the state of a discrete-state first-order Markov process and the entropy rate of that process calculated as described in the study by Davis et al. (2017). We considered alternative strategies for calculating the entropy rate (e.g., based on other Markov chain models; second order and third order) as well as a nonparametric approach based on theoretical results relating data compression to unpredictability of maternal sensory signals and found that results were highly consistent (Spearman's rank correlations for resulting unpredictability measures ranging from 0.91 to 0.98; Vegetabile et al., 2019). The entropy rate measurement can be thought of as capturing how random or uncertain a mother's next behavior would seem to someone making a guess based on previous observed behavior. Entropy rate can range from 0 (transitions are perfectly predictable, e.g., speech is always followed by touch) to a maximum of 2.807 (unpredictable, the next observed behavior among them appears to occur at random). The resulting unpredictability rates were calculated separately for each visit (at 6 and 12 months) and averaged. A comprehensive description of the calculation regarding maternal unpredictability and the entropy rate quantification is described in the study by Davis et al. (2019), and an R package for the calculation of entropy is available at https://contecenter.uci.edu/shared-resources.

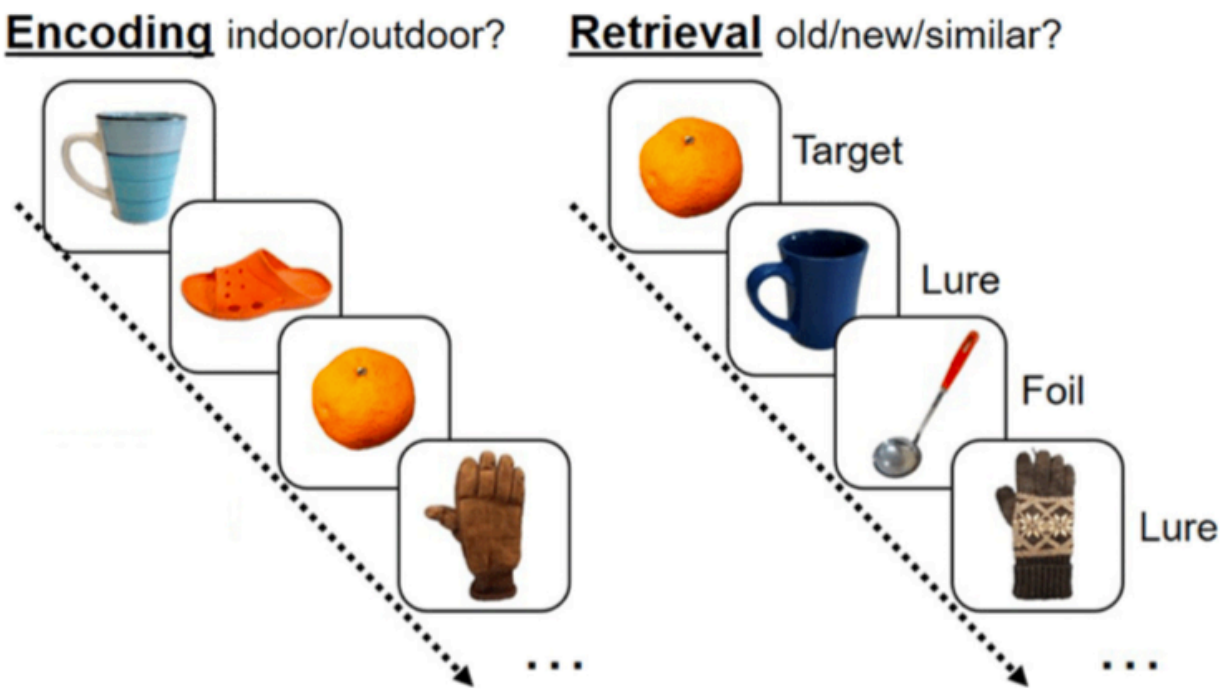

Figure 6: The MST consists of two phases: an incidental encoding phase and a retrieval (testing) phase. The incidental encoding phase consists of a series of 64 images where children are asked to indicate whether the items would appear indoor or outdoor. Upon completion of the incidental encoding phase, children completed the retrieval or testing portion of the MST. During test, children were presented with 32 target images (identical images that appeared during encoding), 32 foil images (images that did not appear during encoding), and 32 lure images (variants of images presented during encoding). Children were asked to indicate whether the presented object was "old" (they had seen the image before), similar (the images were slightly different from images presented during test), or "new" (images were novel and not seen during test). Lure items were varied by similarity ratings on a scale from 1 to 5, with 1 being the most similar (bin 1: most difficult to dis- criminate) and 5 being the least similar (bin 5: easier to discriminate).

Episodic memory: mnemonic similarity task.

The MST was administered on average 99 ± 12.13 days from the date of the MRI scan. The MST consists of the following two phases: an incidental encoding phase and a surprise memory test (Figure 6). During the incidental encoding phase, children are presented with a series of objects appearing on the screen for 2.0 s (interstimulus

interval, 0.5 s). At this time, the children were asked to rate the objects as being found "indoor" or "outdoor" via computer keyboard presses. A total of 64 images was presented during the testing phase. During the retrieval (testing) portion, children were presented with 32 target images (identical images that appeared during encoding), 32 foil images (images that did not appear during encoding), and 32 lure images (variants of images presented during encoding). During the test, children were asked to indicate whether the presented object was "old" (they had seen the image before), "similar" (the images were slightly different from images presented during the test), or "new" (images were novel and not seen during the test). Lure items were varied by similarity ratings on a scale from 1 to 5 with 1 being the most similar (bin 1: most difficult to discriminate) and 5 being the least similar (bin 5: easier to discriminate). Lure items were distributed across bin similarity in the following way: bin 1 (6 items), bin 2 (7 items), bin 3 (7 items), bin 4 (6 items), and bin 5 (6 items). As measures of performance, we calculated a lure discrimination index (LDI), which is defined as the probability of indicating similar when given a lure minus the probability of indicating similar given a foil. In this fashion, this measure controls for response bias (indicating similar for every item). The LDI is used as the index of episodic memory. We analyzed the low-similarity conditions (average, L4 and L5) as previous research using the MST demonstrated that children this age exhibit chance-level performance on the more difficult high-similarity conditions (Rollins and Cloude, 2018). A significant advantage of the MST task is the concurrent ability to assess traditional recognition memory by evaluating the recognition of target items versus novel foils. We used performance on this recognition condition as a control to determine the specificity of the relationship between hippocampal pattern separation

and unpredictable maternal sensory signals.

Measurement of possible confounding variables:

To assess whether associations with unpredictable maternal sensory signals are influenced by confounding factors, we evaluated maternal mental health, quality of maternal care, and household income. These variables are further described below. Maternal depression/anxiety. Symptoms of maternal depression and anxiety were assessed at the two postnatal visits (at 6 and 12 months). The Edinburgh Postnatal Depression Scale (EPDS; Cox et al., 1987) and State Anxiety Inventory (STAI; Spielberger et al., 1983) were administered. Scores were standardized and then averaged as an index of maternal mental health (Davis et al., 2019). Quality of maternal care: maternal sensitivity. To determine whether the unpredictability of maternal signals was associated with brain outcomes beyond more standard measures of quality of maternal care, we evaluated a measure of maternal sensitivity during the same observation period as the quantification of maternal unpredictability. Maternal sensitivity was coded using a protocol developed for the Eunice Kennedy Shriver National Institute of Child Health and Human Development (NICHD) Study of Early Child Care and Youth Development (NICHD Early Child Care Research Network, 1999). Maternal behavior was evaluated for sensitivity to non-distress, intrusiveness (reverse scored), and positive regard (1 = not at all characteristic to 4 = highly characteristic). A sum of ratings of sensitivity were calculated and used according to the NICHD Early Child Care Research Network (1999).

Income-to-needs ratio.

The income-to-needs ratio (INR) was determined by comparing household income to the federal poverty line for a given year and a given household size. Ratios < 1.00 indicate that household income is below the federal poverty line; in contrast, a ratio of ≥ 1.00 indicates income above the federal poverty level (Grieger et al., 2009).

Diffusion imaging protocol and processing

MRI were collected on a 3.0 tesla Philips Achieva scanner at the Neuroscience Imaging Center at the University of California, Irvine, using a 32-channel head coil. The diffusion-weighted imaging scheme consisted of six separate runs of 11 volumes (including one b = 0 volume) each. The first two runs were collected using a b value of 500 s/mm2, the third and fourth runs were collected using a b value of 1000 s/mm2, and the fifth and sixth runs were collected using a b value of 2000 s/mm2. Thus, the final scan consisted of a multishell sequence with 60 noncollinear directions and six B0 volumes. The following scanning parameters were used: direction of acquisition was anterior to posterior, the field of view was 216 (Anterior-Posterior), 216 (Foot-Head), 151.2 (Right-Left); the scan resolution was 108 (10), 127 (y); number of slices = 84; voxel size = 1.69 x 1.68 x 1.68 mm; TR = 11 502.76; TE = 89. Raw data were corrected for motion and eddy currents using FSLs eddy program (Andersson & Sotiropoulo, 2016). Data were analyzed using DSI-Studio (http://dsi-studio. labsolver.org; July 26, 2017 build). Corrected data were then reconstructed using the DSI-Studio Q-spin Diffeomorphic Reconstruction (QSDR) function, which uses a powerful diffeomorphic algorithm to warp model-free orientation distribution functions (ODFs) to Montreal Neurologic Institute (MNI) space (Yeh & Tseng, 2011). ODFs were reconstructed with the default diffusion sampling length ratio of 1.25, which was sufficient to model

crossing fibers at the intersection of the corticospinal tract and corpus callosum. This value was additionally validated by varying the diffusion sampling length ratio at intervals of 0.2 and visually examining this intersection using generalized q-sampling imaging. Other reconstruction parameters included the following registration method: norm 7–9-7, eightfold ODF tessellation, number of fibers resolved (5). Output resolution was increased to 1 mm. Quality control for fit to the template space was implemented by setting a criterion on R^2 at .0.6. Four subjects of the total of 73 were eliminated based on these criteria, leaving a final sample size of 69 subjects (29 females). Subject head motion was assessed by the eddy_movement_rms file exported from eddy (movement relative to the previous volume) and included as a nuisance regressor. Subject T1-weighted images were used for the quantification of intracranial brain volume. Structural MPRAGE scans were collected at the time of the diffusion scan with the following parameters: 1 mm isotropic resolution; 208 sagittal slices; field of view = 208 x 256 x 256 mm; flip angle=8°; TR = 8 ms; TE=3.7 ms; matrix size= 256 x 210 mm. Intracranial volume was calculated using Freesurfer version 6.0 and used to rule out whether differences in GFA were because of intracranial volume.

Region of interest-based approach

Masks of regions of interest (ROIs) were obtained through the Johns Hopkins white matter atlas (in MNI space), which is available within DSI Studio. Regions included limbic white matter regions, namely, the uncus of the uncinate fasciculus and the hippocampal cingulum bilaterally. Averaged generalized fractional anisotropy (GFA) values were extracted for each ROI and averaged across hemispheres. GFA is one of

several model-free diffusion measures and is known to correlate with fractional anisotropy of the tensor model. GFA was used to assess the structural integrity of complex tissues in a clinical setting, particularly when there are heterogeneous fiber tissues (Koh et al., 2018; Yamada et al., 2018), and has been used in studies of affective disorders (Chiang et al., 2016; Lo et al., 2017). However, it should be noted that the accuracy of GFA depends on the type of tissue being evaluated as well as the b value at which the raw data are collected (Tuch et al., 2002; Tuch, 2004; Gorczewski et al., 2009; Fritzsche et al., 2010).

Statistical analysis

Covariates were identified based on theoretical links to either maternal behavior or child outcomes. Covariates included in all analyses were child sex, maternal depressive and anxiety symptoms, maternal sensitivity, and income-to-needs ratio. Correlational analysis was conducted using Prism GraphPad 7 with two-tailed tests of Pearson correlation coefficients. Multiple linear regression models were implemented using RStudio to assess the association between unpredictable maternal sensory signals and the integrity of the white matter tract (uncinate fasciculus and hippocampal cingulum) after the consideration of covariates. Mediation analyses were conducted using the “mediation” package in RStudio. Each mediation model was tested using bias-corrected and accelerated procedures with 10,000 simulations. One case of missing data were imputed for the measurement of maternal depression and anxiety using all possible covariates and uncinate fasciculus GFA (Sinharay et al., 2001). Three cases of

missing data were imputed for INR in a similar manner using all possible covariates (including maternal depression/anxiety and uncinate fasciculus GFA).

Results

Exposure to unpredictable maternal sensory signals during infancy is associated with higher uncinate fasciculus integrity at age 9–11 years First, we tested the hypothesis that exposure to unpredictable maternal sensory signals in infancy is associated with the integrity of the uncinate fasciculus in 9- to 11-year-old children using GFA as our primary outcome measure. Exposure to unpredictable maternal sensory signals during infancy predicted greater uncinate fasciculus GFA ($r = 0.37$, $p = 0.0017$; Figure 7a). Multiple regressions with covariates (maternal depression/anxiety, maternal sensitivity, income-to-needs ratio, and sex) did not change the association between unpredictable maternal sensory signals and uncinate fasciculus GFA ($b = 0.26$, $R^2 = 0.35$, $p = 0.020$; Table 2). Sex was significant as an independent predictor of uncinate fasciculus GFA. However, the sex by unpredictability interaction was nonsignificant.

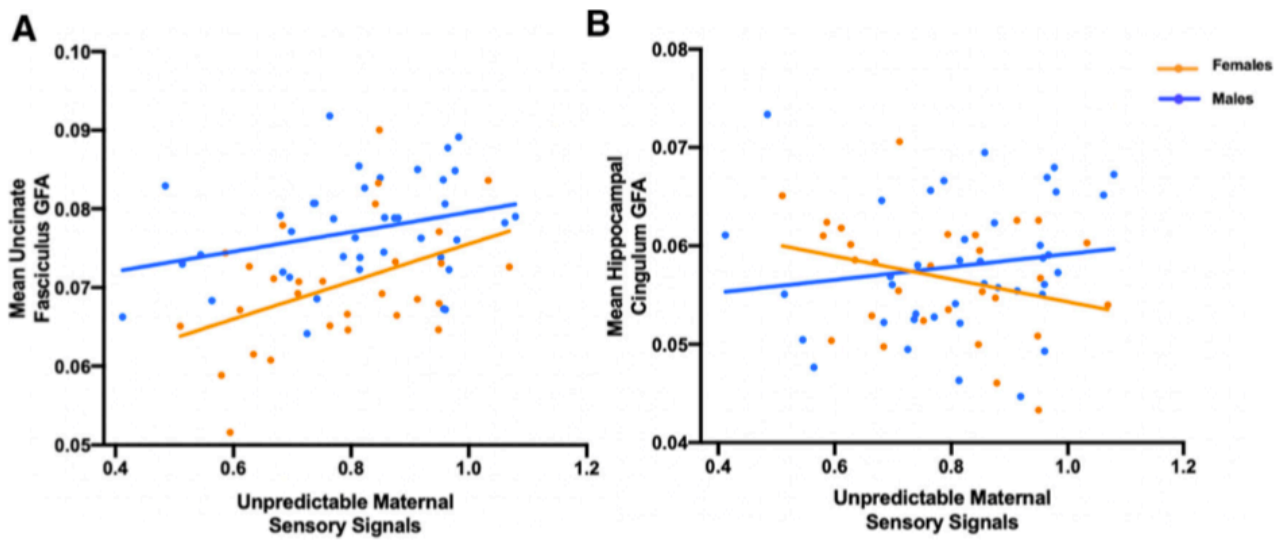

Figure 7. Generalized fractional anisotropy results. A) A significant positive association between exposure to unpredictable maternal sensory signals during infancy and mean uncinate fasciculus GFA primarily in girls (r = 0.44, p = 0.016) 9–11 years of age. This association was not significant in boys (r = 0.30, p = 0.057). B) No association between exposure to unpredictable maternal sensory signals during infancy and mean hippocampal cingulum GFA in girls (r = -0.29, p = 0.13) or boys (r = 0.15, p = 0.35) 9–11 years of age.

To rule out the possibility that age at scan and in-scanner head motion (derived from eddy) were responsible for differences in uncinate fasciculus GFA, we included them as nuisance regressors in an additional model with all previously mentioned covariates. The association between unpredictable maternal sensory signals and uncinate fasciculus GFA (b = 0.26, R^2 = 0.38, p = 0.017) remained significant after accounting for age and head motion. Additionally, neither age, subject head motion, nor their interaction predicted uncinate fasciculus GFA. Additionally, intracranial volume did not predict uncinate fasciculus GFA (r = -0.023, p = 0.85). Finally, including age and intracranial volume (calculated from T1-weighted images) as covariates in our analyses did not alter the statistical significance of the relationships between unpredictable maternal sensory signals and uncinate fasciculus GFA.

Because the functional output of brain circuits is a combinatorial sum of the activity of each of their components, we conducted similar analyses in the hippocampal cingulum bundle, a second component of the corticolimbic circuit that connects the connects the medial temporal lobe (MTL) with the PFC via a posterior pathway through the retrosplenial cortex (Bubb et al., 2018). While unpredictable maternal sensory signals did not significantly predict hippocampal cingulum GFA (r = -0.0026, p = 0.98; Figure 7b), the sex by unpredictability interaction was marginally significant (Table 3; b = -1.22, R^2 = 0.052, p = 0.086). The directionality of the associations identified in the uncinate fasciculus and marginal interaction with sex in the cingulum prompted us to ask whether the two findings are related to an imbalance in the integrity or maturation of these two circuits. We calculated a simple ratio measure of uncinate fasciculus

Table 2. Unpredictability of maternal sensory signals related to increased uncinate fasciculus GFA accounting for possible covariates

Regression Model	R^2	F	β	Standardized β	SE(β)	P-value
Overall Model	0.35	6.73				
Unpredictability of maternal sensory signals			$1.34x10^{-2}$	0.26	$5.62x10^{-3}$	0.020
Maternal depression anxiety			$5.054x10^{-4}$	0.065	$7.96x10^{-4}$	0.53
Maternal sensitivity			$-1.56x10^{-3}$	-0.21	$8.041x10^{-4}$	0.057
Income-to-needs ratio			$-1.01x\ 0^{-6}$	-0.066	$1.60x10^{-6}$	0.53
Sex			$-6.30x10^{-3}$	-0.39	$1.67x10^{-3}$	0.00036

/cingulum GFA to capture this imbalance. We found a significant association between the unpredictability of maternal sensory signals and the ratio of uncinate fasciculus GFA to hippocampal cingulum GFA ($r = 0.28$, $p = 0.018$; Figure 8a).

Corticolimbic circuit imbalance is associated with impaired episodic memory performance Based on prior work across species (Davis et al., 2017), we hypothesized that the unpredictability of maternal sensory signals would be associated with worse performance on cognitive tasks. In the current study, we used the LDI to assess episodic memory performance. Interestingly, we observed that unpredictable maternal sensory signals did not significantly predict impaired episodic memory performance ($r = 0.022$, $p = 0.86$). We then probed whether the observed circuit changes related to unpredictable maternal sensory signals were associated with episodic memory performance.

Table 3. Results of interaction model with unpredictability of hippocampal cingulum GFA predicted by unpredictability of maternal sensory signals, sex, and their interaction.

Regression Model	R^2	F	β	Standardized β	SE(β)	P-value
Overall Model	0.052	1.18				
Unpredictability of maternal sensory signals			0.025	0.59	0.015	0.11
Sex			0.013	1.024	0.0084	0.12
Sex*unpredictability			-0.018	-1.22	0.010	0.086

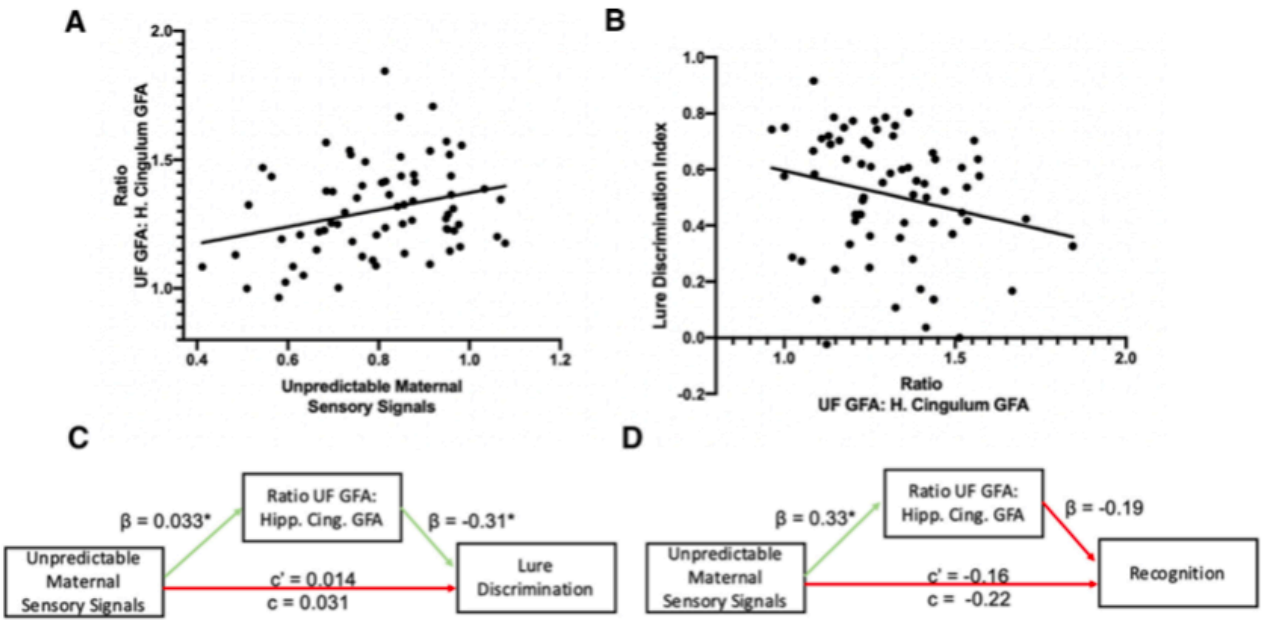

Figure 8. Results of uncinate fasciculus /cingulum ratio analyses. A, Shows the statistically significant positive association between unpredictable maternal sensory signals and the ratio of anterior MTL–PFC connectivity (uncinate fasciculus GFA) to posterior MTL–PFC connectivity (hippocampal cingulum GFA; r = 0.28, p = 0.018). B, The marginally significant association between a greater ratio of anterior MTL–PFC connectivity to posterior MTL–PFC connectivity and impaired lure discrimination on low-similarity lure items (r = -0.23, p = 0.058). C, D, The results of the mediation analyses. b values represent the coefficient for the arrows effect. c' represents the direct effect, and c represents the total effect of unpredictable maternal sensory signals on low-similarity lure dis- crimination. C, Shows the significant indirect effect of the ratio of uncinate fasciculus GFA to hippocampal cingulum GFA mediating the association between unpredictable maternal sensory signals and low similarity lure discrimination. D, The nonsignificant indirect effect of the ratio of uncinated fasciculus GFA to hippocampal cingulum GFA mediating the association between unpredictable maternal sensory signals and recognition performance is statistically significant at $p < .05$.

Uncinate fasciculus GFA was not significantly associated with episodic memory performance assessed with the LDI (r = -0.091, p=0.46). However, we found that decreased hippocampal cingulum GFA was marginally associated with lower LDI (r = 0.22, p = 0.072). A higher uncinate fasciculus/cingulum GFA ratio was also marginally

associated with lower LDI (r = 0.23, p = 0.058; Figure 8b). The interaction between sex and the uncinate fasciculus /cingulum ratio in association with LDI did not reach statistical significance (b = 1.28, p = 0.13).

We observed a significant indirect association through which higher levels of unpredictable maternal sensory signals was associated with a higher uncinate fasciculus /cingulum GFA ratio, which, in turn, was associated with worse LDI. In separate mediation models, neither uncinate fasciculus GFA (indirect effect = -0.061, CI = -0.24 to 0.097, p = 0.44) nor cingulum GFA (indirect effect = -0.0008, CI = -0.088 to 0.11, p = 0.99) were significant mediators of the association between unpredictable maternal sensory signals and LDI; however, the uncinate fasciculus/cingulum GFA ratio measure was a marginally significant mediator of the association between unpredictable maternal sensory signals and LDI (indirect effect = -0.10, p = 0.049, CI = -0.28 to -0.0081; Figure 8c). Critically, this association was specific to lure discrimination and did not generalize to general recognition memory; the indirect association was not statistically significant with the recognition memory outcome (indirect effect = -0.063, p = 0.31, CI = -0.27 to 0.034; Figure 8d).

Discussion

There are three key findings of this study. First, we show that infant exposure to unpredictable patterns of maternal-derived sensory signals is associated with greater integrity of the uncinate fasciculus in late childhood. Second, this finding is specific to the uncinate fasciculus and is not present in the hippocampal cingulum. Last, we find that the ratio of uncinate fasciculus (anterior MTL–PFC connectivity) to hippocampal

cingulum GFA (posterior MTL–PFC connectivity; Figure 9) mediates the association between experiencing greater unpredictability of maternal sensory signals and impaired performance on an episodic memory task. Together, these data suggest that one possible consequence of early life unpredictability is desynchronized maturation of two key corticolimbic pathways resulting in selective impairments in episodic memory tasks requiring nuanced and fine-tuned MTL– PFC connectivity. Such findings are consistent with those of other studies, suggesting that these connections are vulnerable to early life adversity (Gee et al., 2013; Tottenham & Galván, 2016).

Unpredictable maternal sensory signals have been identified as a novel type of early life adversity, associated with reduced memory and executive functioning (Davis, 2017, 2019) an association that has been observed in independent cohorts, such as FinnBrain (Karlsson et al., 2018; Davis, 2019). Evidence that patterns of sensory input contribute to the maturation of brain pathways has been previously shown in rodents (Molet et al., 2016a; Bolton et al., 2018b) and affects emotional (Walker et al., 2017) as well as cognitive circuits (Chen & Baram, 2016). Here we provide evidence that corticolimbic circuits are associated with infant exposure to unpredictability from the mother in early life and that imbalance among these circuits serves as a possible mechanism explaining differences in cognitive function observed here and in previous studies (Davis, 2017, 2019).

Past literature on the association of uncinate fasciculus with various types of early life adversity report mixed results. For example, several studies have found reductions in fractional anisotropy associated with early life maltreatment and deprivation (Eluvathingal et al., 2006; Govindan et al., 2010; Hanson et al., 2015; Ho et

al., 2017). In contrast, other studies reported increased diffusion properties of the uncinate fasciculus in premature infants exposed to prenatal maternal stress (Lautarescu et al., 2019) and among adults exposed to childhood trauma (Tatham et al., 2016). Discrepancies may be because of differences in the type of adversity and developmental stage at assessment, and none of these prior studies evaluated unpredictability. We focus on unpredictability as a type of early adversity that has been associated with long-term consequences for development (Glynn et al., 2018, 2019; Howland et al., 2020; Noraña-Zhou et al., 2020). Patterns of sensory signals are known to shape the development of neural circuits involved in sensory systems, and we show that circuits involved in cognitive functions also may be affected. Further, almost all previous studies have quantified the integrity of the uncinate fasciculus using tensor-based measures such as fractional anisotropy, axial, and radial diffusivity. These measures rely on the tensor model, which assumes a single fiber orientation per voxel and does not properly account for fiber crossing, bending, or twisting (Alexander et al., 2001). A strength of our approach of modeling multiple fiber orientations using orientation distribution functions is possibly more likely to approximate microstructural properties of complex neural tissue than the tensor model (Gorczewski et al., 2009; Fritzsche et al., 2010; Yamada et al., 2018).

Anatomically, the uncinate fasciculus is a U-shaped, fanning white matter bundle with complex structure (Ebeling & von Cramon, 1992; Bhatia et al., 2012, 2017, 2018; Riva-Posse et al., 2014; Vergani et al., 2016) and a number of termination points in the medial temporal lobes (Ebeling & Von Cramon, 1992; Thiebaut de Schotten et al., 2012; Von Der Heide et al., 2013). It has only recently been visualized using Q-space imaging

methods that model the U-shaped uncus and orbitofrontal cortex branching and turning patterns (Leng et al., 2016; Bhatia et al., 2017). Developmental studies have shown that white matter rapidly develops during early infancy, with MTL–PFC pathways like the uncinate (as well as cingulum) continuing to develop until the age of 35 years (Hermoye et al., 2006; Asato et al., 2010; Von der Heide et al., 2013; Simmonds et al., 2014; Olson et al., 2015). In animal models, a very similar pattern exists as the amygdala–prefrontal connection is relatively slow to develop and continues into adolescence with very rapid growth during the first 10 postnatal days of life followed by synaptic pruning in adolescence (Cunningham et al., 2002; Johnson et al., 2016). Although histologic evidence is needed to truly determine the significance of age-related increased anisotropy across maturation, evidence points to very rapid limbic white matter change in the first 2 years of life, possibly indicating a period of sensitivity in which environmental stimuli could more drastically affect the development of limbic white matter (Yu et al., 2020). In contrast to the association with the uncinate fasciculus, early life exposure to unpredictability was not related to integrity in the cingulum bundle, which is in contrast with previous reports suggesting that this pathway is vulnerable to early life adversity (Choi et al., 2009; Huang et al., 2012; El Marroun et al., 2018).

The function of the uncinate fasciculus is still not well understood, although recent studies have suggested that it plays a role in episodic memory, and in particular the adjudication among similar mnemonic representations during retrieval (Von Der Heide et al., 2013; Alm et al., 2016). It is well established that episodic memory involves the MTL, the PFC, as well as their interactions (Jones & Wilson, 2005; Van Kesteren et al., 2010; Preston & Eichenbaum, 2013; Brincat & Miller, 2015; Eichenbaum, 2017).

Further, the ability to adjudicate among competing memory representations is thought to rely on hippocampal pattern separation. With this in mind, our primary behavioral outcome measure (LDI) was based on the mnemonic similarity task, which is designed to assess hippocampal pattern separation. Our results provide evidence that an imbalanced ratio of uncinate connectivity to cingulum connectivity is related to impaired performance on the mnemonic similarity task. Additionally, our mediation analyses suggest that this imbalanced connectivity, a possible indicator of imbalanced maturation, is a putative mechanism that links the experience of unpredictable maternal sensory signals early in infancy to impaired memory function in childhood.

The ratio of integrity parameters of the uncinate fasciculus to cingulum was a mediator in the association between unpredictable maternal sensory signals and performance in our task. This should not be surprising, as both of these projections comprise components of the corticolimbic brain circuitry, which is critical for executing complex behaviors such as memory. Notably, the overall function of the circuit can be thought of as the combinatorial sum of the function and connectivity of its distinct components (Redish & Gordon, 2017). Thus, whereas augmented maturation of a single component or a deficit in another in and by itself may not suffice to distort circuit function, their combined existence may be synergistic, leading to unbalanced functional output (Figure 9).

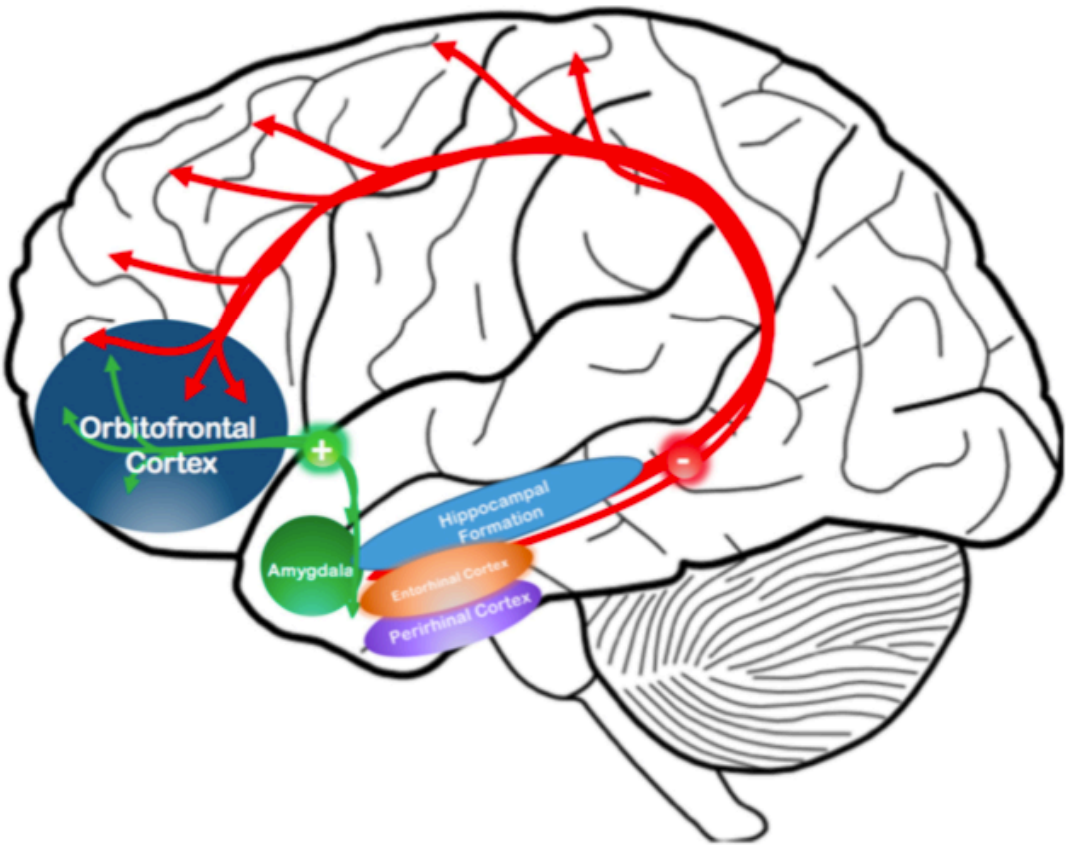

Figure 9. Anterior and posterior MTL–PFC circuits in humans. The circuit schematic summarizes our results demonstrating that (1) the anterior MTL–PFC pathway (i.e., the uncinate fasciculus in green lines), which connects the amygdala and rhinal cortex directly to the orbitofrontal cortex is enhanced in relationship to the increased unpredictability of maternal sensory signals and (2) the posterior MTL–PFC pathway (i.e., the cingulum in red and white), which connects the hippocampus and rhinal cortex with the retrosplenial cortex as well as medial prefrontal and orbitofrontal cortex is not related to the increased unpredictability of maternal sensory signals. These aberrations in circuitry are consistent with a developmental scenario, primarily in female children 9–11 years of age, in which unpredictable maternal sensory signals bias connectivity in favor of the anterior pathway at the expense of the posterior pathway and possibly lead to episodic memory dysfunction.

In conclusion, our findings demonstrate that infant exposure to unpredictable patterns of maternal care is associated with imbalanced maturation of the uncinate fasciculus and the cingulum detected during childhood, and that this imbalance may be

associated with deficits in memory function. This is consistent with our prior work in rodents showing that early life unpredictability leads to increased structural connectivity of the amygdala to prefrontal cortex pathway in rats (Bolton et al., 2018b) and to deficits in hippocampal memory (Molet et al., 2016b). This study, along with future investigations, will yield novel insight into neurobiological mechanisms of vulnerability to cognitive deficits as a result of unpredictable early environments.

Chapter 3: Function of the Uncinate Fasciculus in Emotional Pattern Separation

All findings of this study have been published in Granger et al., (2021b)

Introduction

Episodic memory – memory for facts and events – involves contributions from the medial temporal lobe (MTL), prefrontal cortex (PFC), and their interactions (Eichenbaum, 2017; Preston & Eichenbaum, 2013). While a considerable imaging literature in humans has focused on the MTL, relatively few studies have examined the role of white matter pathways connecting the MTL to the PFC in supporting episodic memory computations.

One such anatomical connection, the uncinate fasciculus, is a major white matter bundle connecting the MTL to the orbitofrontal cortex (OFC) in primates. This particular connection forms an “anterior pathway” by which the MTL can communicate with the PFC. Although often described as innervating the hippocampus, human dissection and axonal tracing studies in primates indicate that this bundle more accurately innervates

the basolateral amygdala (BLA) and the entorhinal cortices of the MTL and projects to a number of prefrontal regions including the OFC (Figure 10; Ebeling & Von Cramon, 1992; Von Der Heide et al., 2013; Thiebaut de Schotten et al., 2012).

In humans, abnormalities of the uncinate fasciculus have been implicated in psychiatric disorders characterized by emotional dysregulation such as major depression and anxiety, as well as in response to early life stress and maltreatment (Eluvathingal et al., 2006; Hanson et al., 2015; Ho et al., 2017; Taylor, et al., 2007; Zhang et al., 2012; Olson et al., 2015).

While the exact functional role of the uncinate fasciculus remains unclear, it is broadly thought to be involved in episodic memory, language, and socio-emotional processing (Von Der Heide et al., 2013). Von Der Heide et al., (2013) provide a review of the origins of research on the uncinate fasciculus derived from humans and monkeys with selective ventral frontal lobe and anterior temporal lobe damage writing that the first theory of the uncinate fasciculus in episodic memory function was derived from Markowitsch (1982) who wrote *"The task of the uncinate fascicle will be to guide and channel this information flow to the prefrontal cortex and to transmit preprocessed information back to the temporal cortex for the final act of representation".* This hypothesis was followed by studies in monkeys showing that performance on conditional rule learning tasks were impaired after uncinate fasciculus transection or transection of the connecting tissue within the orbital and ventral prefrontal cortex and inferotemporal cortex. In one such study, bilateral resection of the uncinate fasciculus in cynomolgus monkeys resulted in impairment in a visuomotor conditional rule learning task requiring monkeys to discriminate between two digitally presented stimuli and

provide the appropriate motor response for reward delivery. In this experiment, in order to receive a reward, monkeys had to learn to respond to one of two stimuli presented one at a time on the screen. If stimulus A was presented, monkeys had to touch and maintain contact with the stimulus for 1 second before the reward was delivered. If stimulus B (a different multicolored pattern) was presented the monkey was required to tap the stimulus 8 times in order to receive a reward. Errors across 10 different stimulus pairs before and after surgery were calculated. Monkeys displayed more errors in discriminating motor responses to the two stimuli after uncinate fasciculus transection. In several follow-up experiments, this study also showed that the deficit observed in this task was not related to mild motor impairment nor visual impairment (Eacott & Gaffan, 1992). In rhesus macaques, selective ablation of the orbital/ventral prefrontal cortex and inferotemporal cortex (regions connected by the uncinate fasciculus) resulted in impaired performance on a conditional rule learning task that required animals to associate two of 8 digital stimuli with a particular corner location on a screen in order to receive reward (Bussey et al., 2002). More specifically, animals were tasked with correctly recalling which of the four choice locations were paired with each one of the highly similar target objects. Interestingly, object–reward association learning, reversal learning, configural learning, and delayed matching-to-sample are unimpaired by uncinate fasciculus disconnection in monkeys (Von der Heide et al., 2013; Eacott & Gaffan, 1992; Gaffan & Eacott, 1995; Gutnikov et al., 1997). One hypothesis derived from this work was suggested by Alm et al., (2016) which purports that these conditional rule learning tasks require a great deal of retrieval competition and therefore the uncinate fasciculus may play a role in adjudicating among competing episodic memory

representations at retrieval. In order to test this notion in humans, Alm et al., (2016) employed the use of diffusion tensor imaging to assess uncinate fasciculus integrity and correlated structural measures with three separate tasks to assess retrieval competition. In experiment 1, young adults learned to associate names with faces through feedback provided at the end of each trial. Here the faces contained retrieval competition and it was found that structural measures of uncinate fasciculus integrity were associated with performance on this task. In experiment 2, participants learned to associate fractal images with cued locations through feedback provided at the end of each trial. Here retrieval competition was manipulated among fractals and uncinate fasciculus structural measures were associated with performance on this task. In experiment 3, participants were asked to recall unique faces in a paradigm that required low retrieval competition among faces. Integrity measurements of the uncinate fasciculus were not associated with performance on this task (Alm et al., 2016).

Competition among memory traces during retrieval could be mediated, at least in part, by pattern separation. This process is defined as the neural computation used to orthogonalize overlapping similar stimuli, a process that particularly involves the dentate gyrus and CA3 regions of the hippocampus (Yassa & Stark, 2011; Leal & Yassa 2018; Leutgeb et al., 2007). Functional MRI studies have noted pattern separation related activity in the DG/CA3 region during incidental encoding of similar lure items (Bakker et al. 2008; Lacy et al., 2010) as well as explicit performance of mnemonic discrimination tasks (Yassa et al., 2010; Reagh et al. 2018). These tasks require participants to determine during retrieval if items highly similar to the previously encoded items are “new” or “old”, which requires suppression of interference from competing memory

representations. In the context of emotional memories, we have previously shown this process extends to the amygdala (Leal et al., 2014a; Zheng et al. 2019). Given this prior work, we reasoned that tasks assessing pattern separation would be particularly well-suited to understanding the impact of the uncinate fasciculus connection on emotional episodic memory discrimination. However, its role in this process has never before been investigated.

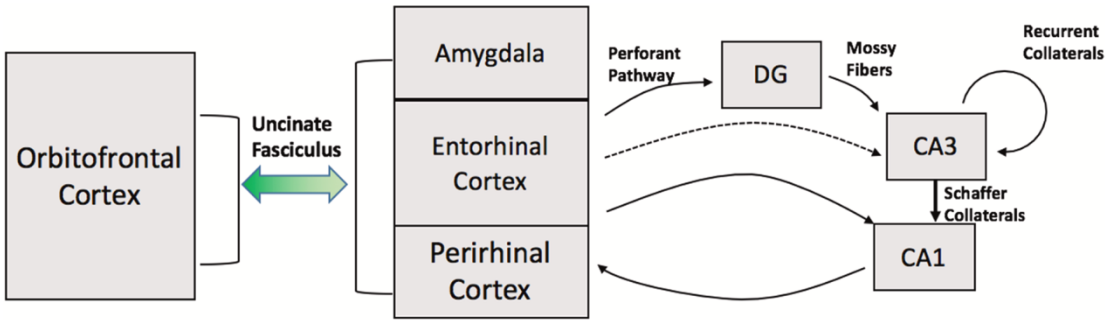

Figure 10: Circuitry of orbitofrontal connectivity with the medial temporal lobe subfields via the uncinate fasciculus. The uncinate innervates both the lateral amygdala and cortices of the MTL. The cortices of the MTL feed into the hippocampal subfields of DG, CA3, and CA1 via multiple pathways one of which includes the perforant path. The perforant pathway feeds into the DG/CA3 subfields where the neuronal computation known as pattern separation is thought to occur. In this manner, the uncinate fasciculus is a possible direct route of inhibitory information to these regions.

Using multimodal neuroimaging, we tested the hypothesis that the uncinate fasciculus may play a role in regulating mnemonic discrimination specifically for emotional items by modulating BOLD fMRI activity in the DG/CA3 region, which, would predict emotional discrimination performance. To assess the structure of the uncinate fasciculus, we implemented a new method to anatomically track the pathway using non-tensor-based deterministic tractography and utilized a model-free diffusion metric (normalized quantitative anisotropy – nQA) designed to capture the degree of diffusion

among primary fiber orientations accounting for partial volume effects inherent in the tensor model (Yeh et al., 2013). To assess the functional role of the DG/CA3 region of the hippocampus, we used high-resolution (1.5 mm isotropic) BOLD fMRI capable of resolving hippocampal subfields, while participants performed the emotional discrimination (i.e. pattern separation) task (Figure 11). The outcome measure was the "lure discrimination index", a measure of how well participants are able to discriminate among similar emotional and neutral scenes, corrected for response bias.

Materials and Methods

Participants

Table 4. Participant Demographics and Neuropsychological Results.

N = 27 (15 female)	**Mean (±SD)**
Age	21 ± 3.38
Beck Depression Inventory-II	10.55 ± 11.48
RAVLT Immediate Recall	12.59 ± 1.97
RAVLT Delayed Recall	11.63 ± 3.44
Digit Span Forward	11.96 ± 1.85
Digit Span Backward	8.29 ± 2.03
Mini Mental State Exam	29.22 ± 0.97
Trails Making Test A	19.58 ± 5.31
Trails Making Test B	45.59 ± 11.91

A total sample of 27 participants (15 female) were recruited from Johns Hopkins University and received monetary compensation for their participation. Informed consent was given by all participants and all procedures approved by the Johns Hopkins University Institutional Review Board. Subjects were administered a neuropsychological battery which is summarized in Table 4. All participants were screened against major medical or psychiatric morbidities, substance abuse history, and additional criteria of

MRI contraindications like metal in the body. Results of the fMRI analysis of this dataset were previously published in Leal et al. (2014b) with the exception of a single subject who did not complete the DWI scan.

Imaging data collection

All data were collected on a 3 Tesla Philips scanner. We collected an ultrahigh-resolution structural MPRAGE scan that we developed for accurate delineation of hippocampal subfields and high-resolution diffeomorphic alignment (0.55 mm isotropic resolution; 273 sagittal slices, field of view = 240 × 240 mm, flip angle = 9, TR/TE = 13/5.9 ms, matrix size = 448 × 448, inversion pulse TI = 1110 ms). SENSE parallel imaging was used in two directions (2 × 1.5). The SAR (<10%) and PNS (<75%) were within required limits based on the scanner-calculated values. Task-activated functional data were collected and processed in the same manner as Leal et al. (2014b). Briefly, these data were collected with a high-speed EPI single-shot pulse sequence (1.5 mm isotropic, 19 oblique axial slices parallel to the principal axis of the hippocampus, field of view = 96 × 96 mm, flip angle = 70, SENSE parallel reduction factor = 2, TR/TE = 1500/30 ms, matrix size = 64 × 64. Diffusion weighted imaging were collected with an echo planar imaging sequence. The data were 3 mm isotropic, TR/TE = 6800/67 ms, 65 slices, 32 non- collinear directions, one B0, b-value = 700 s/mm2. Diffusion MR data were collected during the same scan session as the fMRI scanning.

Emotional pattern separation task

The emotional pattern separation task consists of an incidental encoding phase where subjects are instructed to rate the valence of each image from positive, negative,

or neutral based on a priori ratings outlined in Leal et al. (2014a). Subjects were later tested during the “Old/ New Recognition” portion of the task. In this portion, foils (new images), targets (same images), and high and low similarity lures were presented. Subjects were asked to make “Old” or “New” recognition judgments (Figure 11). In this case, correctly identifying that a lure item was “New” is termed as a Correct Rejection (CR) and falsely claiming that a lure item is “Old” would be termed a False Alarm (FA). We assessed behavioral discrimination on this task by quantifying a lure discrimination index (LDI) which measures performance on the task accounting for response bias: P(“New”|Lure) – P(“New”|Target) or lure correct rejections minus target misses. This was calculated for high and low similarity lures across the three valence types. This is a measure we have frequently employed in the past as it accounts for response bias (e.g. Leal et al. 2014a; Reagh et al., 2018). LDI of highly similar lure items was chosen in this case because of the uncinate fasciculus’ purported role in adjudicating between similar items during retrieval.

Functional MRI image analysis

Task data were analyzed using the open source package Analysis of Functional Neuroimages (AFNI) (Cox, 1996) and are previously described in detail in Leal et al. (2014b). Briefly, images were corrected for slice timing and subject motion censoring motion of 3◦ of rotation or 2 mm translocation in any direction relative to prior acquisition. Upon processing for motion we then registered our functional images to the structural (MPRAGE) using AFNI/s 3dAllineate program. We use Advanced Normalization Tools (Avants et al., 2011) which implements a robust diffeomorphic algorithm to warp structural scans to a common template based on the entire sample.

The same transformations were then applied to the functional data. Finally, behavioral vectors were created based on trial type orthogonalizing trials unique in emotion, similarity, and behavioral decision. These vectors there then used in a deconvolution approach based on multiple linear regression and the resulting fit coefficients (betas) estimated activity versus novel foils as an implicit baseline for a given time points and trial type in a voxel was calculated. We used the sum of the fit coefficients over an expected hemodynamic response of 3–12 s after trial onset as the model's estimate of response to each trial type as described in Leal et al. (2014b). Finally, fit coefficients were extracted using a region of interest approach for the DG/CA3 and CA1 subfields of the hippocampus according to Leal et al. (2014b).

Diffusion weighted imaging analysis

Diffusion data were processed for eddy correction using FSLs eddy_correct and analyzed using DSI-Studio (http://dsi-studio.labsolver.org). Individual subject data were then processed using DSI-Studios Q-Spin Diffeomorphic Reconstruction (QSDR) method which calculates the orientational distribution of the density of diffusing water in MNI space (Yeh & Tseng, 2011). All subjects met the criterion of fitting to the template space by obtaining an R-squared value of greater than 0.63 as suggested by the software developers. QSDR was chosen as the reconstruction method in order to overcome several limitations of the tensor model. First, QSDR provides reconstruction in a template space allowing the creating of standardized "regions-of-avoidance" to filter out known false-projecting fibers. Second, QSDR allowed for the computation of

orientation distribution functions rather than tensor-based computation of diffusion signals. This is important because the orientation distribution functions calculated with this method are presumed to resolve partial volume fractions, model crossing-fibers, and are thought to result in more accurate deterministic tractography (Yeh et al., 2013; Maier- Hein, 2017). Our tractography protocol included a customized region- of-avoidance by merging three intersecting planes (one axial, one coronal, one sagittal) with a sphere over the striatum and nucleus accumbens complex (Figure 12). The use of this region allowed us to filter out false projections along the inferior longitudinal fasciculi and projections extending medially toward the striatum and anterior cingulate cortex. We included bilateral uncinate fasciculus regions from the Johns Hopkins White Matter Atlas available through DSI-Studio as “seed regions” and Brodmann’s areas 11 and 47 as “end regions”. The tractography settings were: seed count = 500,000, threshold index = QA, FA threshold = 0.0, seed plan = “0”, initial direction = “0”, interpolation = “0”, step size = “0”, turning angle = “55”, smoothing = 0.6, min length = 0, max length = 150. The tractography protocol was repeated for the left and right hemisphere separately by using the left or right uncinate seed region in each iteration. In order to quantify the integrity of the resulting streamlines we used the model-free measure of normalized quantitative anisotropy (nQA) to quantify the degree of diffusion along principle orientations on an ODF. This measure is thought to more accurately represents the degree of diffusion among principal axonal directions within a single voxel rather than fractional anisotropy (FA), which is a singular tensor-based measure that does not account for multiple orientations. The nQA measure also accounts for the isotropic component of diffusion and, similar to FA, is normalized on a scale from 0 to 1

and reflects greater diffusivity among primary fiber orientations (Yeh et al., 2013; Yeh, et al., 2010). Together, these methods allowed for consistent modeling of the uncinate fasciculus in a standardized and automated way with no manual intervention.

Statistical Analysis

All statistical analyses were conducted using Prism GraphPad 7 and R-studio. We conducted all correlational analysis in Prism 7 computing two-tailed Pearson correlation coefficients with 95% confidence intervals. Unlike our previous work, we did not choose an arbitrary cutoff to be used for a binary classification of “healthy” and “depressed” as we did not recruit a clinically assessed sample. Instead, multiple linear regressions were used to assess the influence of Beck Depression Inventory-II (on a continuous basis) on relationships between behavior, fMRI, and diffusion measures and were conducted in R-studio. Bootstrap analysis were conducted in R-studio using the Boot package with 1000 repetitions. 95% confidence intervals are reported. Statistical values were considered significant at an alpha level of 0.05. Since we only tested targeted hypotheses and used a priori planned comparisons, correction for multiple comparisons was not necessary (Rothman, 1990; Saville, 1990).

Results

Uncinate fasciculus integrity predicts DG/CA3 activity during emotional lure discrimination

To test the hypothesis that uncinate fasciculus structural integrity is associated with MTL subregional activation profiles involved in discrimination of highly similar lures, we used normalized quantitative anisotropy (nQA) to quantify the uncinate fasciculus and the average of beta coefficients of signal in the DG/ CA3 region during correct

discrimination as our variables of interest. Here we separately assessed the magnitude of this relationship (between uncinate fasciculus integrity and DG/CA3 activity) in highly similar negative, neutral, and positive correct discrimination trials within each hemisphere. We investigated each hemisphere separately as recent investigations modeling the uncinate fasciculus using diffusion spectrum imaging have reported hemispheric differences (Leng et al., 2016). We focused on highly-similar lures as prior work suggested that DG/CA3 signals are particularly sensitive to this more challenging condition (Leal et al., 2014b). We found a significant negative correlation between left uncinate fasciculus nQA and left DG/CA3 activity for highly similar negative ($r = -0.41$, $p = 0.035$) and positive ($r = -0.44$, $p = 0.022$) but not neutral ($r = 0.12$, $p = 0.55$) CRs (Figure 13a–c). To rule out the possibility of individual points having a large contribution to the aforementioned effects we conducted bootstrap analysis with 1000 simulations. The 95% confidence interval for the Pearson correlation coefficient bootstrap effect of the relationship between left uncinate fasciculus nQA and left DG/CA3 activity for negative CRs ranged from −0.69 to −0.12 (SE = 0.14). The 95% confidence interval for the Pearson correlation coefficient bootstrap effect of the relationship between left uncinate fasciculus nQA and left DG/CA3 activity for positive CRs ranged from −0.82 to −0.11 (SE = 0.18). As a result of these analyses, we then tested if the slope of the relationship between uncinate fasciculus integrity and DG/CA3 activity during "emotional" CRs was significantly different the relationship between uncinate fasciculus integrity and DG/CA3 activity during neutral lure discrimination. We found that the slope of the relationship between uncinate fasciculus integrity and DG/CA3 activity during negative correct rejections was significantly different than the slope of the relationship

between uncinate fasciculus integrity and DG/CA3 activity during neutral lure CRs ($Z = 2.057$, $p = 0.040$). Similarly, we found that the slope of the relationship between uncinate fasciculus integrity and DG/CA3 activity during positive correct rejections was significantly different than the slope of the relationship between uncinate fasciculus integrity and DG/CA3 activity during neutral lure CRs ($Z = 2.22$, $p = 0.027$). These data suggest that lower integrity of the left uncinate fasciculus is associated with higher levels of activity in the left DG/CA3 during correct emotional but not neutral discrimination, suggesting a possible role in limiting the activity of this subregion during emotional conditions.

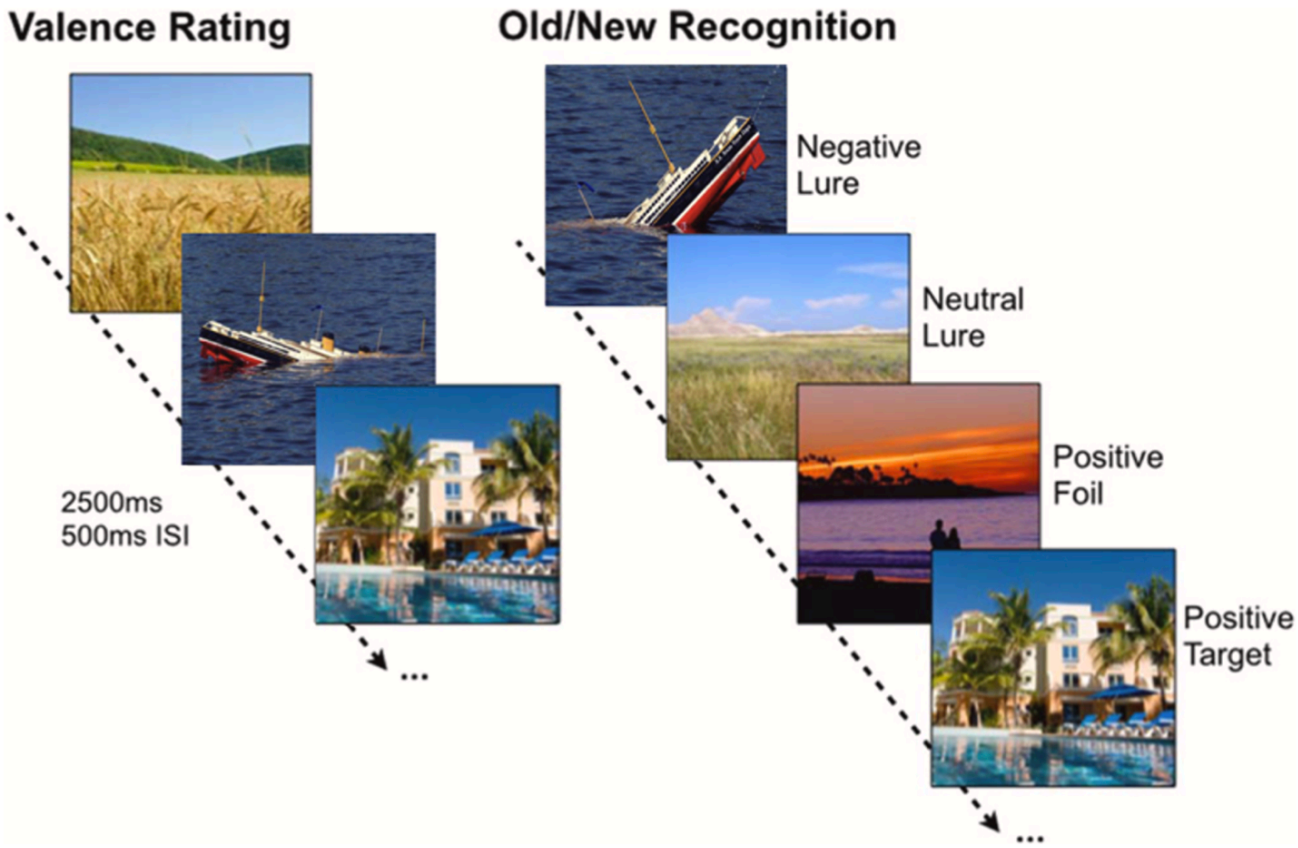

Figure 11: Schematic of the emotional pattern separation task. The left side of the image shows the incidental encoding phase of the task where participants are asked to rate images as “negative”, “neutral”, or “positive”. On the right side of the image is the memory portion of the task. This phase, known as the Old/New Recognition phase shows participants several variants of previously seen images (lures), as well as repeated images (repeats), and never before seen images (foils). Subjects are asked to make “old” or “new” judgements during the trial and response times are recorded.

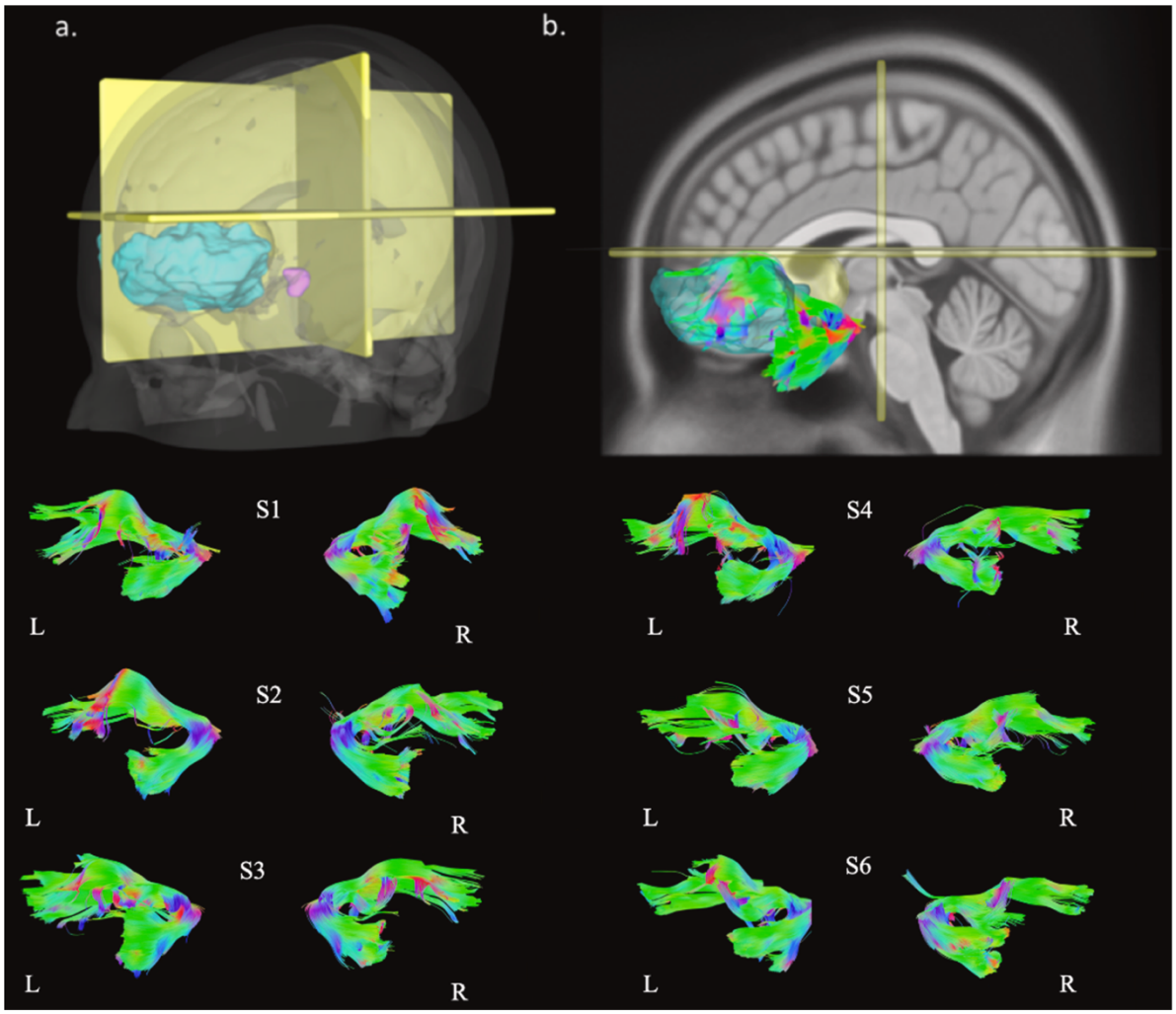

Figure 12. In-vivo dissection of the uncinate fasciculus derived from model-free QSDR and deterministic tractography in the template space. (a) The “region-of- avoidance” is depicted in yellow, uncinate fasciculus “seed region” depicted in purple, and “end” region in blue containing merged Brodmanns areas 11 and 47. (b) The resulting uncinate fasciculus tractography for the left hemisphere. The tractography shows branching in the prefrontal cortex region as anatomical studies suggest. We also provide tractography results for 6 random subjects viewed from a sagittal perspective in the template space. Here we show the consistent nature of the custom protocol in modeling of this complex pathway. In each of the subjects the U-shaped fanning bundle is clearly seen with individual difference in the amount of branching in the prefrontal cortex.

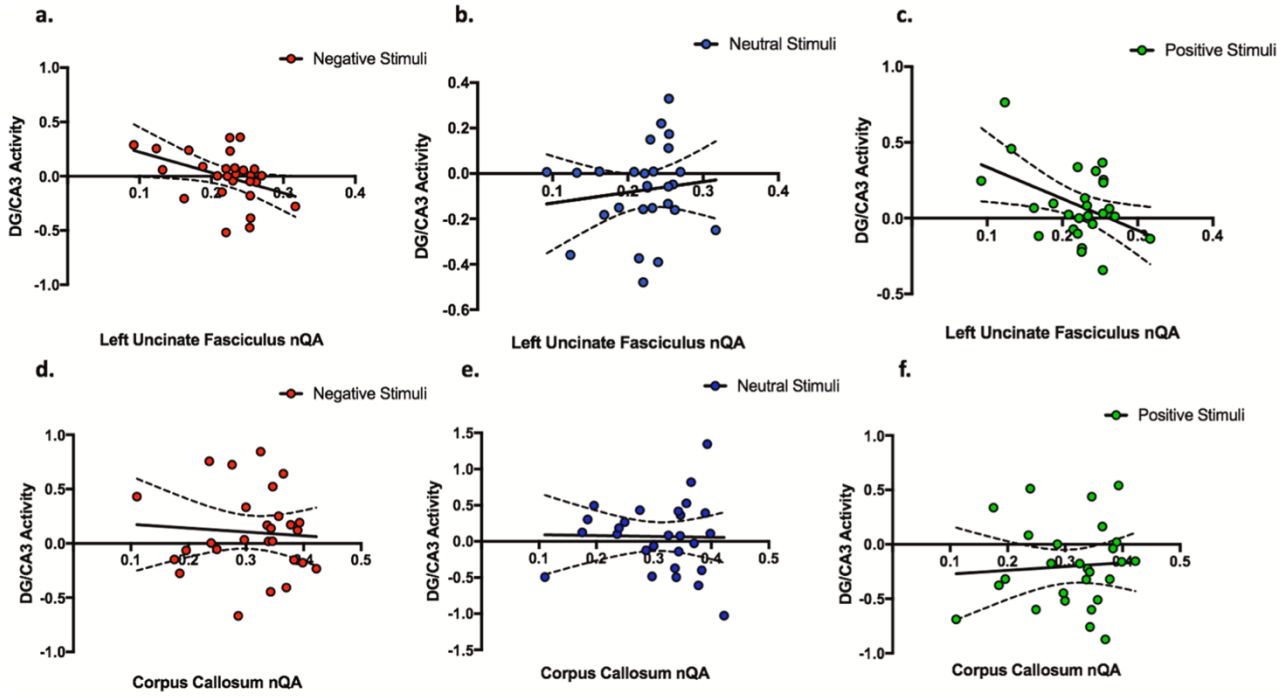

Figure 13. Relation between structural integrity (nQA) predicting BOLD activation of DG/CA3 during correct lure discrimination trials. The top row (a–c) shows left uncinate fasciculus nQA predicting left DG/CA3 BOLD activity during highly similar lure correct rejections. Specifically, we show that greater left uncinate fasciculus nQA predicts decreased DG/CA3 BOLD response during the correct discrimination of (a) negative (r = − 0.41, p = 0.035) and (c) positive (r = − 0.44, p = 0.022) highly similar lure items but not (b) neutral (r = 0.12, p = 0.55). (d–f) Shows the corpus callosum as our negative control. We show there is no relationship between corpus callosum nQA and average left and right DG/CA3 activity during the correct discrimination of (d) negative, (e) neutral, and (f) positive highly similar lure items.

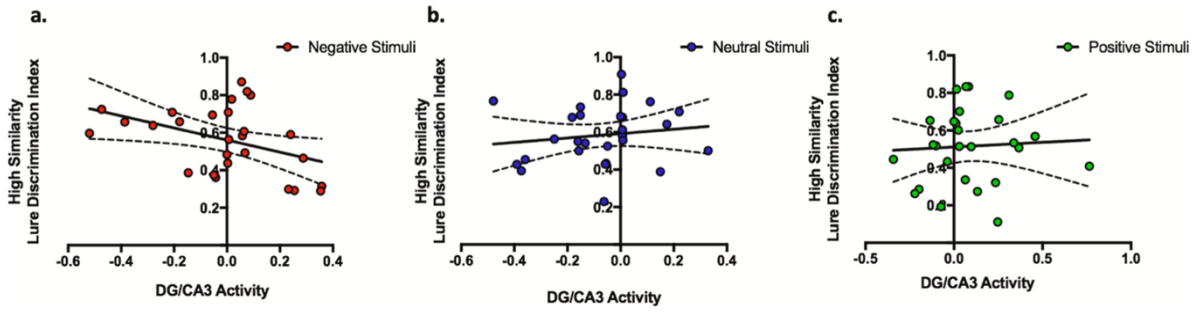

Figure 14. Relationship between DG/CA3 BOLD response during highly similar lure discrimination and lure discrimination behavior. Here left DG/CA3 activity during high similarity CRs is inversely related with lure discrimination for (a) negative (r = − 0.42, p-value = 0.029), but not (b) neutral or (c) positive stimuli.

As the uncinate fasciculus has been previously implicated in psychiatric disorders characterized by emotional disturbances, we asked if this effect could be related to symptoms of depression. Using the Beck Depression Inventory II (BDI-II) we quantified depressive symptoms in all participants and included the overall score in a regression model (BDI-II and uncinate fasciculus nQA predicting DG/CA3 activity). We found that the relationship between left uncinate fasciculus nQA and left DG/CA3 activity for highly similar negative lure correct discrimination trials remained significant (B = − 1.8, p = 0.048) after accounting for BDI-II scores (B = − 0.0029, p = 0.46). Similarly, the relationship between left uncinate fasciculus nQA and left DG/CA3 activity for highly similarly positive items remained significant (B = − 1.94, p = 0.032) after accounting for BDI-II scores (B = − 0.0045, p = 0.24).

In order to assess the specificity of our findings, we conducted several additional control analyses. First, we asked whether this relationship between activation and white matter is specific to the uncinate fasciculus or if it is a general feature of white matter connectivity. We tested the relationship between general connectivity and DG/CA3

activity using the corpus callosum as a control pathway. Specifically, we tested if corpus callosum nQA predicted averaged DG/CA3 response during high similarity negative, positive and neutral lures. We found that none of the relationships were statistically significant (Figure 13d–f). Second, we asked whether the relationship between uncinate fasciculus nQA and DG/CA3 activity generalizes to other hippocampal subfields. We tested whether uncinate fasciculus integrity was associated with CA1 activity and found left uncinate fasciculus nQA did not predict with the responses of the left CA1 subfield during highly similar lure correct rejection trials of any valence (Supplementary Table 1a). Additionally, these effects seem specific to the left hemisphere. Right uncinate fasciculus integrity did not predict right DG/CA3 nor CA1 activity during highly similar lure discrimination for any valence type (Supplementary Table 1b). Finally, to test the specificity of uncinate fasciculus nQA predicting DG/CA3 activity during highly similar emotional lure discrimination, we asked whether uncinate fasciculus nQA also predicted DG/CA3 activity during low similarity lure correct rejections. Left uncinate fasciculus nQA did not predict DG/CA3 activity for negative ($r = 0.084$, $p = 0.68$), neutral ($r = 0.21$, $p = 0.28$), or positive ($r = 0.15$, $p = 0.45$) low similarity correct rejections.

Uncinate fasciculus Integrity, DG/CA3 functional activity, and lure discrimination performance

Given the relationship between uncinate fasciculus integrity and DG/CA3 activity during correct rejections of emotional stimuli, we asked whether left uncinate fasciculus integrity was directly associated with lure discrimination performance. We found that uncinate fasciculus integrity did not directly predict lure discrimination performance. We then asked whether the relationship between DG/CA3 subfield activity during discrimination of highly similar lure was associated with overall performance on those

trial types. Past work in our group and others has suggested that higher levels of activity in the DG/CA3 region is associated with overgeneralization errors. We found a significant negative correlation between left DG/CA3 activity during correct discrimination of negative stimuli and the lure discrimination index on the same trials ($r = -0.42$, $p = 0.029$, Figure 14). We once again assessed whether depressive symptoms impacted this relationship by including BDI-II score as a regressor and found that that the relationship between left DG/CA3 activity and negative LDI remained significant ($B = -0.31$, $p = 0.039$) after accounting for depressive symptoms ($B = 0.00089$, $p = 0.76$).

Discussion

In this study, we tested the hypothesis that the integrity of the uncinate fasciculus is associated with medial temporal lobe dynamics during an emotional pattern separation task. This stems from the observation that prefrontal cortex modulation of MTL signaling is implicated in memory processing (Jones & Wilson, 2005; Kim et al., 2011; Brincat & Miller, 2015; Van Kesteren et al., 2010), however, the exact pathways by which this modulation occurs in humans have remained elusive. Studies in rodents have been hindered by the major species differences in PFC anatomy as well as the absence of certain anatomical connections that are present in primates, thus this study offers novel insight into human MTL-PFC interactions.

Accounting for depressive symptoms, we found that in the left hemisphere, lower uncinate fasciculus integrity predicted greater activation of the DG/CA3 subfield of the hippocampus during emotional (positive and negative but not neutral) highly similar correct discrimination trials. To our knowledge, this is the first demonstration that differences in uncinate fasciculus integrity may be associated with alterations of

functional activity in the DG/CA3 subfields of the hippocampus during discrimination of similar information.

In addition to providing a link between uncinate structure and DG/ CA3 activity, we found that greater left DG/CA3 activity during highly similar negative correct rejections was related to poorer memory performance for highly similar negative items (i.e. higher rate of false alarms). Although at first this result seems surprising, given what is known about the role of DG/CA3 in pattern separation, a finding of increased activation in DG/CA3 linked to poor performance has been previously reported in older age (Yassa et al., 2011; Sinha et al., 2018).

An interesting possibility is that the increased activation is related to CA3′s recurrent collateral network which is thought to play a role in pattern completion (or overgeneralization in the case of a discrimination task). While the noted activity occurred during the correct trials, pattern completion is assumed to occur also during lure discrimination (i.e. “recall to reject”). Here, much like the data in older adults, higher levels of DG/CA3 activity during correct lure discrimination is linked to poorer overall memory performance at the individual subject level. Overall, this suggests that greater activation in this subfield is associated with worse cognitive outcomes. That said, other work has shown that a within- subject increase in DG/CA3 activity as a function of mild aerobic exercise is associated with enhanced discrimination (Suwabe et al. 2018), however this finding also was associated with increased functional connectivity with regions involved in high precision recollection of memories (e.g. retrosplenial cortex, angular gyrus). Given this evidence, it is possible that there is an inverted U-shaped dose–response relationship where activity in DG/CA3 needs to be held in balance, with

too much or too little activity being associated with worse outcomes. This particular topic should be subject to further investigation.

Our analysis of lure discrimination performance provides evidence that while the structural integrity of the uncinate fasciculus is not related to lure discrimination, it is possible that the impact of this MTL-PFC bundle on memory is directed by its impact on DG/CA3 function. Further research is needed in order to test this hypothesis appropriately. The lack of correlation between uncinate integrity and discrimination performance is consistent with other results from Bennett et al. (2015), who found no link between uncinate integrity and object discrimination performance. Instead, the authors found a relationship between the fornix and performance, a relationship that was consistent across young and older adults. The possibility that the uncinate's impact on behavior is mediated by functional signals in the DG/CA3 is consistent with a top-down modulatory control from the PFC to the MTL during discrimination.

Although we tested a focused hypothesis about the uncinate fasciculus and checked its specificity against a control pathway (the corpus callosum), one possible limitation is that other pathways might influence these emotional memory processes. In general, the relative contribution of the uncinate fasciculus, cingulum, and fornix bundles in innervating their respective targets within the medial temporal lobe are poorly understood in humans. The 3-dimensional structures of these pathways have not been extensively resolved in humans or non-human primates. Along these lines, it is possible that information flow is segregated according to information content and valence. Signaling involving emotional items could be reliant on OFC integration and thus be communicated via the uncinate fasciculus, whereas signaling involving non-emotional

items could be reliant on mPFC (or other PFC region) integration and thus be communicated via the cingulum or fornix. This may be too simplified, as it is not currently known whether these pathways innervate overlapping subdivisions of the PFC, and it is unclear what the functional consequences of these dissociations may be. Another possible limitation is the relatively small sample size collected in this investigation. While we provide additional statistical analysis to demonstrate these results are not sensitive to outliers, it is still unclear how these results would generalize in larger clinically-assessed populations.

One issue is the difficulty of even modern tractography algorithms and data acquisition schemes to accurately and non-invasively model even the largest white matter bundles with sufficient accuracy in humans (Maier-Hein, 2017). Tractography of the uncinate fasciculus is a particularly challenging endeavor due to its branching and turning pattern and the possibility for false continuation medially toward the striatum and posteriorly along the inferior fronto-occipital fasciculus and inferior longitudinal fasciculus. In this manner, the use of more sophisticated tractography algorithms that might account for multiple fiber orientations within each voxel might aid in the delineation of this morphologically complex fiber. To address these issues we used normalized quantitative anisotropy, a measure that resolves multiple fiber orientations within a voxel and appropriately accounts for the isotropic component of diffusion, which addresses partial volume confounds. We combined this approach with anatomical regions of avoidance consisting of three intersecting planes and a sphere over the striatal area to ultimately generate a highly reproducible scheme for tractography of the uncinate fasciculus while avoiding common false continuations with respect to anatomy.

In this study, we have shown that decreased uncinate fasciculus integrity is associated with greater activity of DG/CA3 during emotional lure discrimination and that greater DG/CA3 activity is associated with poor performance on an emotional pattern separation task. As a result of this finding, we hypothesize that these results reflect a possible scenario in which the uncinate fasciculus mediates important top-down control from the OFC to the MTL which is critical for processing of emotional memories, but that the relationship between uncinate fasciculus integrity and behavior is mediated by functional activation of the hippocampal network.

Together our results suggest that uncinate fasciculus integrity may be a marker for emotional and cognitive health, which is consistent with prior work implicating the uncinate fasciculus in emotional dysregulation conditions including major depressive disorder and anxiety (Zhang et al., 2012), as well as work linking uncinate fasciculus integrity with early life stress and maltreatment (Eluvathingal et al., 2006). Future studies are needed to determine whether these effects manifest beyond emotional discrimination tasks or if there are alterations in the relationship between uncinate fasciculus and functional signals across the lifespan.

Chapter 4: Summary and Synthesis of Findings

This Dissertation is directed at investigating altered circuits as a result of exposure to maternal sensory unpredictability and is comprised of two major experiments focused on the white matter that connects the medial temporal lobe and prefrontal cortex. The first experiment is targeted at investigating the impact of

experiencing maternal sensory unpredictability in infancy on MTL-PFC white matter later in adolescence. The second experiment is targeted at the investigation of the function of the uncinate fasciculus in episodic memory functioning in adults.

In the first investigation, we determined that maternal sensory unpredictability was associated with augmented uncinate fasciculus GFA. This effect remained after controlling for several other confounding factors of early life adversity including maternal depression/anxiety, maternal sensitivity, income-to-needs ratio, and sex. To determine the specificity of this finding and because the functional output of a brain circuit is a combinatorial sum of the activity of each of their components, we asked if maternal sensory unpredictability was also associated with a second white matter bundle, the hippocampal cingulum. Hippocampal cingulum GFA was not associated with maternal sensory unpredictability. However, we did find an association between greater maternal sensory unpredictability and an increased uncinate to hippocampal cingulum GFA ratio suggesting an imbalance of this medio-frontal white matter circuit as a result of maternal unpredictability in infancy. The behavioral relevance of this circuit was assessed with the lure discrimination index from the mnemonic similarity task. Using this task, we provide evidence that a greater uncinate to hippocampal cingulum GFA imbalance mediated the relationship between greater somatosensory unpredictability and impaired mnemonic separation performance. Together, in Chapter 2, we provide a key mechanistic link between experiencing this form of early life adversity and episodic memory impairment in humans.

The second major investigation of this Dissertation was directed at investigating the function of the uncinate fasciculus and pursue its hypothesized role in adjudicating

between competing memory traces (Alm et al., 2016). To investigate this question, Chapter 3 focused on parsing the 3-dimensional uncinate fasciculus using deterministic tractography aided by quantitative anisotropy. This work provided the first evidence that in the left hemisphere, greater uncinate fasciculus integrity predicted reduced activation of the DG/CA3 subfield of the hippocampus during emotional (positive and negative but not neutral) highly similar lure discrimination trials. Of importance, this relationship was only true for high similarity lures and uncinate fasciculus integrity was not associated with activity of the CA1 subfield.

Accelerated Development of the Uncinate Fasciculus

One question which was not extensively discussed in Chapter 2 of this work is how the imbalanced white matter connectivity might occur. Researchers in the field who have investigated the impact of maternal deprivation on amygdala-prefrontal cortex resting state functional connectivity have observed more adult-like, or accelerated, functional connectivity between these two regions and have hypothesized that accelerated development of this pathway may be an adaptive response which reprioritizes developmental goals to match the demands of an adverse early life environment (Gee et al., 2013). Here I refer to an adaptive response as a neurobiological or behavioral response made by an organism in order to increase evolutionary fitness.

While the explanation suggested by Gee et al., (2013) is reasonable, it does not address the cognitive or neurobiological sequalae that might lead to this adaptation of developmental processes and constitutes a different form of early life adversity.

Research in animal models has sought to determine if corticosterone and the receptor mediating its impact (glucocorticoid receptor; GR) are solely responsible for deficits in hippocampal structure as a result of maternal unpredictability (Bolton et al., 2020). This work employed the LBN model and RNA-sequencing and provided evidence for a myriad of genes in dorsal hippocampus that were differentially expressed between the control and LBN-exposed animals. More specifically, at a false discovery rate of 0.05, this investigation found 35 genes that were significantly upregulated and 107 genes that were significantly repressed in dorsal hippocampus as a result of exposure to LBN. Interestingly, these gene clusters were thought to be broken into two distinct groups namely it appeared that genes involved in maintenance of membrane potentials and neuronal firing were repressed whereas genes contributing to cell metabolism and oxidative stress were augmented (Bolton et al., 2020).

It has been shown that neonatal stress exposure induced from the LBN paradigm from postnatal day (PND) 1 to 7 in rats accelerated the development of the amygdala assessed via 2-deoxyglucose (2-DG) autoradiography (Moriceau et al., 2009). This finding was further corroborated by showing that corticosteroid infusion into the amygdala of rats reared in normal conditions produced similar effects (Moriceau et al., 2006) and blocking the impact of early life stress exposure from PND 1-7 with a corticosteroid receptor antagonist prevents accelerated amygdala maturation (Moriceau et al., 2009). Male mice exposed to early weaning (known to induce a biological stress response) showed precocious accumulation of galactosylceramide, a myelin constituent, in the amygdala (Ono et al., 2008).

Due to these findings, one might hypothesize that numerous epigenetic

modifications or activation of CRF-expressing neurons of the uncinate fasciculus may be responsible for the observed increases in GFA values in the uncinate fasciculus in humans. In other words, one might hypothesize that the mechanisms of augmented amygdala maturation and myelination described previously might extent to its neurons that project to the prefrontal cortex or perhaps there is a myriad of genes that are upregulated to enhance the myelination of the uncinate fasciculus over development which is responsible for the observed increase in GFA in the current work or increased streamline count shown in animals exposed to LBN (Bolton et al., 2018b).

One challenge in investigating this question is the ability to compare the amygdala-prefrontal cortex white matter across species. Tractography derived from diffusion weighted imaging of animals exposed to LBN shows a potential disparity in the morphology of the uncinate fasciculus across species or perhaps may point out that different tractography protocols can produce differing results. The predominant difference in this cross-species approach to the amygdala-prefrontal cortex white matter being that in animals the amygdala and prefrontal cortex was defined as 'regions-of-interest' (streamlines must pass through each region) whereas this work in humans (from the protocols in Chapter 3) used a combination of regions of avoidance to avoid falsely projecting streamlines and seed region of the uncinate fasciculus from a pre-existing atlas. The other possibility is that there is a cross-species difference where the morphology of the uncinate fasciculus simply does not exist in rodents.

While this study was among the first to employ the use of the metric of GFA as an outcome of early life adversity, other studies have shown reductions of FA values as a result of prolonged institutionalized care (Eluvathingal et al., 2006; Govindan et al.,

2010) and reductions of FA in individuals who have shown a higher sensitivity to early life stress (Ho et al., 2017). Figure 3 of this Dissertation shows the possibilities of how FA values can be low whilst generalized fractional anisotropy values can be high in the context of complex underlying tissue. Thus, another possibility is that low fractional anisotropy values of other studies that largely operationalize the uncinate fasciculus from FA-aided tractography (and not GFA of the uncus) may be due to the inability of fractional anisotropy to properly model complex underlying white matter across the various portions of the uncinate fasciculus. Regardless of this distinction, this type of criticism is reflective of a broader need for histological confirmation of diffusion signals across tissue types for both humans and rodents.

In response to this notion, Appendices B and C of this Dissertation are directed at advancing the study of diffusion imaging in humans by taking advantage of high-resolution sequences. This work, although it may seem tangential to the primary goals of this Dissertation, is designed to mirror findings in animal models that compared histological tissue properties of the CA1, DG, and perforant path with diffusion metrics. In these works, we show that high-resolution imaging yields novel insights into hippocampal subfield structure that maps onto work in animals that compare diffusion metrics with histology. It's possible one future direction of uncinate fasciculus work in humans would be to adapt the high-resolution sequences used in Appendices B-C to focus on the anterior MTL in order to more accurately parse and image the uncinate fasciculus in humans as a result of exposure to novel early life adversities.

Additional potential explanations for observing increased or accelerated development of the uncinate fasciculus in response to exposure to maternal sensory

unpredictability may be derived from other works. In introducing a novel tool to retrospectively assess environmental unpredictability Glynn et al., (2019) refer to complementary conceptual models that recognize unpredictability as a primary and unique determinant of development from an evolutionary-developmental perspective. This literature and its seminal theory proposed by Ellis et al., (2009) purports that environmental harshness and unpredictability are fundamental dimensions that influence an individual's life-history traits (characteristics determining growth, aging, and parental investment; Liu & Fischer, 2022; Belsky et al., 2012). In a review entitled *Theory and Measurement of Environmental Unpredictability*, Young et al., (2020) discuss possible ways in which environmental unpredictability can be described in statistical terms, the mechanisms in which organisms detect environmental unpredictability, and what information triggers a response from an individual once unpredictability is detected. This work suggests two potentially overlapping hypotheses about the proximate mechanisms evolved to detect environmental unpredictability. One of which, the authors suggest, is a statistical learning approach where organisms respond to the statistical patterns of change in its environment and suggest that cue reliability (the extent to which experiences or events provide information about current or future environmental conditions) is an important property. In this model, the statistical structure of cues over time is integrated to build predictions of the organism's environment. Further, an organism responds to environmental unpredictability when it detects a prediction error. Predictability is necessary in order to build predictions and consequently detect and respond to prediction errors. In the case of experiencing an unpredictable environment, it is possible that the statistical structure and unreliability of

cues over time from the environment may impair the function of prediction error signaling ultimately changing the organism's frequency of adaptive responses. One suggestion is that when predictions are constantly violated a flurry of prediction errors ensues resulting in many adaptive responses. This literature suggests that when individuals perceive their environment as more unpredictable (unpredictability in this sense perhaps detected by many prediction errors and adaptive responses over time) they are more likely to adopt faster or accelerated life history strategies to promote evolutionary fitness (Belsky et al., 2012). Importantly, this theory of accelerated development (driven by accumulated prediction errors perhaps) is similar to the theory proposed by Gee et al., (2013) which suggested that accelerated development of the amygdala-prefrontal cortex connection is an adaptive response which reprioritizes developmental goals to match the demands of an adverse early life environment. The literature on unpredictability and statistical learning theory has also provided evidence that faster life history strategies are related to internalizing and externalizing psychopathology symptoms (Del Giudice, 2014; Hurst & Kavanaugh, 2017; Liu & Fischer, 2022). Despite this overlap in literatures, there are several limitations to the cue-reliability and statistical learning perspective proposed by Young et al., (2020) as a mechanism for how environmental unpredictability can be described and influence developmental outcomes. More specifically, this theory does not take into account the developmental timing and sources of exposures to environmental unpredictability and does not address the specific biological or cognitive mechanisms that mediate response to unpredictability beyond the suggestion that cue-reliability and prediction error may be involved.

Neuro-Computational Model for the Influence of Maternal Sensory Unpredictability on Cognitive and Emotional Outcomes

Aside from both the literature of maternal sensory unpredictability and the developmental-evolutionary statistical learning theory of Ellis et al., (2009) and Young et al., (2020) there is a rich literature describing the cognitive, computational, and neurobiological mechanisms of prediction error. Incorporating or coalescing these literatures with the findings of maternal sensory unpredictability has important implications when considering anhedonia as a primary outcome of exposure to unpredictability in early life.

The historical roots of this literature are embedded in reinforcement learning (Rescorla & Wagner, 1972) and the role of dopamine (DA) in computing a reward prediction error (RPE; the difference between an actual and expected reward; Schultz, 2016). Generally speaking, dopaminergic neurons in the ventral tegmental area (VTA) are known to increase their firing rate when a reward occurs without a prediction, maintain firing rates in response to a reward that was predicted but increase firing in response to the cue signaling the reward, and decrease their firing rate in response to the absence of a reward when it is expected (Schultz et al., 1997; Schultz, 1997; Schultz, 2016; Watabe-Uchida et al., 2017). In addition, as greater time elapses between the reward-predicting cue and reward, dopaminergic response to the cue is reduced--a phenomenon known as temporal discounting (Kobayashi & Schultz, 2008). These firing rate properties and prediction error mechanisms are thought to facilitate new learning and adaptive responses when predictions are not met. It is important to note that recent research of the prediction error calculating properties of these dopaminergic neurons suggest that dopamine acts as a generalized prediction error

mechanism (all sensory prediction errors) and not necessarily dependent on the associational binding of rewarding stimulus (Gardner et al., 2018).

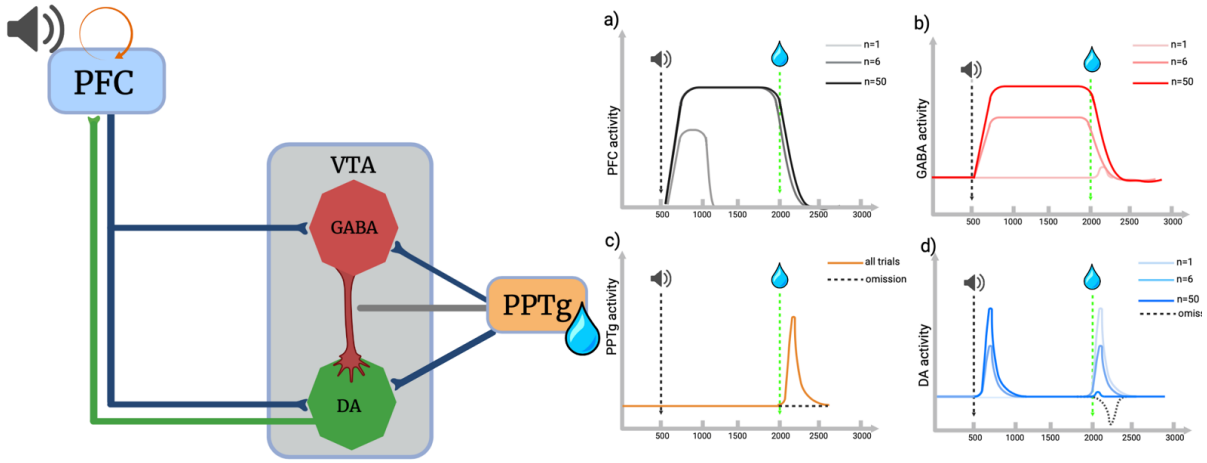

Figure 15. Simplified computational model for reward prediction error (adapted from Deporrois et al., 2019). (a) Shows the recurrent excitation of PFC signaling the response to the conditioned stimulus. After many trials, (n = 50) the PFC is able to hold the response to the cue (tone) for an interval delay until the outcome (water reward in this case) is presented (b) Shows GABA neurons activation to inhibit DA activity. (c) Shows PPTg activity signaling the presentation of reward (d) DA VTA neurons compute a subtraction between actual and expected reward and are regulated by GABAergic VTA neurons. Here "n" refers to the number of trials or pairings of associated stimuli (tone and water delivery). This functional neuronal network is able to replicate and produce the dopaminergic activity when a reward presentation is not predicted (n=1; DA neurons increase there firing in response to reward). After some predictable pairings of cue and reward, DA neurons shift their response to an 'expectation' signal firing in response to the cue predicting the reward (n = 50). When the reward is omitted, DA neurons reduce their firing rate. This model serves as an example of how (un)predictability engages the reward system.

There have been several computational models proposed to explain the prediction error firing properties of these neurons, many of which incorporate the associational binding of neutral cues and rewarding outcomes. A recently proposed computational model for RPE firing suggests an integration of important upstream regions and local inhibitory dynamics that influence the responsivity of RPE neurons in the ventral tegmental area (VTA). The model by Deporrois and colleagues incorporates the dynamics of four neuronal populations including "glutamatergic (from PFC and

PPTg) and cholinergic (from PPTg) inputs to VTA DA and GABA neurons, as well as local inhibition of DA neurons by GABA neurons" which are thought to "encode reward expectations with a persistent cue response proportional to the expected reward" (Deporrois et al., 2019; Cohen et al., 2012; Eshel et al., 2015; Tian et al., 2016). Put simply, the PFC explicitly integrates the reward predicting stimulus (i.e. a tone) while the PPTg responds phasically to the reward itself (i.e. a water reward). Recurrent-excitation of the PFC mimics electrophysiological recordings in monkeys during delayed-match-to-sample tasks where the PFC maintains its activity to the cue until the subsequent stimulus is presented thus maintaining the cue in working memory (Funahashi et al., 1989).

Both of these signals converge on VTA DA neurons that compute the difference (subtraction) between the actual and expected rewards or outcomes. GABAergic neurons in the VTA aid DA neurons by inhibiting DA neurons when a reward is expected (Eshel et al., 2015). DA VTA neurons themselves then synapse on the PFC to provide a negative feedback loop which modulates PFC recurrent excitation. Using this network architecture and optogenetic simulation, Deporrois and colleagues provide evidence that this simplified network is able to reproduce many of the firing properties of RPE DA neurons. It is important to note that this is only one model of many that work to compute RPE responses and there are certainly more regions involved in its calculation. Thus, both predictability and unpredictability engage the reward system, however, the history of cue-reliability or cue-outcome pairings shifts the dynamics of the reward system to act as an expectation signal (firing in response to the cue with learning) or error signal.

With respect to the neuro-computational model of prediction error described above, one possibility is that unpredictable maternal sensory signals during sensitive periods of brain development result in impaired synaptic tuning of the prediction error mechanisms that involve the reward system described above. In other words, perhaps cue-reliability or cue-outcome predictability is necessary for the tuning of neurons that are involved in prediction error signaling. This type of consideration is interesting considering the link between maternal sensory unpredictability and anhedonia in animals as measured by sucrose preference and social play (Bolton et al., 2018b; Molet et al., 2018) as well as impaired reward learning as measured by performance on a probabilistic reward learning task (Kangas et al., 2022).

The idea that early life experience results in synaptic tuning and modification of neurons to respond to specific input comes from the Nobel Award winning work of Hubel & Wiesel (1959;1962) which provided the first basis for the notion that the development of feature selectivity (the ability of neurons to respond to specific patterns of input such as lines of a particular orientation or sounds of a specific frequency) in visual and auditory systems are dependent on visual and auditory input (respectively) during critical periods. Bienenstock, Cooper, and Munro (BCM; Bienenstock, et al., 1982; Law & Cooper,1994) proposed one of the most poignant and lasting mathematical theories for the development of feature selectivity in visual cortex indicating that a combination of long-term potentiation and long-term depression facilitate the developmental change from low feature selectivity (before environmental input or in the case of monocular deprivation) to high feature selectivity (after environmental input or when the eye is receiving sequences of patterns of different line

orientation). In this manner, the BCM theory provides a distinguishable benefit from Hebbian-based plasticity mechanisms by providing a mechanism for some connections to become weaker and creates an upper-bound for how strong connections can become (cells that fire together, wire together but not indefinitely). An example simulation derived from the BCM Theory is shown in Figure 16.

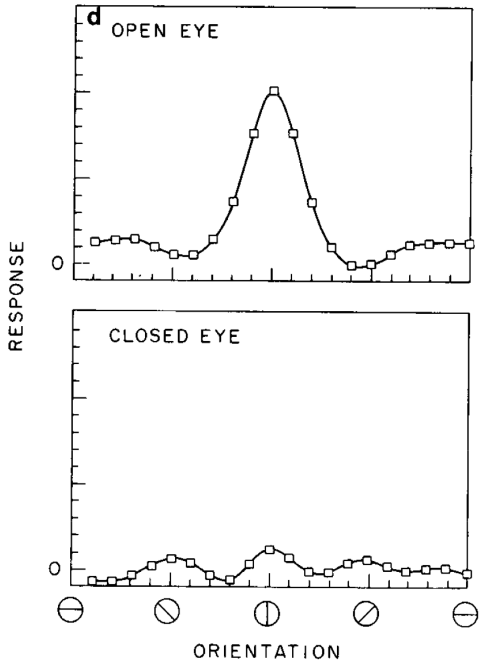

Figure 16. Adapted from Bienenstock, Cooper, and Munro (1982). An example of the functionality of the BCM-theory in developing feature selection of neurons in the visual cortex. This mathematical formulation is able to replicate the development of feature selectivity through experience dependent 'tuning' of cortical neurons that respond to lines of particular orientation but not other lines. Before learning (or in the example of the closed eye), there is very low feature selectivity for any line orientation. After learning (in the example of the open eye) and as a result of tuning via the BCM theory the neuron increases its response to a particular (in this case) vertical line (via LTP) while selectivity reducing its firing rate to lines of similar but different line orientations (via LTD). This model was proposed to address the saturation issue of Hebbian Plasticity; where there is no proposed mechanism to selectivity weaken synapses.

In the case of an infant exposed to maternal sensory unpredictability (where the probability of transitioning from one behavior to another is low), one possibility is that

there is also a relative deficit in cue-outcome pairings (a deficit in cue-reliability) or an array of other behaviors following a given behavior resulting in a lack of timely cue-outcome pairing over time in early infancy (Figure 17a). Baram et al., 2013 outline this conceptualization providing the example that measuring maternal unpredictability is similar to asking “whether smiling always follows eye contact (in humans) or grooming always follows nursing (in rodents)”. Thus, as feature selectivity of visual and auditory system is dependent on environmental input of patterns of lines and tones, perhaps the development of feature selectivity of the prediction error system (where the evolved feature is to integrate sensory input through learning and calculate prediction errors) might require predictable environmental signals to develop the ability to properly organize and respond to the statistics of the environment.

Going back to the model proposed by Deporrois et al., (2019), a functioning adult-like prediction error system integrates the associational binding of cues and outcomes over time and “holds them” in working memory via the prefrontal cortex after a history of cue-outcome pairings. In other words, consistent cue-outcome or cue-reward parings or a large number of trials (n=50; Figure 15a) are needed for the PFC to “learn” to hold this recurrent excitatory activity. One possibility is that during early development the lack of cue-reliability through intervening stimuli may result in an inability of the prediction error circuitry to develop the feature selectivity of responding and holding cues in working memory thus interrupting the recurrent-excitation and attractor state of the PFC (see Figure 17b curves for “Normal PFC Recurrent Activity” vs. “Interrupted PFC Recurrent Activity: High Entropy Mothers”).

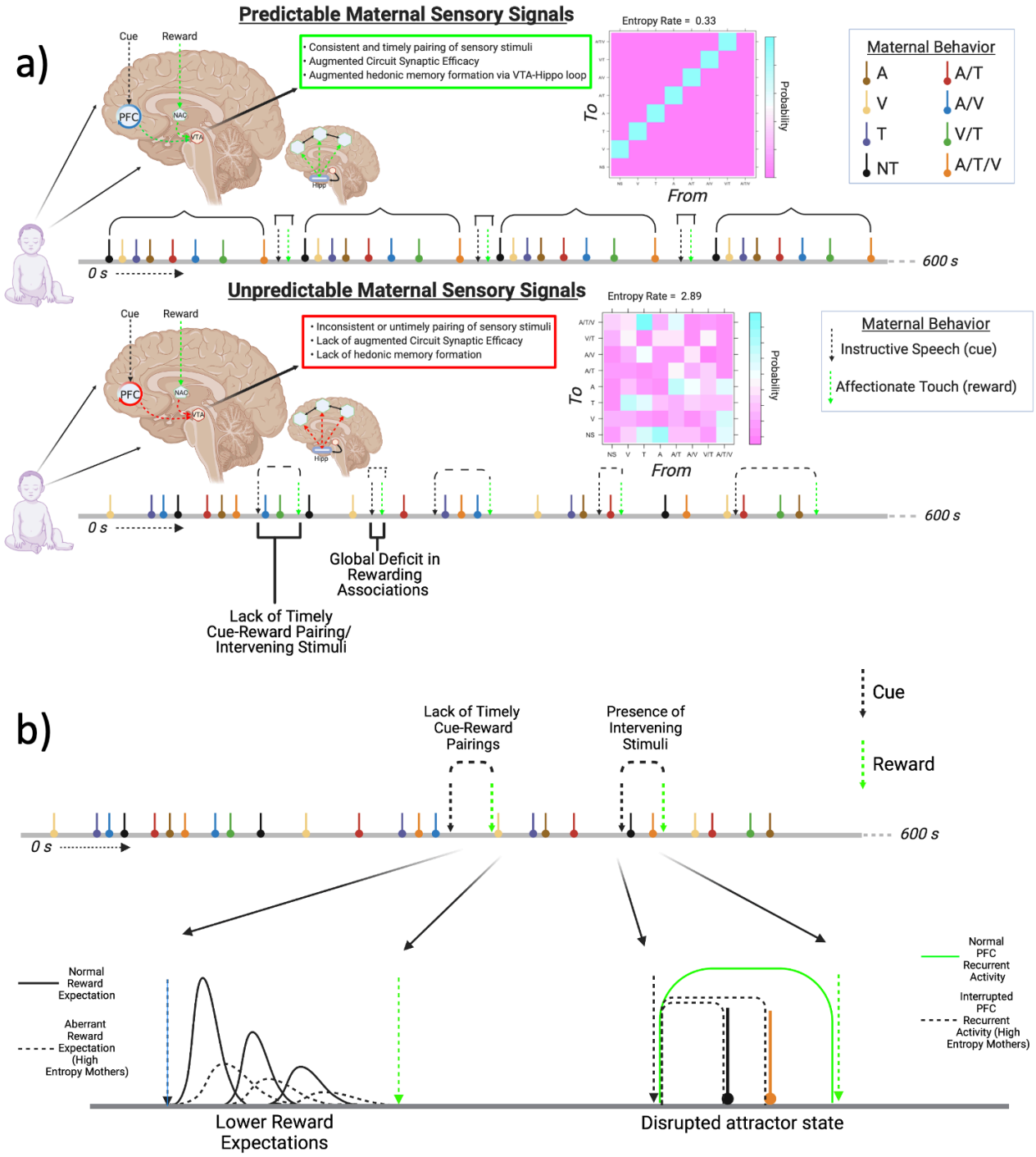
a)
Predictable Maternal Sensory Signals
Cue
Reward
PFC
NAC
VTA
Hipp
• Consistent and timely pairing of sensory stimuli
• Augmented Circuit Synaptic Efficacy
• Augmented hedonic memory formation via VTA-Hippo loop
Entropy Rate = 0.33
To
From
Probability
Maternal Behavior
A
A/T
V
A/V
T
V/T
NT
A/T/V
0 s
600 s
Unpredictable Maternal Sensory Signals
• Inconsistent or untimely pairing of sensory stimuli
• Lack of augmented Circuit Synaptic Efficacy
• Lack of hedonic memory formation
Entropy Rate = 2.89
Maternal Behavior
Instructive Speech (cue)
Affectionate Touch (reward)
Global Deficit in Rewarding Associations
Lack of Timely Cue-Reward Pairing/ Intervening Stimuli
b)
Lack of Timely Cue-Reward Pairings
Presence of Intervening Stimuli
Cue
Reward
Normal Reward Expectation
Aberrant Reward Expectation (High Entropy Mothers)
Normal PFC Recurrent Activity
Interrupted PFC Recurrent Activity (High Entropy Mothers)
Lower Reward Expectations
Disrupted attractor state

Figure 17. (a) The Top Panel shows predictable (low entropy) maternal sensory input to the infant. Here the probability of transitioning from any given behavior to another behavior is high. In the probability matrix, 'A' represents an auditory stimulus, 'T' represents a tactile stimulus, 'V' represents a verbal stimulus, and 'NS' represents "no state". Combinations of these behaviors are also included as a discrete event. It is possible that predictable mothers provide predictable sensory cues and sensory outcomes (in this example the sensory outcome is a rewarding stimulus) over early development. This predictability between cue and outcome engages the prediction error mechanisms of the brain to 'tune', develop feature selectivity, and detect and respond to prediction error accordingly. The Bottom Panel shows an unpredictable (high entropy) mother. Here, an infant exposed to an unpredictable mother may be exposed to a relative global deficit in cue-outcome pairings or a lack of timely cue-outcome pairings via intervening stimuli. This may be a likely possibility given that the probability of transitioning from one behavior to another is low across the transition probability matrix from which entropy is calculated. The outcome is the possibility of an attenuated synaptic efficacy of reward circuits involved in prediction error. (b) This panel explores the change in synaptic tuning of specific components of the prediction error system as a result of experiencing a lack of timely cue-outcome (cue-reward) pairings and presence of intervening stimuli via a low probability of transitioning from one behavior to another. Here two overlapping possibilities may exist where infants with high entropy mothers may be exposed to the presence of intervening stimuli thereby disrupting prefrontal cortex (PFC) recurrent excitation that 'learns' to look for the corresponding outcome. The lack of timely cue-outcome pairing might also impair the ability of dopaminergic neurons to 'shift' their activity to respond to cues that signal an expected outcome.

As mentioned previously, it is also possible that maternal sensory unpredictability results in a lack of timely cue-outcome (or cue-reward) pairing as a result of experiencing a large probability of other behaviors given any single behavior. One aspect of this notion is the potential for a variable time interval between cue stimulus and the time elapsed between the outcome which may result in an inability to learn about the structure of events (including rewards) more generally. Evidence for this has been shown in animal studies where rodents working under variable-interval reinforcement schedules failed to learn the timing and predictability of a reward over time whereas rodents working under the fixed-interval schedule did learn the timing of reward (Hernandez et al., 2007). Thus, perhaps what is being adapted as a result of exposure to somatosensory unpredictability is the tuning curves that specify the temporal window between cue and outcome.

Fiorillo et al., (2008) describe the temporal precision of reward prediction in dopamine neurons suggesting that individuals are able to respond to rewards at

variable times after cue presentation. Fiorillo and colleagues suggests that there is a 'basis set' of temporal windows that enable reward expectation at different time intervals. These time intervals resemble a gamma function where there is a robust neuronal 'expectation signal' to rewards near the cue presentation, then smoothly tailing off as time goes on (see Figure 17b curve for "Normal Reward Expectation'). In this case, individuals are most sensitive to rewards presented not too quickly but also not too long after the presentation of the reward-predicted cue. These neurons are only activated through the shifting of dopaminergic activity towards the actual onset time of the cue after learning (n = 50 from Figure 15d).

Together then perhaps during the critical period of dopaminergic development (when maternal sensory signals are thought to impact reward responsiveness) the "default" shape of these temporal windows are adjusted or adapted. If reliable pairings are less likely, this shape will have a less-pronounced peak and fatter/longer tails (see Figure 17b curve for "Aberrant Reward Expectation: High Entropy Mothers"). This notion is similar to the lack of proper environmental input in the development of visual feature selectivity (Figure 16). This developmental framework and incorporation of prediction error mechanisms in maternal sensory unpredictability could predict a few things. First, that individuals exposed to maternal sensory unpredictability may generally develop persistently lower reward expectations as evidence by reduced dopaminergic activity in response to a lack of timely cue-outcome pairings (Figure 17b curve for "Aberrant Reward Expectation: High Entropy Mothers"). In this case, the tuning or feature selectivity of the prediction error neurons may be compromised over development. In other words, it's possible that unpredictability which induces a relative deficit in cue-

outcome pairings results in an inability or reduction in the ability of dopamine neurons to 'shift' their response to respond to the cue and predict the outcome.

Second, this developmental framework and incorporation of prediction error could describe a mechanism where individuals exposed to maternal sensory unpredictability may be impaired in learning the structure of transitions more generally. Rouhani et al., (2020) provide evidence that reward prediction errors create event boundaries in memory and were among the first to hypothesize that these RPE-induced event boundaries lead to mnemonic separation (facilitated by the DG) of subsequent experiences from what came before (Rouhani et al., 2020). This fits well with the notion that a prediction error results in the need for an adaptive response or for new learning to occur. In adults, it is hypothesized that people adjust their learning rates to the overall volatility of the environment which consequently blunts prediction errors in noisy (unpredictable) environments and enhances prediction errors in stable (predictable) environments (Behrens et al., 2007). Thus, in an unpredictable early life environment (where volatility is high) perhaps the sensitivity to naturally-occurring event boundaries is reduced (Siefke et al., 2019). When event boundaries are highly uncertain, the contingency between actions and outcomes is also highly unpredictable which results in persistently lowered expectations of reward. Thus, when large rewards are received, they are taken to be isolated, non-contingent events, with little predictive value for future gain (effectively discounting future rewards). Jiang et al., (2015) outline the possibility that when transition structure is more uncertain it becomes more optimal to plan fewer steps ahead — in other words, to have a steep discount factor. Thus, either of these above models predicts less "lookahead" activity in these subjects, and commensurate

effects on risk-seeking and exploration commiserate with the findings of Ross & Hill (2002) mentioned in the introduction of this Dissertation.

Critically, this developmental and neuro-computational framework that bridges the literature of maternal sensory unpredictability and the statistical learning theory of Ellis et al., (2002) and Young et al., (2020) has important implications as an explanatory factor for developing the outcome symptom of anhedonia in Major Depression which has a similar behavioral phenotype.

For instance, adult subjects with depression underestimate the frequency of positive feedback and reinforcement received over time (Nelson & Craighead, 1977; Pizzagalli, 2014). Similarly, children expressing greater depressive symptoms showed decreased ratings of the probability of positive events happening in the future when events referred to the self (Muris & van der Heiden, 2006). In a sample of adults with depression, subjects predicted fewer positive outcomes in the future, relative to controls and those with anxiety (Miranda & Mennin, 2007). Pizzagalli (2014) suggests that depressed subjects contain “a perception of the past which is characterized by an underestimation of positive reinforcements received, whereas their future is colored by a reduced expectation of positive reinforcement”. Together, the developmental mechanisms described above which provide a link between maternal sensory unpredictability and (reward) prediction error are a possible and important feature given that not receiving expected reward has been extensively tied to depression as well as the amygdala-prefrontal cortex connection (Rolls, 2016; Holland & Gallagher, 2004; Beck, 2008; Drevets, 2007; Eshel & Roiser, 2010; Harmer & Cowen, 2013; Price, 2012).

To conclude, a single work that coalesces the ideas of how the brain detects

unpredictability and a consideration of how unpredictability impacts the development of the reward circuits responsible for prediction error and their link to anhedonia as a specific outcome is not currently represented in the literature. The union of these ideas may also have important implications for the altered development of some circuits but not others. It is also important to note that the plasticity mechanism mentioned above is not mutually exclusive from other works that highlight the role of CRF in the plasticity of the reward system as a result of exposure to early life maternal unpredictability (Birnie et al., 2019). The plasticity mechanism mentioned above is also complementary to work that has made analogy between the hierarchical nature of visual, auditory, and memory circuit development and the impact of somatosensory unpredictability in shaping the development of emotional brain systems (Birnie & Baram, 2022; Birnie et al., 2019). One future direction based on this Dissertation would be to provide such an amalgamation as it has important implications for the field of neuropsychiatry and the pathophysiology of mental illness.

Uncinate Fasciculus Associated with DG/CA3 Activity During Emotional Pattern Separation

In Chapter 2 of this Dissertation, emphasis was placed on the cingulum bundle which shares the role of connecting the MTL with the PFC. In Chapter 2, because the functional output of brain circuits is a combinatorial sum of the activity of each of their components (Redish & Gordon, 2017), we also conducted analyses using the ratio of uncinate to hippocampal cingulum connectivity as a measure of imbalance across these two pathways. In Chapter 3 of this Dissertation, we asked if the relationship between

greater uncinate fasciculus integrity and reduced DG/CA3 activity during emotional lure discrimination was a general feature of white matter connectivity. We found that corpus callosum integrity did not predict DG/CA3 activity during highly similar lure discrimination for any emotional valence.

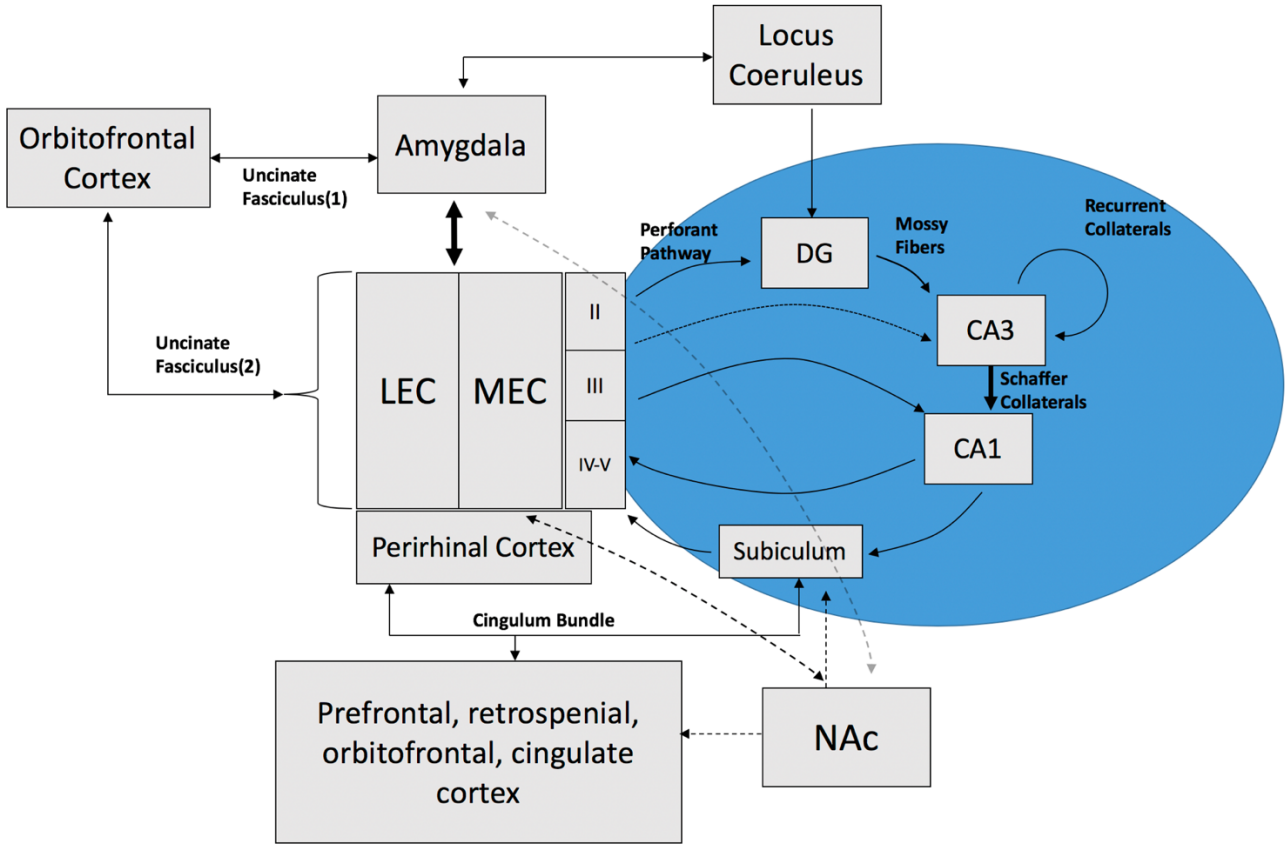

Figure 18. Summary of circuitry under investigation in this work. Results of Chapter 2 provide evidence for the link between experiencing early life maternal sensory unpredictability and imbalanced uncinate fasciculus-hippocampal cingulum integrity. Results of Chapter 3 show the link between reduced uncinate fasciculus integrity and greater DG/CA3 activity during emotional lure discrimination. Appendix B investigates the integrity of MTL gray matter nodes in older adults. Appendix C investigates the structural connectivity within the MTL including a novel approach at detecting the perforant pathway using diffusion imaging.

Despite this nuance, it would be interesting to consider a more comprehensive approach to disentangling the contributions of the uncinate fasciculus and cingulum

bundle and their subcomponents to episodic memory processes and regions depicted in Figure 18. Using diffusion spectrum imaging of the uncinate fasciculus, one investigation was able to identify and parse 2 predominant fanning sections of the uncinate fasciculus that terminate in different areas within the frontal segment. This investigation provided evidence that the cortical innervation of the uncinate fasciculus to and from the temporal lobe includes the middle frontal gyrus including Brodmann's areas 10 and 11 and the inferior frontal gyrus including the pars triangularis (Brodmann's area 45) and the pars orbitalis (Brodmann's area 47), excluding the pars opercularis (Brodmann's area 44; Leng et al., 2016). Histological evidence has shown that in the temporal lobe the uncinate fasciculus is thought to innervate the temporal pole including the basolateral amygdala, perirhinal, and the rostrolateral entorhinal cortex (Ebeling & Von Cramon, 1992; Von Der Heide et al., 2013; Thiebaut et al., 2012; Leichnetz & Astruc, 1975).

In comparison, the cingulum is connected to a wide array of cortical regions including the orbitofrontal, prelimbic, anterior cingulate, and retrospenial cortices (Bubb et al., 2018). Within the MTL, histological evidence has shown that the cingulum fibers innervate the subiculum, CA1, medial entorhinal, parahippocampal, and perirhinal cortices (Figure 15; Bubb et al., 2018; Wouterlood et al., 1990). From the perspective of diffusion weighted imaging, some investigators have proposed to divide the cingulum into several distinct portions. Budisavljevic et al., (2015) suggest that the cingulum can best be divided into a dorsal and ventral component. The dorsal component reflecting the white matter connecting the cingulate gyrus and the ventral component being composed of the hippocampal cingulum both subcomponents however include fibers

projecting toward the retrosplenial cortex. Jones et al., (2013) suggest the cingulum can be divided into three units that represent different bundles along both the anterior-posterior and medial-lateral axis. These three subdivisions include the subgenual (located anterior, medial, and dorsal in comparison to the retrosplenial), retrosplenial (located posterior and ventral in comparison to the subgenual), and parahippocampal division (located along the hippocampal axis projecting to the retrosplenial cortex when restricted and anterior cingulate when unrestricted; Jones et al., 2013). Some histological evidence suggests that almost all prefrontal regions contribute at least some fibers to the cingulum (Heilbronner & Haber, 2014; Bubb et al., 2018). Fiber tracing studies in marmoset monkeys provide evidence that the orbitofrontal cortex fibers projected through the uncinate fasciculus but also joined the cingulum bundle (Leichnetz & Astruc, 1974). Together, this work highlights the two routes in the marmoset by which the prefrontal cortex reaches the entorhinal and subicular areas; the first being the uncinate fasciculus projecting to the lateral entorhinal cortex (among others) and the second being the cingulum which projects to the medial entorhinal cortex and subiculum (among others; Leichnetz & Astruc, 1974).

Other researchers in the field have outlined the relative contributions of the prefrontal cortex inputs to the medial temporal lobe in the context of episodic memory performance proposing the Posterior-Medial Anterior-Temporal (PMAT) Framework (Ritchey et al., 2015; Ranganath & Ritchey, 2012). This framework suggests that the contributions of the posterior-medial system (connected via the cingulum) and the anterior-temporal system (connected via the uncinate) subserve distinct roles in memory processing and cognition. More specifically, the PMAT Framework suggests

that the posterior-medial system (composed of the parahippocampal cortex, medial entorhinal cortex, retrosplenial cortex, precuneus, angular gyrus, anterior thalamus, medial prefrontal cortex, and cingulate cortex) has extensively been linked to memory for the context of an event or the memory for spatial information (Norman & Eacott, 2005; Vann & Aggleton, 2002; Libby et al., 2014; Reagh & Yassa, 2014; Ritchey et al., 2015). Conversely, the anterior-temporal system (composed of the anterior temporal cortex, lateral entorhinal cortex, perirhinal cortex, amygdala, and orbitofrontal cortex) is thought to be involved in visual object or item recognition, associative memory, and affective processing (Ritchey et al., 2015). As mentioned in Chapter 1 of this Dissertation, our laboratory previously investigated the dissociable function of the medial and lateral entorhinal cortex providing some of the first evidence in humans that the medial entorhinal cortex is involved in the mnemonic discrimination of spatial lure items whilst the lateral entorhinal cortex is involved in taxing the mnemonic discrimination of objects (Reagh & Yassa, 2014). This dissociation also extended to perirhinal and parahippocampal cortex whilst the DG/CA3 demonstrated signals consistent with resolution of mnemonic interference across domains. Importantly, the PMAT framework mentioned above does not consider or mention the possible impact of differences in integrity of the nuanced white matter subserving this dissociation and instead focuses on the role of each gray matter region.

In considering this framework, one future direction stemming from the work of this Dissertation would be to reproducibly and systematically parse subcomponents of the uncinate and cingulum using advanced DWI methods including high-spatial high-angular resolution images, and quantitative anisotropy informed tractography. If these

bundles and their subcomponents can be parsed reproducibly, it would be interesting to test their roles in supporting both spatial and object mnemonic discrimination processes and what subcomponents might be more influential in each condition. If this could be accomplished one could ask: which component of uncinate morphology (the middle frontal gyrus and inferior frontal gyrus subdivisions) and cingulum morphology (the subgenual, retrosplenial, parahippocampal subdivisions) might contribute to spatial or object mnemonic discrimination processes? Does integrity of the restricted parahippocampal division of the cingulum which connects the MTL with retrospenial cortex contribute more to spatial mnemonic discrimination processes than the unrestricted parahippocampal division which extends to the prefrontal cortex? In addition, it would be interesting to know if differences in uncinate fasciculus or cingulum microstructural or macrostructural integrity would impact the activation of not only the DG/CA3 subfield but also the lateral and medial entorhinal cortices using a task that manipulates emotional valence, as well as object and spatial lure discrimination. One approach would be to pursue these kinds of questions with adapted high resolution diffusion imaging methods similar to those of Appendices B-C. In general, investigations involving both the uncinate fasciculus and cingulum in episodic memory function rarely co-occur and further study is an exciting research direction based on the findings of this Dissertation.

Conclusion

To conclude, this work provides evidence that an imbalance of MTL-PFC connectivity is associated with a novel operationalization or form of early life adversity and mediates the association of this early life adversity with episodic memory impairment where adjudication between stimuli is necessary. This Dissertation then provides the first evidence that uncinate fasciculus integrity is associated with DG/CA3 subfield activity during the mnemonic discrimination of highly similar emotional (stimuli of the positive and negative valence) but not neutral stimuli. Together, this work mobilizes new and exciting research avenues within the discipline of diffusion weighted MRI and applies them to concepts within the fields of early life adversity and episodic memory.

While not a direct link to the work at hand, the Appendices provided in this document are influenced by Chapters 2 and 3 and in some fashion might inform future research in the work described here. This work is able to provide insight into the structure and function of gray matter nodes of the MTL as a function of age. The published work in Appendix A recognizes the comorbidity of memory dysfunction in clinical populations and the influence of symptoms clusters (negative affect, anhedonia, somatic anxiety, and cognitive anxiety) on episodic memory performance in clinical populations. Together, with the addition of Appendices A-C, this work provides a comprehensive example of the impact of diffusion weighted MRI in transdiagnostic neuroscience research and yields new insights to the etiology of cognitive and emotional impairment associated with exposure to early life adversity.

References

Ahun, M. N., Gapare, C., Gariépy, G., & Côté, S. M. (2021). Sex differences in the association between maternal depression and child and adolescent cognitive development: a systematic review and meta-analysis. *Psychological medicine*, 51(9), 1431–1440.

Ainsworth, M. D. S., Bell, S. M., & Stayton, D. F. (1974). Infant-mother attachment and social development: Socialization as a product of reciprocal responsiveness to signals. In M. P. M. Richards (Ed.), *The integration of a child into a social world* (pp. 99–135). Cambridge University Press.

Ainsworth, M. D., & Bell, S. M. (1970). Attachment, exploration, and separation: illustrated by the behavior of one-year-olds in a strange situation. *Child development*, 41(1), 49–67.

Ainsworth, M., Blehar, M., Waters, E., & Wall, S. (1978). Patterns of attachment: A psychological study of the strange situation. Hillsdale, NJ: Erlbaum.

Alexander, A.L., Hasan, K.M., Lazar, M., Tsuruda, J.S., Parker, D.L. (2001). Analysis of partial volume effects in diffusion-tensor MRI. *Magn Reson Med*, 45:770–780.

Alexander, A.L., Hurley, S.A., Samsonov, A. A., Adluru, N., Hosseinbor, A. P., Mossahebi, P., Tromp do P. M., Zakszewski E., Field, A. S. (2011). Characterization of cerebral white matter properties using quantitative magnetic resonance imaging stains. *Brain Connectivity*, 1: 423–46.

Alexander, A.L., Lee, J.E., Lazar, M., Field, A.S. (2007). Diffusion tensor imaging of the brain. *Neurotherapeutics: the journal of the American Society for Experimental Neuro Therapeutics,* 4: 316–329.

Alm, K.H., Rolheiser, T., Olson, I. R. (2016). Inter-individual variation in fronto- temporal connectivity predicts the ability to learn different types of associations. *Neuroimage*, 132:213–224.

Anda, R. F., Croft, J. B., Felitti, V. J., Nordenberg, D., Giles, W. H., Williamson, D. F., & Giovino, G. A. (1999). Adverse childhood experiences and smoking during adolescence and adulthood. *JAMA*, 282(17), 1652–1658.

Anda, R. F., Felitti, V. J., Bremner, J. D., Walker, J. D., Whitfield, C., Perry, B. D., Dube, S. R., & Giles, W. H. (2006). The enduring effects of abuse and related adverse experiences in childhood. A convergence of evidence from neurobiology and epidemiology. *European archives of psychiatry and clinical neuroscience*, 256(3), 174–186.

Andersen, S. L., Teicher, M. H. (2008). Stress, sensitive periods and maturational events in adolescent depression. *Trends Neurosci,* 31:183–191.

Andersson, J. L., Skare, S., Ashburner, J. (2003). How to correct susceptibility distortions in spin-echo echo-planar images: application to diffusion tensor imaging. *Neuroimage*, 20:870–88.

Andersson, J. L. R., Sotiropoulo, S.N. (2016). An integrated approach to correction for off-resonance effects and subject movement in diffusion MR imaging. *Neuroimage,* 125:1063–1078.

Arp, J. M., Ter, Horst, J.P., Loi, M., den Blaauwen, J., Bangert, E., Fernández, G. (2016). Blocking glucocorticoid receptors at adolescent age prevents enhanced freezing between repeated cue-exposures after conditioned fear in adult mice raised under chronic early life stress. *Neurobiology of Learning and Memory*, 133:30–38.

Asato, M.R., Terwilliger, R., Woo, J., Luna, B. (2010). White matter development in adolescence: a DTI study. *Cereb Cortex,* 20:2122–2131.

Avants, B. B., Tustison, N. J., Song, G., Cook, P. A., Klein, A., & Gee, J. C. (2011). A reproducible evaluation of ANTs similarity metric performance in brain image registration. *NeuroImage*, 54, 2033–2044.

Bagot, R. C., Labonté, B., Peña, C. J., Nestler, E. J. (2014). Epigenetic signaling in psychiatric disorders: stress and depression. *Dialogues Clin Neurosci,* 6:281–95.

Bakker, A., Kirwan, C.B., Miller, M. Stark, C.E. (2008). Pattern separation in the human hippocampal CA3 and Dentate gyrus. *Science*, 219: 1640-1642.

Balderston, N. L., Mathur, A., Adu-Brimpong, J., Hale, E. A., Ernst, M., Grillon, C. (2017) Effect of anxiety on behavioural pattern separation in humans. *Cogn. Emot.,* 31 (2), 238–248.

Bale T. L. (2011). Sex differences in prenatal epigenetic programming of stress pathways. *Stress*, 14(4), 348–356.

Bale, T. L., Baram, T. Z., Brown, A. S., Goldstein, J. M., Insel, T. R., McCarthy, M. M., Nemeroff, C. B., Reyes, T. M., Simerly, R. B., Susser, E. S., Nestler, E. J. (2010). Early life programming and neurodevelopmental disorders. *Biol Psychiatry,* 68: 314–319.

Baram, T. Z., Davis, E. P., Obenaus, A., Sandman, C. A., Small, S. L., Solodkin, A., Stern, H. (2012) Fragmentation and unpredictability of early-life experience in mental disorders. *Am J Psychiatry,* 169:907–915.

Baram, T. Z., Solodkin, A., Davis, E., Stern, H., Obenaus, A., Sandman, C. A., & Small, S. L. (2013). Fragmentation and Unpredictability of Early-Life Experience in Mental Disorders. *American Journal of Psychiatry*, 169(9), 907–915.

Bath KG, Nitenson AS, Lichtman E, Lopez C, Chen W, Gallo M, Goodwill H, Manzano-Nieves G (2017) Early life stress leads to developmental and sex selective effects on performance in a novel object placement task. *Neurobiol Stress*, 7:57–67.

Beck, A. T. (2008). The evolution of the cognitive model of depression and its neurobiological correlates. *The American journal of psychiatry*, 165(8), 969–977.

Beck, C. T. (1998). The effects of postpartum depression on child development, *Arch Psychiatr Nurs*, 12: 12–20.

Behrens, T. E., Woolrich, M. W., Walton, M. E., & Rushworth, M. F. (2007). Learning the value of information in an uncertain world. *Nature neuroscience*, 10(9), 1214–1221.

Belsky, J., Schlomer, G. L., & Ellis, B. J. (2012). Beyond cumulative risk: distinguishing harshness and unpredictability as determinants of parenting and early life history strategy. *Developmental psychology*, 48(3), 662–673.

Bennett, I. J., Huffman, D. J., & Stark, C. E. L. (2015). Limbic Tract Integrity Contributes to Pattern Separation Performance Across the Lifespan. *Cerebral Cortex*, 25, 2988–2999.

Bhatia, K., Henderson, L., Yim, M., Hsu, E., Dhaliwal, R. (2017). Diffusion tensor imaging investigation of uncinate fasciculus anatomy in healthy controls: description of a subgenual stem. *Neuropsychobiology,* 75:132–140.

Bhatia, K. D., Henderson, L., Ramsey-Stewart, G., May, J. (2012). Diffusion tensor imaging to aid subgenual cingulum target selection for deep brain stimulation in depression. *Stereotact. Funct. Neurosurg.,* 90:225–232.

Bhatia, K. D., Henderson, L. A., Hsu, E., Yim, M. (2018). Reduced integrity of the uncinate fasciculus and cingulum in depression: a stem-by-stem analysis. *J Affect Disord*, 235:220–228.

Bienenstock, E. L., Cooper, L. N., & Munro, P. W. (1982). Theory for the development of neuron selectivity: orientation specificity and binocular interaction in visual cortex. *The Journal of neuroscience: the official journal of the Society for Neuroscience*, 2(1), 32–48.

Birnie, M. T., Kooiker, C. L., Short, A. K., Bolton, J. L., Chen, Y., Baram, T. Z. (2020) Plasticity of the Reward Circuitry After Early-Life Adversity: Mechanisms and Significance. *Biol Psychiatry*, 15;87:875-884.

Birnie, M. T., & Baram, T. Z. (2022). Principles of emotional brain circuit maturation. *Science*, 376(6597), 1055–1056.

Blair, C., & Raver, C. C. (2016). Poverty, Stress, and Brain Development: New Directions for Prevention and Intervention. *Academic pediatrics*, 16(3 Suppl), S30–S36.

Bohacek, J., Mansuy, I. M. (2016). Epigenetic Risk Factors for Diseases: A Transgenerational Perspective. *Epigenetics Neuroendocrinol*. Springer International Publishing; pp. 79–119.

Bolton, J. L., Molet, J., Regev, L., Chen, Y., Rismanchi, N., Haddad, E., Yang, D. Z., Obenaus, A., & Baram, T. Z. (2018a). Anhedonia Following Early-Life Adversity Involves Aberrant Interaction of Reward and Anxiety Circuits and Is Reversed by Partial Silencing of Amygdala Corticotropin-Releasing Hormone Gene. *Biological psychiatry*, 83(2), 137–147.

Bolton, J. L., Ruiz, C. M., Rismanchi, N., Sanchez, G. A., Castillo, E., Huang, J., Cross, C., Baram, T. Z., & Mahler, S. V. (2018b). Early-life adversity facilitates acquisition of cocaine self-administration and induces persistent anhedonia. *Neurobiology of stress*, 8, 57–67.

Bolton, J. L., Schulmann, A., Garcia-Curran, M. M., Regev, L., Chen, Y., Kamei, N., Shao, M., Singh-Taylor, A., Jiang, S., Noam, Y., Molet, J., Mortazavi, A., & Baram, T. Z. (2020). Unexpected Transcriptional Programs Contribute to Hippocampal Memory Deficits and Neuronal Stunting after Early-Life Adversity. *Cell reports*, 33(11), 108511.

Bolton, J. L., Short, A. K., Simeone, K. A., Daglian, J., & Baram, T. Z. (2019). Programming of Stress-Sensitive Neurons and Circuits by Early-Life Experiences. *Frontiers in behavioral neuroscience*, 13, 30.

Bos, K. J., Fox, N., Zeanah, C. H., & Nelson Iii, C. A. (2009). Effects of early psychosocial deprivation on the development of memory and executive function. *Frontiers in behavioral neuroscience*, 3, 16.

Bos, K., Zeanah, C. H., Fox, N. A., Drury, S. S., McLaughlin, K. A., & Nelson, C. A. (2011). Psychiatric outcomes in young children with a history of institutionalization. *Harvard review of psychiatry*, 19(1), 15–24.

Bowlby, J. (1944). Forty-four juvenile thieves: Their characters and home-life. *International Journal of Psychoanalysis*, 25, 107–128.

Bowlby, J. (1949). The study and reduction of group tensions in the family. *Human Relations*, 2, 123–128.

Bowlby, J. (1951). Maternal care and mental health. World Health Organization Monograph (Serial no. 2). Geneva, Switzerland: World Health Organization.

Bowlby, J. (1952). Maternal care and mental health. *Journal of Consulting Psychology*, 16(3), 232.

Bowlby, J. (1969;1983). Attachment and loss. Volume 1: Attachment. New York, NY: Basic Books (Original work published 1969)

Brennan, P. A., Pargas, R., Walker, E. F., Green, P., Newport, D. J., & Stowe, Z. (2008). Maternal depression and infant cortisol: influences of timing, comorbidity and treatment. *Journal of child psychology and psychiatry, and allied disciplines*, 49(10), 1099–1107.

Brincat, S. L., & Miller, E. K. (2015). Frequency-specific hippocampal-prefrontal interactions during associative learning. *Nat. Neurosci*., 18, 576–581.

Brunson, K. L., Kramár, E., Lin, B., Chen, Y., Colgin, L. L., Yanagihara, T. K., Lynch, G., Baram, T. Z. (2005). Mechanisms of late-onset cognitive decline after early- life stress. *J Neurosci,* 25:9328–9338.

Bubb, E. J., Metzler-baddeley, C., Aggleton, J.P. (2018). The cingulum bundle : Anatomy , function , and dysfunction. *Neuroscience and Biobehavioral Reviews,* 92: 104–127.

Budisavljevic, S., Kawadler, J.M., Dell'Acqua, F., Rijsdijk, F.V., Kane, F., Picchioni, M., McGuire, P., Toulopoulou, T., Georgiades, A., Kalidindi, S., Kravariti, E. (2015). Heritability of the limbic networks. *Soc. Cogn. Affect. Neurosci*, 115, 746–757.

Burghy, C.A., Stodola, D.E., Ruttle, P.L., Molloy, E.K., Armstrong, J.M., Oler, J.A., Fox, M.E., Hayes, A.S., Kalin, N.H., Essex, M.J., Davidson, R.J., Birn, R.M. (2012). Developmental pathways to amygdala- prefrontal function and internalizing symptoms in adolescence. *Nat Neurosci*, 15: 1736-1741.

Burgos-Robles, A., Kimchi, E. Y., Izadmehr, E. M., Porzenheim, M. J., Ramos-Guasp, W. A., Nieh, E. H., Felix-Ortiz, A. C., Namburi, P., Leppla, C. A., Presbrey, K. N., Anandalingam, K. K., Pagan-Rivera, P. A., Anahtar, M., Beyeler, A., & Tye, K. M. (2017). Amygdala inputs to prefrontal cortex guide behavior amid conflicting cues of reward and punishment. *Nature neuroscience*, 20(6), 824–835.

Bussey, T. J., Wise, S. P., Murray, E. A. (2002). Interaction of ventral and orbital prefrontal cortex with inferotemporal cortex in conditional visuomotor learning. *Behavioral Neuroscience*,116(4):703–715.

Calabrese, E. J., Bachmann, K. A., Bailer, A. J., Bolger, P. M., Borak, J., Cai, L., Cedergreen, N., Cherian, M. G., Chiueh, C. C., Clarkson, T. W., Cook, R. R., Diamond, D. M., Doolittle, D. J., Dorato, M. A., Duke, S. O., Feinendegen, L., Gardner, D. E., Hart, R. W., Hastings, K. L., Hayes, A. W., … Mattson, M. P. (2007). Biological stress response terminology: Integrating the concepts of adaptive response and preconditioning stress within a hormetic dose-response framework. *Toxicology and applied pharmacology*, 222(1), 122–128.

Carballedo, A., Amico, F., Ugwu, I., Fagan, A. J., Fahey, C., Morris, D., Meaney, J. F., Leemans, A., & Frodl, T. (2012). Reduced fractional anisotropy in the uncinate fasciculus in patients with major depression carrying the met-allele of the Val66Met brain-derived neurotrophic factor genotype. American journal of medical genetics. *Part B, Neuropsychiatric genetics : the official publication of the International Society of Psychiatric Genetics*, 159B(5), 537–548.

Chatterjee, D., Chatterjee-Chakraborty, M., Rees, S., Cauchi, J., de Medeiros, C.B., & Fleming, A.S. (2007). Maternal isolation alters the expression of neural proteins during development: 'Stroking' stimulation reverses these effects. *Brain Research*, 1158,11–27.

Chen, Y., Baram, T. Z. (2016). Toward understanding how early-life stress repro- grams cognitive and emotional brain networks. *Neuropsychopharmacology*, 41:197–206.

Chiang, H. L., Chen, Y.J., Shang, C.Y., Tseng, W. Y. I., Gau, S. S. F. (2016). Different neural substrates for executive functions in youths with ADHD: a diffusion spectrum imaging tractography study. *Psychol Med,* 46:1225–1238.

Choi, J., Jeong, B., Rohan, M. L., Polcari, A. M., Teicher, M. H. (2009). Preliminary evidence for white matter tract abnormalities in young adults exposed to parental verbal abuse. *Biol Psychiatry,* 65:227–234.

Cicchetti, D., Rogosch, F. A. (2001). Diverse patterns of neuroendocrine activity in maltreated children. *Dev Psychopathol*,13:677–93.

Cicchetti, D., Rogosch, F. A., & Toth, S. L. (1998). Maternal depressive disorder and contextual risk: contributions to the development of attachment insecurity and behavior problems in toddlerhood. *Development and psychopathology*, 10(2), 283–300.

Cohen, J. Y., Haesler, S., Vong, L., Lowell, B. B., & Uchida, N. (2012). Neuron-type-specific signals for reward and punishment in the ventral tegmental area. *Nature*, 482(7383), 85–88.

Colonnesi, C., Draijer, E. M., Jan J M Stams, G., Van der Bruggen, C. O., Bögels, S. M., & Noom, M. J. (2011). The relation between insecure attachment and child

anxiety: a meta-analytic review. *Journal of clinical child and adolescent psychology : the official journal for the Society of Clinical Child and Adolescent Psychology, American Psychological Association*, Division 53, 40(4), 630–645.

Cox, J. L., Holden, J. M., & Sagovsky, R. (1987). Detection of postnatal depression. Development of the 10-item Edinburgh Postnatal Depression Scale. *The British journal of psychiatry: the journal of mental science*, 150, 782–786.

Cox, R. W. (1996). AFNI: software for analysis and visualization of functional magneticresonance neuroimages. *Comput Biomed Res,* 29:162–173.

Crittenden, P. M. (2017). Gifts from Mary Ainsworth and John Bowlby. *Clinical child psychology and psychiatry*, 22(3), 436–442.

Cummings, E. M., & Davies, P. T. (1994). Maternal depression and child development. *Journal of child psychology and psychiatry, and allied disciplines*, 35(1), 73–112.

Cunningham, M. G., Bhattacharyya, S., Benes, F. M. (2002). Amygdalo-cortical sprouting continues into early adulthood: implications for the development of normal and abnormal function during adolescence. *J Comp Neurol*, 453:116–130.

Dalgleish, T., Williams, J. M., Golden, A. M., Perkins, N., Barrett, L. F., Barnard, P. J., Yeung, C. A., Murphy, V., Elward, R., Tchanturia, K., Watkins, E. (2007). Reduced specificity of autobiographical memory and depression: the role of executive control. *J. Exp. Psychol. Gen*., 136 (1), 23–42.

Davis, E. P., Stout, S. A., Molet, J., Vegetabile, B., Glynn, L. M., Sandman, C. A., Heins, K., Stern, H., & Baram, T. Z. (2017). Exposure to unpredictable maternal sensory signals influences cognitive development across species. *Proceedings of the National Academy of Sciences of the United States of America*, 114(39), 10390–10395.

Dawson, G., Ashman, S. B., Panagiotides, H., Hessl, D., Self, J., Yamada, E., & Embry, L. (2003). Preschool outcomes of children of depressed mothers: role of maternal behavior, contextual risk, and children's brain activity. *Child development*, 74(4), 1158–1175.

de Kloet, E. R., Sutanto, W., van den Berg, D. T., Carey, M. P., van Haarst, A. D., Hornsby, C. D., et al. (1993). Brain mineralocorticoid receptor diversity: functional implications. *J. Steroid Biochem. Mol. Biol*., 47, 183–190.

Del Giudice, M., & Haltigan, J. D. (2021). An integrative evolutionary framework for psychopathology. *Development and psychopathology*, 1–11. Advance online publication.

Deperrois, N., Moiseeva, V., & Gutkin, B. (2019). Minimal Circuit Model of Reward Prediction Error Computations and Effects of Nicotinic Modulations. *Frontiers in neural circuits*, 12, 116.

Dillon, D. G., Pizzagalli, D. A., (2018). Mechanisms of memory disruption in depression. *Trends Neurosci*, 41 (3), 137–149.

Drevets, W. C. (2007). Orbitofrontal cortex function and structure in depression. *Annals of the New York Academy of Sciences*, 1121, 499–527.

Eacott, M. J., & Gaffan, D. (1992). Inferotemporal-frontal Disconnection: The Uncinate Fascicle and Visual Associative Learning in Monkeys. *The European journal of neuroscience*, 4(12), 1320–1332.

Ebeling, U., von Cramon, D. (1992). Topography of the uncinate fascicle and adjacent temporal fiber tracts. *Acta Neurochir (Wien*), 115:143–148.

Eghbal-Ahmadi, M., Avishai-Eliner, S., Hatalski, C.G., & Baram, T.Z. (1999). Differential regulation of the expression of corticotropin-releasing fac- tor receptor type 2 (CRF2) in hypothalamus and amygdala of the immature rat by sensory input and food intake. *Journal of Neuroscience*, 19, 3982–3991.

Eichenbaum, H. (2017). Prefrontal–hippocampal interactions in episodic memory. *Nat Rev Neurosci*, 18:547–558.

Eichenbaum, H., Sauvage, M., Fortin, N., Komorowski, R., and Lipton, P. (2012). Towards a functional organization of episodic memory in the medial temporal lobe. *Neurosci. Biobehav. Rev*., 36: 97–1608.

El Marroun, H., Zou, R., Muetzel, R. L., Jaddoe, V. W., Verhulst, F. C., White, T., & Tiemeier, H. (2018). Prenatal exposure to maternal and paternal depressive symptoms and white matter microstructure in children. *Depression and anxiety*, 35(4), 321–329.

Ellis, B. H., Fisher, P. A., & Zaharie, S. (2004). Predictors of disruptive behavior, developmental delays, anxiety, and affective symptomatology among institutionally reared romanian children. *Journal of the American Academy of Child and Adolescent Psychiatry*, 43(10), 1283–1292.

Ellis, B. J., Figueredo, A. J., Brumbach, B. H., & Schlomer, G. L. (2009). Fundamental Dimensions of Environmental Risk : The Impact of Harsh versus Unpredictable Environments on the Evolution and Development of Life History Strategies. *Human nature*, 20(2), 204–268.

Eluvathingal, T. J., Chugani, H. T., Behen, M. E., Juhász, C., Muzik, O., Maqbool, M., Chugani, D. C., & Makki, M. (2006). Abnormal brain connectivity in children after

early severe socioemotional deprivation: a diffusion tensor imaging study. *Pediatrics*, 117(6), 2093–2100.

Eshel, N., & Roiser, J. P. (2010). Reward and punishment processing in depression. *Biological psychiatry*, 68(2), 118–124.

Eshel, N., Bukwich, M., Rao, V., Hemmelder, V., Tian, J., & Uchida, N. (2015). Arithmetic and local circuitry underlying dopamine prediction errors. *Nature*, 525(7568), 243–246.

Evans, G.W., Li, D., Whipple, S.S., (2013). Cumulative risk and child development. *Psychol. Bull*., 139 (6), 1342.

Feldman, R., Granat, A., Pariente, C., Kanety, H., Kuint, J., & Gilboa-Schechtman, E. (2009). Maternal depression and anxiety across the postpartum year and infant social engagement, fear regulation, and stress reactivity. *Journal of the American Academy of Child and Adolescent Psychiatry*, 48(9), 919–927.

Feldman, H., Yeatman, J., Lee, E., Barde, L., Gaman-Bean, S. (2014). Diffusion Tensor Imaging: A review for Pediatric Researchers and Clinicians. *J Dev Behav Pediatr*, 31: 346–356.

Felitti, V. J., Anda, R. F., Nordenberg, D., Williamson, D. F., Spitz, A. M., Edwards, V., Koss, M. P., & Marks, J. S. (1998). Relationship of childhood abuse and household dysfunction to many of the leading causes of death in adults. The Adverse Childhood Experiences (ACE) Study. *American journal of preventive medicine*, 14(4), 245–258.

Fiorillo, C. D., Newsome, W. T., & Schultz, W. (2008). The temporal precision of reward prediction in dopamine neurons. *Nature neuroscience*, 11(8), 966–973.

Fritzsche, K. H., Laun, F. B., Meinzer, H. P., & Stieltjes, B. (2010). Opportunities and pitfalls in the quantification of fiber integrity: what can we gain from Q-ball imaging?. *NeuroImage*, 51(1), 242–251.

Funahashi, S., Bruce, C. J., & Goldman-Rakic, P. S. (1989). Mnemonic coding of visual space in the monkey's dorsolateral prefrontal cortex. *Journal of neurophysiology*, 61(2), 331–349.

Gaffan, D., & Eacott, M. J. (1995). Visual learning for an auditory secondary reinforcer by macaques is intact after uncinate fascicle section: indirect evidence for the involvement of the corpus striatum. *The European journal of neuroscience*, 7(9), 1866–1871.

Gardner, M., Schoenbaum, G., & Gershman, S. J. (2018). Rethinking dopamine as generalized prediction error. Proceedings. *Biological sciences*, 285(1891), 20181645.

Gee, D. G., Gabard-Durnam, L. J., Flannery, J., Goff, B., Humphreys, K. L., Telzer, E. H., Hare, T. A., Bookheimer, S. Y., & Tottenham, N. (2013). Early developmental emergence of human amygdala-prefrontal connectivity after maternal deprivation. *Proceedings of the National Academy of Sciences of the United States of America*, 110(39), 15638–15643.

Gilles, E.E., Schultz, L., Baram, T.Z. (1996) Abnormal corticosterone regulation in an immature rat model of continuous chronic stress. *Pediatric neurology*, 15: 114–119.

Glenn, G. R., Helpern, J. A., Tabesh, A., & Jensen, J. H. (2015). Quantitative assessment of diffusional kurtosis anisotropy. *NMR in biomedicine*, 28(4), 448–459.

Glynn, L. M., Baram, T. Z. (2019). The influence of unpredictable, fragmented pa- rental signals on the developing brain*. Front Neuroendocrinol,* 53: 100736.

Glynn, L. M., Howland, M. A., Sandman, C. A., Davis, E. P., Phelan, M., Baram, T. Z., & Stern, H. S. (2018). Prenatal maternal mood patterns predict child temperament and adolescent mental health. *Journal of affective disorders*, 228, 83–90.

Glynn, L. M., Stern, H. S., Howland, M. A., Risbrough, V. B., Baker, D. G., Nievergelt, C. M., Baram, T. Z., & Davis, E. P. (2019). Measuring novel antecedents of mental illness: the Questionnaire of Unpredictability in Childhood. *Neuropsychopharmacology : official publication of the American College of Neuropsychopharmacology*, 44(5), 876–882.

Gonzalez, A. (2013). The impact of childhood maltreatment on biological systems: Implications for clinical interventions. *Pediatrics & child health*, 18(8), 415–418.

Goodman, S. H. (2007). Depression in mothers. *Annu Rev Clin Psychol*, 3: 107–35.

Gorczewski, K., Mang, S., & Klose, U. (2009). Reproducibility and consistency of evaluation techniques for HARDI data. *Magma*, 22(1), 63–70.

Gotlib, I. H., & Hammen, C. L. (Eds.). (2009). *(2nd ed.). The Guilford Press.*

Govindan, R. M., Behen, M. E., Helder, E., Makki, M. I., & Chugani, H. T. (2010). Altered water diffusivity in cortical association tracts in children with early deprivation identified with Tract-Based Spatial Statistics (TBSS). *Cerebral cortex*, 20(3), 561–569.

Granger, S. J., Adams, J. G., Kark, S. M., Sathishkumar, M. T., Chen, I. Y., Benca, R. M., McMillan, L., Janecek, J. T., & Yassa, M. A. (2022). Latent anxiety in clinical depression is associated with worse recognition of emotional stimuli. *Journal of affective disorders*, 301, 368–377.

Granger, S. J., Glynn, L. M., Sandman, C. A., Small, S. L., Obenaus, A., Keator, D. B., Baram, T. Z., Stern, H., Yassa, M. A., & Davis, E. P. (2021a). Aberrant Maturation of the Uncinate Fasciculus Follows Exposure to Unpredictable Patterns of Maternal Signals. *Journal of Neuroscience*, 41(6), 1242–1250.

Granger, S. J., Leal, S. L., Larson, M. S., Janecek, J. T., McMillan, L., Stern, H., & Yassa, M. A. (2021b). Integrity of the uncinate fasciculus is associated with emotional pattern separation-related fMRI signals in the hippocampal dentate and CA3. *Neurobiology of Learning and Memory*, 177, 107359.

Greenberg, P. E., Fournier, A. A., Sisitsky, T., Simes, M., Berman, R., Koenigsberg, S. H., & Kessler, R. C. (2021). The Economic Burden of Adults with Major Depressive Disorder in the United States (2010 and 2018). *PharmacoEconomics*, 39(6), 653–665.

Grieger, L. D., Schoeni, R. F., Danziger, S. (2009). Accurately measuring the trend in poverty in the United States using the panel study of income dynamics. *J Econ Soc Meas,* 34:105–117.

Groh, A. M., Fearon, R. M., IJzendoorn, M. H., Bakermans-Kranenburg, M. H., Roisman, G. I. (2017) Attachment in the early life course: Meta-analytic evidence for its role in socioemotional development. *Child Development Perspectives*,11:70–76.

Guadagno, A., Verlezza, S., Long, H., Wong, T. P., Walker, C.D. (2016). The effects of chronic early-life stress on amygdala morphology and function in neo-natal rats. *Paper presented at Neurobiology of Stress Workshop, Irvine, CA, April.*

Guadagno, A., Wong, T. P., & Walker, C. D. (2018). Morphological and functional changes in the preweaning basolateral amygdala induced by early chronic stress associate with anxiety and fear behavior in adult male, but not female rats. *Progress in neuro-psychopharmacology & biological psychiatry*, 81, 25–37.

Gunnar M. R. (2010). Reversing the Effects of Early Deprivation after Infancy: Giving Children Families may not be Enough. *Frontiers in neuroscience*, 4, 170.

Gutnikov, S. A., Ma, Y. Y., Buckley, M. J., & Gaffan, D. (1997). Monkeys can associate visual stimuli with reward delayed by 1 s even after perirhinal cortex ablation, uncinate fascicle section or amygdalectomy. *Behavioural brain research*, 87(1), 85–96.

Halligan, S. L., Herbert, J., Goodyer, I. M., & Murray, L. (2004). Exposure to postnatal depression predicts elevated cortisol in adolescent offspring. *Biological psychiatry*, 55(4), 376–381.

Hanson, J. L., Knodt, A. R., Brigidi, B. D., & Hariri, A. R. (2015). Lower structural integrity of the uncinate fasciculus is associated with a history of child maltreatment and future psychological vulnerability to stress. *Development and psychopathology*, 27(4 Pt 2), 1611–1619.

Harmer, C. J., & Cowen, P. J. (2013). 'It's the way that you look at it'--a cognitive neuropsychological account of SSRI action in depression. *Philosophical transactions of the Royal Society of London. Series B, Biological sciences*, 368(1615), 20120407.

Hasler, G., Drevets, W.C., Manji, H.K., Charney, D.S. (2004). Discovering Endophenotypes for Major Depression. *Neuropsychopharmacology*, 1765–1781.

Heilbronner, S.R., Haber, S.N., (2014). Frontal cortical and subcortical projections provide a basis for segmenting the cingulum bundle: implications for neuroimaging and psychiatric disorders. *J. Neuroscience,* 34, 10041–10054.

Heim, C., Binder, E. B. (2012). Current research trends in early life stress and depression: review of human studies on sensitive periods, gene-environment interactions, and epigenetics. *Exp Neurol,* 233:102–111.

Henderson, S.E., Johnson, A.R., Vallejo, A.I., Katz, L., Wong, E., Gabbay, V. (2013) A preliminary study of white matter in adolescent depression: relationships with illness severity, anhedonia, and irritability. *Front. Psychiatry,* 4: 152.

Herman, J. P., and Cullinan, W. E. (1997). Neurocircuitry of stress: central control of the hypothalamo-pituitary-adrenocortical axis. *Trends Neurosci*., 20, 78–84.

Hermoye, L., Saint-Martin, C., Cosnard, G., Lee, S.K., Nassogne, M.C., Menten, R., Clapuyt, P., Donohue, P. K., Hua, K, Wakana, S., Jiang, H., van Zijl, P. C., Mori, S. (2006). Pediatric diffusion tensor imaging: normal database and observation of the white matter maturation in early childhood. *Neuroimage,* 29: 493-- 504.

Hernandez, G., Haines, E., Rajabi, H., Stewart, J., Arvanitogiannis, A., & Shizgal, P. (2007). Predictable and unpredictable rewards produce similar changes in dopamine tone. *Behavioral neuroscience*, 121(5), 887–895.

Hill, E. M., Ross, L. T., & Low, B., (1997). The role of future unpredictability in human risk-taking. *Human Nature*, 8, 287-325.

Ho, T. C., King, L. S., Leong, J. K., Colich, N. L., Humphreys, K. L., Ordaz, S. J., & Gotlib, I. H. (2017). Effects of Sensitivity to Life Stress on Uncinate Fasciculus

Segments in Early Adolescence. Social Cognitive and Affective Neuroscience, 12, 1460-1469.

Hoeve, M., Stams, G. J., van der Put, C. E., Dubas, J. S., van der Laan, P. H., & Gerris, J. R. (2012). A meta-analysis of attachment to parents and delinquency. *Journal of abnormal child psychology*, 40(5), 771–785.

Hofer M. A. (1994). Early relationships as regulators of infant physiology and behavior. *Acta paediatrica (Oslo, Norway : 1992)*. Supplement, 397, 9–18.

Hofer, M.A. (1973). The effects of brief maternal separations on behavior and heart rate of two week old rat pups. *Physiology & Behavior*, 10, 423–427.

Hofer, M.A. (1984). Relationships as regulators: A psychobiologic perspective on bereavement. *Psychosomatic Medicine*, 46, 183–197.

Holland, P. C., & Gallagher, M. (2004). Amygdala-frontal interactions and reward expectancy. *Current opinion in neurobiology*, 14(2), 148–155.

Hostinar, C.E., Sullivan, R.M., & Gunnar, M.R. (2014). Psychobiological mechanisms underlying the social buffering of the hypothalamic-pituitary-adrenocortical axis: A review of animal models and human studies across development. *Psychological Bulletin*, 140, 256.

Howland, M. A., Sandman, C. A., Davis, E. P., Stern, H. S., Phelan, M., Baram, T. Z., & Glynn, L. M. (2021). Prenatal maternal mood entropy is associated with child neurodevelopment. *Emotion*, 21(3), 489–498.

Huang, H., Gundapuneedi, T., & Rao, U. (2012). White matter disruptions in adolescents exposed to childhood maltreatment and vulnerability to psychopathology. *Neuropsychopharmacology : official publication of the American College of Neuropsychopharmacology*, 37(12), 2693–2701.

Hubel, D. H.; Wiesel, T. N. (1959). Receptive fields of single neurones in the cat's striate cortex. *The Journal of Physiology*, 124(3): 574–591.

Hubel, D. H.; Wiesel, T. N. (1962). Receptive fields, binocular interaction and functional architecture in the cat's visual cortex. *The Journal of Physiology*, 160 (45): 106–154.

Hughes, K., Bellis, M. A., Hardcastle, K. A., Sethi, D., Butchart, A., Mikton, C., Jones, L., & Dunne, M. P. (2017). The effect of multiple adverse childhood experiences on health: a systematic review and meta-analysis. *The Lancet. Public health*, 2(8), e356–e366.

Humphreys, K. L., Gleason, M. M., Drury, S. S., Miron, D., Nelson, C. A., 3rd, Fox, N. A., & Zeanah, C. H. (2015). Effects of institutional rearing and foster care on psychopathology at age 12 years in Romania: follow-up of an open, randomised controlled trial. *The lancet. Psychiatry*, 2(7), 625–634.

Hurst J.E., Kavanagh P.S. (2017). Life history strategies and psychopathology: the faster the life strategies, the more symptoms of psychopathology. *Evol. Hum. Behav*, 38(1):1–8.

I.H. Gotlib, C.L. Hammen (2009) Handbook of Depression. *Guilford Press, New York*

Inaba, M., Ohira, H., (2009). Reduced recollective memory about negative items in high trait anxiety individuals: an ERP study. *Int. J. Psychophysiol*., 74 (2), 106–113.

Ivy, A. S., Brunson, K. L., Sandman, C., & Baram, T. Z. (2008). Dysfunctional nurturing behavior in rat dams with limited access to nesting material: a clinically relevant model for early-life stress. *Neuroscience*, 154(3), 1132–1142.

Ivy, A. S., Rex, C. S., Chen, Y., Dubé, C., Maras, P. M., Grigoriadis, D. E., Gall, C. M., Lynch, G., & Baram, T. Z. (2010). Hippocampal dysfunction and cognitive impairments provoked by chronic early-life stress involve excessive activation of CRH receptors. *The Journal of neuroscience : the official journal of the Society for Neuroscience*, 30(39), 13005–13015.

Bailey, D. B., Bruer, J. T., Symons, F. J., & Lichtman, J. W. (Eds.). (2001). Critical thinking about critical periods. Baltimore, MD: Brookes.

J. W. Curtis, C. A. Nelson, *in Resilience and Vulnerability: Adaptation in the Context of Childhood Adversities*, S. Luthar, Ed. (Cambridge Univ. Press, London, 2003), pp. 463–488.

Jaworska-Andryszewska, P., & Rybakowski, J. K. (2019). Childhood trauma in mood disorders: Neurobiological mechanisms and implications for treatment. *Pharmacological reports*,, 71(1), 112–120.

Jbabdi, S., Johansen-Berg, H. (2011). Tractography: Where Do We Go from Here? *Brain Connectivity,* 1: 169- 183.

Jiang, N., Kulesza, A., Singh, S., & Lewis, R. (2015). The dependence of effective planning horizon on model accuracy. *In Proceedings of the 2015 International Conference on Autonomous Agents and Multiagent Systems* (pp. 1181-1189).

Joëls, M., & Baram, T. Z. (2009). The neuro-symphony of stress. *Nature reviews. Neuroscience*, 10(6), 459–466.

Johnson, C. M., Loucks, F. A., Peckler, H., Thomas, A. W., Janak, P. H., & Wilbrecht, L. (2016). Long-range orbitofrontal and amygdala axons show divergent patterns of maturation in the frontal cortex across adolescence. *Developmental cognitive neuroscience*, 18, 113–120.

Jones, M. W., & Wilson, M. A. (2005). Theta rhythms coordinate hippocampal-prefrontal interactions in a spatial memory task. *PLoS biology*, 3(12), e402.

Jones, D. K. (2008). Studying connections in the living human brain with diffusion MRI. *Cortex*, 44, 936–952.

Jones, D. K., Cercignani, M. (2010) Twenty-five pitfalls in the analysis of diffusion MRI data. *NMR Biomed*., 23: 803–820.

Jones, D. K., Christiansen, K. F., Chapman, R. J., & Aggleton, J. P. (2013). Distinct subdivisions of the cingulum bundle revealed by diffusion MRI fibre tracking: implications for neuropsychological investigations. *Neuropsychologia*, 51(1), 67–78.

Juruena M. F. (2014). Early-life stress and HPA axis trigger recurrent adulthood depression. *Epilepsy & behavior: E&B*, 38, 148–159.

Kangas, B. D., Der-Avakian, A., & Pizzagalli, D. A. (2022). Probabilistic Reinforcement Learning and Anhedonia. *Current topics in behavioral neurosciences*, 10.1007/7854_2022_349. Advance online publication.

Kangas, B. D., Short, A. K., Luc, O. T., Stern, H. S., Baram, T. Z., & Pizzagalli, D. A. (2022). A cross-species assay demonstrates that reward responsiveness is enduringly impacted by adverse, unpredictable early-life experiences. *Neuropsychopharmacology*, 47(3), 767–775.

Karlsson, L., Tolvanen, M., Scheinin, N. M., Uusitupa, H. M., Korja, R., Ekholm, E., Tuulari, J. J., Pajulo, M., Huotilainen, M., Paunio, T., Karlsson, H., & FinnBrain Birth Cohort Study Group (2018). Cohort Profile: The FinnBrain Birth Cohort Study (FinnBrain). *International journal of epidemiology*, 47(1), 15–16j.

Kaufman, J., Charney, D., (2000). Comorbidity of mood and anxiety disorders. *Depression and anxiety*, 12 (1), 69–76.

Keedwell, P. A., Chapman, R., Christiansen, K., Richardson, H., Evans, J., Jones, D. K. (2012). Cingulum white matter in young women at risk of depression: The effect of family history and anhedonia. *Biol. Psychiatry,* 72: 296–302.

Kheirbek, M.A., Klemenhagen, K.C., Sahay, A., Hen, R. (2012). Neurogenesis and generalization: a new approach to stratify and treat anxiety disorders. *Nat. Neurosci.,* 15, 1613–1620.

Kim J., Delcasso S., Lee I. (2011). Neural correlates of object-in-place learning in hippocampus and prefrontal cortex. *J. Neurosci*., 31, 16991–17006.

Knierim, J. J., and Neunuebel, J. P. (2016). Tracking the flow of hippocampal computation: Pattern separation, pattern completion, and attractor dynamics. *Neurobiol. Learn. Mem*. 129: 38–49.

Knierim, J. J., Neunuebel, J. P., and Deshmukh, S. S. (2013). Functional correlates of the lateral and medial entorhinal cortex: Objects, path integration and local-global reference frames. *Philos. Trans. R. Soc. Lond. B Biol. Sci*. 369: 20130369.

Kobayashi, S., & Schultz, W. (2008). Influence of reward delays on responses of dopamine neurons. *The Journal of neuroscience: the official journal of the Society for Neuroscience*, *28*(31), 7837–7846.

Koh, C., Tang, P., Chen, H., Hsu, Y., Hsieh, C., Tseng, W.I. (2018). Impaired callosal motor fiber integrity and upper extremity motor impairment are associated with stroke lesion location. *Neurorehabil Neural Repair,* 32:602–612.

Korosi, A., Shanabrough, M., McClelland, S., Liu, Z.-W., Borok, E., Gao, X.-B., Horvath, T.L., Baram, T.Z. (2010). Early-life experience reduces excitation to stress-responsive hypothalamic neurons and reprograms the expression of corticotropin-releasing hormone. *Journal of Neuroscience,* 30:703–713.

Koss, K. J., & Gunnar, M. R. (2018). Annual Research Review: Early adversity, the hypothalamic-pituitary-adrenocortical axis, and child psychopathology. *Journal of child psychology and psychiatry, and allied disciplines*, 59(4), 327–346.

Lacy, J.W., Yassa, M.A., Stark, S. M. Muftuler, L.T., Stark, C.E. (2010) Distinct pattern separation related transfer functions in human CA3/dentate and CA1 revealed using high-resolution fMRI and variable mnemonic similarity. *Learn mem*, 18: 15-8.

Lanier, P., Maguire-Jack, K., Lombardi, B., Frey, J., & Rose, R. A. (2018). Adverse Childhood Experiences and Child Health Outcomes: Comparing Cumulative Risk and Latent Class Approaches. *Maternal and child health journal*, 22(3), 288–297.

Lautarescu, A., Pecheva, D., Nosarti, C., Nihouarn, J., Zhang, H., Victor, S., Craig, M., Edwards, D., Counsell, S. J. (2019). Maternal prenatal stress is associated with altered uncinate fasciculus microstructure in premature neonates. *Biol Psychiatry,* 87:559–569.

Law, C. C., & Cooper, L. N. (1994). Formation of receptive fields in realistic visual environments according to the Bienenstock, Cooper, and Munro (BCM) theory. *Proceedings of the National Academy of Sciences of the United States of America*, 91(16), 7797–7801.

Leal S.L., Tighe S.K., Yassa M.A. (2014a). Asymmetric effects of emotion on mnemonic interference. *Neurobiol Learn Mem*, 111:41–48.

Leal, S.L., Yassa, M.A. (2018). Integrating new findings and examining clinical applications of pattern separation. *Nat Neurosci,* 21:163–173.

Leal, S. L., Tighe, S. K., Jones, C. K., Yassa, M. A. (2014b). Pattern separation of emotional information in hippocampal dentate and CA3. *Hippocampus*, 24(9), 1146–1155.

Lebel, C., Walton, M., Letourneau, N., Giesbrecht, G. F., Kaplan, B. J., Dewey, D. (2016) Prepartum and postpartum maternal depressive symptoms are related to children's brain structure in preschool*. Biol Psychiatry*, 80:859– 868.

Lee, A., & Hankin, B. L. (2009). Insecure attachment, dysfunctional attitudes, and low self-esteem predicting prospective symptoms of depression and anxiety during adolescence. *Journal of clinical child and adolescent psychology : the official journal for the Society of Clinical Child and Adolescent Psychology, American Psychological Association, Division 53*, 38(2), 219–231.

Leichnetz, G. R., & Astruc, J. (1975). Efferent connections of the orbitofrontal cortex in the marmoset (Saguinus oedipus). *Brain research*, 84(2), 169–180.

Leng, B., Han, S., Bao, Y., Zhang, H., Wang, Y., Wu, Y., & Wang, Y. (2016). The uncinate fasciculus as observed using diffusion spectrum imaging in the human brain. *Neuroradiology*, 58(6), 595–606.

Leutgeb, J. K., Leutgeb, S., Moser, M. B., & Moser, E. I. (2007). Pattern separation in the dentate gyrus and CA3 of the hippocampus. *Science*, 315(5814), 961–966.

Libby, L. A., Hannula, D. E., & Ranganath, C. (2014). Medial temporal lobe coding of item and spatial information during relational binding in working memory. *The Journal of neuroscience : the official journal of the Society for Neuroscience*, 34(43), 14233–14242.

Liu, D., Diorio, J., Tannenbaum, B., Caldji, C., Francis, D., Freedman, A., Sharma, S., Pearson, D., Plotsky, P. M., & Meaney, M. J. (1997). Maternal care, hippocampal glucocorticoid receptors, and hypothalamic-pituitary-adrenal responses to stress. *Science*, 277(5332), 1659–1662.

Liu, S., & Fisher, P. A. (2022). Early experience unpredictability in child development as a model for understanding the impact of the COVID-19 pandemic: A translational neuroscience perspective. *Developmental cognitive neuroscience*, 54, 101091.

Lo, Y. C., Chen, Y. J., Hsu, Y. C., Tseng, W. I., & Gau, S. S. (2017). Reduced tract integrity of the model for social communication is a neural substrate of social

communication deficits in autism spectrum disorder. *Journal of child psychology and psychiatry, and allied disciplines*, 58(5), 576–585.

Lu, S., Wei, Z., Gao, W., Wu, W., Liao, M., Zhang, Y., Li, W., Li, Z., Li, L. (2013). White matter integrity alterations in young healthy adults reporting childhood trauma: A diffusion tensor imaging study. *Aust N Z J Psychiatry*. 47(139).

Luijk, M. P., Saridjan, N., Tharner, A., van Ijzendoorn, M. H., Bakermans-Kranenburg, M. J., Jaddoe, V. W., Hofman, A., Verhulst, F. C., & Tiemeier, H. (2010). Attachment, depression, and cortisol: Deviant patterns in insecure-resistant and disorganized infants. *Developmental psychobiology*, 52(5), 441–452.

Lumley, M.N., Harkness, K.L., (2007). Specificity in the relations among childhood adversity, early maladaptive schemas, and symptom profiles in adolescent depression. *Cogn. Ther. Res*. 31 (5), 639–657.

Lupien SJ, Ouellet-Morin I, Herba CM, Juster R, McEwen BS. (2016). From Vulnerability to Neurotoxicity: A Developmental Approach to the Effects of Stress on the Brain and Behavior. *Epigenetics Neuroendocrinol. Springer International Publishing*; 2016.; pp. 3–48.

MacLean, K. (2003). The impact of institutionalization on child development. *Development and psychopathology*, 15(4), 853–884.

Madigan, S., Brumariu, L. E., Villani, V., Atkinson, L., & Lyons-Ruth, K. (2016). Representational and questionnaire measures of attachment: A meta-analysis of relations to child internalizing and externalizing problems. *Psychological bulletin*, 142(4), 367–399.

Maier-Hein, K. H. (2017). The challenge of mapping the human connectome based on diffusion tractography. *Nature Communications*, 8(1).

Main, M. & Solomon, J. (1986). Discovery of a new, insecure-disorganized/disoriented attachment pattern. In T. B. Brazelton & M. Yogman (Eds), *Affective development in infancy*, pp. 95-124. Norwood, New Jersey: Ablex.

Markowitsch, H.J. (1982). Thalamic mediodorsal nucleus and memory: a critical evaluation of studies in animals and man. *Neurosci Biobehav Rev*, 6:351–80.

Marr, D. (1971). Simple memory: a theory for archicortex. *Philos Trans R Soc Lond B Biol Sci,* 262:23–81.

Marroun, H. El, Jaddoe, V.W., White, T., Zou, R., Muetzel, R.L., Verhulst, F.C., Tiemeier, H. (2018). Prenatal exposure to maternal and paternal depressive symptoms and white matter microstructure in children. Depress Anxiety 35: 321–329.

McEwen, B. S. (2007). Physiology and neurobiology of stress and adaptation: central role of the brain. *Physiological reviews*, 87(3), 873–904.

McEwen, B. S. (2008). Central effects of stress hormones in health and disease: Understanding the protective and damaging effects of stress and stress mediators. *European journal of pharmacology*, 583(2-3), 174–185.

McEwen, B. S., & Gianaros, P. J. (2011). Stress- and allostasis-induced brain plasticity. *Annual review of medicine*, 62, 431–445.

McEwen, B. S., Bowles, N. P., Gray, J. D., Hill, M. N., Hunter, R. G., Karatsoreos, I. N., & Nasca, C. (2015). Mechanisms of stress in the brain. *Nature neuroscience*, 18(10), 1353–1363.

McGowan, P. O., Sasaki, A., D'Alessio, A. C., Dymov, S., Labonté, B., Szyf, M., Turecki, G., & Meaney, M. J. (2009). Epigenetic regulation of the glucocorticoid receptor in human brain associates with childhood abuse. *Nature neuroscience*, 12(3), 342–348.

Merikangas, K. R., He, J.P., Burstein, M., Swanson, S.A., Avenevoli,. S, Cui, L., Benjet, C., Georgiades, K., Swendsen, J. Lifetime prevalence of mental disorders in U.S. adolescents: results from the National Comorbidity Survey Replication--Adolescent Supplement (NCS-A). J Am Acad Child Adolesc Psychiatry. 2010 Oct;49(10):980-9.

Michel, G. F., & Tyler, A. N. (2005). Critical period: a history of the transition from questions of when, to what, to how. *Developmental psychobiology*, 46(3), 156–162.

Milner, B., Squire, L.R. Kandel, E. R. (1998) Cognitive neuroscience and the study of memory. *Neuron,* 20: 445–468

Mineka, S., Watson, D., & Clark, L. A. (1998). Comorbidity of anxiety and unipolar mood disorders. *Annual review of psychology*, 49, 377–412.

Miranda, R., & Mennin, D. S. (2007). Depression, generalized anxiety disorder, and certainty in pessimistic predictions about the future. *Cognitive Therapy and Research*, 31(1), 71–82.

Molet, J., Heins, K., Zhuo, X., Mei, Y.T., Regev, L., Baram, T.Z., Stern, H. (2016a) Fragmentation and high entropy of neonatal experience predict adolescent emotional outcome. *Transl Psychiatry,* 6:e702.

Molet, J., Maras, P.M., Kinney-Lang, E., Harris, N.G., Rashid, F., Ivy, A..S., Solodkin, A., Obenaus, A., Baram, T.Z. (2016b) MRI uncovers disrupted hippocampal

microstructure that underlies memory impairments after early-life adversity. *Hippocampus,* 26:1618–1632.

Moriceau, S., Shionoya, K., Jakubs, K., & Sullivan, R. M. (2009). Early-life stress disrupts attachment learning: the role of amygdala corticosterone, locus ceruleus corticotropin releasing hormone, and olfactory bulb norepinephrine. *The Journal of neuroscience : the official journal of the Society for Neuroscience*, 29(50), 15745–15755.

Muris, P., & van der Heiden, S. (2006). Anxiety, depression, and judgments about the probability of future negative and positive events in children. *Journal of Anxiety Disorders*, 20(2), 252–261.

Murray, L., Arteche, A., Fearon, P., Halligan, S., Goodyer, I., & Cooper, P. (2011). Maternal postnatal depression and the development of depression in offspring up to 16 years of age. *Journal of the American Academy of Child and Adolescent Psychiatry*, 50(5), 460–470.

Nelson, C. A., 3rd, Zeanah, C. H., Fox, N. A., Marshall, P. J., Smyke, A. T., & Guthrie, D. (2007). Cognitive recovery in socially deprived young children: the Bucharest Early Intervention Project. *Science*, 318(5858), 1937–1940.

Nelson, C. A., 3rd, & Gabard-Durnam, L. J. (2020). Early Adversity and Critical Periods: Neurodevelopmental Consequences of Violating the Expectable Environment. *Trends in neurosciences*, 43(3), 133–143.

Nelson, C. A., 3rd, Zeanah, C. H., Fox, N. A., Marshall, P. J., Smyke, A. T., & Guthrie, D. (2007). Cognitive recovery in socially deprived young children: the Bucharest Early Intervention Project. *Science* (New York, N.Y.), 318(5858), 1937–1940.

Nelson, R. E., & Craighead, W. E. (1977). Selective recall of positive and negative feedback, self-control behaviors, and depression. *Journal of Abnormal Psychology*, 86(4), 379–388

NICHD Early Child Care Research Network (1999) Chronicity of maternal depressive symptoms, maternal sensitivity, and child functioning at 36 months. *Dev Psychol,* 35:1297–1310.

Noraña-Zhou, A. N., Morgan, A., Glynn, L. M., Sandman, C. A., Baram, T. Z., Stern, H. S., Davis, E. P. (2020) Unpredictable maternal behavior is associated with a blunted infant cortisol response. *Dev Psychobiol,* 62:882–888.

Norman, G., & Eacott, M. J. (2005). Dissociable effects of lesions to the perirhinal cortex and the postrhinal cortex on memory for context and objects in rats. *Behavioral neuroscience*, 119(2), 557–566.

O'Reilly, R. C., & Norman, K. A. (2002). Hippocampal and neocortical contributions to memory: advances in the complementary learning systems framework. *Trends in cognitive sciences*, 6(12), 505–510.

Olson, I. R., Von Der Heide, R. J., Alm, K. H., & Vyas, G. (2015). Development of the uncinate fasciculus: Implications for theory and developmental disorders. *Developmental cognitive neuroscience*, 14, 50–61.

Ono, M., Kikusui, T., Sasaki, N., Ichikawa, M., Mori, Y., & Murakami-Murofushi, K. (2008). Early weaning induces anxiety and precocious myelination in the anterior part of the basolateral amygdala of male Balb/c mice. *Neuroscience*, 156(4), 1103–1110.

Parker, S. W., Nelson, C. A., & Bucharest Early Intervention Project Core Group (2005). The impact of early institutional rearing on the ability to discriminate facial expressions of emotion: an event-related potential study. *Child development,* 76(1), 54–72.

Perlman, W.R. Webster, M.J., Herman, M.M., Kleinman, J.E., Weickert, C.S. (2007). Age-related differences in glucocorticoid receptor mRNA levels in the human brain. *Neurobiol. Aging,* 28: 447– 458

Pittenger, C., (2013). Disorders of memory and plasticity in psychiatric disease. *Dialogues Clin. Neurosci*., 15 (4), 455–463.

Pizzagalli, D. A. (2014). Depression, stress, and anhedonia: Toward a synthesis and integrated model. *Annual Review of Clinical Psychology*, 10, 393–423.

Plotsky, P. M., Meaney, M. J. (1993). Early, postnatal experience alters hypothalamic corticotropin-releasing factor (CRF) mRNA, median eminence CRF content and stress-induced release in adult rats. *Mol. Brain Res*. 18, 195–200.

Plotsky, P. M., Thrivikraman, K. V., Nemeroff, C. B., Caldji, C., Sharma, S., & Meaney, M. J. (2005). Long-term consequences of neonatal rearing on central corticotropin-releasing factor systems in adult male rat offspring. *Neuropsychopharmacology:official publication of the American College of Neuropsychopharmacology*, 30(12), 2192–2204.

Preston, A.R., Eichenbaum, H. (2013). Interplay of hippocampus and prefrontal cortex in memory. *Curr Bio*l, 23:R764–R773.

Price, J. L., & Drevets, W. C. (2012). Neural circuits underlying the pathophysiology of mood disorders. *Trends in cognitive sciences*, 16(1), 61–71.

Purewal Boparai, S. K., Au, V., Koita, K., Oh, D. L., Briner, S., Burke Harris, N., & Bucci, M. (2018). Ameliorating the biological impacts of childhood adversity: A review of intervention programs. *Child abuse & neglect*, 81, 82–105.

Raineki, C., Cortes, M.R., Belnoue, L., Sullivan, R.M. (2012) Effects of early-life abuse differ across development: Infant social behavior deficits are followed by adolescent depressive-like behaviors mediated by the amygdala. *Journal of Neuroscience*, 32: 7758–7765.

Ranganath, C., & Ritchey, M. (2012). Two cortical systems for memory-guided behaviour. *Nature reviews. Neuroscience*, 13(10), 713–726.

Reagh, Z. M., & Yassa, M. A. (2014). Object and spatial mnemonic interference differentially engage lateral and medial entorhinal cortex in humans. *Proceedings of the National Academy of Sciences of the United States of America*, 111(40), E4264–E4273.

Reagh, Z. M., Noche, J. A., Tustison, N. J., Delisle, D., Murray, E. A., & Yassa, M. A. (2018). Functional Imbalance of Anterolateral Entorhinal Cortex and Hippocampal Dentate/CA3 Underlies Age-Related Object Pattern Separation Deficits. *Neuron*, 97(5), 1187–1198.

Redish, D. A., Gordon, J. A. (2017). Computational psychiatry: a new perspective on mental illness. *Cambridge*, MA: MIT.

Rescorla RA., Wagner AR. A theory of Pavlovian conditioning: Variations in the effectiveness of reinforcement and nonreinforcement. In: Black AH, Prokasy WF, eds. Classical Conditioning II: Current Research and Theory. New York, NY: Appleton Century Crofts: 1972:64–99.

Rice, C. J., Sandman, C. A., Lenjavi, M. R., & Baram, T. Z. (2008). A novel mouse model for acute and long-lasting consequences of early life stress. *Endocrinology*, 149(10), 4892–4900.

Rincón-Cortés, M., & Sullivan, R. M. (2016). Emergence of social behavior deficit, blunted corticolimbic activity and adult depression-like behavior in a rodent model of maternal maltreatment. *Translational psychiatry*, 6(10), e930.

Ritchey, M., Libby, L. A., & Ranganath, C. (2015). Cortico-hippocampal systems involved in memory and cognition: the PMAT framework. *Progress in brain research*, 219, 45–64.

Riva-Posse, P., Choi, K. S., Holtzheimer, P. E., McIntyre, C. C., Gross, R. E., Chaturvedi, A., Crowell, A. L., Garlow, S. J., Rajendra, J. K., & Mayberg, H. S. (2014). Defining critical white matter pathways mediating successful subcallosal

cingulate deep brain stimulation for treatment-resistant depression. *Biological psychiatry*, 76(12), 963–969.

Rollins, L., Cloude, E. B. (2018). Development of mnemonic discrimination during childhood. *Learn Mem,* 25:294–297.

Rolls E. T. (2016). A non-reward attractor theory of depression. *Neuroscience and biobehavioral reviews*, 68, 47–58.

Ross, L. T., Hill, E. M. (2000). The family unpredictability Scale: Reliability and Validity. *Journal of Marriage and Family*, 62, 549-562.

Ross, L. T., Hill, E. M. (2002). Childhood unpredictability, schemas for unpredictability, and risk taking. *Social Behavior and Personality*, 30, 453 – 474.

Rothman, K.J. (1990). No adjustments are needed for multiple comparisons. *Epidemiology*, 1: 43-46.

Rouhani, N., Norman, K. A., Niv, Y., & Bornstein, A. M. (2020). Reward prediction errors create event boundaries in memory. *Cognition*, 203, 104269.

Rutter, M. (1979). Maternal deprivation, 1972-1978: New findings, new concepts, new approaches. *Child Development*, 283-305.

Saville, D. J. (1990) Multiple Comparison Procedures: The Practical Solution. *The American Statistician*, 44:174-180

Schultz W. (2016). Dopamine reward prediction error coding. *Dialogues Clin Neurosci*. ,18(1):23-32.

Schultz, W. (1997). Dopamine neurons and their role in reward mechanisms. *Current opinion in neurobiology*, 7(2), 191–197.

Schultz, W., Dayan, P., & Montague, P. R. (1997). A neural substrate of prediction and reward. *Science*, 275(5306), 1593–1599.

Shibata, H. (1993a) Direct projections from the anterior thalamic nuclei to the retro-hippocampal region in the rat. *J. Comp. Neurol*. 337, 431–445.

Shibata, H. (1993b) Efferent projections from the anterior thalamic nuclei to the cingulate cortex in the rat. *J. Comp. Neurol*. 330, 533–542.

Short, A. K., Baram, T. Z. (2019) Early-life adversity and neurological disease: age-old questions and novel answers. *Nat Rev Neurol,* 15:657–669.

Siefke, B. M., Smith, T. A., & Sederberg, P. B. (2019). A context-change account of temporal distinctiveness. *Memory & Cognition*, 47(6), 1158–1172.

Simmonds, D. J., Hallquist, M. N., Asato, M., & Luna, B. (2014). Developmental stages and sex differences of white matter and behavioral development through adolescence: a longitudinal diffusion tensor imaging (DTI) study. *NeuroImage*, 92, 356–368.

Sinha, N., Berg, C. N., Tustison, N. J., Shaw, A., Hill, D., Yassa, M. A., & Gluck, M. A. (2018). Neurobiology of Aging APOE ε 4 status in healthy older African Americans is associated with deficits in pattern separation and hippocampal hyperactivation. *Neurobiology of Aging*, 69, 221–229.

Sinharay, S., Stern, H. S., & Russell, D. (2001). The use of multiple imputation for the analysis of missing data. *Psychological methods*, 6(4), 317–329.

Smith, K. E., & Pollak, S. D. (2020). Early life stress and development: potential mechanisms for adverse outcomes. *Journal of neurodevelopmental disorders*, 12(1), 34.

Spielberger, C. D., Gorsuch, R. L., Lushene, R., Vagg, P. R., Jacobs, G.A. (1983) Manual for the State-Trait Anxiety Inventory. *Palo Alto, CA: Consulting Psychologists.*

Spinhoven, P., Elzinga, B.M., Hovens, J.G., Roelofs, K., Zitman, F.G., van Oppen, P., Penninx, B.W., (2010). The specificity of childhood adversities and negative life events across the life span to anxiety and depressive disorders. *J. Affect. Disord*., 126 (1–2), 103–112.

Spruit, A., Goos, L., Weenink, N., Rodenburg, R., Niemeyer, H., Stams, G. J., & Colonnesi, C. (2020). The Relation Between Attachment and Depression in Children and Adolescents: A Multilevel Meta-Analysis. *Clinical child and family psychology review*, 23(1), 54–69.

Squire, L.R., Stark, C.E., Clark, R.E. (2004). The medial temporal lobe. *Annu. Rev. Neurosci*. 27: 279–306.

Stark, S. M., Kirwan, C. B., Stark, C. (2019). Mnemonic similarity task: A tool for assessing hippocampal integrity. *Trends in cognitive sciences,* 23:938– 951.

Stratakis, C. A., and Chrousos, G. P. (1995). Neuroendocrinology and pathophysiology of the stress system. *Ann. N.Y. Acad. Sci.* 771, 1–18.

Substance Abuse and Mental Health Services Administration. (2021). Key substance use and mental health indicators in the United States: Results from the 2020 National Survey on Drug Use and Health (HHS Publication No. PEP21-07-01-

003, NSDUH Series H-56). Rockville, MD: Center for Behavioral Health Statistics and Quality, Substance Abuse and Mental Health Services Administration. Retrieved from https://www.samhsa.gov/data/report/2020-nsduh-annual-national-report.

Suwabe, K., Byun, K., Hyodo, K., Reagh, Z. M., & Roberts, J. M. (2018). Rapid stimulation of human dentate gyrus function with acute mild exercise, *PNAS*, 115(41).

Tatham, E. L., Ramasubbu, R., Gaxiola-Valdez, I., Cortese, F., Clark, D., Goodyear, B., Foster, J., & Hall, G. B. (2016). White matter integrity in major depressive disorder: Implications of childhood trauma, 5-HTTLPR and BDNF polymorphisms. *Psychiatry research. Neuroimaging*, 253, 15–25.

Tatham, E.L., Hall, G.B., Clark, D., Foster, J., Ramasubbu, R. (2017). The 5-HTTLPR and BDNF polymorphisms moderate the association between uncinate fasciculus connectivity and antidepressants treatment response in major depression. *European Archives of Psychiatry and Clinical Neuroscience*, 267: 135–147.

Taylor, W. D., MacFall, J. R., Gerig, G., & Krishnan, R. R. (2007). Structural integrity of the uncinate fasciculus in geriatric depression: Relationship with age of onset. *Neuropsychiatric Disease and Treatment*, 3(5), 669–674.

Thiebaut de Schotten, M., Dell'Acqua, F., Valabregue, R., & Catani, M. (2012). Monkey to human comparative anatomy of the frontal lobe association tracts. *Cortex; a journal devoted to the study of the nervous system and behavior*, 48(1), 82–96.

Tian, J., Huang, R., Cohen, J. Y., Osakada, F., Kobak, D., Machens, C. K., Callaway, E. M., Uchida, N., & Watabe-Uchida, M. (2016). Distributed and Mixed Information in Monosynaptic Inputs to Dopamine Neurons. *Neuron*, 91(6), 1374–1389.

Tofalini, E., Mirandola, C., Coli, T., Cornoldi, C., (2015). High trait anxiety increases inferential false memories for negative (but not positive) emotional events. *Personal. Individ. Differ*., 75, 201–204.

Tottenham, N., Galván, A. (2016). Stress and the adolescent brain Amygdala- prefrontal cortex circuitry and ventral striatum as developmental targets. *Neurosci Biobehav Rev*, 70:217–227.

Tuch, D. S. (2004). Q-ball imaging*. Magn Reson Med,* 52:1358–1372.

Tuch, D. S., Reese, T. G., Wiegell, M. R., Makris, N., Belliveau, J. W., & Wedeen, V. J. (2002). High angular resolution diffusion imaging reveals intravoxel white matter fiber heterogeneity. *Magnetic resonance in medicine*, 48(4), 577–582.

Ulrich-Lai, Y. M., & Herman, J. P. (2009). Neural regulation of endocrine and autonomic stress responses. *Nature reviews. Neuroscience*, 10(6), 397–409.

van Bodegom, M., Homberg, J. R., & Henckens, M. (2017). Modulation of the Hypothalamic-Pituitary-Adrenal Axis by Early Life Stress Exposure. *Frontiers in cellular neuroscience*, 11, 87.

Van Groen, T., Wyss, J.M. (1990). The connections of presubiculum and parasubiculum in the rat. *Brain Res*. 518: 227–243.

van Kesteren, M. T., Fernández, G., Norris, D. G., & Hermans, E. J. (2010). Persistent schema-dependent hippocampal-neocortical connectivity during memory encoding and postencoding rest in humans. *Proceedings of the National Academy of Sciences of the United States of America*, 107(16), 7550–7555.

VanTieghem, M. R., & Tottenham, N. (2018). Neurobiological Programming of Early Life Stress: Functional Development of Amygdala-Prefrontal Circuitry and Vulnerability for Stress-Related Psychopathology. *Current topics in behavioral neurosciences*, 38, 117–136.

Vanderwert, R. E., Zeanah, C. H., Fox, N. A., & Nelson, C. A., 3rd (2016). Normalization of EEG activity among previously institutionalized children placed into foster care: A 12-year follow-up of the Bucharest Early Intervention Project. *Developmental cognitive neuroscience*, 17, 68–75.

Vann, S. D., & Aggleton, J. P. (2002). Extensive cytotoxic lesions of the rat retrosplenial cortex reveal consistent deficits on tasks that tax allocentric spatial memory. *Behavioral neuroscience*, 116(1), 85–94.

Vegetabile, B. G., Stout-Oswald, S. A., Davis, E.P., Baram, T.Z., Stern, H.S. (2019). Estimating the entropy rate of finite Markov chains with application to behavior studies. *J Educ Behav Stat,* 44:282–308.

Verbeek, T., Bockting, C. L., van Pampus, M. G., Ormel, J., Meijer, J. L., Hartman, C. A., & Burger, H. (2012). Postpartum depression predicts offspring mental health problems in adolescence independently of parental lifetime psychopathology. *Journal of affective disorders*, 136(3), 948–954.

Vergani, F., Martino, J., Morris, C., Attems, J., Ashkan, K., & Dell'Acqua, F. (2016). Anatomic Connections of the Subgenual Cingulate Region. *Neurosurgery*, 79(3), 465–472.

Vilgis, V., Vance, A., Cunnington, R., & Silk, T. J. (2017). White matter microstructure in boys with persistent depressive disorder. *Journal of affective disorders*, 221, 11–16.

Von Der Heide, R. J., Skipper, L. M., Klobusicky, E., & Olson, I. R. (2013). Dissecting the uncinate fasciculus: disorders, controversies and a hypothesis. *Brain: a journal of neurology*, 136(Pt 6), 1692–1707.

Drevets, W.C. (2007). Orbitofrontal cortex function and structure in depression. *Ann. N. Y. Acad. Sci.,* 1121, 499-527

Walker, C. D., Bath, K. G., Joels, M., Korosi, A., Larauche, M., Lucassen, P. J., Morris, M. J., Raineki, C., Roth, T. L., Sullivan, R. M., Taché, Y., & Baram, T. Z. (2017). Chronic early life stress induced by limited bedding and nesting (LBN) material in rodents: critical considerations of methodology, outcomes and translational potential. *Stress*, 20(5), 421–448.

Watabe-Uchida, M., Eshel, N., & Uchida, N. (2017). Neural Circuitry of Reward Prediction Error. *Annual review of neuroscience*, 40, 373–394.

Wedeen, V.J., Hagmann, P., Tseng, W.Y., Reese, T.G., Weisskoff, R.M. (2005) Mapping complex tissue architecture with diffusion spectrum magnetic resonance imaging. *Magn. Reson. Med*. 54: 1377–1386.

Williams, J.M., Barnhofer, T., Crane, C., Herman, D., Raes, F., Watkins, E., Dalgleish, T., (2007). Autobiographical memory specificity and emotional disorder. *Psychol. Bull*. 133 (1), 122–148.

Windsor, J., Glaze, L. E., Koga, S. F., & Bucharest Early Intervention Project Core Group (2007). Language acquisition with limited input: Romanian institution and foster care. *Journal of speech, language, and hearing research*, 50(5), 1365–1381.

Wise, T., Radua, J., Nortje, G., Cleare, A. J., Young, A. H. (2016). Archival Report Voxel-Based Meta-Analytical Evidence of Structural Disconnectivity in Major Depression and Bipolar Disorder. *Biological Psychiatry*, 79: 293–302.

Witter, M.P., Doan, T.P., Jacobsen, B., Nilssen, E.S., Ohara, S. (2017). Architecture of the Entorhinal Cortex A Review of Entorhinal Anatomy in Rodents with Some Comparative Notes. *Front Syst Neurosci,* 11(June): 1–12.

Wouterlood, F.G., Saldana, E., Witter, M.P. (1990). Projection from the nucleus reuniens thalami to the hippocampal region: light and electron microscopic tracing study in the rat with the anterograde tracer Phaseolus vulgaris-leucoagglutinin. *J. Comp. Neurol.* 296: 179–203.

Wyman, P.A., (2003). Emerging perspectives on context specificity of children's adaptation and resilience: evidence from a decade of research with urban children in adversity. *Resilience and Vulnerability: Adaptation in the Context of Childhood Adversities*, pp. 293–317.

Yamada, N., Ueda, R., Kakuda, W., Momosaki, R., Kondo, T., Hada, T., Sasaki, N., Hara, T., Senoo, A., & Abo, M. (2018). Diffusion Tensor Imaging Evaluation of Neural Network Development in Patients Undergoing Therapeutic Repetitive Transcranial Magnetic Stimulation following Stroke. *Neural plasticity*, 2018, 3901016.

Yan, C.G., Rincón-Cortés, M., Raineki, C., Sarro, E., Colcombe, S., Guilfoyle, D.N., Yang, Z., Gerum, S., Biswal, B.B., Milham, M.P., Sullivan, R.M., Castellanos, F.X. (2017) Aberrant development of intrinsic brain activity in a rat model of caregiver maltreatment of offspring. *Translational Psychiatry*, 7, e1005.

Yang, X. H., Wang, Y., Wang, D. F., Tian, K., Cheung, E., Xie, G. R., & Chan, R. (2017). White matter microstructural abnormalities and their association with anticipatory anhedonia in depression. Psychiatry research. *Neuroimaging*, 264, 29–34.

Yang, X.-D., Liao, X.-M., Uribe-Marino, A., Liu, R., Xie, X.-M., Jia, J., Su, Y.A., Li, J.T., Schmidt, M.D., Wang, X.D., Si, T.-M. (2015). Stress during a critical postnatal period induces region- specific structural abnormalities and dysfunction of the prefrontal cortex via CRF1. *Neuropsychopharmacology*, 40: 1203– 1215.

Yassa, M. A., Mattfeld, A. T., Stark, S. M., & Stark, C. E. (2011). Age-related memory deficits linked to circuit-specific disruptions in the hippocampus. *Proceedings of the National Academy of Sciences of the United States of America*, 108(21), 8873–8878.

Yassa, M. A., Stark, C.E.L. (2011) Pattern separation in the hippocampus. *Trends Neurosci*, 34:515–525.

Yeh, F. C., & Tseng, W. Y. I. (2011). NTU-90: A high angular resolution brain atlas constructed by q-space diffeomorphic reconstruction. *NeuroImage*, 58(1), 91–99.

Yeh, F. C., Verstynen, T. D., Wang, Y., Fernández-Miranda, J. C., & Tseng, W. Y. I. (2013). Deterministic diffusion fiber tracking improved by quantitative anisotropy. *PLoS ONE*, 8(11), 1–16.

Yeh, F. C., Wedeen, V. J., & Tseng, W. Y. (2010). Generalized q-sampling imaging. *IEEE transactions on medical imaging*, 29(9), 1626–1635.

Yoshikawa, H., Aber, J. L., & Beardslee, W. R. (2012). The effects of poverty on the mental, emotional, and behavioral health of children and youth: implications for prevention. *The American psychologist*, 67(4), 272–284.

Young, C.B., Eijndhoven, P. Van, Nusslock, R., Schene, A., Beckmann, C.F., Tendolkar, I. (2016). Brain Disorders and Treatment Decreased Hippocampal

Volume is Related to White Matter Abnormalities in Treatment-Resistant Depression. *ClinMed*, 2(1), 1–6.

Young, E. S., Frankenhuis, W. E., Ellis, B. J., (2020). Theory and measurement of environmental unpredictability. *Evolution and Human Behavior*, 41, 550-556.

Yu, Q., Peng, Y., Kang, H., Peng, Q., Ouyang, M., Slinger, M., Hu, D., Shou, H., Fang, F., & Huang, H. (2020). Differential White Matter Maturation from Birth to 8 Years of Age. *Cerebral cortex*, 30(4), 2673–2689.

Zeanah, C. H., Nelson, C. A., Fox, N. A., Smyke, A. T., Marshall, P., Parker, S. W., & Koga, S. (2003). Designing research to study the effects of institutionalization on brain and behavioral development: the Bucharest Early Intervention Project. *Development and psychopathology*, 15(4), 885–907.

Zeanah, C. H., Smyke, A. T., Koga, S. F., Carlson, E., & Bucharest Early Intervention Project Core Group (2005). Attachment in institutionalized and community children in Romania. *Child development*, 76(5), 1015–1028.

Zhang, A., Leow, A., Ajilore, O., Lamar, M., Yang, S., Joseph, J., Medina, J., Zhan, L., & Kumar, A. (2012). Quantitative tract-specific measures of uncinate and cingulum in major depression using diffusion tensor imaging. *Neuropsychopharmacology : official publication of the American College of Neuropsychopharmacology*, 37(4), 959–967.

Appendix A: Latent anxiety in clinical depression is associated with worse recognition of emotional stimuli

This appendix in its entirety is published as Granger et al., (2022)

Granger, S. J., Adams, J. G., Kark, S. M., Sathishkumar, M. T., Chen, I. Y., Benca, R. M., McMillan, L., Janecek, J. T., & Yassa, M. A. (2022). Latent anxiety in clinical depression is associated with worse recognition of emotional stimuli. *Journal of affective disorders,* 301, 368–377.

Introduction

Major depressive disorder (MDD) is one of the most pressing public health challenges facing our society today. As many as 17.3 million adults in the United States 18 years and older were thought to have at least one major depressive episode in 2017 (NIMH, 2017). Characterized by depressed mood, loss of pleasure or interest, fatigue, insomnia, and suicidal ideation, MDD is also highly comorbid with anxiety disorders (Mineka, Watson, & Clark, 1998). As the prevalence of comorbidity of anxiety disorders with MDD may be as high as 60% of cases (Kaufman & Charney 2000) an extensive effort is being made to take a more dimensional approach to understanding the comorbid profiles of these mental illnesses. Prior work has explored both the constructs of depression and anxiety in large clinical cohorts using exploratory factor analyses to uncover latent clusters of variables from the Beck Anxiety Inventory (BAI) and Beck Depression Inventory-II (BDI-II) scales. These investigations yield evidence of a tripartite model of depression and anxiety (consisting of negative affect, low positive affect, and physiological hyper-arousal) and theorize that while these constructs share general negative affect, they can perhaps be differentiated based on the basis of factors specific to each syndrome (Lee et. al., 2016, Clark & Watson, 1991).

Cognitive affective biases have been well documented in MDD (Murrough et al., 2011; Chamberlain & Sahakian, 2006), can be detected even during remission and are associated with persistent psychosocial impairment (Conradi et al., 2011; Hasselbalch et al., 2011; Lam et al., 2014). Prior work has reported memory disturbances in depression and anxiety (Pittenger, 2013; Dillon & Pizzagalli, 2018; Leal & Yassa, 2018). Evidence has linked both MDD diagnosis as well as depressive symptom severity to augmented memory for negative items both in terms of recognition (Bai et al., 2017; Hamilton et al., 2008) and discrimination (Leal et al., 2014a), as well as reduced specificity of autobiographical retrieval (Dillon & Pizzagalli, 2018; Dalgleish et al., 2007; Williams et al., 2007). Other studies have demonstrated that those with greater symptoms of anxiety exhibit impaired memory of negative stimuli (Tofalini et al., 2015; Inaba & Ohira, 2009) suggesting a cognitive affective bias that leads to overgeneralization of negative emotional memories (Leal & Yassa, 2018; Kheirbek et al., 2012; Balderston et al., 2017).

We have previously shown that individuals with more depressive symptoms show augmented memory discrimination for negative items (Leal et al., 2014a) and exhibit unique neurobiological signatures which include reduced hippocampal dentate gyrus/CA3 activity and increased amygdala activity during the correct discrimination of highly similar negative (but not neutral) items (Leal et al., 2014b). These results were consistent with other literature on depression that find evidence of a negativity bias (for review see Haas & Canli, 2008; Hasler et al., 2004) and functional and structural differences in the amygdala (MacMillan et al., 2003; Sheline et al., 2001; Whalen et al., 2002) and the hippocampus (Stockmeier et al., 2004).

Given prior work, there is uncertainty as to how greater depressive symptoms can be associated with augmented negative memory performance while greater anxiety symptoms can be associated with impaired negative episodic memory performance given that these two constructs are often comorbid and present together. Prior work, however, did not take into consideration the comorbidity of depression and anxiety, and the presence of subthreshold anxiety symptoms. In this investigation, we used exploratory factor analysis, applied to the BDI and BAI to uncover latent constructs of anxiety and depression in a clinically assessed cohort. We then tested the association of individual factors with memory performance, focusing on two primary outcome measures including target recognition (TR) assessing gist or generalized knowledge and Lure Discrimination Index (LDI) assessing detail knowledge or high precision memories (Norman, 2010; Yonelinas et al., 2010; Leal et al., 2014a).

Methods

Participants

Participants were recruited in collaboration with the department of Psychiatry and Human Behavior at the UC Irvine Medical Center and compensated for their participation. Participants were of 79 young adults (58 female) aged 18 to 41 years-old. This sample was comprised of 22 healthy participants (14 female) and 58 participants with a clinical diagnosis (44 females; see Clinical Diagnosis section). All procedures were in accordance with protocols approved by the UC Irvine Institutional Review Board. All participants provided informed consent prior to participation in the study. Participants were pre-screened before enrollment in the study for the presence of active

depressive symptoms. These participants filled out a version of the Beck Depression Inventory without question nine (related to suicidality) online as part of their eligibility pre-screening. A score of 16 or higher on the pre-screening BDI-II determined eligibility to enroll in the study group. A matched sample of healthy control participants were recruited and had to satisfy the inclusion criterion of a BDI score less than 12. Once enrolled in the main study, the full version of the Beck Depression Inventory (BDI-II) was administered in person during the first study visit along with the Beck Anxiety Inventory (BAI) and other mood and sleep questionnaires. This in person administration of the BDI-II was used in all of our calculations. Table A1.1 describes the sample demographics.

Table A1.1. Participant demographics (N=79). The subgroup of participants able to complete the emotional pattern separation task is denoted by n.

	Full Sample$N = 79n = 73$	**H(Healthy)$N = 22n = 20$**	**D(Depression)$N = 29n = 28$**	**$D + A$(Depression + Anxiety)$N = 18n = 18$**	**O(Other)$N = 10n = 7$**
Age	23.21 ± 5.71 (1 missing)	26.38 ± 6.78 (1 missing)	22.61 ± 5.18	20.91 ± 3.76	22.46 ± 5.59
Sex	58 Female 21 Male	14 Female 8 Male	23 Females 6 Males	15 Females 3 Males	6 Females 4 Males
Trails A	37.83 ± 22.20	36.27 ± 25.00	37 ± 22.83	38.83 ± 19.74	41.88 ± 20.67
Trails B	39.31 ± 22.38	39.50 ± 24.43	36.55 ± 21.27	43.17 ± 18.66	39.91 ± 28.77
MMSE	28.87 ± 1.19	28.73 ± 1.16	28.97 ± 1.09	28.78 ± 1.17	29.10 ± 1.66
BDI-II	23.23 ± 15.05	4.86 ± 5.79	29.1 ± 8.33	34.17 ± 11.43	26.90 ± 15.23
BAI	16.67 ± 13.12	3.96 ± 3.89	20.9 ± 10.20	24.00 ± 12.22	19.20 ± 16.86
RAVLT Immediate Recall	12.63 ± 2.35	12.32 ± 2.21	13.69 ± 1.47	11.33 ± 2.99	12.6 ± 2.41
RAVLT Delayed Recall	12.58 ± 2.69	12.5 ± 2.99	13.45 ± 1.74	11.50 ± 2.75	12.2 ± 3.65
Digit Span Forward	11.04 ± 2.46	10.73 ± 2.43	11.62 ± 2.58	10.22 ± 2.32	11.50 ± 2.17
Digit Span Backward	7.70 ± 2.51	7.59 ± 2.42	8.41 ± 2.63	6.78 ± 2.39	7.5 ± 2.27

Structured Clinical Interview (SCID)

As part of the study procedure, all participants underwent a two-hour semi-structured clinical interview with a clinician (I.Y.C. or R.B.) as outlined by the Structured Clinical Interview for DSM-5 Research Version (SCID-5-RV). The SCID-5-RV is a semi structured interview guide for making the major Diagnostic and Statistical Manual of Mental Disorders (DSM-5) diagnoses. After completing this clinical interview, the

clinician completed an accompanying summary sheet to determine the participant's current and past diagnoses. The summary sheet additionally allowed the clinician to indicate whether a participant met sub-threshold criteria for any relevant diagnosis. In the DSM-5 there are often multiple criteria or symptom types that need to be met in order to meet the full diagnosis requirements. A sub-threshold diagnosis was marked if the participant met a number of the criteria outlined in the DSM-5 corresponding to a particular disorder but did not meet ALL of the criteria necessary for a full diagnosis under the DSM-5.

Clinical Diagnosis

In order to incorporate the SCID diagnoses into the analysis, we used a tag system to simplify the variety of clinical diagnoses. Healthy (H) participants (N = 22) underwent the full SCID Interview and had no history of psychopathology or clinical diagnosis. Participants whose SCID diagnosis revealed a past, subthreshold or active unipolar depression were designated with a Depression (D) tag (N=29). For this sample, every participant with the "D" tag had a history of Major Depressive Disorder, a small subset (n=3) also had a comorbid Persistent Depressive Disorder diagnosis and one (n=1) had a comorbid Premenstrual Dysphoric Disorder diagnosis. The tag D+A (depression comorbid with anxiety; N=18) was given to participants who were eligible for the "D" tag but also had clinically identifiable anxiety. We considered this to be any participant with an active threshold or sub-threshold anxiety disorder or obsessive-compulsive disorder. In this population, this included Generalized Anxiety Disorder (n=6), Agoraphobia (n=2), Panic Disorder (n=5), Social Anxiety Disorder (n=4), Specific

Phobia (n=7), Obsessive-compulsive Disorder (n=7). Obsessive-compulsive disorder (included in the obsessive-compulsive and related disorders), was previously considered an anxiety disorder in the DSM-4. While it now has its own chapter in the DSM-5, these disorders are still considered to be closely related. Remaining participants receiving a SCID diagnosis that did not include an element of unipolar depression were tagged with the “Other” designation (“O”; N=10). These participants were included despite not having a depression diagnosis to increase sample size and examine the effect of symptom severity even in the absence of a depression diagnosis. A full description of all clinically relevant diagnoses derived from the SCID for each participant is described in Table A1.2.

Table A1.2. Table of Diagnosis and comorbidities

ID	Tag	Stuctured Clinical Inteview of DSM-5 Diagnosis																					
		Major Depressive Disorder (MDD)	Persistent Depressive Disorder (PDD)	Premenstrual Disphoric Disorder (PMDD)	Generalized Anxiety Disorder (GAD)	Agoraphobia	Panic Disorder	Social Anxiety Disorder	Specific Phobia	Obsessive Compusive Disorder (OCD)	Body Dysmorphic Disorder	Post Traumatic Stress Disorder (PTSD)	Bipolar II Disorder	Attention Deficit Hyperactive Disorder (ADHD)	Adjustment Disorder	Binge Eating Disorder	Bulimia Nervosa	Anorexia Nervosa	Other Feeding/Eating Disorder	Alcohol Abuse Disorder			
115	H	-	-	-	-	-	-	-	-	-	-	-	-	-	-	-	-	-	-	-			
119	H	-	-	-	-	-	-	-	-	-	-	-	-	-	-	-	-	-	-	-			
120	H	-	-	-	-	-	-	-	-	-	-	-	-	-	-	-	-	-	-	-			
122	H	-	-	-	-	-	-	-	-	-	-	-	-	-	-	-	-	-	-	-			
124	H	-	-	-	-	-	-	-	-	-	-	-	-	-	-	-	-	-	-	-			
130	H	-	-	-	-	-	-	-	-	-	-	-	-	-	-	-	-	-	-	-			
153	H	-	-	-	-	-	-	-	-	-	-	-	-	-	-	-	-	-	-	-			
155	H	-	-	-	-	-	-	-	-	-	-	-	-	-	-	-	-	-	-	-			
157	H	-	-	-	-	-	-	-	-	-	-	-	-	-	-	-	-	-	-	-			
159	H	-	-	-	-	-	-	-	-	-	-	-	-	-	-	-	-	-	-	-			
161	H	-	-	-	-	-	-	-	-	-	-	-	-	-	-	-	-	-	-	-			
162	H	-	-	-	-	-	-	-	-	-	-	-	-	-	-	-	-	-	-	-			
166	H	-	-	-	-	-	-	-	-	-	-	-	-	-	-	-	-	-	-	-			
167	H	-	-	-	-	-	-	-	-	-	-	-	-	-	-	-	-	-	-	-			
168	H	-	-	-	-	-	-	-	-	-	-	-	-	-	-	-	-	-	-	-			
170	H	-	-	-	-	-	-	-	-	-	-	-	-	-	-	-	-	-	-	-			
171	H	-	-	-	-	-	-	-	-	-	-	-	-	-	-	-	-	-	-	-			
172	H	-	-	-	-	-	-	-	-	-	-	-	-	-	-	-	-	-	-	-			
173	H	-	-	-	-	-	-	-	-	-	-	-	-	-	-	-	-	-	-	-			
174	H	-	-	-	-	-	-	-	-	-	-	-	-	-	-	-	-	-	-	-			
188	H	-	-	-	-	-	-	-	-	-	-	-	-	-	-	-	-	-	-	-			
207	H	-	-	-	-	-	-	-	-	-	-	-	-	-	-	-	-	-	-	-			
103	D	●	-	●	-	-	-	-	-	-	-	-	-	-	-	-	-	-	-	-			
123	D	◐	●	-	-	-	-	-	-	-	-	-	-	-	-	-	-	-	-	◐			
125	D	◐	◐	-	-	-	-	-	-	-	-	-	-	-	-	-	-	-	-	-			
131	D	●	-	-	-	-	-	-	-	-	-	-	-	-	-	-	-	-	-	-			
132	D	●	-	-	-	-	-	-	-	-	-	-	-	-	-	-	-	-	-	-			
143	D	●	●	-	-	-	-	-	-	-	-	-	-	-	-	-	-	-	-	-			
144	D	●	-	-	-	-	-	-	-	-	-	-	-	-	-	-	-	-	-	-			
145	D	●	-	-	-	-	-	-	-	-	-	-	-	-	-	-	-	-	-	-			
146	D	●	-	-	-	-	-	-	-	-	-	-	-	-	-	-	-	-	-	-			
150	D	●	-	-	-	-	-	-	-	-	-	-	-	-	-	-	-	-	-	-			
151	D	◐	-	-	-	-	-	-	-	-	-	-	-	-	-	-	-	-	-	-			
156	D	◐	-	-	-	-	-	-	-	-	-	-	-	-	-	-	-	-	-	-			
158	D	●	●	-	-	-	-	-	-	-	-	-	-	-	-	-	-	-	-	-			

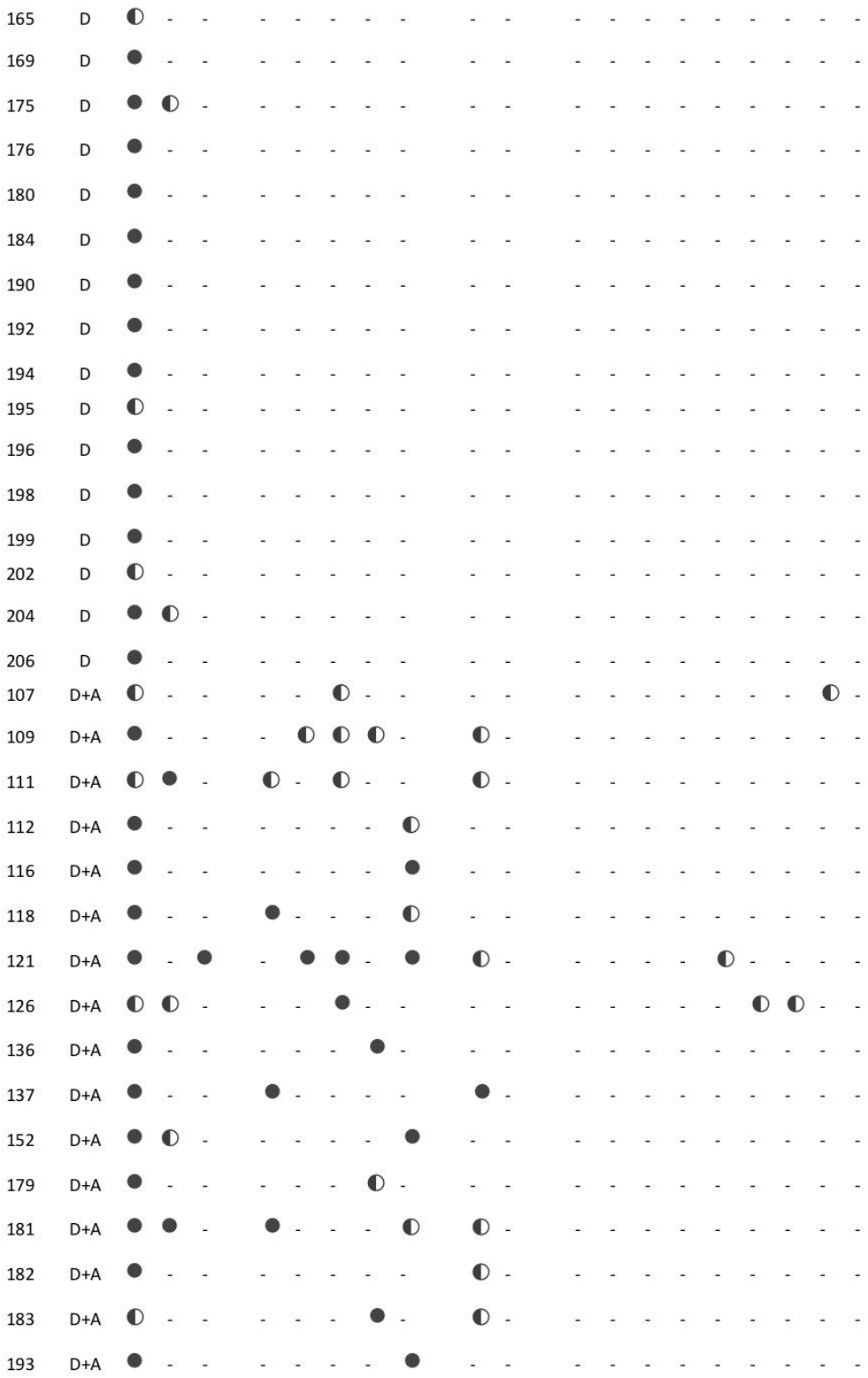
165 D
169 D
175 D
176 D
180 D
184 D
190 D
192 D
194 D
195 D
196 D
198 D
199 D
202 D
204 D
206 D
107 D+A
109 D+A
111 D+A
112 D+A
116 D+A
118 D+A
121 D+A
126 D+A
136 D+A
137 D+A
152 D+A
179 D+A
181 D+A
182 D+A
183 D+A
193 D+A

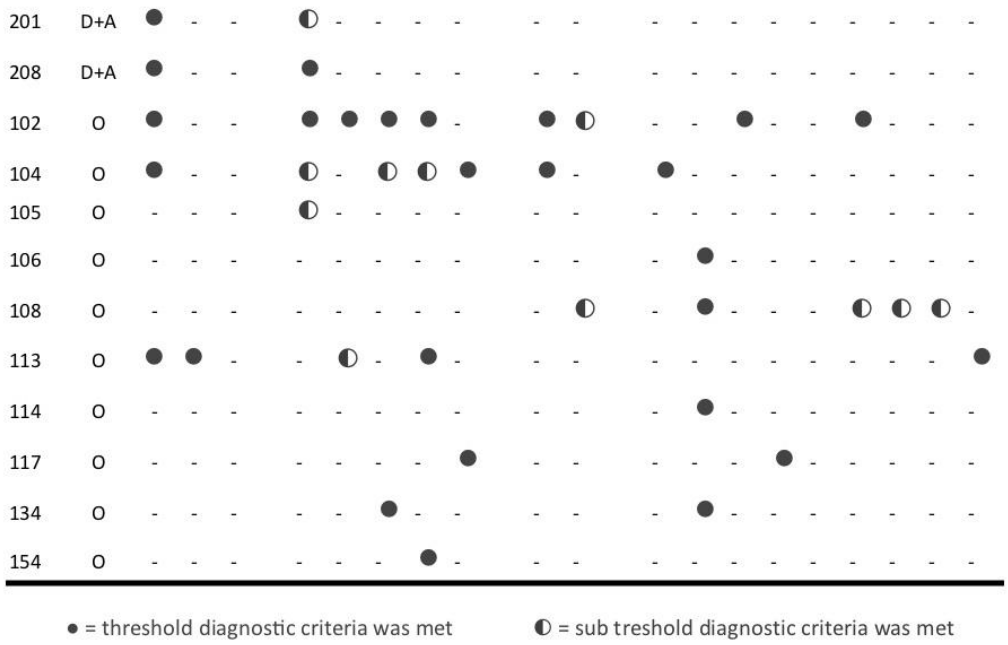

Emotional Pattern Separation (EmoPS) Task

The Emotional Pattern Separation task was administered on a subsample of 73 participants. The task consisted of a study phase and a test phase. The study phase consisted of 149 trials. In each trial a randomized series of emotional and non-emotional scene images were presented at the center of the screen with a black background for 2500ms each, separated by an inter-stimulus interval of 500 ms (fixation cross) (Figure A1.1a).

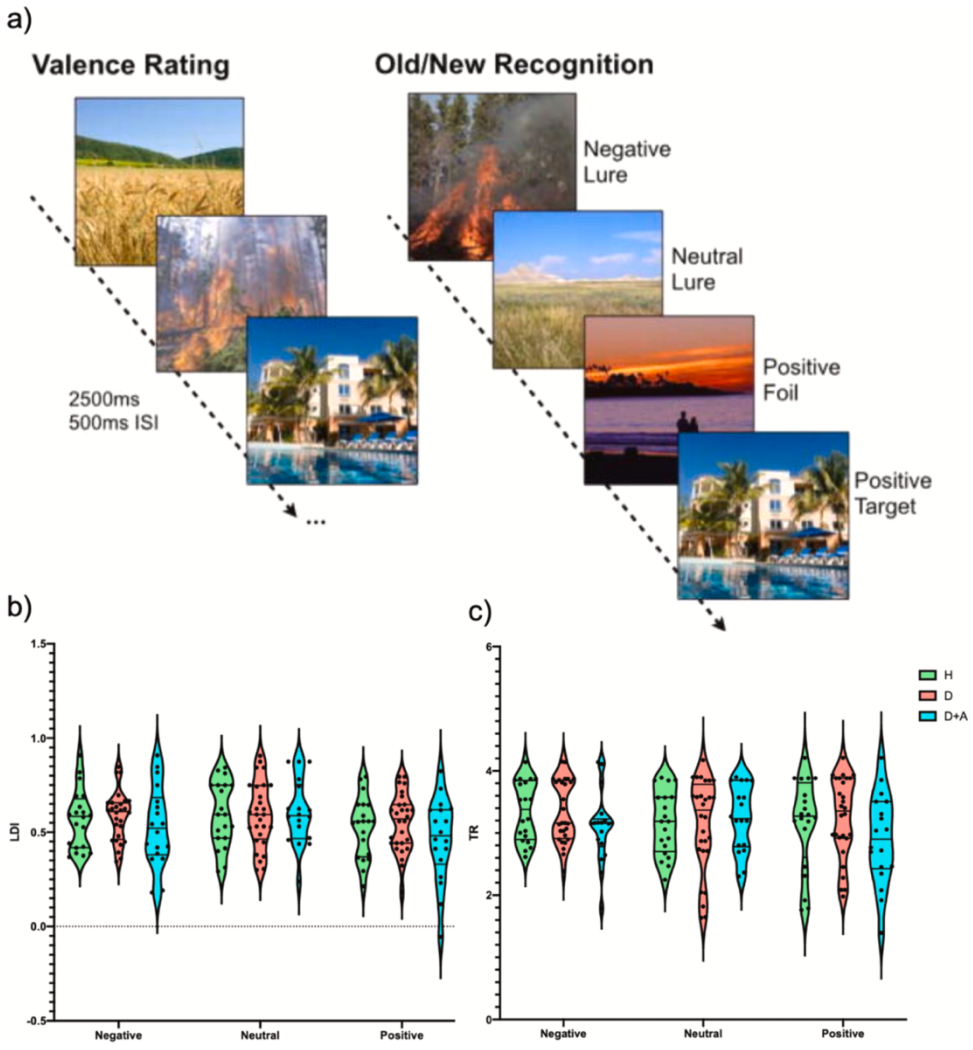

Figure A1.1. (a) The emotional pattern separation paradigm. During study participants are asked to rate the valence of the images either positive, negative, or neutral. During test, participants are asked to make "old" or "new" judgements. Images are varied from study such that some images are slightly altered 'lures', other images are novel 'foils', or repeated (targets). Images are varied as a function of emotional valence (positive, negative, neutral) as described in our previous work (Leal et al., 2014a, 2014b). (b, c) No difference between clinically assessed groups on emotional pattern separation performance for (b) lure discrimination and (c) target recognition (TR).

Participants were asked to identify the valence associated with each image (Negative, Neutral, Positive). The subsequent test phase consisted of 291 trials. During these trials participants viewed stimuli which were either (1) seen once before during

the study phase (targets), (2) stimuli that were similar to ones seen in the study phase but not identical (lures), and (3) novel images never seen before (foils). Targets, lures, and foils were evenly distributed across the three emotional valences. Participants were asked to indicate via button press whether they believed the items were “Old” or “New”. They were explicitly told that “Old” images had to be the exact same image they had seen in the previous encoding phase. Images were characterized *a priori* for emotional valence (negative, neutral, positive), arousal (very calming to very exciting), and similarity (median split of similarity ratings into “high” and “low”) (Leal et al., 2014).

Behavioral performance on the task was quantified using two key measures. First we quantified target recognition (TR) using d-prime, a standard discriminability index that quantifies target hit rate, while correcting for false alarms. It is operationalized as z(Target Hit rate) – z(Foil False Alarm rate). Additionally, we calculated a lure discrimination index (LDI) operationalized as p(“New”|Lure) – p(“New”|Target) which quantifies lure discriminability and corrects for a “New” response bias. Extreme hit and false alarms rates (for lures and foils) were corrected following the methods of Stanislaw and Todorov (1999).

Two versions of the task were administered due to change in software. Twenty-six participants completed the task administered via version one conducted on MATLAB (RRID:nlx_153890, Version R2010a, Natick, MA) software with PsychToolbox version 3.0. Forty-seven participants completed the task using version 2 conducted using PsychoPy. Task versions varied slightly in the size of the images used. In addition, the PsychToolbox version of the task was conducted with visual confirmation of the study

responses. Additional analyses are included in Figure A1.2 to rule out any behavioral differences between task versions.

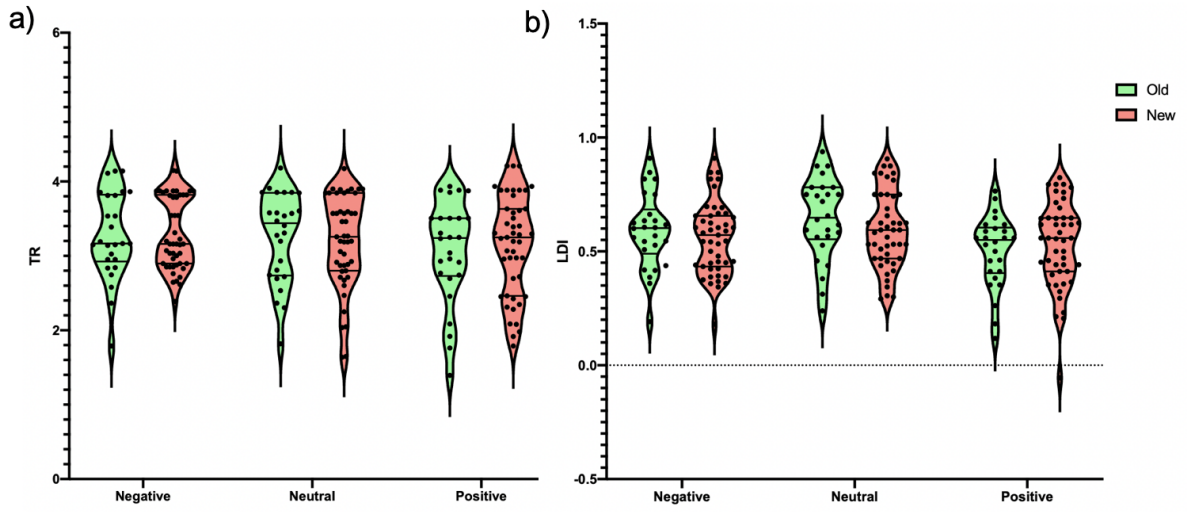

Figure A1.2 No significant difference in task performance across the Old and New task versions. (a) We found no difference ($F_{2,213} = 0.26$, $P = 0.77$) on performance on Target Recognition (TR) across task versions. (b) We found no difference ($F_{2,213} = 0.98$, $P = 0.37$) on lure discrimination performance across valence.

Statistical Analysis

Exploratory Factor analysis were conducted on questions derived from the BDI-II and BAI using the 'Psych' toolbox available in R (https://rstudio.com). Verimax rotated principal components were used. Similar to Lee et al. (2018) we allocated items to a specific factor using the criterion of a loading of more than 0.30 on the corresponding factor and items were excluded if the difference of the factor loading was less than 0.10 for a particular item. We tested if continuous measures of anxiety (BAI), and depression (BDI-II), as well as Factors 1 through 5, were normally distributed using the Shapiro-Wilk normality test from the 'stats' package in R (Royston, 1995). The results confirmed no continuous measure of depression, anxiety, nor the factor scores were normally distributed. As such, Spearman's correlation coefficients (r_s) were calculated using R to

evaluate the relationships between continuous measures of anxiety and depression and memory performance. Multiple linear regression analyses were conducted in R to account for confounding variables including age and sex in the relation between anxiety and depression and memory performance. Standardized beta coefficients are reported in-text and were calculated using the 'lm.beta' package in R. Two-way ANOVA was used to determine differences in task performance across versions and task performance as a function of clinical diagnosis. To ensure Multiple comparisons were corrected for within-family (emotional valence) bivariate analyses of the factor relation to emotional pattern separation behavior using the Benjamini-Hochberg procedure implemented in R (Benjamini & Hochberg, 1995). Bootstrap analysis were conducted using the Boot package available in R-Studio with 1000 repetitions and 95% confidence intervals are reported.

Results

Overall EmoPS Performance Does not Vary by Clinical Diagnosis

We first asked if behavioral performance differed as a function of clinical diagnosis. There was no significant interaction between diagnosis and emotional valence for LDI performance ($F_{4,189}$ = 0.50, *P* = 0.74; Figure A1.1b) or TR performance ($F_{4,189}$ = 0.89, *P* = 0.47; Figure A1.1c). Across the whole sample, LDI performance was significantly different ($F_{2,216}$ = 5.40, *P* = 0.005; Figure A1.3.a) with participants performing worse for positive stimuli compared to neutral (*adjusted P* = 0.0034). We found no behavioral difference in TR across emotional valence for all participants ($F_{2,216}$ = 1.50, *P* = 0.22; Figure A1.3b).

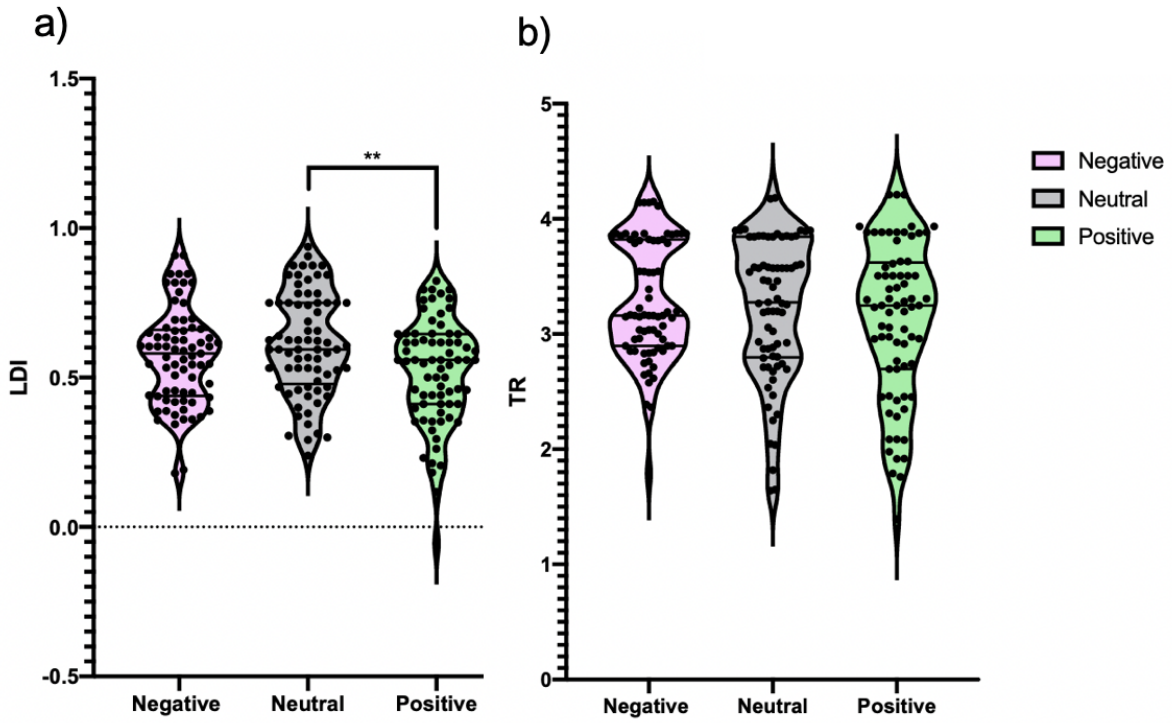

Figure A1.3. Emotional pattern separation performance for all participants on lure discrimination (LDI; a), target discriminability normalized by lure false alarm rate (b), and target discriminability normalized by foil false alarm rate (c).

For all subsequent analyses, we chose to focus on the negative and neutral items and not consider the positive items as they were not well-matched to the negative for arousal ratings, however, results with positive stimuli are represented for reference in Figure A1.4.

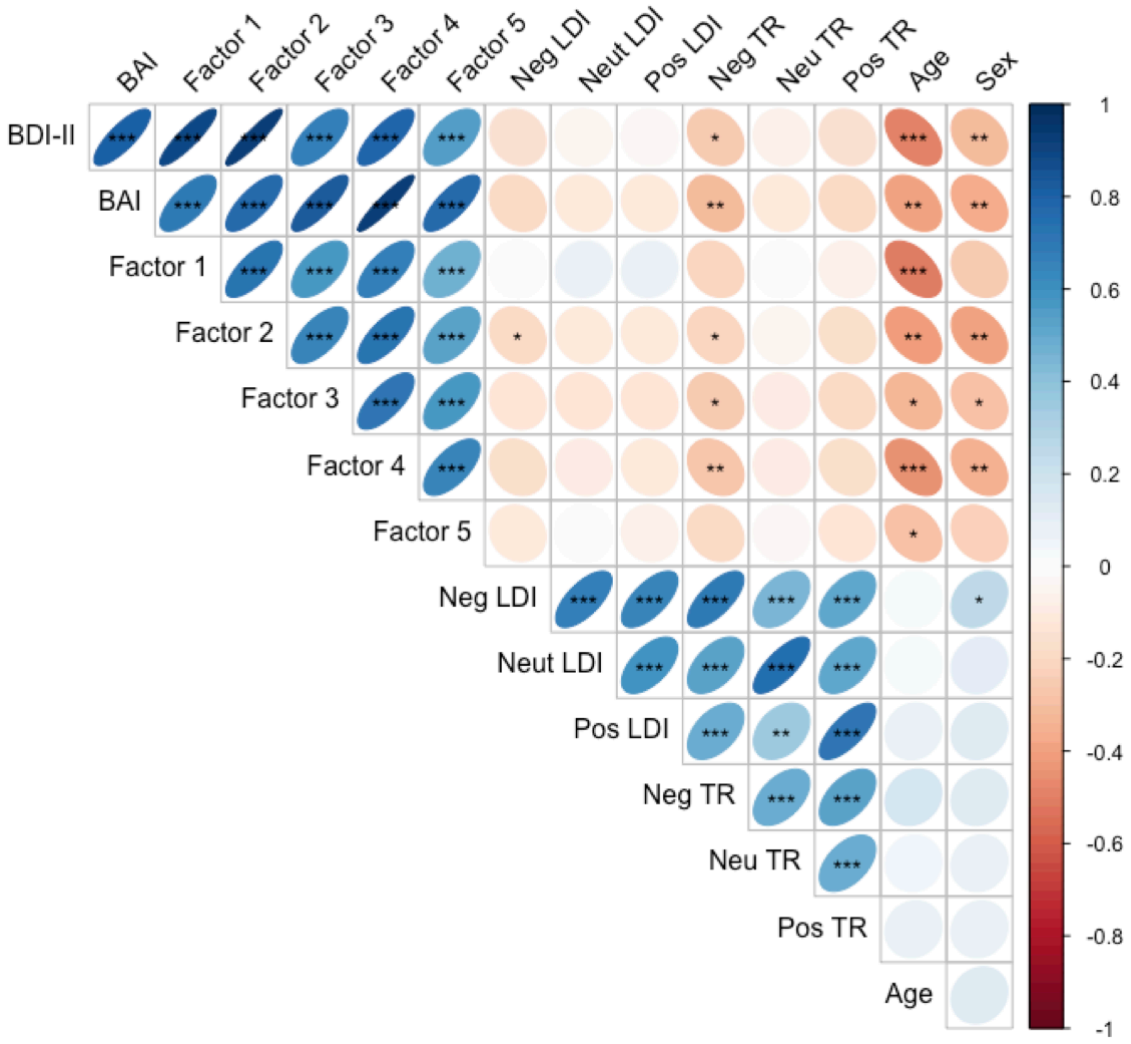

Figure A1.4. Correlations among Factors 1 through 5, LDI, Target Recognition (TR) as well as age and sex. Observationally, we note that negative TR is related to several Factors. Additionally, we identify that age as well as sex (males = 1, females =0) are inversely related to greater Factor totals. *Indicates P < 005. ** Indicates P < 0.01. ***Indicates P < 0.001.

Anxiety Symptom Severity is Associated with Impaired Memory Performance for Negative Items

We first explored the degree to which anxious and depressive symptoms, across all participants, were related to one another using the cumulative inventory totals from

the BAI and BDI-II inventories. We found a strong association between scores on BDI-II and BAI across all participants (r_s = 0.80, P < 0.0001; **Figure A1.5**.).

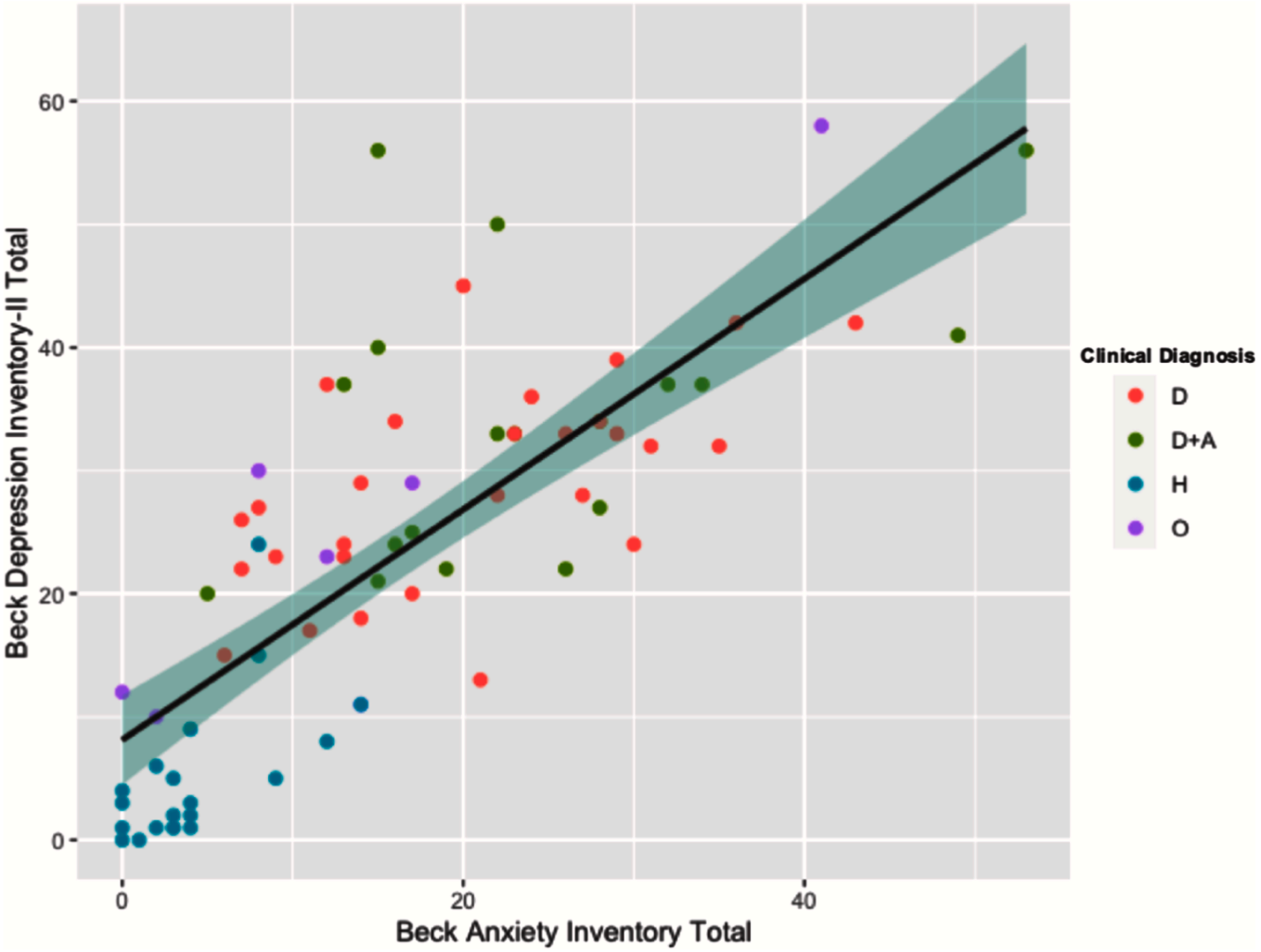

Figure A1.5. Clinical diagnosis plotted as a function of BDI-II inventory and BAI inventory total scores.

We then asked if depression and anxiety scales were associated with LDI and TR for negative and neutral items. We found that greater depressive symptoms were not associated with LDI for negative (r_s = -0.14, P = 0.22) or neutral (r_s =-0.055, P = 0.65) items. Similarly, total anxiety symptoms were not associated with LDI for negative

(r_s = -0.19, *P* = 0.10) or neutral (r_s = -0.10, *P* = 0.39) items. We found that more depressive symptoms (r_s = -0.25, *P* = 0.032; Figure A1.6a) and more anxiety symptoms (r_s = -0.31, *P* = 0.0081; Figure A1.6c) were associated with lower TR for negative items.

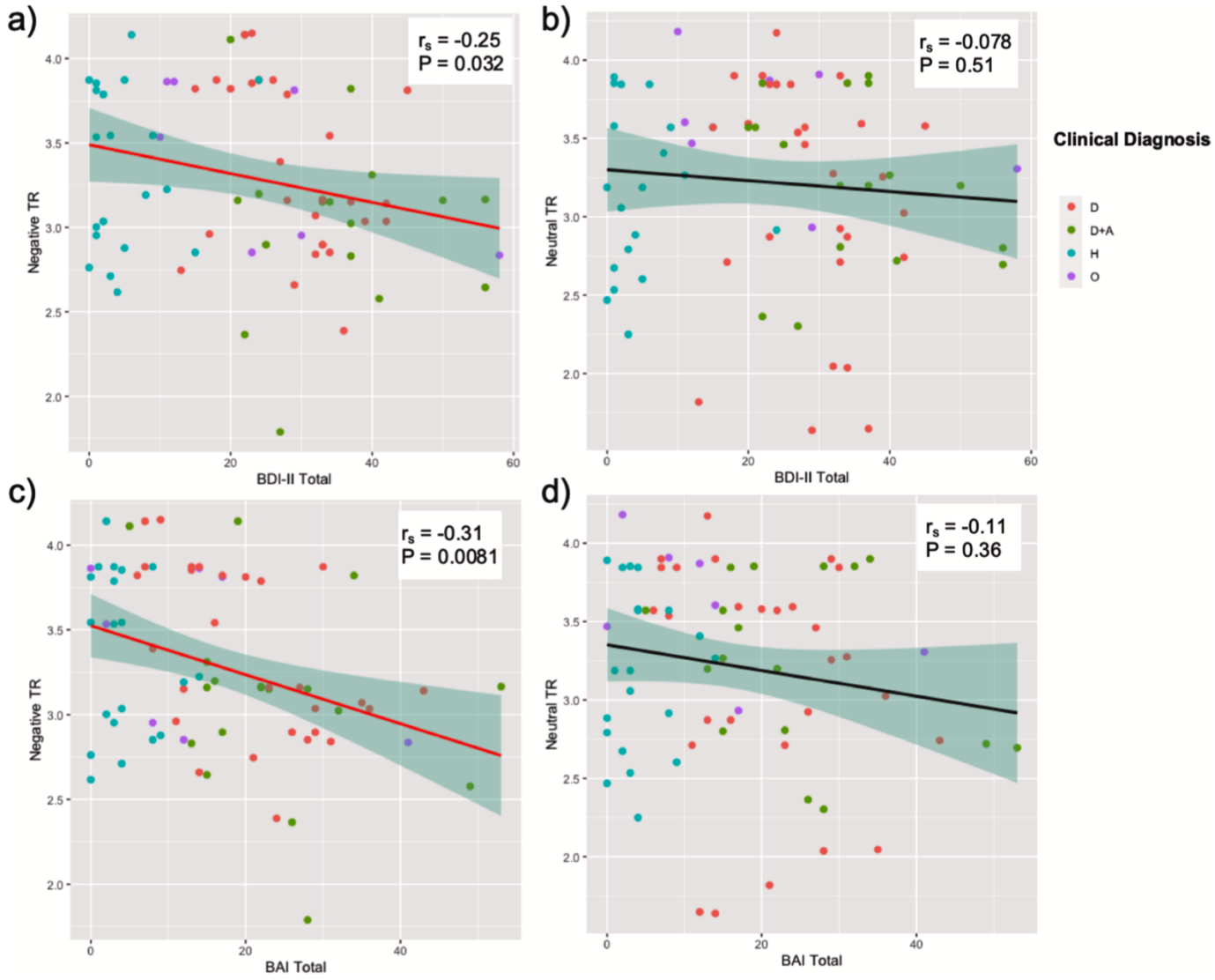

Figure A1.6. Association between BDI-II (a, b) and BAI (c, d) inventory totals and target recognition (TR) for negative (a, c) and neutral (b, d) items.

The relationship between depressive symptoms and lower TR for negative items did not remain significant after accounting for age and sex (β = -0.22, *P* = 0.11). However, the relationship between anxiety symptoms and lower TR for negative stimuli

did remain significant after accounting for age and sex (β = -0.35, *P* = 0.0088). We then tested if depression or anxiety was related to TR for neutral items. Neither depressive symptoms (r_s = -0.087, *P* = 0.51; Figure A1.6b) nor anxiety symptoms (r_s = -0.11, *P* = 0.36; Figure A1.6d) were associated with TR for neutral items. Interestingly, the relationship between symptoms of anxiety and lower TR for negative stimuli was driven by targets hit rate for negative stimuli (r_s = -0.37, *P* = 0.0013) and not false alarm rate (r_s = 0.020, *P* = 0.87).

Exploratory Factor Analysis and Relation to Clinical Diagnoses

As a result of the strong association between depressive and anxious symptoms we sought to determine if sub-clusters of symptoms were more strongly associated with difference facets of emotional memory performance. Utilizing the full sample (N=79) we found that the Kaiser-Meyer-Olkin measure (0.85) and Barrett's test of sphericity (approximate Chi-square = 876.55, 661 degrees of freedom, *P* < 0.0001) provided evidence that the use of the exploratory factor approach was appropriate for these data and that 5 factors were sufficient. Factor analysis revealed that the following 5 factors explained approximately (59%) of the variance. We note that some factors include symptoms that may typically be associated with other clinical constructs. **Factor 1 (Negative Affect)** is composed of 6 items from the BDI-II which include "Pessimism", "Past Failure", "Self-dislike", "Self-criticalness", "Suicidal thoughts or wishes", "Worthlessness". **Factor 2** (**Anhedonia-like**) is composed of 8 items from the BDI-II which include "Loss of pleasure", "Punishment feelings", "Loss of energy", "Irritability", "Crying", "Loss of interest", "Concentration difficulty", "Tiredness or fatigue". **Factor 3**

(**Somatic Anxiety**) is composed of 7 items from the BAI including “Feeling hot”, “Dizzy or lightheaded”, “Feeling of choking”, “Faint lightheaded”, “Face flushed”, “Hot/cold sweats”, “Difficulty breathing”. **Factor 4** (**Cognitive Anxiety**) is composed of 5 items on the BAI and one item on the BDI-II which include “Unable to relax”, “Fear of worst happening”, “Unsteady”, “Nervous”, “Fear of losing control”, “Changes in sleeping pattern”. **Factor 5 (Somatic Anxiety)** is composed of 3 items on the BAI which include “Wobbliness in legs”, “Hands trembling”, “Shaky unsteady”. The factor loadings are summarized in Table A1.3. In order to quantify the external validity of the item factor identities calculated in our sample, we quantified a normalized mutual information (NMI) score representing the degree of consistency of our results with previously published reports. In direct comparison to item factor identities of a large (n=406) clinical population, we report a NMI of 0.67 indicating moderate overlap within the clustering of BAI and BDI-II questions across samples (Lee et al., 2018). Factor scores were quantified by summing respective items within each factor.

Table A1.3. Exploratory factor analysis on 42 items from the BDI-II and BAI.

Inventory Identity	Items	Factor1	Factor2	Factor3	Factor4	Factor5	Uniqueness
D	**Pessimism**	**0.77712804**	0.26485042	0.24539489	0.13132086	0.18068717	0.2158115
D	**Past.Failure**	**0.72389638**	0.28607047	0.15753857	0.21679833	0.04211347	0.3205434
D	**Self.Dislike**	**0.82989106**	0.17227467	0.21814166	0.18228313	0.16831923	0.1724534
D	**Self.Criticalness.**	**0.64141483**	0.41729106	0.04350299	0.27373267	0.1111219	0.325283
D	**Suicidal.Thoughts.or.Wishes**	**0.50809463**	0.25129772	0.19716152	0.17658526	-0.0708959	0.6036264
D	**Worthlessness**	**0.76938677**	0.27262725	0.23716295	0.14848121	0.19582645	0.2170714
D	**Loss.of.Pleasure**	0.39160704	**0.74175296**	0.10688447	0.25363353	0.25373843	0.1563097
D	**Punishment.Feelings.**	0.15389157	**0.51866528**	0.41344227	0.38453728	0.07981183	0.3821329
D	**Loss.of.Energy**	0.30080003	**0.66582562**	0.34871762	0.12285838	0.05939576	0.3259721
D	**Irritability**	0.19712994	**0.69748212**	0.31468192	0.19986512	0.15477788	0.3117314
D	**Crying**	0.3797373	**0.51038543**	0.33966752	0.23245771	0.08895584	0.4179916
D	**Loss.of.Interest**	0.498363	**0.67982493**	0.11051959	0.17688203	0.15742587	0.2211836
D	**Concentration.Difficulty.**	0.34972679	**0.61252432**	0.37267319	0.24507253	0.14257013	0.2832343
D	**Tiredness.or.Fatigure**	0.43846048	**0.54759452**	0.19561457	0.25802558	0.11055606	0.3908366
A	**Feeling.hot**	0.06833009	0.28447635	**0.54870155**	0.15790325	0.09230075	0.5798775
A	**Dizzy.or.lightheaded**	0.17921664	0.29255929	**0.45197241**	0.20154835	0.31058593	0.5409226
A	**Feeling.of.choking**	0.27931474	0.04698573	**0.61724742**	0.12018748	0.24938522	0.4621248
A	**Faint…lightheaded**	0.10020839	0.16722285	**0.58430755**	0.1223727	0.20330428	0.5642958
A	**Face.flushed**	0.07680063	0.29889648	**0.52385807**	0.33669589	0.01042321	0.51686
A	**Hot.cold.sweats**	0.16979326	0.17184826	**0.60430486**	0.1738053	0.08897877	0.5383305
A	**Difficulty.in.breathing**	0.13198328	0.17879972	**0.5613848**	0.31377414	0.31635837	0.4369234
A	**Unable.to.relax**	0.36887081	0.42389236	0.1115699	**0.61417268**	0.27255906	0.2203042
A	**Fear.of.worst.happening**	0.35786713	0.1422663	0.27689994	**0.75375787**	0.09252536	0.198305
A	**Unsteady**	0.12037013	0.23477716	0.37798279	**0.5345359**	0.40700198	0.336145
A	**Nervous**	0.36023396	0.41327091	0.26772248	**0.60153356**	0.19531759	0.227773
A	**Fear.of.losing.control**	0.26797756	0.12804534	0.33455202	**0.47816862**	0.14844334	0.5491919
D	**Changes.in.Sleeping.Pattern**	0.1413271	0.33987445	0.30367662	**0.45596967**	0.04537547	0.5623314
A	**Wobbliness.in.legs**	0.14593026	0.11333084	0.17566114	0.04102021	**0.68420866**	0.4651598
A	**Hands.trembling**	0.19485941	0.10195464	0.39229553	0.21331583	**0.67657523**	0.2944797
A	**Shaky…unsteady**	0.19484544	0.16675031	0.33721594	0.41908604	**0.59418618**	0.2918279
A	**Terrified.or.afraid**	0.30510065	0.0837911	0.51328803	0.55796227	0.13328116	0.3073458
A	**Heart.pounding.racing**	0.1930554	0.27914337	0.38177393	0.4551212	0.34185197	0.4150663
A	**Fear.of.dying**	0.28820349	0.00985847	0.35279735	0.13337594	0.09094666	0.766345
A	**Scared**	0.23180329	0.13712659	0.56696583	0.52408894	0.19122457	0.2947798
A	**Indigestion**	0.21175663	0.30901897	0.38752316	0.03652352	0.0933679	0.6994472
D	**Indecisiveness**	0.46768346	0.4038309	0.29903708	0.32355287	0.18977075	0.3880737
D	**Changes.in.Appetite**	0.42127916	0.37261221	0.22696136	0.16330213	0.12367281	0.5902289
D	**Loss.of.Interest.in.Sex**	0.19114233	0.20696626	0.00992127	0.0111293	0.06832415	0.9158702
A	**Numbness.or.tingling**	-0.0629523	0.33115013	0.07546944	0.44474363	0.46753476	0.4642973
D	**Agitation**	0.34320327	0.40338675	0.12151812	0.29733925	0.09631173	0.6070728
D	**Guilty.Feelings**	0.37364309	0.38201784	0.26216535	0.34768085	0.21968799	0.4765714
D	**Sadness**	0.54186282	0.49744825	0.3999217	0.16048047	0.09065003	0.2650229
SS Loadings		6.166	5.806	5.322	4.671	2.717	
Proportion of Variance Explained		0.15	0.14	0.13	0.11	0.06	
Cumulative Variance Explained		0.15	0.29	0.41	0.52	0.59	

We then asked if factors from our exploratory factor analysis were able to distinguish among different clinical diagnoses (H, D, D+A, and A). We found a significant main effect of factor ($F_{4,330}$= 56.35, P < 0.0001), clinical diagnosis ($F_{2,330}$ = 147.6, P < 0.0001), as well as a significant factor x clinical diagnosis interaction ($F_{8,330}$= 8.41, P < 0.0001). Post-hoc comparisons revealed that Factors 1 (Negative Affect), 2 (Anhedonia), 3 (Somatic Anxiety), and 4 (Cognitive Anxiety) were able to distinguish the H and D groups as well as H and D+A groups (Figure A1.7). No factor was able to distinguish the D and D+A group. Factor 5 (composed from 3 questions from the BAI)

was not sufficient to dissociate the H from clinical groups (D, D+A). Due to this analysis, we decided not to include Factor 5 in subsequent analyses.

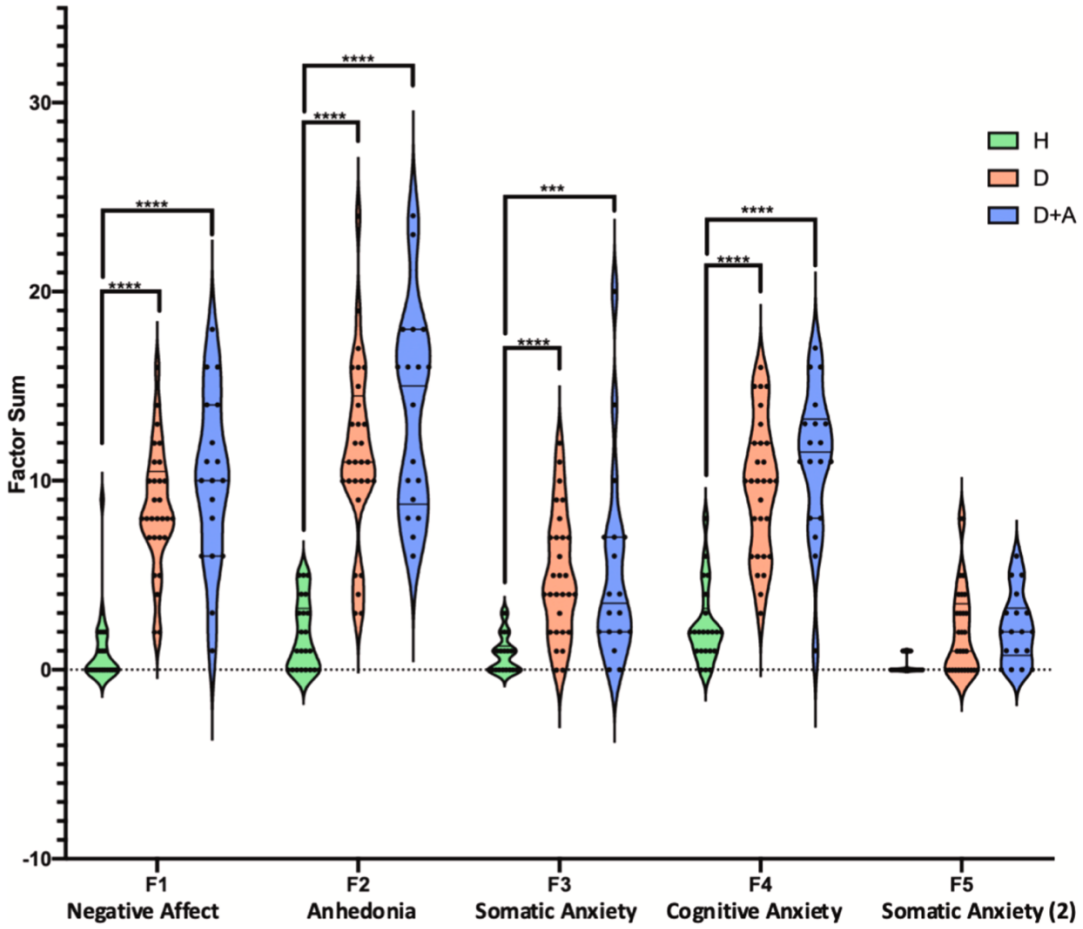

Figure A1.7. Factor analytics dissociate healthy from psychiatric diagnoses as well as those with anxiety from those with comorbid depression. ****Indicates P < 0.0001, ***Indicates P < 0.001, **Indicates P < 0.01, *Indicates P < 0.05.

Factor Relation to EmoPS Performance

We then sought to determine if latent factors of anxiety and depression were associated with impaired EmoPS performance. In separate analyses, we correlated each factor with EmoPS performance for negative and neutral stimuli correcting for multiple comparisons within family using the Benjamini-Hochberg procedure.

First, we found that greater total scores for Somatic Anxiety (r_s = -0.24, un*adjusted P* = 0.038; Figure 5c) and Cognitive Anxiety (r_s = -0.27, un*adjusted P* = 0.019; Figure A1.8d) were associated with impaired negative TR. The association between Somatic Anxiety and negative TR performance was significant after accounting for age and sex (β = -0.27, *P* = 0.036). Similarly, the association between Cognitive Anxiety and negative TR performance was significant after accounting for age and sex (β = -0.33, *P* = 0.020). However, after correcting for multiple comparisons, neither Somatic Anxiety (*adjusted P* = 0.077) nor Cognitive Anxiety (*adjusted P = 0.077*) were significantly associated with negative TR performance. In addition, we note that greater measures of Negative Affect (r_s = -0.20, *unadjusted P* = 0.082; Figure A1.8a) and Anhedonia-Like factors (r_s = -0.21, *unadjusted P* = 0.074; Figure A1.8b) were marginally associated with impaired negative TR.

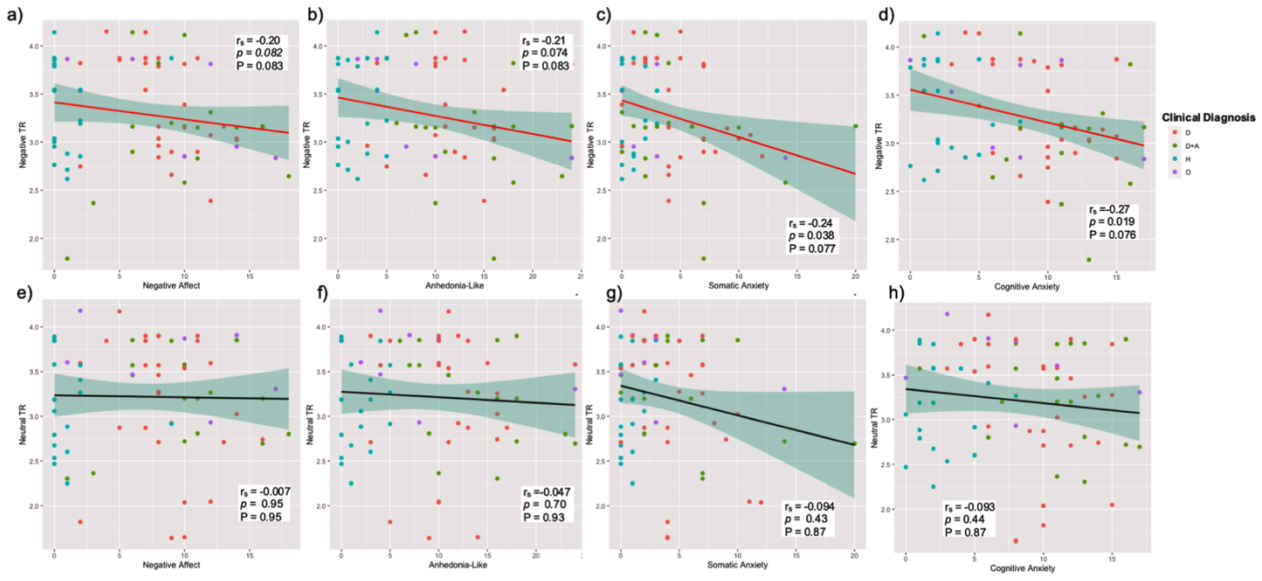

Figure A1.8. (a–d) Show the relationship between Factors 1–4 and Target Recognition (TR) for negative items. (e–h) Show the relationship between Factors 1–4 and TR for neutral items. p indicates p-value prior to correcting for multiple comparisons. P indicates p-value after correcting for multiple comparisons.

As a result of the non-normal distribution of Somatic Anxiety scores and Cognitive Anxiety scores and to ensure these effects were not driven by individual points having a large effect we conducted bootstrap analysis with 1000 simulations. The 95% confidence interval for the Spearman's correlation coefficient bootstrap effect for the relationship between Somatic Anxiety and negative TR ranged from -0.46 to -0.045 (SE = 0.11). The 95% confidence interval for the Spearman's correlation coefficient bootstrap effect for the relationship between Cognitive and negative TR ranged from -0.45 to -0.03 (SE = 0.11). No Factor was associated with negative or neutral LDI after correcting for multiple comparisons (Figure A1.9).

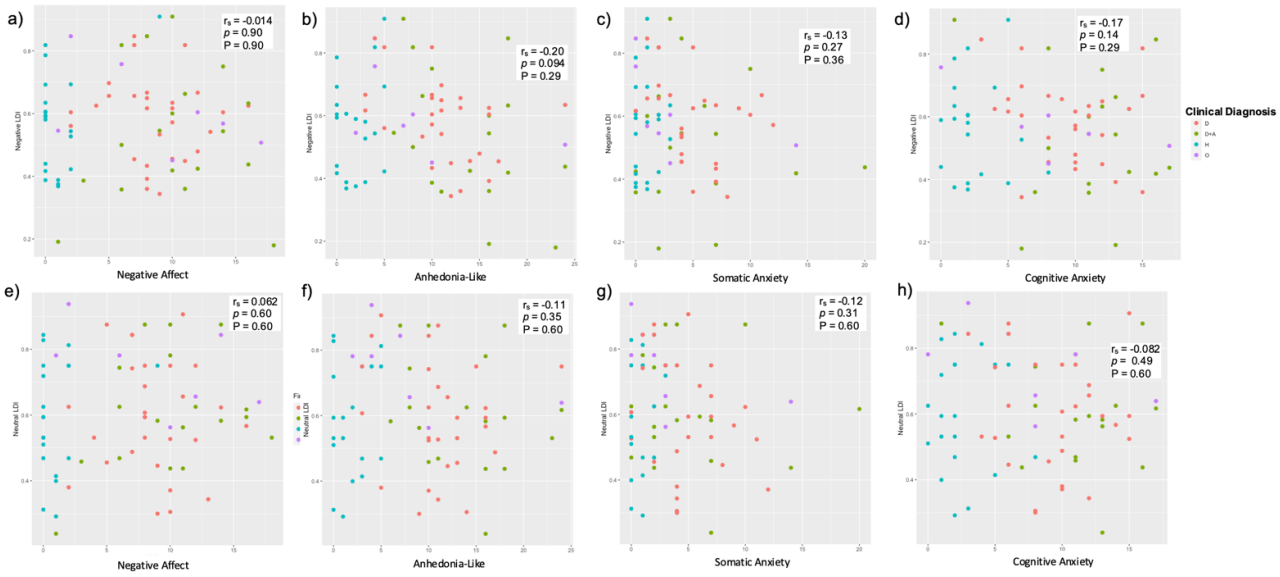

Figure A1.9: (a-d) Show the relationship between Factors 1-4 and LDI for negative items. (e-h) Show the relationship between Factors 1-4 and LDI for neutral items.

Discussion

There are three key findings in this study. First, our exploratory factor analysis provides evidence that symptoms of anxiety and depression may be broken into

constituent components namely Negative Affect, Anhedonia-Like symptoms, Somatic, and Cognitive Anxiety. Second, we find that factors from our exploratory factor analysis are able to dissociate clinical diagnoses from healthy controls, however, diagnoses of depression and depression comorbid with anxiety are not differentiable in this small sample using these latent factors. Third, we find that greater symptoms of anxiety are associated with impaired recognition for negative items but not neutral items. The contributions of anxiety and depression to emotional episodic memory disruption have long been a target of investigation in humans, however, most work has focused on sub-clinical symptoms and the comorbidity of anxiety and depression symptoms are often left untested (Dillon & Pizzagalli, 2018).

A general framework for the episodic memory dysfunction in depression suggests a negativity memory bias or augmented memory for negative material (Dillon & Pizzagalli, 2018; Leal et al., 2014; Burt et al., 1995) whilst also displaying impaired recollection or “overgeneralized” autobiographical retrieval (Dalgleish et al., 2007; Williams et al., 2007). These performance differences are often coupled with volumetric and functional differences in the hippocampus (Stockmeier et al., 2004) as well as amygdala (MacMillan et al., 2003; Sheline et al., 2001; Whalen et al., 2002). We have previously shown in an undiagnosed sample that individuals reporting a high frequency of depressive symptoms show augmented discrimination for negative items (Leal et al., 2014a). We have also shown that higher depressive symptoms were associated with augmented amygdala activity and attenuated DG/CA3 activity during correct discrimination of negative items compared to neutral items (Leal et al., 2014b).

In this investigation, we provide evidence that symptoms of anxiety are associated with impaired recognition for negative stimuli and not neutral stimuli. This relationship also persists after accounting for age and sex. However, across the whole sample, continuous measures of depression and anxiety were highly correlated, which suggests that multiple regression on its own may not be the most suitable method for capturing the effects of depressive symptoms when highly comorbid with anxiety.

To address this concern, we implemented the use of exploratory factor analysis to uncover latent constructs of anxiety and depression and to determine whether symptoms could be meaningfully clustered together. We identified 5 factors, two composed of questions derived from the BDI-II generally reflecting Negative Affect (Factor 1) and Anhedonia-like symptoms (Factor 2) and 3 composed of questions derived largely from the BAI (Factor 3/5: Somatic Anxiety/hyperarousal; Factor 4: Cognitive Anxiety). While we note we were able to derive factors that included largely separable factors of depression and anxiety, we note that factor 4 (Cognitive Anxiety) is composed of 5 items from the BAI and 1 item (changes in sleeping pattern) from the BDI-II. This approach has been previously used to test the hypothesis that coexisting symptoms of anxiety and depression (derived from the BAI and BDI-II) can be differentiated into a tripartite model including general negative affectivity (NA), anxiety (physiological hyper-arousal), and depression (low positive affectivity) (Lee et al., 2018; Clark et al., 1991). In this sample, we demonstrate considerable overlap in the clustering of item-factor identities compared to previously published reports (Lee et al., 2018) and note that questions related to BDI and BAI largely clustered onto separate factors.

While we found that our item-factor identities were comparable with other investigations and were able to dissociate healthy participants from clinical groups (D, D+A), we did not find evidence that our factors were able to dissociate individuals with a depression diagnosis alone from those with depression and a comorbid anxiety disorder indicating similar degree of negative affect, anhedonia-like symptoms, cognitive and somatic anxiety across clinical groups. Thus, it is possible that while similar factor constructs have been successful at separating clinical depression and anxiety diagnoses (Lee et al., 2018), the factor identity approach in this investigation is not capable of dissociating depression and depression with comorbid anxiety symptoms. One possibility is the prevalent presence of subsyndromal or subthreshold anxiety in depression which may make the distinction based on factors and symptoms more difficult.

Regardless of this distinction, we used these factors to determine if specific aspects of depression or anxiety were associated with impaired recognition for negative stimuli. We found that both constructs of anxiety, including somatic anxiety/hyperarousal as well as cognitive anxiety, were associated with impaired recognition of negative stimuli but not neutral stimuli. We also report a marginally significant relationship between anhedonia related symptoms (Factor 2) and impaired recognition for negative stimuli (at the corrected level).

The hypothesis that anxiety-like symptoms are related to impaired episodic memory dysfunction has been tested before. Notably, experimentally induced symptoms of anxiety in both humans and animal models suggest an effect of overgeneralization and impaired memory performance. For instance, animals who have

undergone fear conditioning freeze when exposed to a similar but not identical operant chamber (Kheirbek et al., 2012). In humans, experimentally induced symptoms of somatic anxiety (via shock expectancy) were associated with impaired performance on a pattern separation task (Balderston et al., 2017). Others have suggested that anxiety leads to overgeneralization through impairments in pattern-separation mediated mechanisms (Sahay et al., 2011; Leal et al., 2018). However, here we show for the first time that clinical levels of cognitive and somatic anxiety, distinguished from depressive symptoms, are related to impaired recognition memory for negative stimuli in a clinical sample.

In a recent review, Dillon & Pizzagalli (2018) suggest that while depressive symptoms have been linked with augmented pattern separation for negative stimuli, it is possible that impaired pattern separation may be a feature in depressed individuals who also express comorbid anxiety. The current study suggests that anxiety is associated with worse recognition recognition rather than worse discrimination, after accounting for depressive symptoms. This performance pattern is consistent with the notion that anxiety impairs episodic memory function for negative stimuli (Tofalini et al., 2015; Inaba & Ohira, 2009).

Certainly, the interplay between depression and anxiety may be even more complex and includes factors such as the duration of expression of each type of symptom or the age of onset of symptoms. For example, we have previously shown that post-encoding stress in healthy individuals is able to enhance the discrimination of negative stimuli but not neutral stimuli (Cunningham et al., 2018). Similarly, also in healthy adults, an exaggerated noradrenergic response elicited by viewing threatening

images yielded augmented memory performance for negative but not neutral items (Segal and Cahill, 2008). Perhaps memory performance is a function of severity of psychiatric morbidity. In this case, we may observe augmented discrimination of negative events early in subclinical levels of depression, however as depression progresses, stress levels become more elevated and the storage of negative experiences accumulates, subsequently leading to impaired discrimination or recognition as the disease progresses and the comorbidity with anxiety becomes more established, similar to the theory proposed by Dillon & Pizzagalli (2018).

It is hypothesized that the EmoPS task used in this investigation engages a neuronal computation known as pattern separation which is thought to be heavily reliant on the dentate gyrus (DG) and the CA3 regions of the hippocampus (Yassa & Stark, 2011). The CA3 is thought to maintain a balance between storing new experiences using pattern separation and re-instantiating previously stored experiences using "pattern completion". The latter function in particular is thought to be reliant on the recurrent collateral network of the CA3 (Yassa & Stark, 2011; Rolls, 2007). One possibility is that the relation between greater anxiety and impaired recognition for negative stimuli may be attributed to impaired CA3 function. In animals, chronic stress is thought to induce preferential loss of CA3 apical dendrite length and branching as well as dendritic spine density (Sousa et al., 2000; Magariños & McEven, 1995; Magariños et al., 1996; Vyas et al., 2002; Soetanto et al., 2010). Similar evidence has been found in ex-vivo samples in humans of those with clinical depression, namely decreased dendrite and spine densities in the CA3 region (Soetanto et al., 2010), although we note that these histological effects are not entirely specific to the CA3 region with other

studies finding differences in the amygdala (Vyas et al., 2003), prefrontal cortex (Radley et al., 2004) as well as other regions. The stress-induced loss of CA3 connectivity in particular could impair its ability to process input from the entorhinal cortex thereby leading to an impairment in pattern completion or recognition. This could potentially explain the failure of recognition we observe in individuals with high levels of anxiety. Future research could test the hypothesis that CA3 function may be a mechanistic contributor to the recognition failure in anxiety.

One potential limitation of this study is the use of a clinical sample with mixed pathology that includes varying levels of depression and anxiety. While this may be more representative of the population, it does make interpretations more difficult with respect to depression alone, anxiety alone, or comorbid depression and anxiety given the smaller sample sizes. Additionally, we note that while our sample did contain a group of subjects with clinical history of depression and history of clinically diagnosed co-morbid depression and anxiety, continuous measures of symptoms were not sufficient to dissociate the two. Additionally, we note that we did not explicitly test the relationship between symptom severity and memory discrimination or recognition of positive stimuli. This was intentionally the case for two reasons. First, our prior work focused on the differences between negative and neutral stimuli specifically (Leal et al., 2014ab). Second the positive stimuli were not matched for arousal ratings compared to the negative images and thus would be difficult to compare. Future work could perhaps examine a different kind of positive stimulus such as stimuli that elicit stronger hedonic value.

In conclusion, we provide evidence that symptoms of anxiety, controlling for co-morbid depression, are associated with impaired recognition for negative stimuli. Our exploratory factor analysis revealed that this relationship is present in both somatic and cognitive symptoms of anxiety. These results are consistent with a dimensional understanding of psychiatric pathology and pave the path to more mechanistic studies to understand the neural mechanisms of memory impairment in anxiety and depression.

References

Bai, T., Xie, W., Wei, Q., Chen, Y., Mu, J., Tian, Y., Wang, K., 2017. Electroconvulsive therapy regulates emotional memory bias of depressed patients. Psychiatry Res. 257, 296–302.

Balderston, N.L., Mathur, A., Adu-Brimpong, J., Hale, E.A., Ernst, M., Grillon, C., 2017. Effect of anxiety on behavioural pattern separation in humans. Cogn. Emot. 31 (2), 238–248.

Benjamini, Y., Hochberg, Y., 1995. Controlling the false discovery rate: a practical and powerful approach to multiple testing. J. R. Stat. Soc. Ser. B 57, 289–300.

Burt, D.B., Zembar, M.J., Niederehe, G., 1995. Depression and memory impairment: a meta-analysis of the association, its pattern, and specificity. Psychol. Bull. 117, 285–305.

Chamberlain, S.R., Sahakian, B.J., 2006. The neuropsychology of mood disorders. Curr. Psychiatry Rep. 8 (6), 458–463.

Clark, L.A., Watson, D., 1991. Tripartite model of anxiety and depression: psychometric evidence and taxonomic implications. J. Abnorm. Psychol. 100 (3), 316–336.

Conradi, H.J., Ormel, J., de Jonge, P., 2011. Presence of individual (residual) symptoms during depressive episodes and periods of remission: a 3-year prospective study. Psychol. Med. 41, 1165–1174.

Cunningham, T.J., Leal, S.L., Yassa, M.A., Payne, J.D., 2018. Post-encoding stress enhances mnemonic discrimination of negative stimuli. Learn. Mem. 25 (12), 611–619 (Cold Spring Harbor, N.Y.).

Dalgleish, T., Williams, J.M., Golden, A.M., Perkins, N., Barrett, L.F., Barnard, P.J., Yeung, C.A., Murphy, V., Elward, R., Tchanturia, K., Watkins, E., 2007. Reduced specificity of autobiographical memory and depression: the role of executive control. J. Exp. Psychol. Gen. 136 (1), 23–42.

Dillon, D.G., Pizzagalli, D.A., 2018. Mechanisms of memory disruption in depression. Trends Neurosci. 41 (3), 137–149.

Haas, B.W., Canli, T., 2008. Emotional memory function, personality structure and psychopathology: a neural system approach to the identification of vulnerability markers. Brain Res. Rev. 58, 71–84.

Hamilton, J.P., Gotlib, I.H., 2008. Neural substrates of increased memory sensitivity for negative stimuli in major depression. Biol. Psychiatry 63 (12), 1155–1162.

Hasler, G., Drevets, W.C., Manji, H.K., Charney, D.S., 2004. Discovering endophenotypes for major depression. Neuropsychopharmacology 29 (10), 1765–1781.

Hasselbalch, B.J., Knorr, U., Kessing, L.V., 2011. Cognitive impairment in the remitted state of unipolar depressive disorder: a systematic review. J. Affect. Disord. 134, 20–31.

Inaba, M., Ohira, H., 2009. Reduced recollective memory about negative items in high trait anxiety individuals: an ERP study. Int. J. Psychophysiol. 74 (2), 106–113 official journal of the international organization of psychophysiology.

Kaufman, J., Charney, D., 2000. Comorbidity of mood and anxiety disorders. Depression and anxiety. 12 (1), 69–76.

Kheirbek, M.A., Klemenhagen, K.C., Sahay, A., Hen, R., 2012. Neurogenesis and generalization: a new approach to stratify and treat anxiety disorders. Nat. Neurosci. 15, 1613–1620.

Lam, R.W., Kennedy, S.H., Mclntyre, R.S., Khullar, A., 2014. Cognitive dysfunction in major depressive disorder: effects on psychosocial functioning and implications for treatment. Can. J. Psychiatry 59 (12), 649–654.

Leal, S.L., Yassa, M.A., 2018. Integrating new findings and examining clinical applications of pattern separation. Nature Neuroscience 21 (2), 163–173.

Leal, S.L., Tighe, S.K., Yassa, M.A., 2014a. Asymmetric effects of emotion on mnemonic interference. Neurobiol. Learn. Mem. 111, 41–48.

Leal, S.L., Tighe, S.K., Jones, C.K., Yassa, M.A., 2014b. Pattern separation of emotional information in hippocampal dentate and CA3. Hippocampus 24 (9), 1146–1155.

Lee, K., Kim, D., & Cho, Y. (2018). Exploratory factor analysis of the beck anxiety inventory and the beck depression inventory-II in a psychiatric outpatient population. 33(16), 1–11.

MacMillan, S., Szeszko, P.R., Moore, G.J., Madden, R., Lorch, E., Ivey, J., Banerjee, S.P., Rosenberg, D.R., 2003. Increased amygdala: hippocampal volume ratios associated with severity of anxiety in pediatric major depression. J. Child Adolesc. Psychopharmacol. 13, 65–73.

Magarin˜os, A.M., McEwen, B.S., Flugge, G., Fuchs, E., 1996. Chronic psychosocial stress causes apical dendritic atrophy of hippocampal CA3 pyramidal neurons in subordinate tree shrews. J. Neurosci. 16 (10), 3534–3540.

Magarin˜os, A.M., McEwen, B.S., 1995. Stress-induced atrophy of apical dendrites of hippocampal CA3c neurons: comparison of stressors. Neuroscience 69 (1), 83–88. Mineka, S., Watson, D., Clark, L.A., 1998. Comorbidity of anxiety and unipolar mood

disorders. Annu. Rev. Psychol. 49 (1), 377–412.
Murrough, J.W., Iacoviello, B., Neumeister, A., Charney, D.S., Iosifescu, D.V., 2011.

Cognitive dysfunction in depression: neurocircuitry and new therapeutic strategies. Neurobiol. Learn. Mem. 96 (4), 553–563.

Norman, K.A., 2010. How hippocampus and cortex contribute to recognition memory: revisiting the complementary learning systems model. Hippocampus 20 (11), 1217–1227.

Pittenger, C., 2013. Disorders of memory and plasticity in psychiatric disease. Dialogues Clin. Neurosci. 15 (4), 455–463.

Radley, J.J., Sisti, H.M., Hao, J., Rocher, A.B., McCall, T., Hof, P.R., McEwen, B.S., Morrison, J.H., 2004. Chronic behavioral stress induces apical dendritic reorganization in pyramidal neurons of the medial prefrontal cortex. Neuroscience 125 (1), 1–6.

Rolls, E.T., 2007. An attractor network in the hippocampus: theory and neurophysiology. Learn. Mem. 14, 714–731.

Royston, Patrick, 1995. Remark AS R94: a remark on Algorithm AS 181: the W test for normality. Appl. Stat. 44, 547–551.

Sahay, A., Wilson, D.A., Hen, R., 2011. Pattern separation: a common function for new neurons in hippocampus and olfactory bulb. Neuron 70 (4), 582–588.

Segal, S.K., Cahill, L., 2009. Endogenous noradrenergic activation and memory for emotional material in men and women. Psychoneuroendocrinology 34 (9), 1263–1271.

Sheline, Y.I., Barch, D.M., Donnelly, J.M., Ollinger, J.M., Snyder, A.Z., Mintun, M.A., 2001. Increased amygdala response to masked emotional faces in depressed subjects resolves with antidepressant treatment: an fMRI study. Biol. Psychiatry 50, 651–658.

Soetanto, A., Wilson, R.S., Talbot, K., Un, A., Schneider, J.A., Sobiesk, M., Kelly, J., Leurgans, S., Bennett, D.A., Arnold, S.E., 2010. Association of anxiety and depression with microtubule-associated protein 2- and synaptopodin-immunolabeled dendrite and spine densities in hippocampal CA3 of older humans. Arch. Gen. Psychiatry 67 (5), 448–457.

Sousa, N., Lukoyanov, N.V., Madeira, M.D., Almeida, O.F., Paula-Barbosa, M.M., 2000. Reorganization of the morphology of hippocampal neurites and synapses after stress- induced damage correlates with behavioral improvement. Neuroscience 97 (2), 253–266.

Stanislaw, H., Todorov, N., 1999. Calculation of signal detection theory measures. Behavior research methods, instruments, & computers : a journal of the Psychonomic Society, Inc. 31 (1), 137–149.

Stockmeier, C.A., Mahajan, G.J., Konick, L.C., Overholser, J.C., Jurjus, G.J., Meltzer, H. Y., Uylings, H.B., Friedman, L., Rajkowska, G., 2004. Cellular changes in the postmortem hippocampus in major depression. Biol. Psychiatry 56, 640–650.

Tofalini, E., Mirandola, C., Coli, T., Cornoldi, C., 2015. High trait anxiety increases inferential false memories for negative (but not positive) emotional events. Personal. Individ. Differ. 75, 201–204.

Vyas, A., Bernal, S., Chattarji, S., 2003. Effects of chronic stress on dendritic arborization in the central and extended amygdala. Brain Res. 965 (1–2), 290–294.

Vyas, A., Mitra, R., Shankaranarayana Rao, B.S., Chattarji, S, 2002. Chronic stress induces contrasting patterns of dendritic remodeling in hippocampal and amygdaloid neurons. J. Neurosci. 22 (15), 6810–6818.

Whalen, P.J., Shin, L.M., Somerville, L.H., McLean, A.A., Kim, H., 2002. Functional neuroimaging studies of the amygdala in depression. Semin. Clin. Neuropsychiatry 7, 234–242.

Williams, J.M., Barnhofer, T., Crane, C., Herman, D., Raes, F., Watkins, E., Dalgleish, T., 2007. Autobiographical memory specificity and emotional disorder. Psychol. Bull. 133 (1), 122–148.

Yassa, M.A., Stark, .E.L, 2011. Pattern separation in the hippocampus. Trends Neurosci. 34 (10), 515–525.

Yonelinas, A.P., Aly, M., Wang, W.C., Koen, J.D., 2010. Recollection and familiarity: examining controversial assumptions and new directions. Hippocampus 20 (11), 1178–1194.

Appendix B: Hippocampal dentate gyrus integrity revealed with ultrahigh resolution diffusion imaging predicts memory performance in older adults

This appendix in its entirety has been submitted to Hippocampus and is under minor revision.

Granger, S. J., Colon-Perez, L., Larson, M. S., Bennet, L. J., Phelan, M., Keator, D. B., Janecek, J. T., Sathishkumar, M. T., Smith, A. P., McMillan, L., Greenia, D., Corrada, M. M., Kawas, C. H., Yassa, M. A. Hippocampal dentate gyrus integrity revealed with ultrahigh resolution diffusion imaging predicts memory performance in older adults. *In Review at Hippocampus.*

Abstract

Medial temporal lobe (MTL) atrophy is a core feature of age-related cognitive decline and Alzheimer's Disease (AD). While regional volumes and thickness are often used as a proxy for neurodegeneration, they lack the sensitivity to serve as an accurate diagnostic test and indicate advanced neurodegeneration. Here, we used a submillimeter resolution diffusion weighted MRI sequence (ZOOMit) to quantify microstructural properties of hippocampal subfields in older adults (63-98 years old) using tensor derived measures: fractional anisotropy (FA) and mean diffusivity (MD). We demonstrate that the high-resolution sequence, and not a standard resolution sequence, identifies dissociable profiles for CA1, dentate gyrus (DG), and the collateral

sulcus. Using ZOOMit, we show that advanced age is associated with increased MD of the CA1 and DG as well as decreased FA of the DG. Increased MD of the DG, reflecting decreased cellular density, mediated the relationship between age and word list recall. Further, increased MD in the DG, but not DG volume, was linked to worse spatial pattern separation. Our results demonstrate that ultrahigh-resolution diffusion imaging enables the detection of microstructural differences in hippocampal subfield integrity and will lead to novel insights into the mechanisms of age-related memory loss.

Introduction

Episodic memory decline and medial temporal lobe (MTL) atrophy are prominent changes associated with age-related cognitive decline (Gomez-Isla et al., 1996; Price et al., 2001; Braak and Braak, 1991; Jack et al., 1999). Early sites of structural atrophy include the hippocampus (Fox and Freeborough, 1997; Sabuncu et al., 2011), including specific subfields such as the dentate gyrus (DG; Ohm, 2007; Yassa et al., 2011, Dillon et al., 2017) and CA1 (Csernansky et al., 2005; Csernansky et al., 2000), as well as the adjacent entorhinal cortex (Gomez-Isla et al., 1996). On a cellular level, structural alterations including reduced neuron count and reduced dendritic arborization are a core biological phenomenon associated with age-related cognitive decline that signal tissue destabilization (Zarow et al., 2005; Ohm, 2007). In humans, changes in regional volumes and thickness are most commonly used as a proxy for large scale structural atrophy and neurodegeneration (Márquez and Yassa, 2019), however, they do not provide any insights regarding microstructural MTL neurodegeneration hallmarks like cellular loss nor dendritic arborization. It has been suggested that the study of volumes lack the specificity to stand alone as an accurate diagnostic test to distinguish normal

aging from Alzheimer's Disease (AD) and usually indicate an advanced stage of neurodegeneration providing little room for targeted interventional therapy (Teipel et al., 2013; Frisoni et al., 2010; Whittaker et al., 2019). Therefore, there is substantial need for sensitive and specific markers of microstructural atrophy due to aging and aging-related pathologies. These potential new biomarkers should provide improved quantification of the microstructural changes that underlie gross volumetric decline and provide insight into cellular atrophy in humans.

Measures derived from diffusion weighted MRI (dMRI) are emerging as strong candidates for novel non-invasive biological markers of hippocampal tissue microstructural organization (beyond the study of volumes) in animal studies across pathologies. Changes in tensor-derived measures in the CA1 and DG subfields of the hippocampus have been related to several gray matter insults in mouse models of amyloid accumulation (Whittaker et al., 2019; Daianu et al., 2015), status epilepticus (Salo et al., 2017), early life stress (Molet et al., 2016), and hippocampal sclerosis (Crombe et al., 2018), and indicate change on a cellular level. Importantly, dMRI metrics do not reflect cell-type specificity nor does dMRI currently have the resolution to observe diffusion at a single-cell level. Instead, dMRI metrics indicate difference among different types of tissue. Here our use of the terms microstructure and microstructural properties refer to the ability of dMRI to measure tissue differences within each voxel.

In humans, the use of dMRI measures as sensitive markers of hippocampal integrity in aging, mild cognitive impairment, and Alzheimer's Disease has been studied,

however, has only scarcely been applied to hippocampal subfields possibly due to image resolution or the use of whole hippocampus instead of subfield anatomical segmentation (Colon-Perez et al., 2015; Reas et al., 2017; Mak et al, 2017; Kantarci et al., 2005; Muller et al., 2007; Dyrba et al., 2015). We have previously shown that the use of ultrahigh resolution dMRI in humans can uncover in vivo microstructural properties of white matter that are otherwise impossible to visualize using sequences with standard image resolutions (Yassa et al., 2010). Thus, it is possible that the use of ultrahigh resolution dMRI in humans is critical to uncover new and robust biomarkers of microstructural properties of gray matter within the MTL and hippocampal subfields that are not otherwise palpable using standard image resolutions.

In this investigation, we employ a state-of-the-art ultrahigh resolution dMRI sequence (0.67 x 0.67 x 3mm) to quantify the microstructural features in MTL regions in a cohort of older adults (63-98 years old). Using diffusion tensor derived measures of mean diffusivity (MD) and fractional anisotropy (FA) we demonstrate the utility of this sequence by comparing its performance against a standard diffusion imaging sequence (1.7 mm isotropic). We assessed FA and MD in two hippocampal subfields (DG and CA1) and quantified relationships with age and episodic memory function, using a word list recall test (Rey Auditory Verbal Learning Test; RAVLT) that is often used to identify age-related memory impairment (Estévez-González et al., 2003). We also tested whether FA and MD in these subfields was related to performance on a spatial pattern separation task that is known to rely on the integrity of the DG (Marr et al. 1971; Yassa et al. 2011; Reagh et al. 2014). We focused on the DG and CA1 as they are both critical for episodic memory processes and are known to be impacted by aging and AD

(Ianov et al., 2017; Burger, 2010; Small et al., 2004; Yassa et al., 2010).

Methods

Participants

Participants were recruited from two separate cohorts (Young-Old and Oldest-Old) at the University of California, Irvine to allow us to examine a large range of ages from 60-100 for a total sample of 78 participants (54 female, mean age 80.18). Demographic and cognitive performance data of the two cohorts are summarized in **Table 1**. Recruitment criteria for the Young-Old (age range 63-86) included being between the ages of 60 and 86, speak fluent English, had adequate visual and auditory acuity for neuropsychological and computerized testing, good health with no disease(s) expected to interfere with the study, willing and able to participate for the duration of the study and in all study procedures including MRI, and had normal cognition defined as a Clinical Dementia Rating of 0 and Mini-Mental State Examination Score of 27 or higher. All procedures were in accordance with protocols approved by the UC Irvine Institutional Review Board. Recruitment criteria for the Oldest-Old (age range 93-98) was largely the same, except for testing visual and auditory acuity and the MMSE cutoff. Oldest-Old participants were screened for visual and auditory impairment as part of initial medical screening. We note that roughly one-third (9 participants) were diagnosed with Cognitive Impairment with No Dementia (CIND) and the average MMSE score for the Oldest-Old was lower than the Young-Old (25.54 compared to 28.15). For reference, we also report scores on the Clinical Dementia Rating Scale Sum of Boxes (CDR Sum of Boxes). Twelve participants from the Young-Old cohort did not complete CDR.

Table A2.1. Participant Demographics

	Full sample	Young-Old	Oldest-Old
N	78	52	26
Sex	Female 54 Male 24	Female 38 Male 14	Female 16 Male 10
Age	80.18 ± 10.61 (Range 63.22 - 98.31)	73.48 ± 5.56 (Range 63.22 - 86.00)	93.59 ± 1.95 (Range 90 – 98.31)
Years of education	16.18 ± 2.50	16.58 ± 2.22	15.38 ± 2.87
Cognitive Impairment *	9 CIND	0 CIND	9 CIND
RAVLT Delayed Recall	9.46 ± 4.26	11.42 ± 3.21	5.54 ± 3.31
Mini Mental State Exam	27.28 ± 2.45	28.15 ± 1.42	25.54 ± 3.10
Completed SPS task	53	36	17
CDR Sum of Boxes	n = 66 0.12 ± 0.35 Range (0.0-2.0)	n = 40 0.025 ± 0.11 Range (0.0-0.5)	n = 26 0.27 ± 0.51 Range (0.0-2.0)
**** CIND – Cognitive Impairment No Dementia***			

MR Image Acquisition

All neuroimaging data were acquired on a 3.0 Tesla Siemens Prisma scanner at the Facility for Imaging and Brain Research (FIBRE) at the University of California, Irvine. A high-resolution 3D magnetization-prepared rapid gradient echo (MPRAGE) structural scan (0.8mm isotropic voxels) was acquired at the beginning of each session: repetition time (TR) = 2300ms, echo time (TE) = 2.38ms, FOV =192, 256, 256mm, flip

angle = 8 degrees. In addition, a T2-weighted high-resolution hippocampal sequence was acquired: TR/TE = 5000/84ms, flip angle = 17 degrees, FOV = 190, 105, 198mm, voxel size = 0.42 x 0.42 x 2.4mm. The ultrahigh-resolution diffusion sequence was collected as oblique coronal slices parallel to the principal axis of the hippocampus with the following parameters: TR/TE = 3500/75ms, FOV = 180, 71, 66mm, voxel size = 0.67 x 0.67 x 3mm, bandwidth = 1696 Hx/Px, echo spacing = 0.69ms, EPI factor = 40, TX acceleration = 2.0, total approximate run time = 3 minutes 42 seconds. These parameters were optimized by Siemen's scanner interface. The sequence consisted of two b = 0 s/mm2 volumes and a total of 60 diffusion weighted volumes acquired as 30 non-collinear directions repeated twice at a b-value of 1000 s/mm2. This sequence (ZOOMit) utilizes inner volume excitation to reduce the field of view and in-plane resolution (Blasche et al., 2012). Here we oriented the FOV of the ZOOMit sequence along the long axis of the hippocampus in hopes to more accurately sample MTL tissue. Upon acquiring the MPRAGE image, trained scanner technicians placed the bottom edge of the square FOV "ON" or along the hippocampal body from a sagittal view. The center of the box was then placed over the hippocampus to cover the entire body of the hippocampus. The MPRAGE was checked to ensure that the FOV covered both the left and right hippocampus in its entirety. In this manner, by orienting the FOV along the hippocampus, we hope to minimize partial volume effects across regions given the 3mm slice thickness projects within hippocampal layers rather than across hippocampal layers. More information on this protocol as well as example MPRAGE and T2-weighted images are supplied in Figure A2.1. A whole brain diffusion sequence was also acquired with the following parameters: TR/TE = 3500/102ms, FOV =218, 221, 189 mm, voxel

size = 1.7 mm isotropic, bandwidth = 1698 Hz/Px, echo spacing = 0.71ms, EPI factor = 110, total approximate run time = 8 minutes and 6 seconds. The sequence consisted of 7 b = 0 s/mm2 volumes and two b-values of 1500 s/mm2, 3000 s/mm2 each with 64 diffusion weighted volumes. To make the ZOOMit and whole brain sequence more comparable, we removed all volumes where b=3000 s/mm2 from the whole brain sequence. All vector orientations were automatically generated by Siemen's Prisma software.

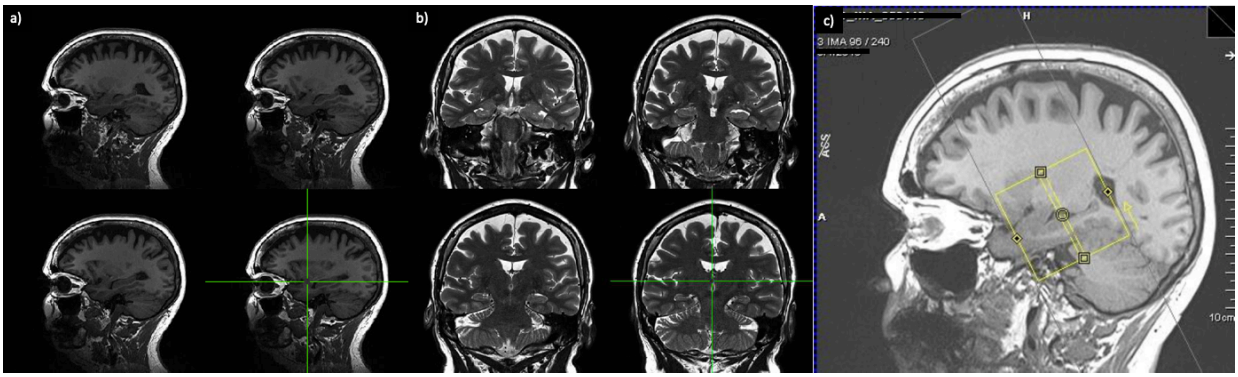

Figure A2.1. (a) Sagittal view of the isotropic (0.8 mm^3) MPRAGE. (b) Coronal view of the high resolution (0.4 x 0.4 x 2mm) T2-weighted image acquired parallel along the long the long axis of the hippocampus. (c) An example of the FOV placement for the ZOOMit sequence also acquired parallel to the long axis of the hippocampus. Upon acquiring the MPRAGE image, trained scanner technicians place the bottom edge of the square FOV "ON" or along the hippocampal body from a sagittal view. The center of the box is then placed over the hippocampus to cover the entire body of the hippocampus. The MPRAGE was checked to ensure that the FOV covered both the left and right hippocampus in its entirety.

Medial Temporal Lobe Subfield Segmentation in Native Diffusion Space

We parsed the subfields of the medial temporal lobe using T1 and T2-weighted images and the Automated Segmentation of Hippocampal Subfields (ASHS; Yushkevich et al., 2015) pipeline to automatically label the T2-weighted images. This method

implements joint label fusion and correcting learning and is a highly accurate method in automatically deriving hippocampal subfield volumes and cortical subregions in the medial temporal lobe. Using ASHS, we calculated the volumes for the following subregions bilaterally in native T2 space: CA1, CA2, CA3, DG, subiculum, sulcus, BA35, BA36, and PHC. For all volumetric analyses, volumes were averaged across hemisphere. To query microstructural differences beyond volume, we used the ANTSRegistrationSyn program offered by Advanced Normalization Tools (ANTS; Avants et al., 2011; Klein et al., 2009) to warp the T2 and associated ASHS regions into the first B0 of the partial FOV ultrahigh-resolution diffusion sequence (Figure A2.2) as well as the first B0 of the whole brain multi-shell diffusion scan. We preprocessed both the high resolution sequence and whole brain sequence using eddy_correct. We quantified motion by calculating the average Euclidian distance in the linear transformation from each subbrick to the first B0 volume prior to any motion correction for each dMRI scan.

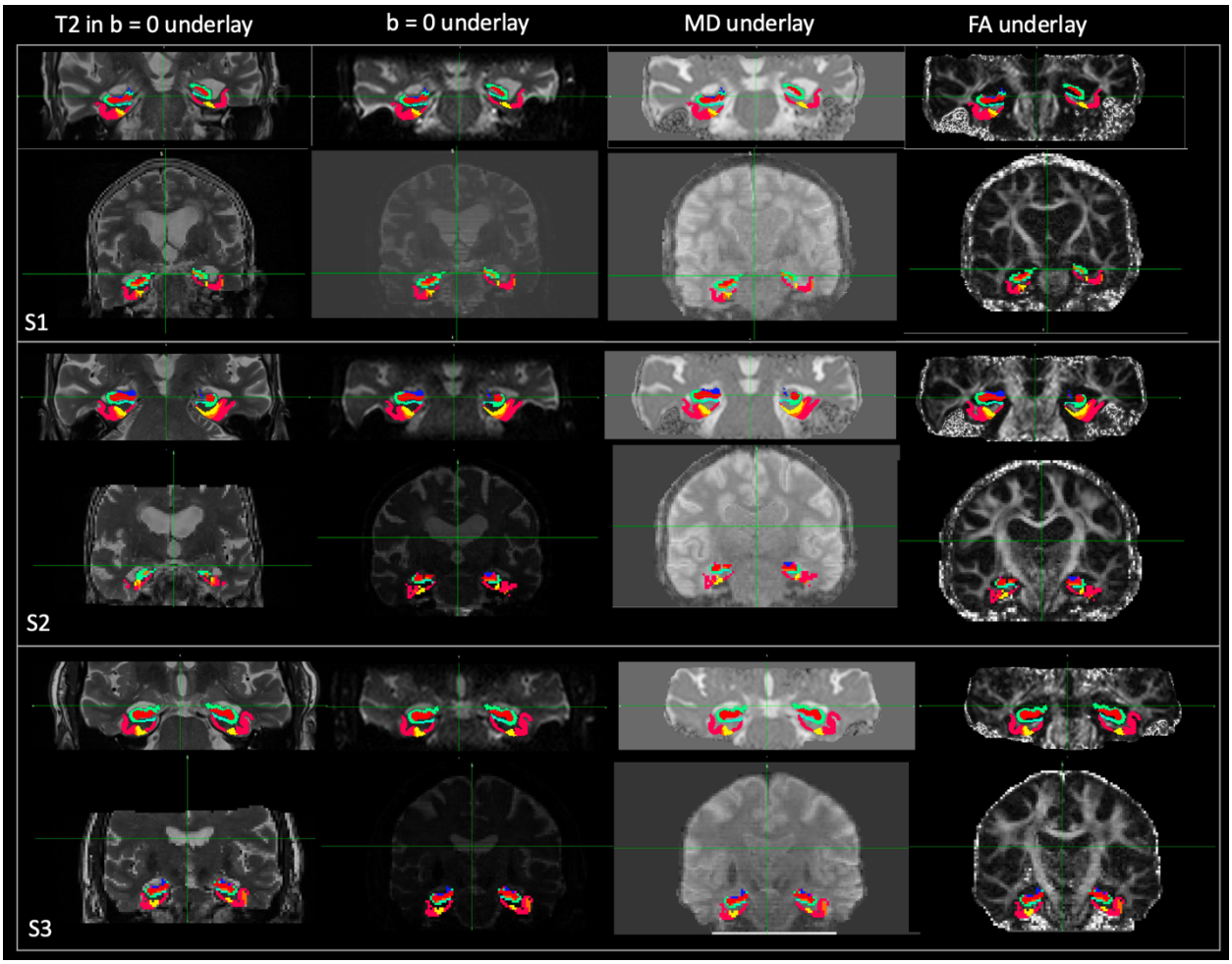

Figure A2.2. MR images of 3 randomly selected subjects (S1-3). Here we provide the ASHS regions of interest with an underlay of the T2-weighted image warped to the b = 0 space, the ASHS regions with the b = 0 volume as an underlay, the ASHS regions with the MD image as an underlay, and the ASHS regions with the FA image as an underlay. We provide each image type for each subject for the high resolution ZOOMit sequence as well as the whole brain sequence.

Computation of Tensor-Based Metrics

We calculated fractional anisotropy (FA) and mean diffusivity (MD) maps using FSL's DTIfit. Fractional anisotropy and mean diffusivity values for each medial temporal lobe subfield (bilaterally) from ASHS output were calculated and averaged across hemispheres using AFNIs 3dmaskave command. This process was completed for both

the ultrahigh resolution dMRI sequence and the whole brain dMRI sequence. For dissociating tissue from non-tissue samples, we compared the sulcus, CA1, DG, and rhinal cortex (defined as averaging BA35, BA36, ERC, and PHC). One subject was removed from the MD whole brain analysis and two subjects were removed from the FA whole brain analysis as clear outliers.

Neuropsychological Testing

Our primary outcome measure in this investigation was performance on the Rey Auditory Verbal Learning Memory Test (RAVLT; Rey 1964) to measure the acuity of verbal memory. Administration of the RAVLT consisted of an examiner reading a list of 15 words, after which the subject was asked to repeat as many words as they could remember (in any order). This study/test trial was be repeated for a total of 5 learning trials (Learning Trials, A1-A5) that were then followed by an immediate recall of a distractor list (B1), then immediate recall of the original list of 15 words (Immediate Recall, A6). The subject was then tested 20 minutes later (Delayed Recall, A7), followed by a recognition test. The RAVLT and delayed recall component is a well-established benchmark for testing and dissociating normal aging, MDI, and Alzheimer's Disease (Estevez-Gonzalez et al., 2003; Jedynak et al., 2012).

Spatial Pattern Separation Task

Table A2.2 Participant Demographics Completing Spatial Pattern Separation Task

	Full sample	Young-Old	Oldest-Old
N	53	36	17

Sex	Female 38 Male 15	Female 28 Male 8	Female 10 Male 7
Age	80.08 ± 10.48 (Range 63.22 - 97.00)	73.68 ± 5.54 (Range 63.22 - 86.00)	93.64 ± 1.56 (Range 91.00 - 97.00)
Years education	16.3 ± 2.27	16.56 ± 2.12	15.76 ± 2.54
Cognitive Impairment *	5 CIND	0 CIND	5 CIND
RAVLT Delayed Recall	9.151± 4.49	11.11 ± 3.50	5 ± 3.45
Mini Mental State Exam	27.19 ± 2.57	28.06 ± 1.47	25.35 ± 3.39
CDR Sum of Boxes	n = 42 0.14 ± 0.40 Range (0.0-2.0)	n = 25 0.04 ± 0.14 Range (0.0-0.5)	n = 17 0.29 ± 0.59 Range (0.0-2.0)
**** CIND – Cognitive Impairment No Dementia***			

In a subset of participants (n=53, Table A2.2), we administered the spatial pattern separation task (Figure A2.8a) to probe DG function specifically. This task has been used previously to assess dentate-gyrus dependent pattern separation (Reagh et al., 2014). During incidental encoding, subjects were asked to rate objects as either 'Indoor' or 'Outdoor' as objects appeared in various positions on the screen. For the Young-Old cohort, each trial lasted 2.5 seconds with a 0.5s ISI. In the Oldest-Old cohort, each trial was self-paced due to concerns regarding motor speed. The Oldest-Old cohort was instructed to respond as soon as they were able. For both cohorts, 160 items were presented during incidental encoding. During test, 40 target images (objects appearing in the same location as encoding), 80 lures (same objects in slightly different locations), and 40 pseudo-foil images (objects originally presented in one corner location at study and in another corner location at test) were presented. Lure images

were binned as either large move (low similarity, 40 images) or small move (high similarity, 40 images). Pseudo-random images were the only set to appear in the corners of the screen. During test, participants were asked if the object was in the “Old Location” or in a “New Location”. We quantified a Lure Discrimination Index (LDI) for highly similar lure items which measures performance on the task accounting for response bias: P(“New Location”|Lure) – P(“New Location”|Target) and did not consider the pseudo-foil images in these analyses. This measure is frequently employed as it not only accounts for response bias but is also sensitive to changes in ageing (Reagh et al., 2018; Reagh et al., 2015; Stark et al., 2015). Here we chose the high-similarity lure bins under the assumption that the ability to adjudicate between stimuli with greater interference (greater similarity) would be more sensitive to aging. We excluded participants who couldn’t respond to more than 75% of the test phase of the task. Additionally, all participants who had a negative LDI were eliminated under the assumption of the response being entirely driven by response bias or inattention to the task instructions. Exclusion based on these criteria let to a final subsample of 53 participants.

Statistical Analysis

Statistical analyses were computed using a mixture of Prism 7, R-Studio Software, and Python. K-means clustering was implemented using Python using sklearn.cluster to identify 4 clusters (selected a priori), with a random state initialization of 0. Normalized mutual information scores were calculated in Python to compare the known identities of regions with the clusters identified from K-means. Regression

models were completed using R-Studio Software and standardized beta coefficients are reported in-text. All correlational analyses were done using two-tailed tests of Pearson correlation coefficients. To assess the impact of the bimodal distribution of age on measures of DG MD and DG volume, we compared the slopes of DG MD and DG volume using a simple test of slopes. Mediation analyses were conducted using the mediation package in R, each model was tested using bias corrected and accelerated (BCa) bootstrapping with 5000 replications.

Results

Ultrahigh-resolution diffusion MRI detects subregion-specific gray matter diffusion profiles

We first tested the hypothesis that the ultrahigh resolution dMRI approach (0.67 x 0.67 x 3mm) will reveal microstructural features of hippocampal subfields and rhinal cortical subregions that would be otherwise indiscernible using traditional diffusion imaging methods. We used k-means clustering to compute and label clusters of FA and MD values from the hippocampus (CA1 and DG), rhinal cortex, and collateral sulcus (the latter as a control). Using data derived from the ultrahigh-resolution sequence, we calculated the overlap between the labels derived from k-means clustering and known anatomical labels (CA1, DG, rhinal cortex, or sulcus). We obtained a normalized mutual information (nMI) score of 0.623, indicating a moderate overlap in the k-means cluster label (Figure A2.3b) and known anatomical label (Figure A2.3a).

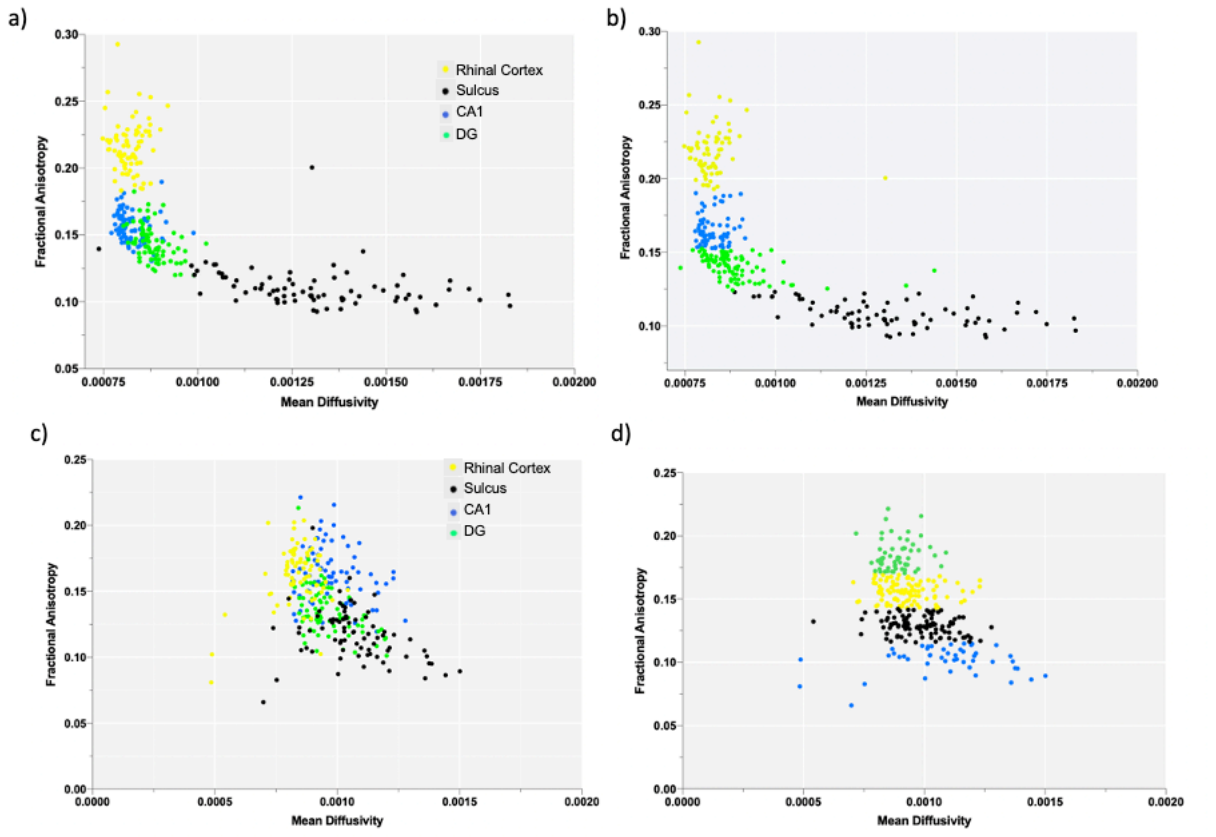

Figure A2.3: (a) Shows the FA and MD data for each area of interest: CA1 (in blue), DG (in green), rhinal cortex (in yellow), and sulcus (in black) derived from the *high-resolution DWI sequence*. (b) Shows the same data points categorized into 4 clusters via unsupervised K-means clustering. We note the large degree of visual overlap (Normalized mutual information score =0.623). (c) Shows the actual FA and MD data plotted for each area of interest: CA1 (in blue), DG (in green), rhinal cortex (in yellow), and sulcus (in black) derived from the *whole brain DWI sequence*. (d) Shows the same data points clustered into 4 clusters using unsupervised K-means clustering. Here we note the minimal degree of overlap between the actual data and predicted data identities (Normalized mutual information score = 0.242)

To determine whether these regions were differentiated by their FA values, we compared regional FA values CA1, DG, rhinal cortex, and sulcus using one-way ANOVA. We found a significant difference across regions ($F_{2, 308} = 700.8$, $P < 0.0001$). Tukey's multiple comparison test revealed each region contained significantly different FA values than the other (Figure A2.4a). Similarly, we compared MD values in each of the same regions and found a significant difference across regions ($F_{3,308}$ =

342.3, P < 0.0001). Tukey's multiple comparisons revealed that each region contained unique MD values except for MD values of the CA1 and rhinal cortex (adjusted p = 0.99; Figure A2.4b). These analyses demonstrate that the medial temporal lobe regions could be discerned based on their microstructural properties, agnostic to their anatomical label.

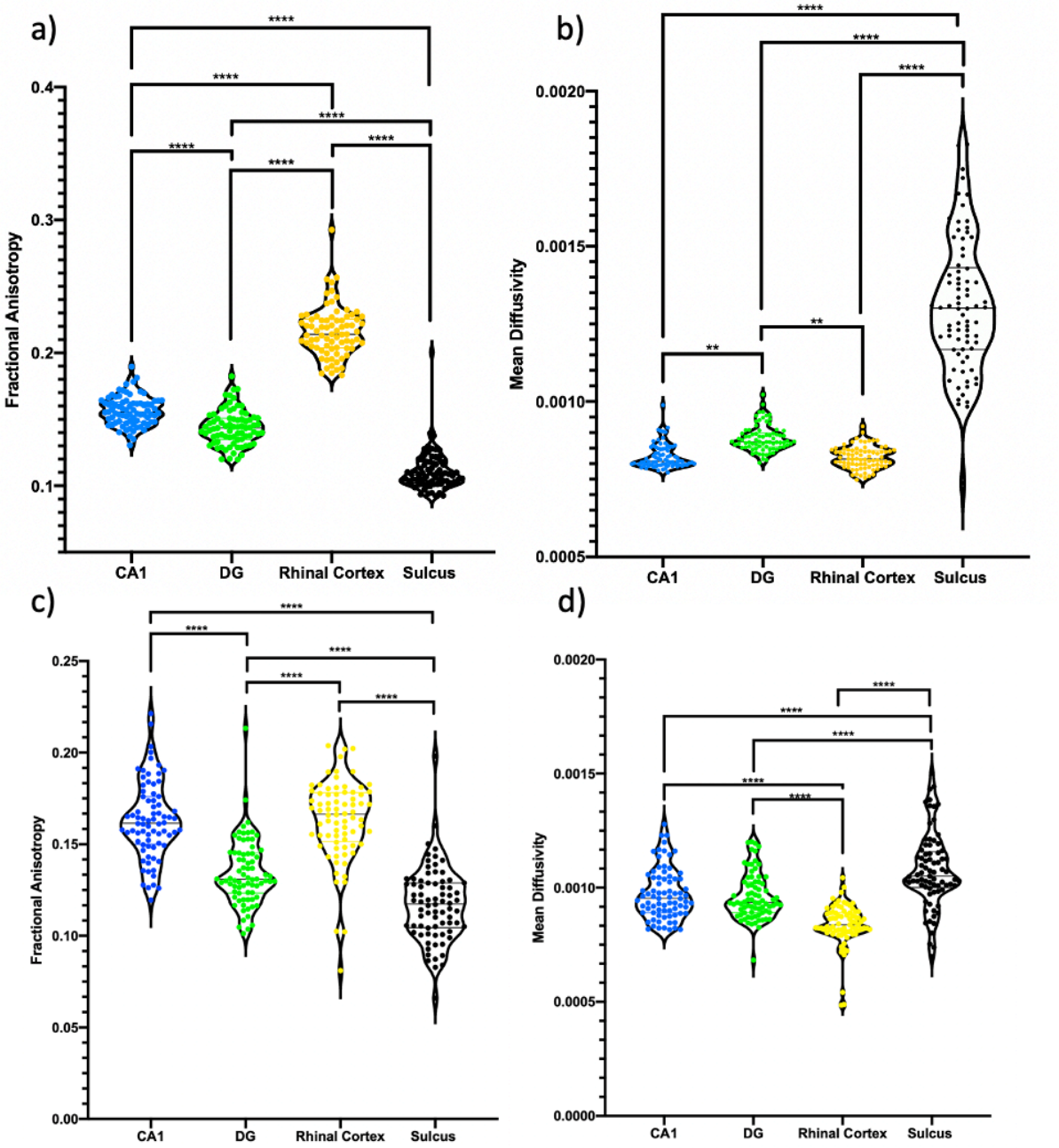

Figure A2.4. (a-b) Diffusion data of the high-resolution dwMRI sequence**.** (a) Shows fractional anisotropy values of the CA1, DG, rhinal cortex, and sulcus of the high-resolution scan. Using one-way ANOVA, we found a significant difference in region ($F_{2, 308} = 700.8$, $p < 0.0001$) and all Tukey's post-hoc comparisons were statistically significant. (b) Shows mean diffusivity values of the CA1, DG, rhinal cortex, and sulcus of the high-resolution scan. There was a statistically significant difference between regions ($F_{3,308} = 342.3$, $p < 0.0001$) however, there was no statistically significant difference between the CA1 and rhinal cortex (adjusted p = 0.994). (c-d) Shows the FA and MD values derived from the whole brain sequence for the CA1, DG, rhinal cortex and sulcus. (c-d) Diffusion data of the whole brain dwMRI sequence. (c) Shows fractional anisotropy data of the CA1, DG, rhinal cortex and a significant difference between regions ($F_{3,300} = 95.96$, $p < 0 .0001$), however, FA values of the CA1 and rhinal cortex were not statistically different (adjusted $p = 0.99$). (d) Shows mean diffusivity data of the CA1, DG, rhinal cortex and DG. We found a difference between regions ($F_{3,304} = 50.71$, $p < 0.0001$), however, values of the CA1 and DG were not statistically significant (adjusted $p = 0.93$).

To determine whether the same information could be gleaned from traditional whole brain DWI imaging, we repeated the same analyses as above with 1.7 mm isotropic data acquired during the same sessions for the same participants. The overlap between the labels derived from k-means clustering and known anatomical labels resulted in a nMI score of 0.242 indicating very minimal overlap between K-means cluster identity (Figure A2.3d) and known anatomical identity (Figure A2.3c). Similarly, we tested weather these regions were differentiated by their FA values. One-way ANOVA revealed a significant difference between regions ($F_{3,300} = 95.96$, $p < 0.0001$), however post-hoc analysis revealed that FA values derived from the CA1 were not statistically different than FA values of the rhinal cortex (adjusted $p = 0.99$, Figure A2.4c). We then compared MD values in each of the same regions and found significant difference across regions ($F_{3,304} = 50.71$, $p < 0.0001$), however, post-hoc analyses revealed that MD values derived from the CA1 were not statistically different than MD valued derived from the DG (adjusted $p = 0.93$, Figure A2.4d).

Higher MD and lower FA in the dentate gyrus are associated with increased age

We then asked if these microstructural properties derived from the ultrahigh resolution dMRI were associated with increasing age. In the DG, we found a negative association between age and FA (Pearson r = -0.47, p <0.0001; Figure A2.5c), as well as positive association between age and MD (Pearson r = 0.66, p < 0.0001; Figure A2.5d). In the CA1, we found a significant positive association between age and MD (Pearson r = 0.52, p < 0.0001; Figure A2.5b. The relationship between age and CA1 FA was not significant (Pearson r = -0.13, p = 0.26; Figure A2.5a).

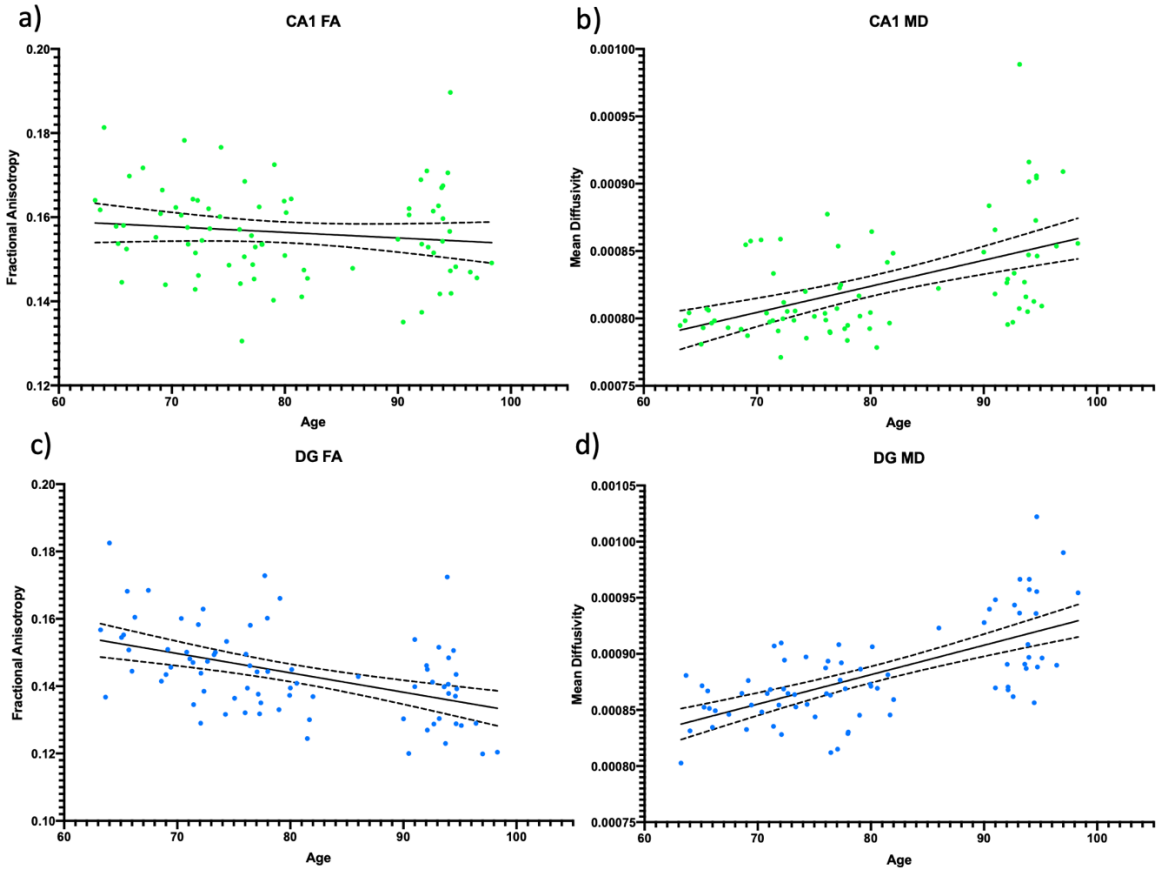

Figure A2.5. (a-b) Shows the results of CA1 structural differences across the age range. (c-d) Show the results of DG structural differences across the age range. (a) Shows the non-significant relation between age and CA1 FA (r = -0.13, *p* = 0.26). (b) Shows the positive relation between age and CA1 MD (r = 0.52, *p* < 0.0001). (c) Shows the negative association between age and DG FA (r = -0.47, *p* <0.0001). Finally, (d) shows the positive relation between age and DG MD (r = 0.66, *p* < 0.0001).

Importantly, we note that our sample contains a bimodal distribution of age as data were collected from two cohorts (63- 86 and 90-98 years old). To ensure that our findings were not driven by one particular age group, we assessed the difference in the slope of the relationship between age and the diffusion measures reported above across the two age groups. As a result, we investigated the relation between age and DG MD, age and DG FA, and age and CA1 MD within each age range separately. We found that there was no difference ($Z = -0.96$, $p = 0.34$) between the slope of the relation between age and DG MD in the young cohort ($\beta = 1.50 \times 10\text{-}6$, $p = 0.023$) compared to the slope of the relation in the old cohort ($\beta = 5.73 \times 10\text{-}6$, $p = 0.20$). We found no difference ($Z = -0.34$, $p = 0.74$) between the slope of the relation between age and DG FA in the young cohort ($\beta = -0.00095$, $p = 0.0014$) and the slope of the relation between age and DG FA in the old cohort ($\beta = -0.001386$, $p = 0.2834$). Similarly, we found no difference ($Z = -0.75$, $p = 0.45$) between the slope of the relation between age and CA1 MD ($\beta = 8.52$ x 10-7, $p = 0.18$) compared to the slope of the relation in the old cohort ($\beta = 4.49$ x 10-6, $p = 0.36$). These analyses are further described in Figure A2.5..

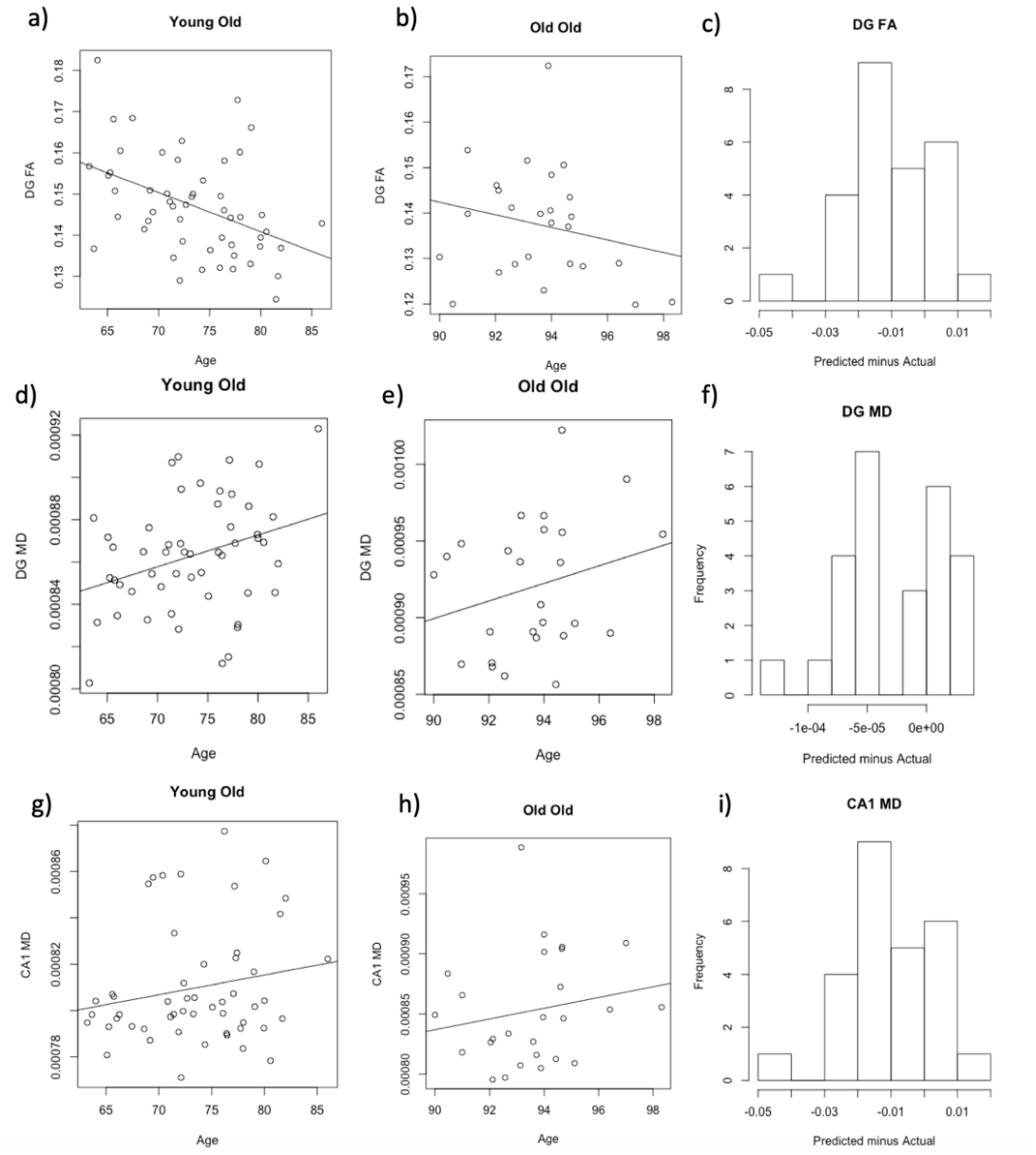

Figure A2.5. Given the bimodal distribution of age and our evidence of age-related differences in DG FA, DG MD, and CA1 MD we tested the relation between age and DG MD, DG FA, and CA1 MD in each age group separately. (a-c) We found no difference ($Z = -0.34$, $p = 0.74$) between the slope of the relation between age and DG FA in the young cohort ($\beta = -0.00095$, $p = 0.0014$; a) and the slope of the relation between age and DG FA in the old cohort ($\beta = -0.001386$, $p = 0.2834$; b). (c) Shows the distribution of the difference between the predicted DG FA values for the Oldest-Old cohort using the slope of the line from the young cohort. (d-f) shows there was no difference ($Z = -0.96$, $p = 0.34$) between the slope of the relation between age and DG MD in the young cohort ($\beta = 1.50 \times 10^{-6}$, $p = 0.023$; d) compared to the slope of the relation in the old cohort ($\beta = 5.73 \times 10^{-6}$, $p = 0.20$; e). (f) Shows the distribution of the difference between the predicted DG MD values for the Oldest-Old cohort using the slope of the line from the young cohort. (g-i)

Shows no difference (Z = -0.75, p = 0.45) between the slope of the relation between age and CA1 MD ($\beta = 8.52 \times 10^{-7}$, p = 0.18; g) compared to the slope of the relation in the old cohort ($\beta = 4.49 \times 10^{-6}$, p = 0.36; h). (f) Shows the distribution of the difference between the predicted CA1 MD values for the Oldest-Old cohort using the slope of the line from the young cohort

Increased dentate gyrus MD predicts worse performance on word list delayed recall

Aging is associated with episodic memory decline (Burke & Barnes, 2006; Levine et al., 2002; Mark & Rugg, 1998). In particular, the Rey Auditory Verbal Learning Test (RAVLT) delayed recall measure has been used in the past to assess general hippocampal integrity with age (Rey 1964; Estevez-Gonzalez et al., 2003; Jedynak et al., 2012). We tested the hypothesis that increased DG MD and decreased FA would predict age-related impairments in RAVLT delayed recall performance. We found that DG MD (Pearson r = -0.54, P < 0.0001; Figure A2.6a) was a significant predictor of delayed recall, however, DG FA was borderline (Pearson r = 0.21, p = 0.064; Figure A2.6b).

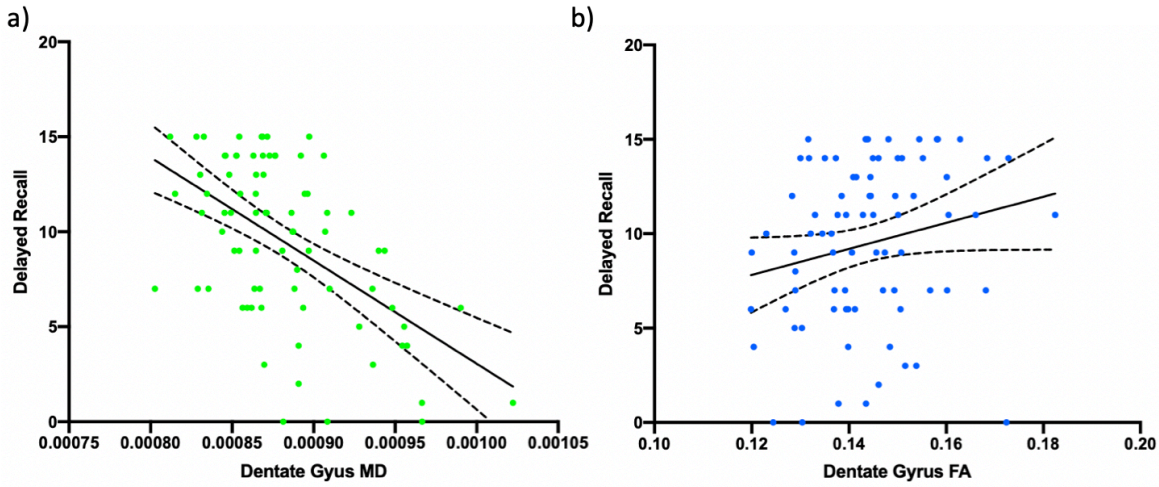

Figure A2.6. Here we report the results of DG MD, FA, and volume predicting delayed recall performance. (a) Shows the significant association between DG MD and delayed

recall performance (r = -0.54, $p < 0.0001$). (b) Shows the non-significant but trending relation between DG FA and delayed recall performance (r = 0.21, $p = 0.064$).

To ensure that these effects are not driven by in-scanner head motion, we assessed whether average Euclidean distance moved during the ultrahigh-resolution scan was associated with DG MD and found the effect to be not significant (Pearson r = 0.16, p = 0.16). To ensure that these effects were not driven by DG volume we asked if DG MD predicted delayed recall performance while regressing out the effects of DG volume. We found that DG MD (β = -0.393, p = 0.00025) was associated with delayed recall performance accounting for DG volume (β = 0.32, p = 0.0021). Although, we note that DG MD and DG volume are related to one another (r = 0.45, p < 0.0001).

To assess the impact of confounding variables such as age and sex, we used multiple regression with age, sex, and DG MD as predictors and RAVLT delayed recall as the outcome. We found that both age (β = -0.42, p = 0.00066) and DG MD (β = -0.26, p = 0.030) were independent predictors of delayed recall. Sex was not a significant predictor, although the effect was borderline or trending towards significance (β = -0.15, p = 0.098). Given the correlated structure across age, DG MD, and delayed recall performance, we conducted mediation analyses in an effort to understand whether changes in DG MD are a neurobiological mechanism that mediates the relationship between age and episodic memory performance. We found that DG MD mediated the relationship between age and RAVLT delayed recall. The bootstrapped unstandardized indirect effect was -0.069 and the 95% confidence interval ranged from -0.13 to -0.0082. The indirect effect was statistically significant (p = 0.029; Figure A2.7).

This result suggests that increased DG MD may serve as a mechanistic biomarker for age-related episodic memory decline.

Figure A2.7 Results of structural equation (mediation) model shows DG MD is a statistically significant mediator between age and delayed recall performance (Indirect Effect = -0.069*, C.I. = -0.13 to -0.0082). *Indicated $p < 0.05$, ** indicates $p < 0.01$, *** indicates $p < 0.0001$

Higher DG MD predicts worse performance on a spatial pattern separation task

While the RAVLT can be used to assess general episodic memory and has been used to index hippocampal function more broadly, the DG is specifically associated with pattern separation, a neurocomputational mechanism by the brain reduces overlap across experiences and store them as unique memories (Marr et al. 1971; Yassa et al. 2011). We have previously developed a spatial pattern separation task (Reagh et al. 2014) to assess age-related changes in spatial memory and demonstrated that it engages the hippocampal DG preferentially over other subfields (Reagh and Yassa, 2014; Reagh et al. 2018). This task was administered to a subset of the participants in the current study (n=53). As in our prior work, the lure discrimination index (LDI) was used as the principal behavioral outcome measure of interest. We replicated our previous finding of decreased LDI as a function of age (Pearson $r = -0.32$, $p = 0.019$). We also show that target recognition (no spatial displacement) is associated with age

(Pearson r = -0.31, p = 0.022). Next, we tested the relationship between DG MD and LDI and found that increased DG MD was associated with worse LDI (Pearson r = -0.39, p = 0.0051; Figure A2.8b), but not with target recognition (Pearson r = -0.22, p = 0.12). We then tested if DG volume was related to LDI, the relation between DG volume and LDI was not a statistically significant (r = 0.12, p = 0.40; Figure A2.8c). Similar to the RAVLT analysis, we asked if increased DG MD was a mediator of the relationship between age and LDI. We found a marginally significant effect whereby DG MD mediated the relationship between age and LDI (indirect effect = -0.0026, C.I. = -0.0063 to 0.00013, p = 0.076).

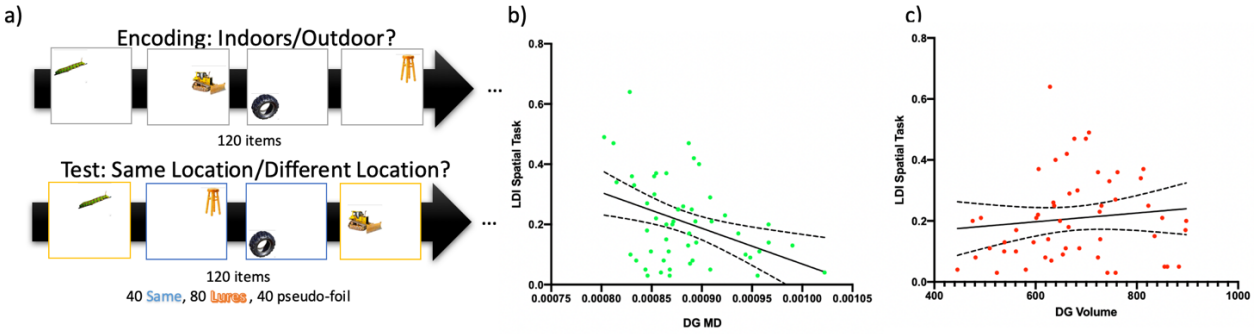

Figure A2.8 In a subset of participants, we tested whether DG MD might also predict performance on a Spatial Pattern Separation Task. (a) The Spatial Pattern Separation Task. During incidental encoding, subjects are shown a series of objects placed in different spatial locations on a screen. Subjects are asked during incidental encoding to rate the images as appearing as “Indoor” or “Outdoor”. During test, targets or objects appearing in the same location as encoding are presented as well as lures which present the same objects in slightly different locations. Here subjects are asked if the object was in a “New Location” or “Old Location”. (b) There is a statistically significant association between DG MD and LDI on the spatial task (r = -0.39, p = 0.0051). (c) However, there is not a statistically significant association between DG volume and LDI (r = 0.12, p = 0.40).

Discussion

There are four major findings of this study. First, we show that the ultrahigh resolution dMRI sequence outperforms the standard resolution whole brain dMRI

sequence in detecting subtle microstructural differences between MTL regions. Second, we show that increased age is associated with distinct microstructural changes within the CA1 (increased MD) and DG (decreased FA and increased MD). Third, we show that increased MD in the dentate gyrus mediates the relationship between advanced age and episodic memory impairment. Finally, we provide evidence that DG MD derived from the ultrahigh-resolution sequence may offer critical information regarding the role of DG in spatial pattern separation. Overall, the approach described in this article provides enhanced sensitivity to regional microstructural differences in the MTL which enhances our ability to elucidate the neural mechanisms of age-related cognitive decline and AD.

We demonstrate that CA1, DG, and surrounding cortex have unique diffusion profiles and that the discrimination of these profiles is improved with the use of the ultrahigh resolution dMRI sequence. Our data-driven approach was able to more accurately cluster unlabeled FA and MD data points according to their true anatomical labels in the ultrahigh sequence compared to the standard isotropic resolution sequence. Interestingly, our evidence suggests that the CA1 and DG are dissociable based on measures of FA and MD derived from the ultrahigh-resolution sequence, but not the whole brain sequence. More specifically, we provide evidence that the CA1 and DG of the hippocampus contain different FA and MD values such that the CA1 contains greater FA and lesser MD compared to the DG. While direct histological evidence is needed to validate this claim, it is possible that the pyramidal cell layer contributes to greater FA in the CA1 as compared to the granule and mossy cells that constitute the DG (McKiernan et al., 2017; Amaral et al., 2007). Interestingly, the directionality of these

signals is consistent with prior research in animals (Stolp et al., 2018) suggesting cross-species consistency of these profiles and that they might map onto cytoarchitectural and cellular differences within these regions (Stolp et al., 2018; Wu & Zhang, 2016). These analyses serve as a benchmark of the ability of ultrahigh resolution dMRI to differentiate between hippocampal structure and surrounding cortices using the collateral sulcus as an additional indicator.

Investigations attempting to dissociate hippocampal subfields based on diffusion profiles have predominantly been done in rodents and have been to some extent related to histological tissue properties (Stolp et al., 2018; Wu & Zhang, 2016). In humans, possibly due to resolution limitation (Colon-Perez et al., 2015), investigations have mainly studied diffusion properties of the hippocampus as a whole (Mak et al., 2017; Reas et al., 2017) with only a few studies segmenting hippocampal body into either anterior/posterior segments (Fjell et al., 2019) or along the head and tail (Hong et al., 2010). A few investigations have probed hippocampal subfield diffusion properties as they relate to aging and memory processes in vivo, however, these approaches had not been benchmarked for sensitivity to subfield differences (Radhakrishnan et al., 2020; Yassa et al., 2011). However, one study using data derived from the Human Connectome Project implemented non-negative matrix factorization to identify components or groupings of similar FA and MD values of the MTL (Patel et al., 2020). Using this method, they were able to identify numerical partitions of the medial temporal lobe that contain clusters of similar MD and FA values; however, it is unclear how the identifiable partitions map onto known subfields of the hippocampus. Another study using the ADNI dataset investigated the use of diffusion imaging within subfields to

improve the detection and prediction of AD using MD (as well as volumes) of hippocampal subfields, however they did not report subfield-specific patterns of association with cognitive performance (Hett et al., 2019). Our current work is distinct from past contributions in that it demonstrates clear subfield-specific diffusion feature profiles and provides evidence for subfield-specific features predictive of memory performance.

Ultrahigh resolution diffusion imaging has previously been used to quantify directional anisotropy in specific white matter pathways (e.g., the perforant path), which was not possible using traditional approaches (Yassa et al., 2011). In the current investigation we improved on this method by using the ZOOMit scan procedure which utilizes inner volume excitation to increase the in-plane resolution (Blasche et al., 2012) in a limited field of view (in this case positioned along the hippocampal axis) under the assumption that we might also be able to detect differences in gray matter microstructure that might otherwise not be detectable. Variants of this sequence have primarily been used for imaging deep small organs including the prostate, spinal cord, pancreas, and optic nerve (Liney et al., 2015; Saritas et al., 2008; Sim et al., 2020; Seeger et al., 2018). Interestingly, only a handful of studies have implemented the ZOOMit sequence in brain tissue and have provided evidence of distinct advantages over their standard sequence counterparts. For instance, some evidence shows that the ZOOMit acquisition applied to BOLD contrast may be superior to conventional BOLD sequences in detecting hand-motor cortex (Fang et al., 2020). Additionally, the use of a structural ZOOMit sequence (paired with EEG) has been shown to facilitate localization of epileptic foci in patients whose focal cortical dysplasia went previously undetected

using standard structural sequences (Aydin et al., 2017). Here, we demonstrate the utility and feasibility of this approach to identify hippocampal subfield-level microstructural property profiles, which was not possible with standard diffusion sequences, and further validate the approach using anatomical a-priori knowledge as well as by testing associations with hypothesized cognitive outcomes. The relevant main anatomical a priori knowledge used here is that the collateral sulcus would provide a diffusion profile consistent with non-tissue (unrestricted free diffusion profile, hence lower FA and higher MD compared to tissue samples).

In addition to providing evidence of regionally specific diffusion properties, we show that increased MD within CA1 and increased MD and decreased FA in DG are associated with age. In this investigation, we note that the measures of FA and MD were calculated from within subject-specific subfield volumes, thus, changes of FA and MD inherently yield additional information regarding tissue microstructural organization across the aging spectrum that may supplement gross volumetric changes. In addition to showing an effect of age, we also show that DG volume and DG MD are associated with memory performance as assessed by the delayed recall portion of the RAVLT, relationships that persisted after accounting for age and sex. Additionally, our structural equation modeling analyses suggest that DG MD mediates the relationship between age and delayed recall performance, suggesting a putative mechanism for age-related episodic memory decline. While the cell type specificity in the interpretation of greater MD is unclear, this metric captures restricted diffusion and can generally be thought of as inversely related to “cellularity” or cellular density (Yeh et al., 2017). In other words, a smaller number of cells results in greater unrestricted diffusion (greater MD). While this

could potentially signify cellular loss in the DG, which is consistent with the volumetric decline we also observe with age, this interpretation remains speculative.

The DG is thought to play an important role in the neurocomputational process known as pattern separation, or the process by which similar experiences are encoded using distinct memory traces (Yassa & Stark, 2011). Recently, we have shown that spatial pattern separation is compromised in aged-impaired groups (Reagh et al., 2013). To further probe DG function, we asked whether DG MD was related to performance on a spatial pattern separation challenge. Here, we provide evidence that increased DG MD is associated with impaired spatial pattern separation performance whereas DG volume was not. Unlike the RAVLT, pattern separation tasks tend to be specific to DG impairment (Leal and Yassa, 2018), thus this directed test of the relationship between DG MD and spatial pattern separation performance provides further specificity. It is important to note that the diffusion profiles observed and their relationships with memory measures occur in the absence of clinical dementia as this is a nondemented sample of older adults. Our results suggest that microstructural alterations in the DG may be a more sensitive biomarker of age-related memory loss than DG volume or overall hippocampal volume.

A limitation of this study is the use of tensor derived measures which are susceptible to partial volume effects and in gray matter can lead to difficulty in interpretation (Assaf et al., 2018; Alexander et al., 2007, Alexander et al., 2011; Jdabdi & Johansen-Berg, 2011). While our approach employing high in-plane resolution limits the degree of partial volume averaging compared to sequences of standard voxel resolution, the single tensor characterization of DTI is another source of volume

averaging which we did not address with this work. Model-free reconstruction methods such as NODDI (Zhang et al., 2012) and ActiveAx (Alexander et al., 2010) have shown promise in alleviating the limitations of DTI and have successfully detected microstructural differences associated with amyloidosis (Colon-Perez et al., 2019) and aging pathology in humans in the hippocampus (Reas et al., 2017; Radhakrishnan et al., 2020). However, such model free methods typically require multiple b-shells, which was not the case with our ZOOMit acquisition. Future work using this ultrahigh resolution sequence may incorporate several diffusion weightings to probe microstructural integrity more thoroughly.

In addition, we note that in this investigation there were multiple differences in scan parameters across the ZOOMit dMRI sequence and whole brain dMRI sequence and the impact of these differences were not systematically evaluated. Indeed, the whole brain dMRI sequence is superior in terms of the number of sampling directions. Thus, we suggest that the high resolution of the ZOOMit sequence as well as its acquisition plane along the principal axis of the hippocampus could potentially serve to both limit partial volume effects and enhance the spatial fitting of ASHS regions to the native diffusion space. Future work is needed to systematically investigate how differences in number of non-diffusion weighted images, number of diffusion weighted images, b-value, scan resolution, and acquisition plane may impact the quantification of hippocampal subfield diffusion profiles and their association with age-related cognitive decline. In addition, we note in this investigation eddy_correct was used rather than eddy, future research should seek to both preprocess high resolution data with eddy as

well as to implement opposite phase encoding in order to correct for magnetization induced susceptibility distortions.

Finally, it is possible that slight differences in the alignment of the ZOOMit FOV during acquisition could have some impact on these results. While we took measures to mitigate operator differences in FOV alignment along the hippocampus with standard operator protocols and training we note that this possibility is not completely excluded.

In conclusion, we have shown using the ZOOMit ultrahigh resolution dMRI sequence that hippocampal subfields contain unique and dissociable diffusion properties. We have shown that these diffusion properties become compromised with increased age and compromised integrity of the DG may mediate the link between age and impaired episodic memory function.

References

Alexander, A.L., Hurley, S.A., Samsonov, A. A., Adluru, N., Hosseinbor, A. P., Mossahebi, P., Tromp do P. M., Zakszewski E., Field, A. S. (2011). Characterization of cerebral white matter properties using quantitative magnetic resonance imaging stains. *Brain Connectivity,* 1: 423–46.

Alexander, A.L., Lee, J.E., Lazar, M., Field, A.S. (2007). Diffusion tensor imaging of the brain. *Neurotherapeutics: the journal of the American Society for Experimental Neuro Therapeutics,* 4: 316–329.

Alkadhi K. A. (2019). Cellular and Molecular Differences Between Area CA1 and the Dentate Gyrus of the Hippocampus. *Molecular neurobiology,* 56(9), 6566–6580.

Amaral, D. G., Scharfman, H. E., & Lavenex, P. (2007). The dentate gyrus: fundamental neuroanatomical organization (dentate gyrus for dummies). *Progress in brain research,* 163, 3–22.

Assaf, Yaniv. (2018). Imaging laminar structures in the gray matter with diffusion MRI. *NeuroImage,* 197.

Avants, B.B., Tustison, N.J., Song, G., Cook, P.A., Klein, A., Gee, J.C. (2011). A reproducible evaluation of ANTs similarity metric performance in brain image registration. *Neuroimage,* 54: 2033–44.

Aydin, Ü., Rampp, S., Wollbrink, A., Kugel, H., Cho, J. -., Knösche, T. R., Grova, C., Wellmer, J., & Wolters, C. H. (2017). Zoomed MRI Guided by Combined EEG/MEG Source Analysis: A Multimodal Approach for Optimizing Presurgical

Epilepsy Work-up and its Application in a Multi-focal Epilepsy Patient Case Study. *Brain topography,* 30(4), 417–433.

Blasche, M., Riffel, P., Lichy, M. (2012). TimTX TrueShape and syngo ZOOMit Technical and Practical Aspects. *Magnetom Flash,* 1:74–84.

Braak, H., Braak, E. (1991). Neuropathological stageing of Alzheimer-related changes. *Acta Neuropathol,* 82:239– 259.

Burger C. (2010). Region-specific genetic alterations in the aging hippocampus: implications for cognitive aging. *Frontiers in aging neuroscience,* 2, 140.

Burke, S. N., & Barnes, C. A. (2006). Neural plasticity in the ageing brain. Nature reviews. *Neuroscience*, 7(1), 30–40.

Colon-Perez, L. M., King, M., Parekh, M., Boutzoukas, A., Carmona, E., Couret, M., Klassen, R., Mareci, T. H., & Carney, P. R. (2015). High-field magnetic resonance imaging of the human temporal lobe. *NeuroImage. Clinical* 9, 58–68.

Colon-Perez, L.M., Ibanez, K.R., Suarez, M., Torroella, K., Acuna, K., Ofori, E., Levites, Y., Vaillancourt, D.E., Golde, T.E., Chakrabarty, P., Febo, M. (2019). Neurite orientation dispersion and density imaging reveals white matter and hippocampal microstructure changes produced by Interleukin-6 in the TgCRND8 mouse model of amyloidosis. *Neuroimage,* 202, 116138.

Crombe, A., Planche, V., Raffard, G., Bourel, J., Dubourdieu, N., Panatier, A., Fukutomi, H., Dousset, V., Oliet, S., Hiba, B., & Tourdias, T. (2018). Deciphering the microstructure of hippocampal subfields with in vivo DTI and NODDI: Applications to experimental multiple sclerosis. *NeuroImage,* 172, 357–368.

Csernansky, J. G., Wang, L., Joshi, S., Miller, J. P., Gado, M., Kido, D., McKeel, D., Morris, J. C., & Miller, M. I. (2000). Early DAT is distinguished from aging by high-dimensional mapping of the hippocampus. Dementia of the Alzheimer type. *Neurology,* 55(11), 1636–1643.

Csernansky, J. G., Wang, L., Swank, J., Miller, J. P., Gado, M., McKeel, D., Miller, M. I., & Morris, J. C. (2005). Preclinical detection of Alzheimer's disease: hippocampal shape and volume predict dementia onset in the elderly. *NeuroImage,* 25(3), 783–792.

Daianu, M., Jacobs, R. E., Weitz, T. M., Town, T. C., & Thompson, P. M. (2015). Multi-shell hybrid diffusion imaging (hydi) at 7 tesla in tgf344-Ad transgenic Alzheimer rats. *PLoS ONE,* 10(12), 1–18.

Dillon, S. E., Tsivos, D., Knight, M., Mccann, B., Shiel, A. I., Conway, M. E., Newson, M.A., Kauppinen, R.A., Coulthard, E. J. (2017). The impact of ageing reveals distinct roles for human dentate gyrus and CA3 in pattern separation and object recognition memory. *Scientific Reports,* 1–13.

Dyrba, M., Barkhof, F., Fellgiebel, A., Filippi, M., Hausner, L., Hauenstein, K., Kirste, T., Teipel, S.J., (2015). EDSD study group. Predicting prodromal Alzheimer's disease in subjects with mild cognitive impairment using machine learning classification of multimodal multicenter diffusion-tensor and magnetic resonance imaging data. *J Neuroimaging*, 25(5):738–47.

Estévez-González, A., Kulisevsky, J., Boltes, A., Otermin, P., & García-Sánchez, C. (2003). Rey verbal learning test is a useful tool for differential diagnosis in the preclinical phase of Alzheimer's disease: Comparison with mild cognitive

impairment and normal aging. *International journal of geriatric psychiatry,* 18. 1021-8

Fang, S., Bai, H. X., Fan, X., Li, S., Zhang, Z., Jiang, T., & Wang, Y. (2020). A Novel Sequence: ZOOMit-Blood Oxygen Level-Dependent for Motor-Cortex Localization. *Neurosurgery,* 86(2), E124–E132.

Fjell, A. M., Sneve, M. H., Sederevicius, D., Sørensen, Ø., Krogsrud, S. K., Mowinckel, A. M., & Walhovd, K. B. (2019). Volumetric and microstructural regional changes of the hippocampus underlying development of recall performance after extended retention intervals. *Developmental Cognitive Neuroscience,* 40.

Fox, N.C., Freeborough, P.A. (1997) Brain atrophy progression measured from registered serial MRI: validation and application to Alzheimer's disease. *J Magn Reson Imaging,* 7:1069–75.

Frisoni, G.B., Fox, N.C., Jack, C.R., Scheltens, P.Thompson, P.M. (2010). The clinical use of structural MRI in Alzheimer disease. *Nat Rev Neurol*, 6:67–77

Gall, C. (1990). Comparative Anatomy of the Hippocampus. In: Jones E.G., Peters A. (eds) *Cerebral Cortex*, vol 8B. Springer, Boston, MA

Gomez-Isla, T., Price, J.L., McKeel, D.W.J., Morris, J.C., Growdon, J.H., Hyman, B.T. (1996). Profound loss of layer II entorhinal cortex neurons occurs in very mild Alzheimer's disease. *Neuroscience,* 16, 4491–4500

Hett, K., Ta, V. T., Catheline, G., Tourdias, T., Manjón, J. V., Coupé, P., & Alzheimer's Disease Neuroimaging Initiative (2019). Multimodal Hippocampal Subfield Grading For Alzheimer's Disease Classification. *Scientific reports*, 9(1), 13845.

Holden, H. M., & Gilbert, P. E. (2012). Less efficient pattern separation may contribute to age-related spatial memory deficits. *Frontiers in aging neuroscience, 4*, 9.

Hong, Y. J., Yoon, B., Shim, Y. S., Cho, A. H., Lim, S. C., Ahn, K. J., & Yang, D. W. (2010). Differences in microstructural alterations of the hippocampus in Alzheimer disease and idiopathic normal pressure hydrocephalus: A diffusion tensor imaging study. *American Journal of Neuroradiology,* 31(10), 1867–1872.

Ianov, L., De Both, M., Chawla, M. K., Rani, A., Kennedy, A. J., Piras, I., Day, J. J., Siniard, A., Kumar, A., Sweatt, J. D., Barnes, C. A., Huentelman, M. J., & Foster, T. C. (2017). Hippocampal Transcriptomic Profiles: Subfield Vulnerability to Age and Cognitive Impairment. *Frontiers in aging neuroscience,* 9, 383.

Insausti, R., Tuñón, T., Sobreviela, T., Insausti, A. M., & Gonzalo, L. M. (1995). The human entorhinal cortex: A cytoarchitectonic analysis. *Journal of Comparative Neurology,* 355(2), 171–198.

Jack, C.R., Petersen, R.C., Xu, Y.C., O'Brien, P.C., Smith, G.E., Ivnik, R.J., Boeve, B.F., Waring, S.C., Tangalos, E.G., Kokmen, E. (1999). Prediction of AD with MRI-based hippocampal volume in mild cognitive impairment. *Neurology*, 52:1397–1403.

Jbabdi, S., Johansen-Berg, H. (2011). Tractography: Where Do We Go from Here? *Brain Connectivity,* 1: 169- 183.

Jedynak, B.M., Lang, A., Liu, B., Katz, E., Zhang, Y., Wyman, B.T., Raunig, D., Jedynak, C.P., Caffo, B., Prince, J.L., (2012). A computational neurodegenerative disease

progression score: method and results with the Alzheimer's disease neuroimaging initiative cohort. *NeuroImage,* 63, 1478e1486.

Kantarci, K., Petersen, R. C., Boeve, B. F., Knopman, D. S., Weigand, S. D., O'Brien, P. C., Shiung, M. M., Smith, G. E., Ivnik, R. J., Tangalos, E. G., & Jack, C. R., Jr. (2005). DWI predicts future progression to Alzheimer disease in amnestic mild cognitive impairment. *Neurology,* 64(5), 902–904.

Klein, A., Andersson, J., Ardekani, B.A., Ashburner, J., Avants, B., Chiang, M.C., Christensen, G.E., Collins, D.L., Gee, J., Hellier, P., Song, J.H., Jenkinson, M., Lepage, C., Rueckert, D., Thompson, P., Vercauteren, T., Woods, R.P., Mann, J.J., Parsey, R.V. (2009). Evaluation of 14 nonlinear deformation algorithms applied to human brain MRI registration. *Neuroimage,* 46:786–802.

Leal, S. L., & Yassa, M. A. (2015). Neurocognitive Aging and the Hippocampus across Species. *Trends in neurosciences*, 38(12), 800–812.

Leal, S. L., Tighe, S. K., Yassa, M. A. (2014). Asymmetric effects of emotion on mnemonic interference. *Neurobiol Learn Mem,* 1(949), 41–48.

Liney, G. P., Holloway, L., Al Harthi, T. M., Sidhom, M., Moses, D., Juresic, E., Rai, R., & Manton, D. J. (2015). Quantitative evaluation of diffusion-weighted imaging techniques for the purposes of radiotherapy planning in the prostate. *The British journal of radiology,* 88(1049), 20150034.

Levine, B., Svoboda, E., Hay, J. F., Winocur, G., & Moscovitch, M. (2002). Aging and autobiographical memory: dissociating episodic from semantic retrieval. *Psychology and aging*, 17(4), 677–689.

Mak, E., Gabel, S., Su, L., Williams, G. B., Arnold, R., Passamonti, L., Rodriguez, P.V., Surendranathan, A., Bevan-Jones, W.R., Rowe, J. B., O'Brien, J. T. (2017). Multi-modal MRI investigation of volumetric and microstructural changes in the hippocampus and its subfields in mild cognitive impairment, Alzheimer's disease, and dementia with Lewy bodies. *International Psychogeriatrics,* 29(4), 545–555.

Mark, R. E., & Rugg, M. D. (1998). Age effects on brain activity associated with episodic memory retrieval. An electrophysiological study. *Brain: a journal of neurology*, 121 (Pt 5), 861–873.

Márquez, F., & Yassa, M. A. (2019). Neuroimaging Biomarkers for Alzheimer's Disease. *Molecular Neurodegeneration,* 14(1), 1–14.

Marr, D. (1971). Simple memory: a theory for archicortex. *Phil. Trans. R. Soc. Lond. B,* 262: 23–81

McKiernan, E. C., & Marrone, D. F. (2017). CA1 pyramidal cells have diverse biophysical properties, affected by development, experience, and aging. *PeerJ*, 5, e3836.

Molet, J., Maras, P. M., Kinney-Lang, E., Harris, N. G., Rashid, F., Ivy, A. S., Solodkin, A., Obenaus, A., & Baram, T. Z. (2016). MRI uncovers disrupted hippocampal microstructure that underlies memory impairments after early-life adversity. *Hippocampus,* 26(12), 1618–1632.

Muller, M.J., Greverus, D., Weibrich, C., Dellani, P.R., Scheurich, A., Stoeter, P., Fellgiebel, A. (2007). Diagnostic utility of hippocampal size and mean diffusivity in amnestic MCI. *Neurobiol Aging,* 28(3):398–403.

Ohm, T. G. (2007). The dentate gyrus in Alzheimer's disease, *Progress in Brain Research*, 163, 723-740.

Patel, R., Steele, C. J., Chen, A. G. X., Patel, S., Devenyi, G. A., Germann, J., Tardif, C. L., Chakravarty, M. M. (2020). Investigating microstructural variation in the human hippocampus using non-negative matrix factorization. *NeuroImage*, 207, 116348.

Price, J.L., Ko, A.I., Wade, M.J., Tsou, S.K., McKeel, D.W., Morris, J.C. (2001). Neuron number in the entorhinal cortex and CA1 in preclinical Alzheimer disease. *Arch. Neurol,* 58, 1395–1402.

Radhakrishnan, H., Stark, S. M., & Stark, C. E. L. (2020). Microstructural alterations in hippocampal subfields mediate age-related memory decline in humans. *Front. Aging Neuroscience,* 12(April), 1–15.

Reagh, Z. M., & Yassa, M. A. (2014). Object and spatial mnemonic interference differentially engage lateral and medial entorhinal cortex in humans. *Proceedings of the National Academy of Sciences of the United States of America,* 111(40), E4264–E4273.

Reagh, Z. M., Noche, J. A., Tustison, N. J., Delisle, D., Murray, E. A., & Yassa, M. A. (2018). Functional Imbalance of Anterolateral Entorhinal Cortex and Hippocampal Dentate/CA3 Underlies Age-Related Object Pattern Separation Deficits. *Neuron,* 97, 1187-1198.

Reagh, Z. M., Roberts, J. M., Ly, M., DiProspero, N., Murray, E., & Yassa, M. A. (2014). Spatial discrimination deficits as a function of mnemonic interference in aged adults with and without memory impairment. *Hippocampus,* 24(3), 303–314.

Reas, E. T., Hagler, D. J., White, N. S., Kuperman, J. M., Bartsch, H., Cross, K., Loi, R. Q., Balachandra, A. R., Meloy, M. J., Wierenga, C. E., Galasko, D., Brewer, J. B., Dale, A. M., McEvoy, L. K. (2017). Sensitivity of restriction spectrum imaging to memory and neuropathology in Alzheimer's disease. *Alzheimer's Research and Therapy,* 9(1), 1–12.

Rey A. (1964). L'examen clinique en psychologie. *Presses Universitaires de France; Paris*.

Sabuncu, M. R., Desikan, R. S., Sepulcre, J., Yeo, B. T., Liu, H., Schmansky, N. J., Reuter, M., Weiner, M. W., Buckner, R. L., Sperling, R. A., Fischl, B., & Alzheimer's Disease Neuroimaging Initiative (2011). The dynamics of cortical and hippocampal atrophy in Alzheimer disease. *Archives of neurology,* 68(8), 1040–1048.

Salo, R. A., Miettinen, T., Laitinen, T., Gröhn, O., Sierra, A. (2017). Diffusion tensor MRI shows progressive changes in the hippocampus and dentate gyrus after status epilepticus in rat – histological validation with Fourier-based analysis, *NeuroImage, 152*, 221-236.

Saritas, E.U., Cunningham, C.H., Lee, J.H., Han, E.T., Nishimura, D.G. (2008). DWI of the spinal cord with reduced FOV single-shot EPI. *Magn Reson Med,* 60:468-473.

Seeger, A., Schulze, M., Schuettauf, F., Ernemann, U., & Hauser, T. K. (2018). Advanced diffusion-weighted imaging in patients with optic neuritis deficit - value of reduced field of view DWI and readout-segmented DWI. *The neuroradiology journal,* 31(2), 126–132.

Shepherd, T. M., Özarslan, E., Yachnis, A. T., King, M. A., & Blackband, S. J. (2007). Diffusion tensor microscopy indicates the cytoarchitectural basis for diffusion

anisotropy in the human hippocampus. *American Journal of Neuroradiology*, 28, 958–964.

Sim, K. C., Park, B. J., Han, N. Y., Sung, D. J., Kim, M. J., & Han, Y. E. (2020). Efficacy of ZOOMit coronal diffusion-weighted imaging and MR texture analysis for differentiating between benign and malignant distal bile duct strictures. *Abdominal radiology (New York), 45*(8), 2418–2429.

Small, S. A., Chawla, M. K., Buonocore, M., Rapp, P. R., Barnes, C. A. (2004). Imaging correlates of brain function in monkeys and rats isolates a hippocampal subregion differentially vulnerable to aging. *Proc Natl Acad Sci,* 101:7181–7186.

Stark, S. M., Stevenson, R., Wu, C., Rutledge, S., & Stark, C. E. (2015). Stability of age-related deficits in the mnemonic similarity task across task variations. *Behavioral neuroscience*, 129(3), 257–268.

Stolp, H. B., Ball, G., So, P. W., Tournier, J. D., Jones, M., Thornton, C., & Edwards, A. D. (2018). Voxel-wise comparisons of cellular microstructure and diffusion-MRI in mouse hippocampus using 3D Bridging of Optically-clear histology with Neuroimaging Data (3D-BOND). *Scientific Reports, 8*(1), 1–12.

Suzuki, W. A., (1996). The anatomy, physiology and functions of the perirhinal cortex. *Current Opinion in Neurobiology,* 6, 179-1867.

Teipel, S.J., Grothe, M., Lista, S., Toschi, N., Garaci, F.G., Hampel, H. (2013). Relevance of magnetic resonance imaging for early detection and diagnosis of Alzheimer disease. *Med Clin North Am,* 97:399–424.

Whittaker, H. T., Zhu, S., Di Curzio, D. L., Buist, R., Li, X. M., Noy, S., Wiseman, F. K., Thiessen, J. D., & Martin, M. (2018). T1, diffusion tensor, and quantitative magnetization transfer imaging of the hippocampus in an Alzheimer's disease mouse model. *Magnetic resonance imaging*, 50, 26–37.

Wu, D., Zhang, J., (2016). In vivo mapping of macroscopic neuronal projections in the mouse hippocampus using high-resolution diffusion MRI. *Neuroimage,* 125: 84-93.

Yassa, M. A., & Stark, C. E. L. (2011). Pattern separation in the hippocampus. *Trends in Neurosciences,* 34(10), 515–525.

Yassa, M. A., Lacy, J. W., Stark, S. M., Albert, M. S., Gallagher, M., & Stark, C. E. (2011). Pattern separation deficits associated with increased hippocampal CA3 and dentate gyrus activity in nondemented older adults. *Hippocampus, 21*(9), 968–979.

Yassa, M. A., Stark, S. M., Bakker, A., Albert, M. S., Gallagher, M., & Stark, C. E. (2010). High-resolution structural and functional MRI of hippocampal CA3 and dentate gyrus in patients with amnestic Mild Cognitive Impairment. *NeuroImage,* 51(3), 1242–1252.

Yassa, M.A., Mattfeld, A.T., Stark, S. M., Stark, C. E. L. (2011). Age-related memory deficits linked to circuit-specific disruptions in the hippocampus. *Proceedings of the National Academy of Sciences*, 108 (21) ,8873-8878.

Yeh, F. C., & Ho, C. (2014). Mapping immune cells infiltration using restricted diffusion MRI. *Magnetic Resonance in Medicine*, 603–612.

Yushkevich, P.A., Pluta, J., Wang, H., Ding, S.L., Xie, L., Gertje, E., Mancuso, L., Kliot, D., Das, S.R., Wolk, D.A. (2014). Automated Volumetry and Regional Thickness Analysis of Hippocampal Subfields and Medial Temporal Cortical Structures in Mild Cognitive Impairment. *Human Brain Mapping*, 36, 258-287.

Zarow, C., Vinters, H. V., Ellis, W. G., Weiner, M. W., Mungas, D., White, L., & Chui, H. C. (2005). Correlates of hippocampal neuron number in Alzheimer's disease and ischemic vascular dementia. *Annals of neurology,* 57(6), 896–903.

Appendix C: Reduced structural connectivity of the medial temporal lobe including perforant path-related connectivity is associated with aging and memory impairment

This appendix in its entirety has been submitted to Neurobiology of Aging and is under review.

Granger, S. J., Colon-Perez, L., Larson, M. S., Bennet, L. J., Phelan, M., Keator, D. B., Janecek, J. T., Sathishkumar, M. T., Smith, A. P., McMillan, L., Greenia, D., Corrada, M. M., Kawas, C. H., Yassa, M. A. Reduced structural connectivity of the medial temporal lobe including perforant path-related connectivity is associated with aging and memory impairment. *In review at Neurobiology of Aging.*

Introduction

It is estimated that currently 5.8 million individuals have Alzheimer's Disease (AD) in the U.S. By 2050 this number is expected to increase to approximately 13.8 million (Hebert et al., 2013), therefore, it is critical to develop new, sensitive, and specific biomarkers to determine early pathological signs of aging and AD.

Episodic memory decline and medial temporal lobe (MTL) atrophy are markedly the most prominent and earliest pathological changes associated with age-related cognitive decline including Alzheimers Disease (Gomez-Isla et al., 1996; Price et al., 2001; Braak and Braak, 1991; Jack et al., 1999).

A key circuit of interest within the medial temporal lobe originates from the entorhinal cortex, one of the earliest sites of accumulation of AD-related tau pathology

(Desikan et al., 2010; Desikan et al., 2011; Desikan et 2012; Eskildsen et al., 2013). Functionally, the entorhinal cortex has shown prominent influence in episodic memory processes as an integrating node that mediates the communication between the hippocampus and the rest of the neocortex (Reagh et al., 2018). Structurally, the entorhinal cortex is known to connect to the dentate gyrus (DG) and CA3 subfields of the hippocampus via a white matter bundle that perforates through the subiculum; the perforant path (Witter, 2007). The integrity of the perforant path is critical for normal hippocampal functioning, is vulnerable to the effects of aging, and is compromised with AD as well as normal aging (Witter et al., 1989; Witter and Amaral, 1991; Witter, 2007; Hyman et al., 1986; Yassa et al., 2010).

There have been several attempts to study this connection using non-invasive diffusion MRI which consist of studies using ex-vivo MTL tissue samples and high angular resolution diffusion imaging (HARDI) protocols that require extensive scan times (Augustinack et al., 2010; Mollink et al., 2019; Colon- Perez et al., 2015; Beaujoin et al., 2018). Our research team has also previously demonstrated that this path can be evaluated in a rudimentary way on in-vivo diffusion weighted imaging (DWI) scans with sufficiently high spatial resolution (Yassa et al. 2010). While we have previously found that tensor-solved signals increase along the medial-lateral axis of the alveus which might correspond to the perforant path, the 2-dimensional nature of this method isn't sufficient to rule out other white matter that project along the anterior-posterior axis of the MTL such as the fornix, cingulum bundle, and stria terminalis. In other words, previous attempts to image the perforant pathway in studies of aging have not resolved

connectivity and integrity based on respective gray matter targets of known anatomical origin consistent with perforant pathway anatomy.

In this investigation, we employ the use of a novel high-resolution (0.67 x 0.67 x 3mm) DWI (ZOOMit) sequence to quantify the structural connectivity of the MTL in a sample of 51 older adults (63 to 98 years old, 32 female). Here we utilized data from two separate cohorts of older adults to make up our sample, the Young-Old group (n = 33, ages 65-86, 21 Female) and the Old-Old group (n = 18, ages 90 to 98, 11 Female). To attempt to delineate the 3-dimensional structure of MTL pathways, we implemented quantitative-anisotropy informed tractography which has been shown to reduce the number of false-positive streamlines compared to a simulated ground truth in global competition (Maier-Hein, et al., 2017) and improve FA-aided deterministic tractography of phantom objects (Yeh at al., 2013). As a measure of memory performance, we focused on the Rey Auditory Verbal Learning Test (RAVLT) delayed recall performance.

We hypothesized that MTL structural connectivity would decline in older adults and in association with reduced delayed recall performance, and further, we hypothesized that perforant pathway-like connectivity (between the entorhinal cortex and dentate gyrus) would be selectively impaired in older adults and in association with reduced verbal memory performance.

Methods

Participants

Participants were recruited in two separate cohorts (Young-Old and Old-Old) at the University of California, Irvine and given appropriate compensation for their

participation. Relevant demographic and RAVLT performance data are summarized in Table A3.1. Recruitment criteria for the Young-Old (age range 63-86) included being between the ages of 60 and 86, speak fluent English, had adequate visual and auditory acuity for neuropsychological and computerized testing, good health with no disease(s) expected to interfere with the study, willing and able to participate for the duration of the study and in all study procedures including MRI, and had normal cognition defined as a Clinical Dementia Rating of 0 and Mini-Mental State Examination Score of 27 or higher. Recruitment criteria for the Old-Old was largely the same, with the exception of testing visual and auditory acuity. Instead participants were screened for visual and auditory impairment as part of an initial medical screening. The Old-Old cohort (age range 90-98) were referred by an existing longitudinal cohort (The 90+ Study; Paganini-Hill et al., 2016) as non-demented as established by their closest visit with a neurologist. We note that approximately 5 individuals were diagnosed with Cognitive Impairment with No Dementia (CIND) from the Old-Old cohort. CIND was evaluated based on protocols from the existing longitudinal cohort study (Peltz et al., 2012). Briefly, CIND diagnosis was decided during a multidisciplinary case conferring session upon death where impairment in the memory domain or two or more other cognitive domains were established for diagnosis.

Table A3.1. Participant Demographics. *Indicates statistically significant t-test between Young-old and Old-old groups. † Indicates marginally significant difference

Age†	80.34 ± 10.76	73.23 ± 5.48	93.39 ± 2.36
Sex	32 Females, 19 Males	21 Females, 12 Males	11 Females, 7 Males

MMSE*	26.82 ± 2.75	27.88 ± 1.52	24.89 ± 3.43
Delayed Recall Performance*	9.67 ± 3.86	11.64 ± 2.73	6.056 ± 2.90
Years of Education*	15.8 ± 2.66	16.42 ± 1.98	14.67 ± 3.36
Clinical Diagnosis	5 CIND	0 CIND	5 CIND
**CIND - Cognitive Impairment No Dementia*			

Imaging Acquisition Parameters

All neuroimaging data were acquired on a 3.0 Tesla Siemens Prisma scanner at the Facility for Imaging and Brain Research (FIBRE) at the University of California, Irvine. A high-resolution 3D magnetization-prepared rapid gradient echo (MPRAGE) structural scan (0.8mm isotropic voxels) was acquired at the beginning of each session: repetition time (TR) = 2300ms, echo time (TE) = 2.38ms, FOV =192, 256, 256mm, flip angle = 8 degrees. In addition, a T2-weighted high-resolution hippocampal sequence was acquired: TR/TE = 5000/84ms, flip angle = 17 degrees, FOV = 190, 105, 198mm, voxel size = 0.42 x 0.42 x 2.4mm. The high-resolution diffusion sequence (ZOOMit) was collected as oblique coronal slices perpendicular to the long axis of the hippocampus with the following parameters: TR/TE = 3500/75ms, FOV = 180, 71, 66mm, voxel size = 0.67 x 0.67 x 3mm. The sequence consisted of two b = 0 s/mm^2 volumes and a total of 60 diffusion weighted volumes acquired as 30 non-collinear directions repeated twice at a b-value of 1000 s/mm^2. This sequence (ZOOMit) utilizes inner volume excitation to reduce the field of view and in-plane resolution (Blasche et al., 2012).

Medial Temporal Lobe Subfield Segmentation in Native Diffusion Space

T1 and T2-weighted images were used to parse the medial temporal lobe using the Automated Segmentation of Hippocampal Subfields (ASHS) pipeline to automatically label the T2-weighted images. This method implements joint label fusion, corrective learning, and is a highly accurate method in automatically deriving hippocampal subfield volumes and cortical subregions in the medial temporal lobe (Yushkevich et al., 2015). Using ASHS, the volumes for the following subregions were generated bilaterally: CA1, CA2, CA3, DG, subiculum, ERC, BA35, BA36, and PHC. The collateral sulcus and miscellaneous binary masks generated by ASHS were excluded from analysis as they represent MTL areas of non-tissue. In order to query medial temporal lobe structural connectivity, we used ANTSRegistrationSyn (Avants et al., 2009; Klein et al., 2009) to warp the T2 and associated ASHS regions to the first B0 of the partial FOV high resolution diffusion sequence (Figure A.3.1a). We preprocessed the ZOOMit sequence using FSLs eddy_corrrect. We quantified motion by calculating the average Euclidian distance in the linear transformation from each sub-brick to the first two b = 0 s/mm2 volume prior to any motion correction.

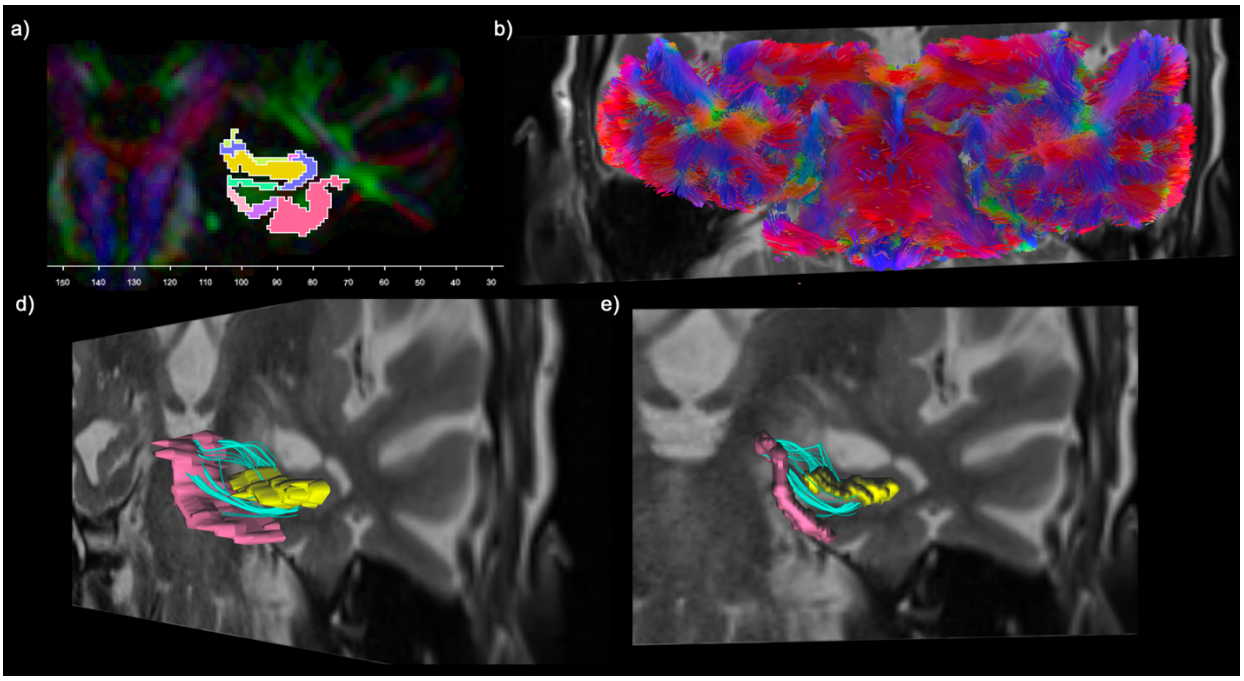

Figure A.3.1. QA-informed whole-brain tractography in the partial FOV high resolution GQI space. (a) Here we show a coronal section of the ASHS ROIs in the subject-specific GQI space with the entorhinal cortex (in pink) and the DG (in yellow). (b) The results of the whole brain tractography a coronal view. (c) A coronal-oblique view of the entorhinal cortex ROI (pink), and DG (yellow) for a single subject with the T2-weighted image in GQI space as the underlay. Blue streamlines here represent the streamlines that connect or 'end' in the entorhinal cortex and DG. These streamlines are representative of those extracted from the whole brain tractography generated with similar tracking parameters with the added filter of the entorhinal cortex and DG as 'end' regions through DSI-Studio's GUI interface.

Tractography and Calculation of Network Measures

Tractography and network-based analyses were conducted using DSI-Studio (http://dsi-studio.labsolver.org; Fang-cheng Yeh. (2019, March 14). The b-table was checked by an automatic quality control routine to ensure its accuracy (Schilling et al., 2019). The diffusion data were reconstructed using generalized q-sampling imaging (Yeh et al., 2010) with a diffusion sampling length ratio of 1.3. A quantitative anisotropy-informed deterministic fiber tracking algorithm (Yeh et al., 2013) was used. A seeding region was placed at the whole brain (within the partial field of view). The qa threshold

was randomly selected. The angular threshold was 65 degrees. The step size was randomly selected from 0.5 voxel to 1.5 voxels. The fiber trajectories were smoothed by averaging the propagation direction with 60% of the previous direction. Tracks with length shorter than 0 or longer than 600 mm were discarded. A total of 10,000,000 seeds were placed. Topology-informed pruning (Yeh et al. 2019) was applied to the tractography with 1 iteration(s) to remove false connections. The resulting restricted FOV tractography can be visualized in Figure A.3.1b. Observationally, the tractography generated via GQI in DSI-Studio software resulted in visually discernable structures including decussating optic chiasm. We further tested if GQI was sufficient at modeling crossing fibers by temporarily "deleting" the fibers decussating at the optic chiasm in subjects whose optic chiasm was discernable and within the field of view using DSI-Studio functions. Upon temporary deletion of the left hemisphere optic nerve, both nerves could be visualized on the other side of the optic chiasm. Upon temporary deletion of the right hemisphere optic nerve, both nerves could be visualized on the other side of the optic chiasm. This visualization technique allowed us to conclude that our diffusion sampling length ratio was appropriate in order to model crossing fibers given the normal protocol for choosing this value relies on the observation of crossing fibers at the intersection of the corticospinal tract and corpus callosum which was not available in the current field of view.

In order to query structural connectivity features of the resulting tractography we implemented DSI-Studio's use of the Brain Connectivity Toolbox (Rubinov & Spourns, 2010; https://sites.google.com/site/bctnet/). The number of streamlines 'ending' within

each ASHS node pair was used as the edge weight. The average left, right, and bilateral connectivity matrices are displayed in Figure A.3.2.

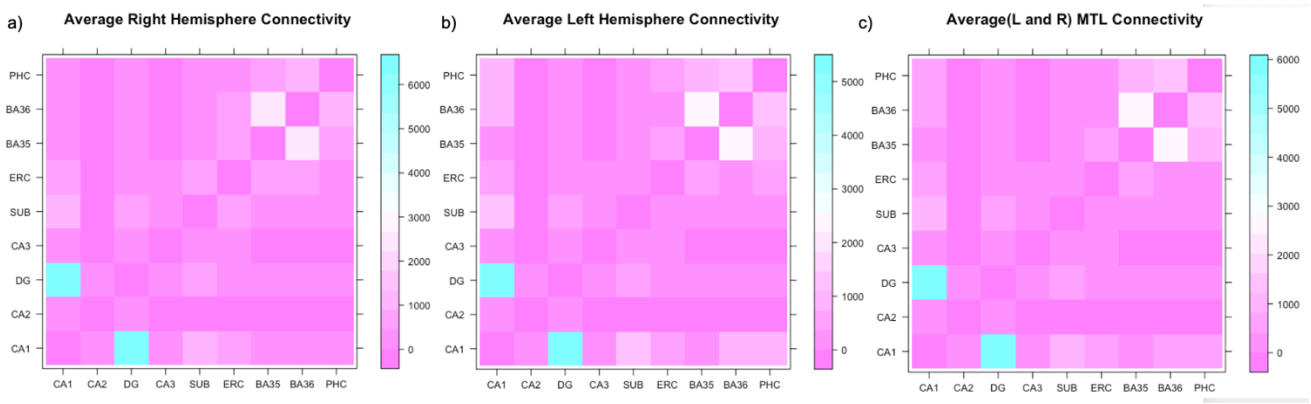

Figure A.3.2. Number of streamlines connecting regions within the medial temporal lobe. (a) Shows the average number of streamlines connecting right hemisphere MTL regions. (b) Shows the average number of streamlines connecting left hemisphere MTL regions. (c) Shows the averaged (left and right) hemisphere MTL connectivity. Left and right hemisphere connectivity values were averaged within individuals and then across individuals to obtain the average connectivity. All adjacency matrices are symmetric across the bottom left to top right diagonal. Visually observable is the apparently large number of streamlines connecting the CA1 and DG of the hippocampus. Other large connectivity's are between BA35 and BA36.

We chose to quantify graph density as a simple summary measure of overall connectedness which is calculated as the proportion of node-to-node connectivity weights that surpass an arbitrary threshold. Graph density was calculated from all ASHS nodes including the CA1, CA2, CA3, DG, subiculum, ERC, sulcus, BA35, BA36, and PHC. Four different thresholds (0.01, 0.001, 0.0001, 0.00001) were chosen to determine if overall "connectedness" of the MTL was associated with aging and episodic memory decline. To better understand ERC projections to the hippocampus to determine which node pair were implicated in aging and memory decline we chose the following regions: ERC, CA1, CA2, CA3, DG, and subiculum.

Neuropsychological Testing

Our primary outcome measure in this investigation was performance on the Rey Auditory Verbal Learning Memory Test (RAVLT; Rey, 1964). The RAVLT is used to evaluate the quality of verbal memory and is a well-established benchmark for testing and dissociating normal aging, MCI, and Alzheimer's Disease (Estevez-Gonzalez et al., 2003). The RAVLT was administered by an examiner who was instructed to read a list of 15 words, after which the subject was asked to repeat as many words as they could remember (in any order). This study/test trial was repeated for a total of 5 learning trials (Learning Trials, A1-A5) and were then followed by an immediate recall of a distractor list (B1), then immediate recall of the original list of 15 words (Immediate Recall, A6). The subject was then tested 20 minutes later making up the Delayed Recall portion. In this investigation we chose the delayed recall measure due to prior work using the tensor signal (Yassa et al., 2010) and relation to hippocampal deficits, aging and Alzheimer's Disease (Stark, 2007). In addition to Delayed Recall, we also quantified performance on the Mini-Mental State Exam (MMSE) to assess general cognitive status and include as a covariate in later regression analyses.

Statistical Analysis

Statistical analyses were computed using a mixture of GraphPad Prism 7 and R Software (https://www.R-project.org/). Multiple linear regression analyses were completed using R. All correlational analyses were done using two-tailed tests of Pearson correlation coefficients (alpha set to 0.05). ANOVA were completed using GraphPad Prism 7 and corresponding post-hoc analyses were conducted using Sidak's

multiple comparisons test. Benjamini-Hochberg procedure was used to correct for multiple comparisons for node-by-node analyses (Benjamini & Hochberg, 1995).

Results

MTL Graph Density Associated with Age and Delayed Recall Performance

We first sought to determine if MTL graph density within each hemisphere was dependent on the assigned arbitrary threshold. We computed graph density using four different thresholds (0.01, 0.001, 0.0001, 0.00001) and evaluated if the threshold impacted the connectedness of each graph. Using two-way analysis of variance, we found a main effect of threshold ($F_{(3, 400)} = 344.2$, $P < 0.0001$; Figure A.3.3).

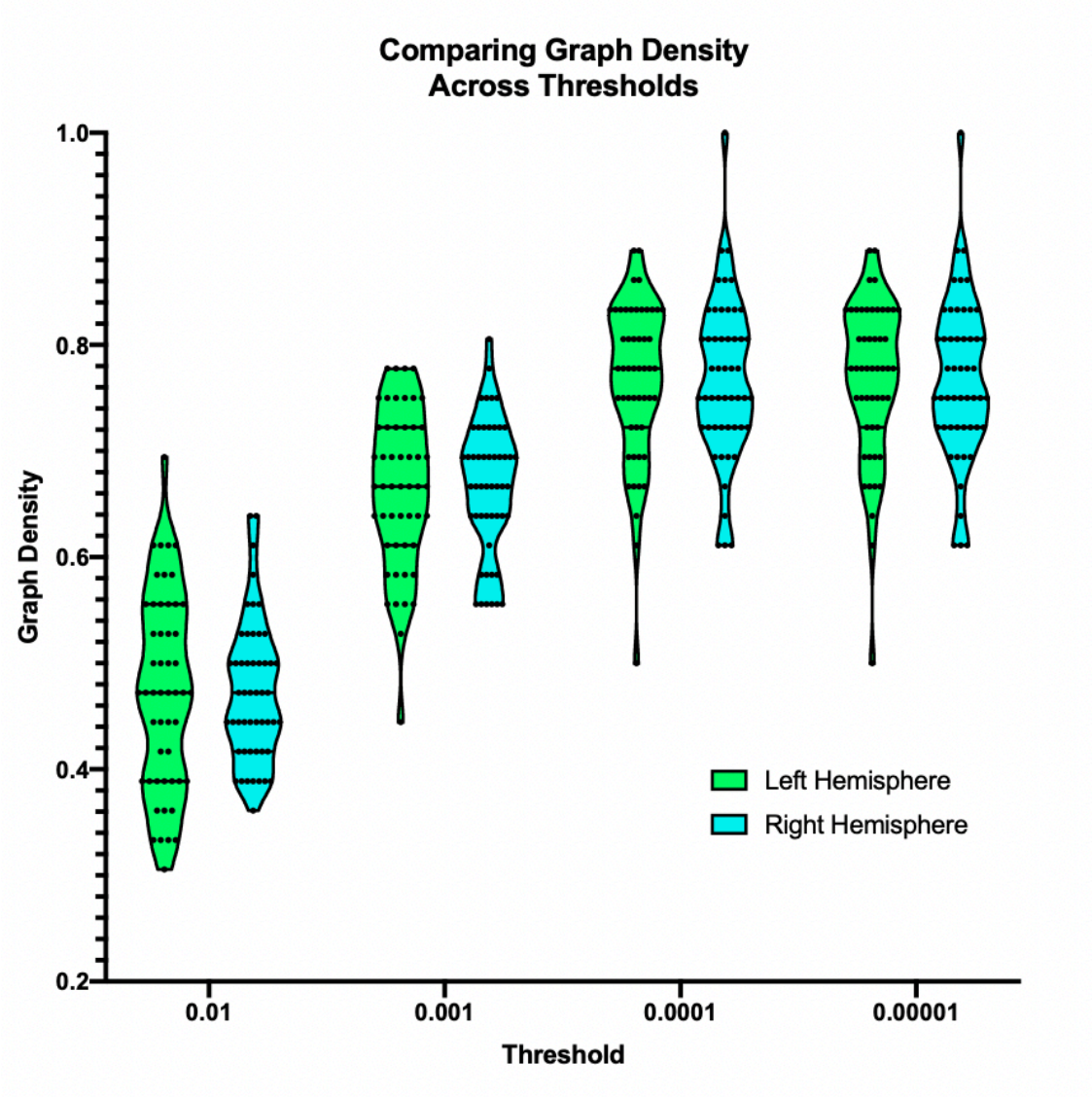

Figure A.3.3. Difference in graph density as a function of threshold. Using two-way ANOVA, we report a main effect of threshold indicating an increase in graph density as threshold moves from more conservative (higher threshold: 0.01) to less conservative (lower threshold: 0.00001). As a result of this analyses we chose to use the threshold of 0.001 to test if difference in MTL structural graph density changes with increased age and impaired memory performance.

Post-hoc comparisons revealed no significant difference between left and right hemisphere graph density within each threshold. Observationally, we note that the graph density in each hemisphere reached an asymptote at 0.0001 which may possibly be too liberal of a threshold. As a result of this and the lack of difference between

hemispheres, we removed analyses with graph density calculated at the smallest threshold (0.00001) and averaged graph densities across the left and right hemisphere for future analyses.

We then tested if average MTL graph density was reduced in the Old-Old cohort compared to the Young-Old cohort. We found a main effect of age group ($F_{(1, 147)}$ = 18.30, P < 0.0001) and a main effect of threshold ($F_{(2, 147)}$ = 308.8, P < 0.0001). Post-hoc analyses revealed that the Old-Old cohort exhibited decreased graph density (t = 3.32, P = 0.0034) compared to the Young-Old cohort only for the 0.01 threshold (Figure A.3.4).

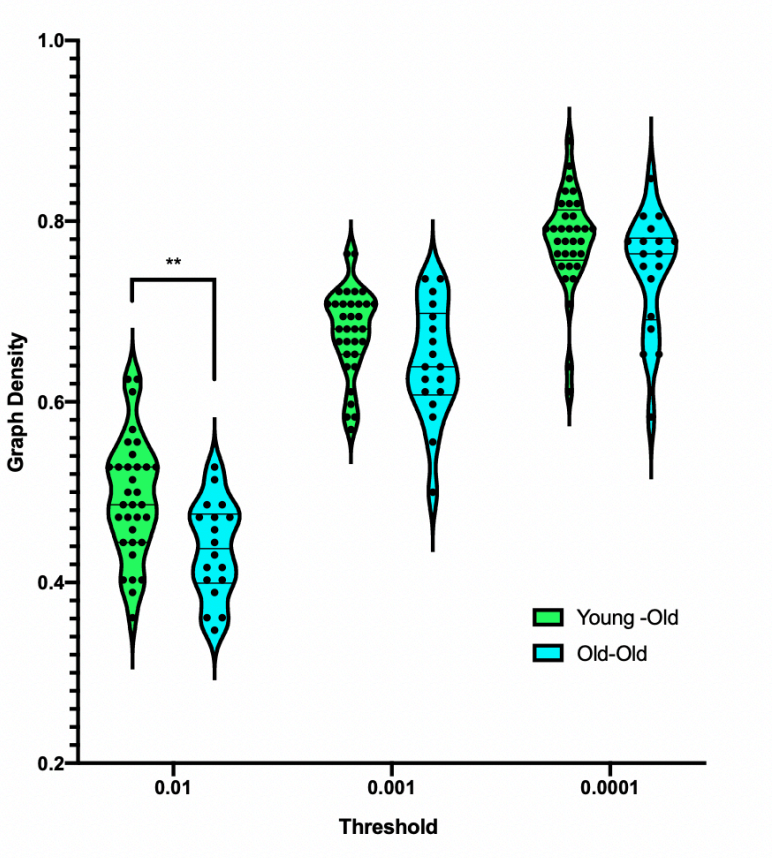

Figure A.3.4. Difference between Young Old and Old Old MTL Graph Density. We report a main effect of age group ($F_{(1, 147)}$ = 18.30, P < 0.0001) and threshold ($F_{(2, 147)}$ =

308.8, $P < 0.0001$). Post-hoc analysis revealed that the Old-Old cohort exhibited decreased graph density ($t = 3.32$, $P = 0.0034$) compared to the Young-Old cohort only for the 0.01 threshold.

We then asked if the graph density of the MTL was associated with performance on the Delayed Recall portion of the RAVLT. We found a significant positive relation between the average graph density and RAVLT Delayed Recall performance for each threshold (0.01: r = 0.38, P = 0.0054; 0.001: r = 0.45, P = 0.001; 0.0001: r = 0.42, P = 0.0021; Figure A.3.5).

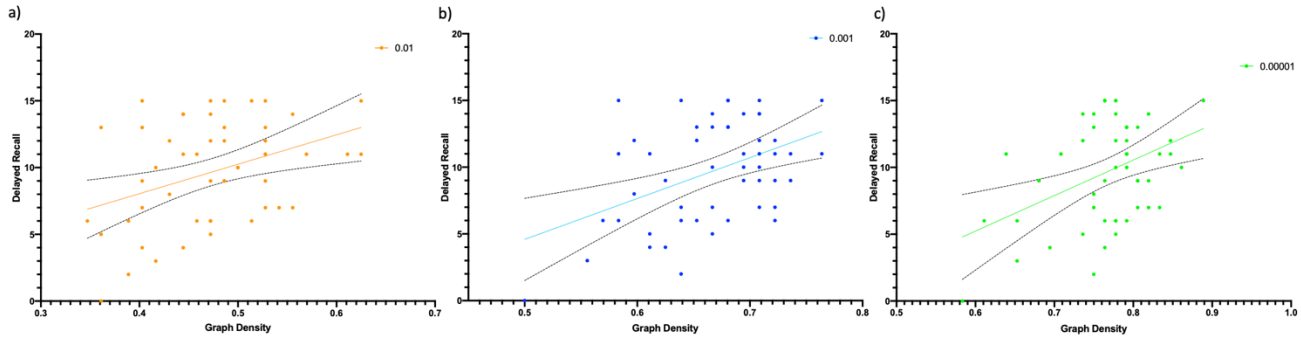

Figure A.3.5. Relation between MTL structural graph density and delayed recall performance. We found that the association between graph density and delayed recall was statistically significant for the (a) 0.01 threshold (r = 0.38, $P = 0.0054$), the (b) 0.001 threshold (r = 0.45, $P = 0.001$), and the (c) 0.0001 threshold (r = 0.42, $P = 0.0021$).

Entorhinal Cortex and DG Streamlines associated with Age

As a result of the differences in MTL graph density across age groups and in association with delayed recall performance, we then sought to test if there were specific connections within the MTL that were responsible for these differences. We focused on streamlines connecting the ERC with hippocampal subfields including CA1, CA2, DG, CA3, and subiculum (SUB).

We tested if there were differences between the Young-Old and Old-Old age groups on a node-by-node basis correcting for multiple comparisons using the

Benjamini-Hochberg method (n = 15). Benjamini-Hochberg corrected t-tests (n = 15; Figure A.3.6) revealed that the number of streamlines between the CA1-Subiculum (t = 2.69, corrected P = 0.048; Figure A.3.6b), entorhinal cortex-DG (t = 3.73, corrected P = 0.0074; Figure A.3.6c), and entorhinal cortex-CA1 (t = 3.40, corrected P = 0.010; Figure A.3.6d) were decreased in the Old-Old age group compared to the Young-Old age group.

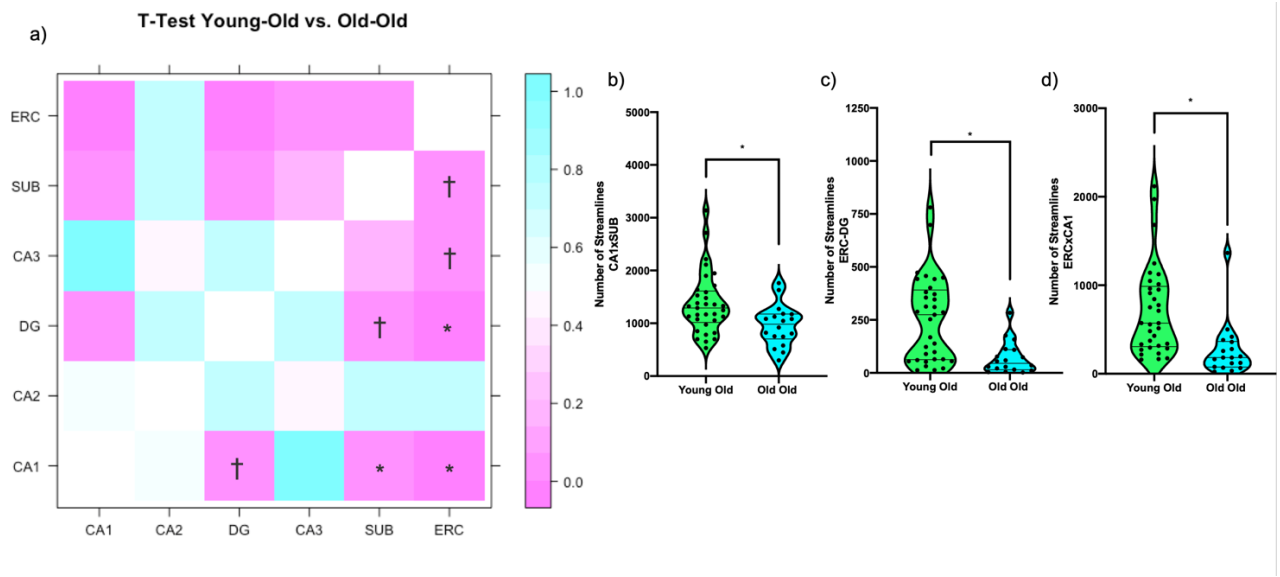

Figure A.3.6. Results of t-test (p-values in color) on a node-by-node basis between Young-old (n = 33) and old-old (n=18). (a) Shows all comparisons between young-old and old-old age groups. (b) shows the statistically significant difference between the CA1 and SUB connection between young-old and old-old. (c) Shows the statistically significant difference between the ERC and DG connection between young-old and old-old. (d) Shows the statistically significant difference between the connectivity of the ERC and CA1 region between young-old and old-old. *Indicate significant differences at the Benjamini-Hochberg corrected level. † indicates significant difference at the uncorrected level.

We note here that there are several different node-by-node differences at the uncorrected level between the DG - CA1 (t = 2.14, uncorrected P = 0.038; Figure A.3.7a), subiculum - DG (t = 2.01, uncorrected P = 0.047; Figure A.3.7b), ERC - CA3 (t

= 2.32, uncorrected P = 0.025; Figure A.3.7c), and ERC-subiculum (t = 2.14, uncorrected P = 0.038; Figure A.3.7d).

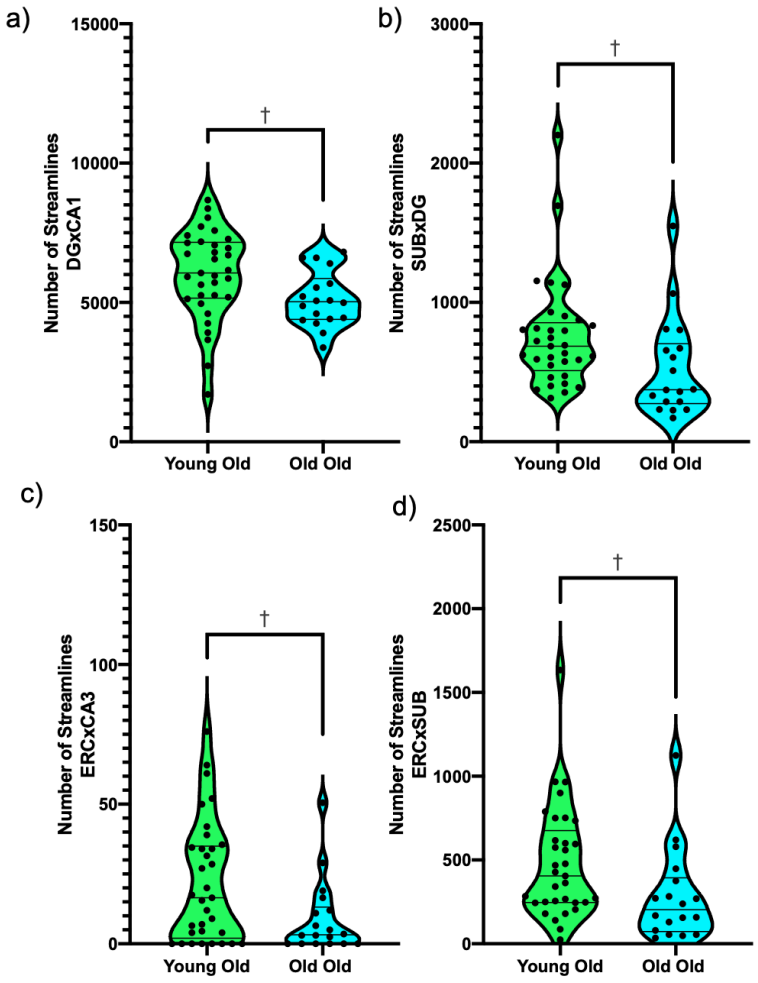

Figure A.3.7. Significant results in node-by-node structural connectivity analysis between young-old and old-old age groups at the uncorrected level (†). (a) At the uncorrected level, there is a difference with old-old showing fewer number of streamlines connecting the DG and CA1 (*t* = 2.14, *uncorrected P* = 0.038). (b) At the uncorrected level, the old-old age group had fewer streamlines connecting the subiculum and DG (*t* = 2.01, *uncorrected P* = 0.047). (c) The old-old cohort also had fewer streamlines connecting the entorhinal cortex and CA3 subregion of the hippocampus (*t* = 2.32, *uncorrected P* = 0.025). (d) Lastly, at the uncorrected level, the old-old cohort exhibited fewer number of streamlines connecting the entorhinal cortex and subiculum (*t* = 2.14, *uncorrected P* = 0.038).

In addition to testing if there was a node-by-node difference across age groups, we also tested if age as a continuous variable was associated with changes in connectivity of ERC-hippocampal subfields on a node-by-node basis. After correcting for multiple comparisons, we found that age was associated with decreased structural connectivity of the entorhinal cortex – CA1 connection (r = -0.44, corrected P = 0.008, Figure A.3.8b) as well as the entorhinal cortex – DG connection (r = -0.50, corrected P = 0.003; Figure A.3.8c).

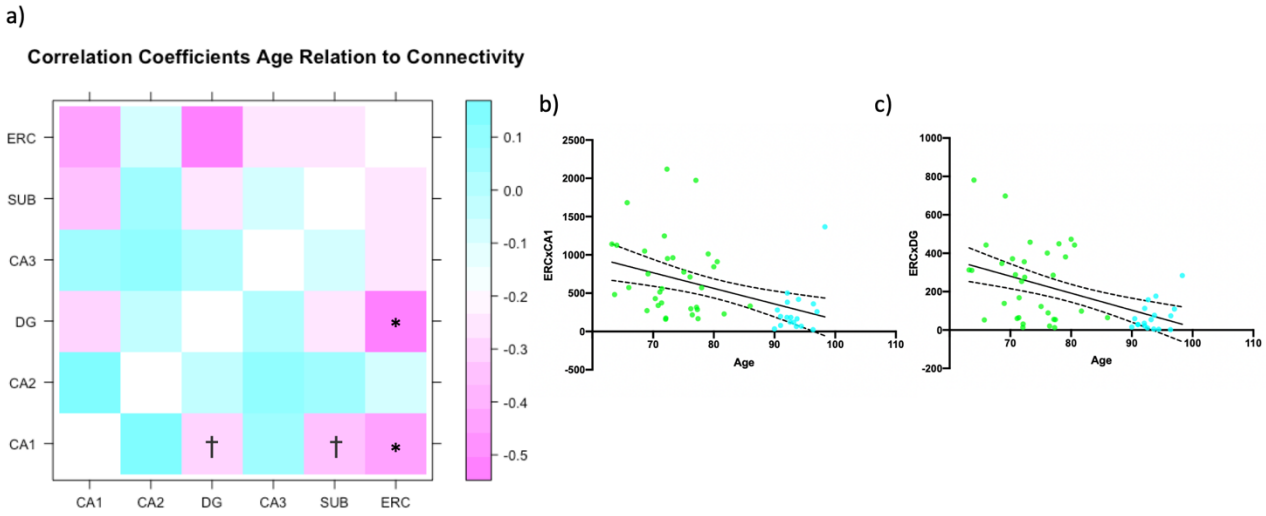

Figure A.3.8. Results of correlation (correlation coefficients in color) of age predicting streamline number on a node-by-node basis. (a) Shows correlation coefficients for all comparisons. (b) Shows ERCxCA1 streamline number declines with advanced age (r = -0.44, *corrected P* = 0.008). (c) Shows ERCxDG streamline number declines with advanced age (r = -0.50, *corrected P* = 0.003).

It is possible that these differences may be biased based on a relative increase in streamlines. To address this we normalized the streamline count for each subject based on the maximum streamline (edge weight) count. The association between age (continuous) and entorhinal cortex – CA1 connectivity persisted after adjusting for the maximum graph edge weight (r = -0.36, P = 0.0086; Figure A.3.9a). Similarly, the

association between age and entorhinal cortex – DG connectivity persisted after adjusting for the maximum graph edge weight (r = -0.45, P = 0.0009; Figure A.3.9b).

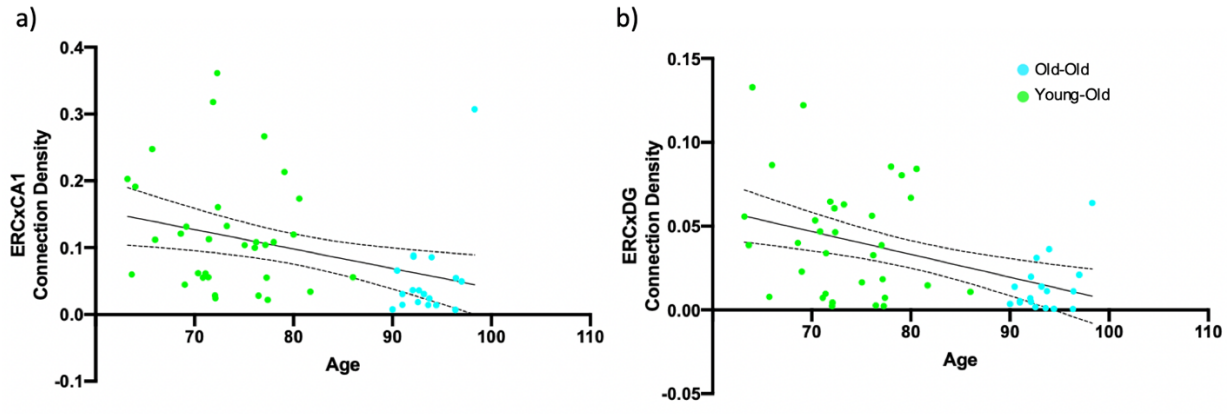

Figure A.3.9. Connection edge weight adjusted by graph edge weight maximum (connection density). (a) Shows the significant relation between age and entorhinal cortex-CA1 connection density (r = -0.36, *P* = 0.0086) (b) Shows the significant relation between and entorhinal cortex – DG connection density (r = -0.45, P = 0.0009).

Entorhinal Cortex and DG Streamlines associated with Delayed Recall Performance

We then asked if particular nodes were associated with delayed recall performance. After correcting for multiple comparisons, we found that fewer streamlines connecting the CA1 and DG (r = 0.38, corrected P = 0.039; Figure A.3.S1b), entorhinal cortex and subiculum (r = 0.40, corrected P = 0.039; Figure A.3.S1c), entorhinal cortex and DG (r = 0.37, corrected P = 0.039; Figure A.3.S1d) were associated with reduced delayed recall performance.

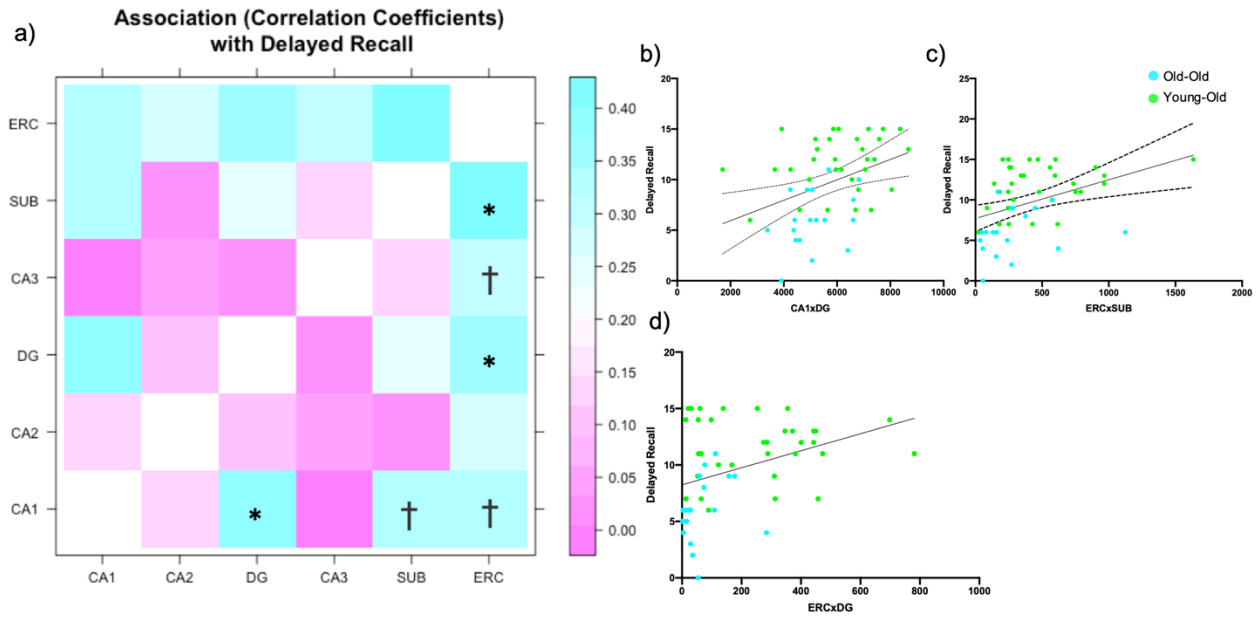

Figure A.3.S1. Relation (correlation coefficients) between the average MTL Connectivity and delayed recall performance. (a) Shows on a node-by-node basis the correlation coefficients of the relation between node-node connectivity and RAVLT Delayed Recall Performance. (b) Shows the significant association between reduced CA1-DG structural connectivity and impaired delayed recall performance (r = 0.38, *uncorrected* P < 0.01). (c) Shows the significant association between reduced entorhinal cortex-subiculum structural connectivity and impaired delayed recall performance (r = 0.40, *uncorrected* P < 0.005). (d) Shows the significant relation between reduced entorhinal cortex-dentate gyrus structural associated with impaired delayed recall performance (r = 0.37, *uncorrected* P < 0.01). * Indicates statistically significant correlation at the Benjamini-Hochberg corrected level. † Indicates significant at the uncorrected level.

The relationship between reduced CA1 and DG connectivity and reduced delayed recall performance did not persist (β = 0.19, P = 0.11) after accounting for MMSE, sex, years of education, and average subject in-scanner head motion. However, the relationship between reduced entorhinal cortex – DG connectivity and reduced delayed recall performance did persist (β = 0.25, P = 0.024) after accounting for MMSE, sex, years of education, and subject motion. Similarly, the relationship between reduced entorhinal cortex-subiculum structural connectivity persisted (β = 0.27, P = 0.013) after

accounting for MMSE, sex, years of education, and subject motion. Relationships between delayed recall and node-by-node connectivity that are statistically significant at the uncorrected level are summarized in Figure A.3.S2.

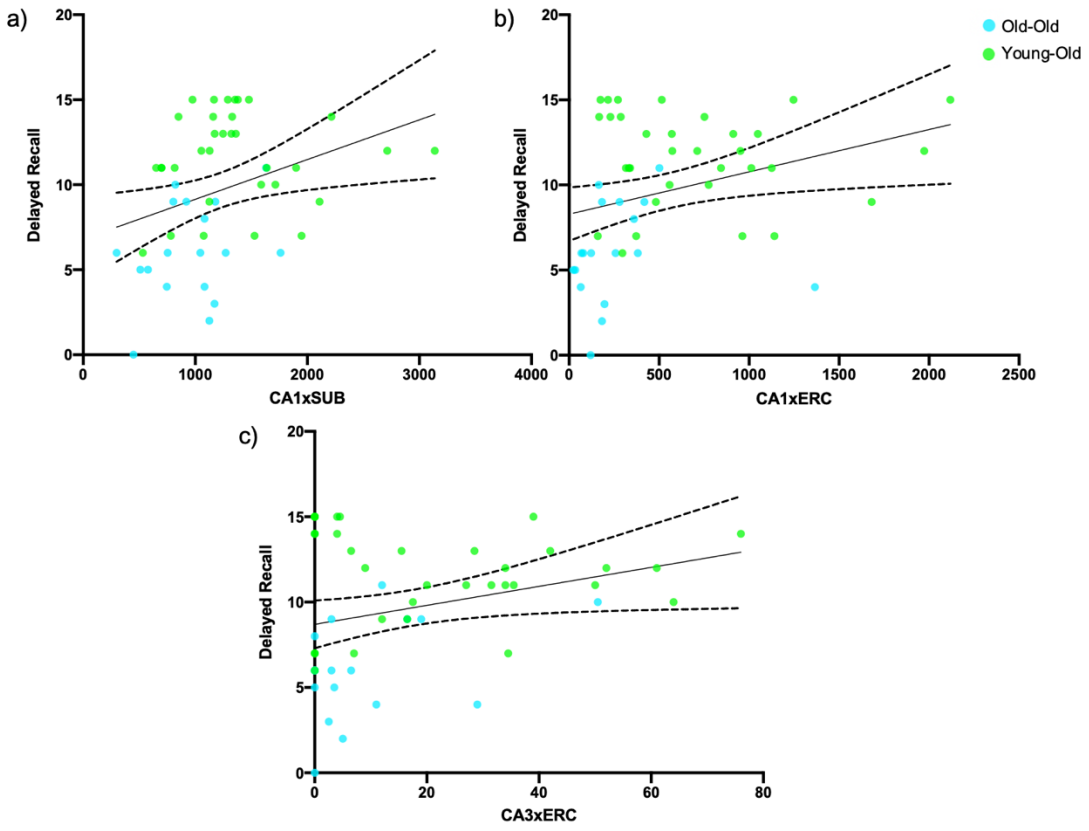

Figure A.3.S2. Significant associations between number of streamlines and delayed recall performance connecting node pairs at the uncorrected level (†). (a) Shows significant relation between the number of streamlines connecting the CA1-subiculum and delayed recall performance at the uncorrected level (r = 0.33, R^2 = 0.11, *uncorrected P* = 0.016). (b) Shows the significant relation between the entorhinal cortex and CA1 subregion of the hippocampus and delayed recall performance (r = 0.32, R^2=0.10, *uncorrected P* = 0.023). (c) Shows the significant relation between the number of streamlines connecting the entorhinal cortex and CA3 subregion of the hippocampus and delayed recall performance (r = 0.29, R^2= 0.083, *uncorrected P* = 0.0405).

Similar to the node-by-node analysis with age, we then asked if the association between node pairs and delayed recall performance was driven by the graph maximum.

To address this, we normalized the streamline count for each subject based on the maximum streamline (edge weight) count. We found that the relationship between entorhinal cortex – DG (r = 0.34, P = 0.015; Figure A.3.S3a) and entorhinal cortex – subiculum (r = 0.31, P = 0.028, Figure A.3.S3b) and delayed recall performance persisted after normalizing for the maximum graph edge weight.

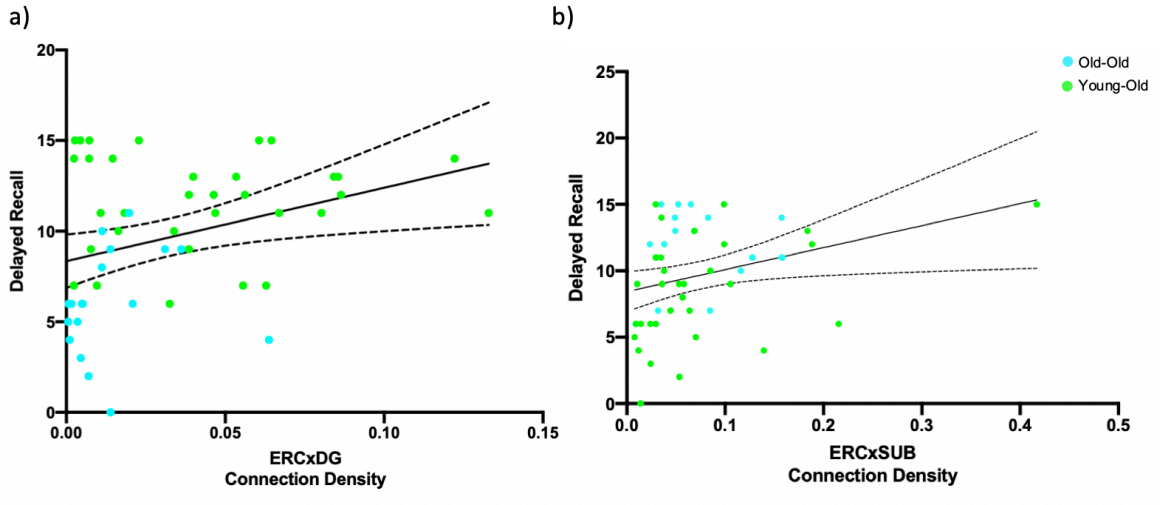

Figure A.3.S3. Normalized connection density by graph maximum. (a) Shows the entorhinal cortex-dentate gyrus connectivity strength normalized by the subject maximum. The resulting connection density measure is associated with delayed recall performance (r = 0.34, *P* = 0.015). (b) Shows the entorhinal cortex-subiculum connection density with is also associated with delayed recall performance although possibly driven by the outlier (r = 0.31, *P* = 0.028).

To address the possibility that a single outlying point is responsible for the positive relationship between entorhinal cortex – subiculum and delayed recall performance we removed that subject and found that the relationship between entorhinal cortex – subiculum connectivity became marginally significant (r = 0.24, P = 0.092). As the CA1 – DG connection was not significant after accounting for covariates and was the maximum graph edge weight for all but 5 subjects, we excluded this connection from this analysis.

Entorhinal Cortex – DG Connectivity Moderates the Association Between Age and Delayed Recall Performance

As a result of the relationship between the entorhinal cortex – DG connection with age and delayed recall performance, we then asked if the entorhinal cortex – DG connectivity moderated the associated between age and delayed recall performance. We found that entorhinal cortex – DG connectivity moderated the association between age and delayed recall performance ($\beta = 2.072$, $P = 0.034$).

Discussion

There are three major findings of this study. First, we provide evidence that structural connectivity within the MTL is reduced in the Oldest-Old and reduced MTL structural connectivity is associated with memory decline. Second, out of all possible entorhinal projections, we provide evidence that streamlines ending in the entorhinal cortex and DG are reduced in the Oldest-Old and reduced in those with memory decline. Finally, we provide evidence that entorhinal cortex - DG connectivity mediates the relationship between age and delayed recall performance.

The perforant pathway, as first visualized by Ramón y Cajal, is thought to originate in layer II and III of the entorhinal cortex and traverse the pyramidal cell layer of the subiculum in order to innervate the dentate gyrus and CA3 subfields of the hippocampal formation (Ramón y Cajal, 1911; Lorente de Nó, 1993; Witter, 2007). It is also understood that the entorhinal cortex projects to a number of other regions

including the subiculum (Witter, 2006) and CA3 subfields of the hippocampus (Steward and Scoville, 1976; Witter and Amaral, 1991), as well as CA1 and CA2 regions (Desmond et al., 1994; Steward, 1976; Steward and Scoville, 1976; Witter, 2007; Naber et al., 2001; Baks-Te-Bulte et al., 2005).

Evidence from rodent studies have shown that the integrity of the perforant path declines in normal aging (Geinisman et al., 1992; Smith et al., 2000). Histological studies from ex-vivo human data suggest that perforant path integrity is associated with AD-pathology (Hyman et al., 1986) and is compromised in those with mild cognitive impairment (Scheff et al., 2006). Extending these findings, using histology from ex-vivo human data, our colleagues have shown that perforant path synaptic loss is related to cognitive impairment and AD-pathology in humans over 90 years old (Robinson et al., 2014).

With the goal of translating these findings to create an early and detectable biological marker of age-related cognitive decline, our laboratory was the first to measure perforant path integrity using in-vivo ultra-high-resolution diffusion weighted imaging targeted at the medial temporal lobe. In this investigation, we used a submillimeter diffusion-weighted imaging sequence to detect anisotropy along the orientation of the perforant path using a composite measure of tensor-derived signals (Yassa et al., 2010). Using this method, we were able to show that the diffusion strength of the perforant path (compared across the medial-lateral axis of the medial temporal lobe) decreased in older adults. As a control, we selected the alveus (forming the anterior portion of the fimbria/fornix), which did not show the same decrease in diffusion parameters associated with age and memory impairment. Critically, this finding

improved previous work that did not utilize sufficiently high voxel resolution to observe the perforant path (Kalus et al., 2006; Rogalski et al., 2009). While our prior work was the first investigation of diffusion anisotropy of the perforant path in-vivo and provided an association with aging and episodic memory performance, others in the field have suggested that this method partially or indirectly captures the perforant pathway (Zeineh et al., 2012) based on its consideration of the perforant path in the 2-dimensional coronal plane rather than with respect to the 3-dimensional morphology of this pathway. In other words, our previous attempt to image the perforant pathway did not resolve connectivity and integrity based on respective gray matter targets of known anatomical origin consistent with perforant pathway anatomy.

In the last decade, other researchers in the field have begun to address these issues using tractography. The perforant path has now been investigated using excised human and non-human primate tissue scanned with high angular resolution diffusion imaging (HARDI) protocols at high magnetic field strengths to resolve 3-dimensional images of the perforant path (Augustinack et al., 2010; Mollink et al., 2019; Colon-Perez et al., 2015; Beaujoin et al., 2018; Zeineh et al., 2017). A smaller number of studies have investigated the perforant path in humans using in-vivo tractography derived from high-resolution diffusion imaging. One such study implemented high-resolution diffusion imaging to visualize the perforant path using fractional anisotropy-aided deterministic tractography (Zeineh et al., 2012). In this investigation, using resampled 1.5mm isotropic data (final resolution 0.7mm isotropic) from 6 human subjects, the authors were able to visualize the perforant path in-vivo operationalized as streamlines connecting the entorhinal cortex with the DG/CA3, CA1, and subiculum.

While this investigation provided one of the first in-vivo 3-dimensional visualizations of entorhinal-hippocampal projections in the high-resolution space, the question remains as to which specific entorhinal-hippocampal projection declines with age and memory decline. To address this issue in this investigation, we focused on improving the existing tractography work, by implementing quantitative anisotropy (QA) informed deterministic tractography (Yeh et. al., 2013). It has been shown that QA-informed tractography improves the accuracy of deterministic tractography of microtubule phantom objects and is less affected by partial volume effects compared to the tensor model (Yeh et al., 2013). In addition, the use of quantitative anisotropy was found to produce fewer false-positive streamlines compared to over 96 different methods released by more than 20 other research groups around the world (Maier-Hein, 2017). In this investigation, by employing the use of generalized q-sampling (GQI) imaging, QA-aided deterministic tractography in the native diffusion space and seeding the high resolution sequence with 10,000,000 seeds (10x the suggest amount for whole brain analysis), we were able to generate a robust model of structural connectivity (Figure A.3.1a). This was made possible by the use of the high-resolution diffusion imaging sequence (ZOOMit; voxel size = 0.67 x 0.67 x 3mm) acquired parallel to the long axis of the hippocampus. This robust tractography derived from ZOOMit, along with acquisition of high-resolution T1 and T2-weighted imaging data, allowed for harmonization with ASHS to delineate MTL regions (see methods). Together, this harmonization approach allowed us to quantify the number of streamlines ending between MTL regions in order to determine which specific entorhinal projection was associated with aging and memory decline.

Using these methods to improve upon prior work, we provide evidence that MTL structural connectedness (graph density) was reduced in those at advanced age. Interestingly, this difference was only apparent for the most restrictive arbitrary threshold of 0.01. Here it is possible that the difference is only apparent at this more restrictive threshold as it might contribute to the removal of spurious streamlines of low count across the network. However, we provide evidence that reduced MTL structural connectedness (across all thresholds) was associated with reduced RAVLT delayed recall performance. Together these results seem to suggest that the degree of white matter connecting the medial temporal lobe is an additional indicator of age-related cognitive decline.

As a result of this first analysis, we then asked which specific entorhinal projections to the subiculum and hippocampal formation were more vulnerable to the effects of aging and cognitive decline. We found that the connectivity of the CA1-subiculum, entorhinal cortex- DG, and entorhinal cortex-CA1 were diminished in those at advanced age. Similarly, we then asked which specific connections between the entorhinal cortex and hippocampal formation were associated with episodic memory decline. We found that reduced connectivity between the CA1 - DG, entorhinal cortex-subiculum, and the entorhinal cortex -DG was related to impaired delayed recall performance.

However, only the relationships between memory performance and entorhinal cortex-subiculum and entorhinal cortex – DG persisted after accounting for sex, MMSE, years of education, and average subject head motion. These relationships also persisted after accounting for the maximum subject streamline count. Here we note that

our usage of the terminology ‘persists’ refers to the ability of the connectivity regressor and corresponding p-value to surpass our arbitrary threshold of alpha. A more general interpretation of these results would suggest that entorhinal – DG connectivity is associated with delayed recall performance when MMSE, years of education, and motion are accounted for. Importantly, we note that the entorhinal cortex – DG projection is the only node-to-node connection that is both reduced in the Oldest-Old and is reduced in those with episodic memory decline.

We have previously reviewed the functional significance of different entorhinal projections in the context of computational theories of DG and CA3 functioning (Yassa & Stark, 2011). It is hypothesized that the direct entorhinal projection to the DG provides input for sparse coding granule cells of the DG to perform pattern separation; a process whereby input is orthogonalized to create unique representations. These newly separated representations are then “collected” by CA3 to reduce interference and support new learning through the mossy fiber pathway (Marr, 1971; Blackstad et al., 1970; Yassa & Stark, 2011). The direct entorhinal projection to CA3 is thought to provide a cue for recall (Rolls, 2007). This theory has been supported by selective lesioning of the mossy fiber pathway which impaired encoding but not retrieval where lesioning of the direct entorhinal – CA3 pathway impaired retrieval but spares encoding (Lee & Kesner, 2004; Yassa & Stark, 2011). Thus, it is tempting to speculate that our findings of reduced entorhinal cortex- DG connectivity would yield impairment in encoding new representations or impairment of pattern separation processes. Indeed, additional research using the fractional anisotropy methodology we have previously developed (Yassa et al., 2010) has found that the perforant path integrity is associated

with behavioral pattern separation performance (Bennett & Stark, 2016; Yassa et al., 2011). However, this work is also subjected to the criticism laid out by Zeineh et al. (2012) as it does not measure the perforant pathway with respect to its gray matter targets and 3-dimensional morphology. Rather, diffusion was accessed locally between the entorhinal cortex and subiculum at a 45-degree angle. Here, we extend this body of work by providing the novel finding that entorhinal cortex – DG streamlines, in particular, decline with aging and are associated with episodic memory performance.

One limitation of this work is that we observed the largest streamline count for most subjects between the CA1 and DG which anatomically is not thought to have a reciprocal connection. In general, future studies should seek to compare the accuracy of streamlines derived from high-resolution diffusion imaging with histological methods from ex-vivo samples that implement anterograde and retrograde tracing. In animal models, one such study has been conducted recently that compared in-vivo 0.1mm resolution tractography with ex-vivo viral tracing (Wu & Zhang, 2016). This investigation found evidence of remarkable similarity between tractography and the viral tracer data in terms of their spatial projection patterns, and also found false positive streamline connectivity between the CA1 and DG of the hippocampus (Wu & Zhang, 2016). Similar techniques should be employed with excised human tissue with the high resolution sequence to better understand the 3-dimensional accuracy of this work.

Another possible limitation of this work is the use of a single shell (single b-value) DWI sequence. It is possible that the implementation of the ZOOMit high resolution sequence adapted to include a multishell diffusion weighted imaging would enhance the tractography results. It is possible that this adaptation would enable the quantification of

separate streamlines projecting from different portions of the entorhinal cortex such as the lateral ("content") and medial ("context") pathways which are known to support different functions (Knierim et al., 2013; Reagh & Yassa, 2014).

Conclusion

In this investigation we provide evidence that the number of streamlines that connect the entorhinal cortex and DG are associated with aging and episodic memory performance. These analyses advance the study of white matter within the medial temporal lobe by supplying 3-dimensional specificity to our previous work (Yassa et al., 2010). Future study should seek to determine if multi-shell acquisition would be able to yield direct visualization of the perforant path using similar state-of-the-art MTL segmentation and tractography procedures.

References

Alexander, A.L., Hurley, S.A., Samsonov, A. A., Adluru, N., Hosseinbor, A. P., Mossahebi, P., Tromp do P. M., Zakszewski E., Field, A. S. (2011) Characterization of cerebral white matter properties using quantitative magnetic resonance imaging stains. *Brain Connectivity* 1: 423–46.

Alexander, A.L., Lee, J.E., Lazar, M., Field, A.S. (2007) Diffusion tensor imaging of the brain. *Neurotherapeutics: the journal of the American Society for Experimental Neuro Therapeutics* 4: 316–329.

Augustinack, J. C., Helmer, K., Huber, K. E., Kakunoori, S., Zöllei, L., & Fischl, B. (2010). Direct visualization of the perforant pathway in the human brain with ex vivo diffusion tensor imaging. neuroscience, 4, 42

Avants, B.B., Tustison, N., Song, G. (2009) Advanced normalization tools (ANTS) (Penn Image Computing and Science Laboratory; University of Pennsylvania, Philadelphia).

Baks-Te-Bulte, L., Wouterlood, F.G., Vinkenoog, M. and Wit-ter, M.P. (2005) Entorhinal projections terminate onto principal neurons and interneurons in the subiculum: aquantitative electron microscopical analysis in the rat. Neuroscience, 136(3): 729–739. A1 to the subiculum. Hippocam-pus, 11(2): 99–104.

Beaujoin, J., Palomero-Gallagher, N., Boumezbeur, F. et al. (2018) Post-mortem inference of the human hippocampal connectivity and microstructure using ultra-high field diffusion MRI

at 11.7 T. Brain Struct Funct 223, 2157–2179
Bennett, I. J., & Stark, C. E. (2016). Mnemonic discrimination relates to perforant path integrity: An ultra-high resolution diffusion tensor imaging study. Neurobiology of learning and memory, 129, 107–112.
Blackstad, T. W., Brink, K., Hem, J., & Jeune, B. (1970). Distribution of hippocampal mossy fibers in the rat. An experimental study with silver impregnation methods. The Journal of comparative neurology, 138(4), 433–449.
Braak H, Braak E. Neuropathological stageing of Alzheimer-related changes. Acta Neuropathol. 1991; 82:239– 259.
Colon-Perez, L. M., King, M., Parekh, M., Boutzoukas, A., Carmona, E., Couret, M., ... Carney, P. R. (2015). High-field magnetic resonance imaging of the human temporal lobe. NeuroImage: Clinical, 9, 58–68.
Desikan RS, McEvoy LK, Thompson WK, Holland D, Brewer JB, Aisen PS, et al. Amyloid-β–Associated Clinical Decline Occurs Only in the Presence of Elevated P-tau. Arch Neurol. 2012;69:709–13.
Desikan RS, Sabuncu MR, Schmansky NJ, Reuter M, Cabral HJ, Hess CP, et al. Selective disruption of the cerebral neocortex in Alzheimer's disease. PLoS One. 2010;5:e12853.
Desmond, N.L., Scott, C.A., Jane, J.A. and Levy, W.B. (1994)Ultrastructural identification of entorhinal cortical synapsesin CA1 stratum lacunosum-moleculare of the rat. Hippo-campus, 4(5): 594–600
Eichenbaum, H., Sauvage, M., Fortin, N., Komorowski, R., and Lipton, P. (2012) Towards a functional organization of episodic memory in the medial temporal lobe. Neurosci. Biobehav. Rev. 36: 97–1608.
Eskildsen SF, Coupé P, García-Lorenzo D, Fonov V, Pruessner JC, Collins DL. Prediction of Alzheimer's disease in subjects with mild cognitive impairment from the ADNI cohort using patterns of cortical thinning. NeuroImage. 2013;65:511–21.
Fang-cheng Yeh. (2019, March 14). DSI Studio (Version 2019 March). Zenodo.
Garrison, K. A., Scheinost, D., Finn, E. S., Shen, X., & Constable, R. T. (2015). The (in)stability of functional brain network measures across thresholds. *NeuroImage*, *118*, 651–661.
Geinisman, Y., deToledo-Morrell, L., Morrell, F., Persina, I.S., Rossi, M. (1992) Age-related loss of axospinous synapses formed by two afferent systems in the rat dentate gyrus as revealed by the unbiased stereological dissector technique. Hippocampus 2:437–444.
Gomez-Isla T, Price JL, McKeel DWJ, Morris JC, Growdon JH, Hyman BT, (1996). Profound loss of layer II entorhinal cortex neurons occurs in very mild Alzheimer's disease. Neuroscience 16, 4491–4500.
Hebert LE, Weuve J, Scherr PA, Evans DA. Alzheimer disease in the United States (2010-2050) estimated using the 2010 Census. Neurology. 2013; 80(19):1778–83.
Hyman, B. T., Van Hoesen, G. W., Kromer, L. J., & Damasio, A. R. (1986). Perforant pathway changes and the memory impairment of Alzheimer's disease. *Annals of neurology*, 20(4), 472–481.
Hyman, B.T., Van Hoesen, G.W., Kromer, L.J., Damasio, A.R. (1986) Perforant pathway changes and the memory impairment of Alzheimer's disease. Ann Neurol 20:472–481.
Jack CR, Petersen RC, Xu YC, O'Brien PC, Smith GE, Ivnik RJ, Boeve BF, Waring SC, Tangalos EG, Kokmen E. Prediction of AD with MRI-based hippocampal volume in mild cognitive impairment. Neurology. 1999; 52:1397–1403.

Jbabdi, S., Johansen-Berg, H. (2011) Tractography: Where Do We Go from Here? *Brain Connectivity* 1: 169- 183.
Kalus, P., Slotboom, J., Gallinat, J., Mahlberg, R., Cattapan-Ludewig, K., Wiest, R., Nyffeler, T., Buri, C., Federspiel, A., Kunz, D., Schroth, G., & Kiefer, C. (2006). Examining the gateway to the limbic system with diffusion tensor imaging: the perforant pathway in dementia. NeuroImage, 30(3), 713–720.
Knierim, J.J., and Neunuebel, J.P. (2016) Tracking the flow of hippocampal computation: Pattern separation, pattern completion, and attractor dynamics. Neurobiol. Learn. Mem. 129: 38–49.
Knierim, J.J., Neunuebel, J.P., and Deshmukh, S.S. (2013) Functional correlates of the lateral and medial entorhinal cortex: Objects, path integration and local-global reference frames. Philos. Trans. R. Soc. Lond. B Biol. Sci. 369: 20130369.
Knierim, J.J., Neunuebel, J.P., and Deshmukh, S.S. (2013) Functional correlates of the lateral and medial entorhinal cortex: Objects, path integration and local-global reference frames. Philos. Trans. R. Soc. Lond. B Biol. Sci. 369: 20130369.
Lee, I., & Kesner, R. P. (2004). Encoding versus retrieval of spatial memory: double dissociation between the dentate gyrus and the perforant path inputs into CA3 in the dorsal hippocampus. Hippocampus, 14(1), 66–76.
Lorente de No´, R. (1933) Studies on the structure of the cer-ebral cortex. J. Psychol. Neurol., 45(6): 26–438.
Maier-Hein, K. H., Neher, P. F., Houde, J. C., Côté, M. A., Garyfallidis, E., Zhong, J., ... Descoteaux, M. (2017). The challenge of mapping the human connectome based on diffusion tractography. Nature Communications, 8(1).
Marr D (1971) Simple memory: a theory for archicortex. Philos Trans R Soc Lond B Biol Sci 262:23–81.
Mollink, J. M. Hiemstra, K. L. Miller, I. N. Huszar, M. Jenkinson, J. Raaphorst, M. Wiesmann, O. Ansorge, M. Pallebage-Gamarallage and A. M. van Cappellen van Walsum (2019). White matter changes in the perforant path area in patients with amyotrophic lateral sclerosis, Neuropathology and Applied Neurobiology (2019) 1– 16.
Naber, P.A., Lopes da Silva, F.H. and Witter, M.P. (2001) Reciprocal connections between the entorhinal cortex andhippocampal fields CA1 and the subiculum are in registerwith the projections from C
Price JL, Ko AI, Wade MJ, Tsou SK, McKeel DW, Morris JC, (2001). Neuron number in the entorhinal cortex and CA1 in preclinical Alzheimer disease. Arch. Neurol 58, 1395–1402.
Ramón y Cajal, S. (1911) Histologie du SystemeNerveux del'Homme et des Vertebres. Maloine, Paris
Reagh, Z. M., & Yassa, M. A. (2014). Object and spatial mnemonic interference differentially engage lateral and medial entorhinal cortex in humans. Proceedings of the National Academy of Sciences of the United States of America, 111(40), E4264‑E4273.
Reagh, Z. M., Noche, J. A., Tustison, N. J., Delisle, D., Murray, E. A., & Yassa, M. A. (2018). Functional Imbalance of Anterolateral Entorhinal Cortex and Hippocampal Dentate/CA3 Underlies Age-Related Object Pattern Separation Deficits. Neuron, 97(5), 1187-1198.e4.
Rey A. L'examen clinique en psychologie. Presses Universitaires de France; Paris: 1964.
Robinson, J. L., Molina-Porcel, L., Corrada, M. M., Raible, K., Lee, E. B., Lee, V. M. Y., … Trojanowski, J. Q. (2014). Perforant path synaptic loss correlates with cognitive

impairment and Alzheimer's disease in the oldest-old. Brain, 137(9), 2578–2587.
Rogalski, E. J., Murphy, C. M., deToledo-Morrell, L., Shah, R. C., Moseley, M. E., Bammer, R., & Stebbins, G. T. (2009). Changes in parahippocampal white matter integrity in amnestic mild cognitive impairment: a diffusion tensor imaging study. Behavioural neurology, 21(1), 51–61.
Rolls, E.T. (2007) An attractor network in the hippocampus: theory and and neurophysiology. Learn. Mem. 14, 714–731
Rubinov M, Sporns O (2010) Complex network measures of brain connectivity: Uses and interpretations. *NeuroImage* 52:1059-69.
Scheff, S. W., Price, D. A., Schmitt, F. A., & Mufson, E. J. (2006). Hippocampal synaptic loss in early Alzheimer's disease and mild cognitive impairment. Neurobiology of aging, 27(10), 1372–1384.
Schilling, Kurt G., et al. "A fiber coherence index for quality control of B-table orientation in diffusion MRI scans." Magnetic resonance imaging (2019)
Smith, T.D., Adams, M.M., Gallagher, M., Morrison, J.H., Rapp, P.R. (2000) Circuit-specific alterations in hippocampal synaptophysin immunoreactivity predict spatial learning impairment in aged rats. J Neurosci20:6587–6593.
Stark CEL (2007) Functional Role of the Human Hippocampus. The Hippocampus Book, eds Andersen P, Morris R, Amaral D, Bliss T, O'Keefe J (Oxford University Press, New York), pp 549–579
Steward, O. (1976) Topographic organization of the projectionsfrom the entorhinal area to the hippocampal formation of therat. J. Comp. Neurol., 167(3): 285–314.Steward, O. and Scoville, S.A. (1976) Cells of origin of ent-orhinal cortical afferents to the hippocampus and fascia den-tata of the rat. J. Comp. Neurol., 169(3): 347–370.
Steward, O. and Scoville, S.A. (1976) Cells of origin of ent-orhinal cortical afferents to the hippocampus and fascia den-tata of the rat. J. Comp. Neurol., 169(3): 347–370.
Tucholka, A., Grau-Rivera, O., Falcon, C., Rami, L., Sánchez-Valle, R., Lladó, A., Gispert, J. D., Molinuevo, J. L., & Alzheimer's Disease Neuroimaging Initiative (2018). Structural Connectivity Alterations Along the Alzheimer's Disease Continuum: Reproducibility Across Two Independent Samples and Correlation with Cerebrospinal Fluid Amyloid-β and Tau. *Journal of Alzheimer's disease : JAD*, 61(4), 1575–1587.
Witter M. P. (2007). The perforant path: projections from the entorhinal cortex to the dentate gyrus. *Progress in brain research*, 163, 43–61.
Witter, M P (2006) Connections of the subiculum of the rat: topography in relation to columnar and laminar organization. Behavioral Brain Research, 174(2) : 251-264.
Witter, M. P. (2007). The perforant path: projections from the entorhinal cortex to the dentate gyrus. Progress in Brain Research, 163, 43–61.
Witter, M. P., & Amaral, D. G. (1991). Entorhinal cortex of the monkey: V. Projections to the dentate gyrus, hippocampus, and subicular complex. *The Journal of comparative neurology*, 307(3), 437–459.
Witter, M. P., Groenewegen, H. J., Lopes da Silva, F. H., & Lohman, A. H. (1989). Functional organization of the extrinsic and intrinsic circuitry of the parahippocampal region. *Progress in neurobiology*, 33(3), 161–253.
Witter, M.P. and Amaral, D.G. (1991) Entorhinal cortex of themonkey. V. Projections to the dentate gyrus, hippocampus,and subicular complex. J. Comp. Neurol., 307(3): 437–459.
Wu, D., & Zhang, J. (2016). In vivo mapping of macroscopic neuronal projections in the mouse

hippocampus using high-resolution diffusion MRI. NeuroImage, 125, 84‑93.
Yassa MA, Mattfeld AT, Stark SM, Stark CEL. Age-related memory deficits linked to circuit-specific disruptions in the hippocampus. Proceedings of the National Academy of Sciences. 2011; 108 (21):8873–8878.
Yassa, M. A., Muftuler, L. T., & Stark, C. E. L. (2010). Ultrahigh-resolution microstructural diffusion tensor imaging reveals perforant path degradation in aged humans in vivo. *Proceedings of the National Academy of Sciences*, 107(28), 12687–12691.
Yeh, F. C., Panesar, S., Barrios, J., Fernandes, D., Abhinav, K., Meola, A., & Fernandez-Miranda, J. C. (2019). Automatic Removal of False Connections in Diffusion MRI Tractography Using Topology-Informed Pruning (TIP). Neurotherapeutics, 1-7.
Yeh, F. C., Verstynen, T. D., Wang, Y., Fernández-Miranda, J. C., & Tseng, W. Y. I. (2013). Deterministic diffusion fiber tracking improved by quantitative anisotropy. PLoS ONE, 8(11), 1–16.
Yeh, Fang-Cheng, Van Jay Wedeen, and Wen-Yih Isaac Tseng, "Generalized-sampling imaging."Medical Imaging, IEEE Transactions on 29.9 (2010): 1626-1635.
Yendiki, A., Koldewyn, K., Kakunoori, S., Kanwisher, N., & Fischl, B. (2014). Spurious group differences due to head motion in a diffusion MRI study. NeuroImage, 88, 79–90.
Yushkevich, P. A., Pluta, J. B., Wang, H. , Xie, L. , Ding, S. , Gertje, E. C., Mancuso, L. , Kliot, D. , Das, S. R. and Wolk, D. A. (2015), Automated volumetry and regional thickness analysis of hippocampal subfields and medial temporal cortical structures in mild cognitive impairment. Hum. Brain Mapp., 36: 258-287.
Zeineh, M. M., Holdsworth, S., Skare, S., Atlas, S. W., & Bammer, R. (2012). Ultra-high resolution diffusion tensor imaging of the microscopic pathways of the medial temporal lobe. NeuroImage, 62(3), 2065–2082.
Zeineh, M. M., Palomero-Gallagher, N., Axer, M., Gräßel, D., Goubran, M., Wree, A., Woods, R., Amunts, K., & Zilles, K. (2017). Direct Visualization and Mapping of the Spatial Course of Fiber Tracts at Microscopic Resolution in the Human Hippocampus. Cerebral cortex (New York, N.Y. : 1991), 27(3), 1779–1794.